325

MASTER

ORNL-3213
UC-34 – Physics
TID-4500 (16th ed. Rev.)

SOLID STATE DIVISION
ANNUAL PROGRESS REPORT
FOR PERIOD ENDING AUGUST 31, 1961

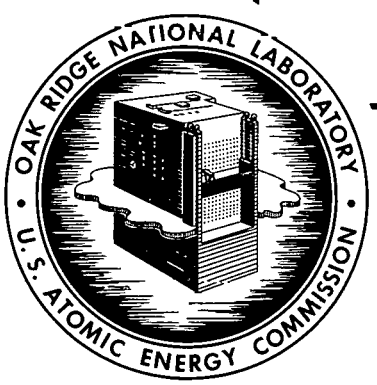

OAK RIDGE NATIONAL LABORATORY
operated by
UNION CARBIDE CORPORATION
for the
U.S. ATOMIC ENERGY COMMISSION

DISCLAIMER

Printed in USA. Price $2.75. Available from the
Office of Technical Services
Department of Commerce
Washington 25, D.C.

ORNL-3213
UC-34 – Physics
TID-4500 (16th ed. Rev.)

Contract No. W-7405-eng-26

SOLID STATE DIVISION
ANNUAL PROGRESS REPORT
For Period Ending August 31, 1961

D. S. Billington, Director
J. H. Crawford, Jr., Associate Director

DATE ISSUED

DEC 29 1961

OAK RIDGE NATIONAL LABORATORY
Oak Ridge, Tennessee
operated by
UNION CARBIDE CORPORATION
for the
U. S. ATOMIC ENERGY COMMISSION

THIS PAGE

WAS INTENTIONALLY

LEFT BLANK

SOLID STATE DIVISION ANNUAL PROGRESS REPORT

SUMMARY

PART I. THEORY

1. Ranges of Primary Atoms

Theoretical calculations have been performed to determine the ranges in solids of atoms having energies from 250 ev to 200 kev. The work makes use of Monte Carlo techniques on an IBM 7090 computer. The lattice atoms of the solid are assumed to be randomly located in such a manner as to preserve the density of the crystal. The collisions between the moving primary atom and the lattice atoms are assumed to be binary. For most of the work to date, a screened Coulomb potential and a hard-sphere approximation to the screened Coulomb potential have been used to represent the interaction between the colliding atoms.

2. Electron Cross Sections for Atomic Displacements

A calculational program has recently been undertaken for theoretically computing the number of atomic displacements in solids by irradiation with fast electrons. The aim of the program is to supplement the rather limited number of theoretical calculations reported in the literature.

3. Electron Transport in a Magnetic Field

The kinetic coefficients which relate the electrical and thermal currents to the electrical and thermal gradients have been calculated for a free electron model. The most interesting result is that the Seebeck and Ettingshausen-Nernst effects are almost purely oscillatory for strong magnetic fields and low temperatures.

4. Statistical Mechanics of Nonmetallic Crystals

An IBM 7090 computer program has been written for hole and electron concentration in the valence and conduction bands, respectively, of nonmetallic crystals, under quite general assumptions. It is being extended to include space and time variation of acceptor and donor concentration.

PART II. METALS AND ALLOYS

5. Low-Temperature Irradiation Studies

Annealing Studies of Various Neutron-Irradiated Metals. – Damage rates and isochronal annealing data for W, Mo, Ni, Pb, Sn, Na, and graphite irradiated near 4°K have been obtained. An interesting anomaly has been found in the resistivity behavior of Na.

Stored Energy in Irradiated B^{10}-Doped Copper. – Using a new technique for specimen isolation the stored energy arising from B^{10} fission damage in copper has been measured as a function of temperature. The associated resistivity changes were measured on the same sample. Estimates of defect concentration and resistivity per defect have been made.

Length Changes in Irradiated B^{10}-Doped Copper. – The resistivity and length changes associated with B^{10} fission damage in copper have been measured simultaneously. Isochronal annealing data are presented from which some conclusions can be made concerning the annealing processes and the properties of the defects involved.

Helium Refrigerator Modifications. – Recent improvements to the low-temperature irradiation facility are described. A bombardment temperature of 3°K can now be maintained at full reactor power.

Twinning in Silver. – Experiments have been conducted on the tensile deformation of twinning in silver. Samples were deformed at 4.2, 77, and 300°K.

6. Quenching Studies in Copper

In order to obtain the energy of formation of vacancies in copper and to study the motion of vacancy defects, copper samples are quenched from high temperatures in a helium refrigerator.

7. Dislocation Interactions

Temperature Dependence from 250 to 370°K of Dislocation Pinning in Copper Single Crystals by Radiation Defects. – Measurements of internal friction and modulus defect at 15 kc have been used to study, in the neighborhood of room temperature, the pinning of dislocations in copper

crystals by fast-neutron-induced defects. By measuring at various constant temperatures the delayed pinning following a short irradiation, a delay-time distribution for the pinning defects was obtained and the process was found to be governed by a single activation energy, 1.1 ev. Although this energy is reasonable for the diffusion of vacancies to dislocations, the shape of the delay-time distribution does not agree with theory, and the apparent number of jumps at the end of the process is anomalously low.

A Thermally Activated Internal Friction Spectrum in Copper Following Neutron Irradiation. – Measurements of the internal friction of copper as a function of temperature from 220 to nearly 400°K after a neutron irradiation of about 1×10^{14} *nvt* indicate a defect-controlled spectrum in which the defect's activation energy for motion plays a role. The present spectrum is characterized by activation energies of 0.39 ev at the low-temperature side and 0.56 ev at the high-temperature side.

8. Investigations of Metal Surfaces

Using chemical and electrochemical techniques, investigations of the effects of both crystallographic orientation and defect structure on the dissolution mechanisms of copper in aqueous solutions have been continued. The effects of neutron irradiation and/or mechanical stress upon the density of dislocations, as well as their motion and multiplication, have been studied by a technique which reveals dislocations as etch pits. The same technique was used to observe dislocations formed about precipitate particles of Cu_2O in copper. An acid saw and an acid polisher, which permit preparation of copper crystals with a very low dislocation density, have been constructed.

9. Alloy Research

Experiments are being continued on the effect of radiation on diffusion-controlled atomic rearrangements in Cu-Al alloys. The dependence of the rate of decrease of resistivity during irradiation at 100°C on the instantaneous neutron flux is being investigated. Preliminary results indicate that recombination annealing is important during earlier stages of the process and linear annealing during later stages.

Atomic rearrangements following cold working are being studied in Cu-Si alloys. Measurements have been made of the electrical resistivity, hardness, and yield strength upon isochronal annealing up to 850°C following cold drawing to 42–45% reduction in area. The changes in these properties are being compared with changes in microstructure and x-ray patterns. A preliminary discussion of the results is given in terms of the introduction of vacancies and stacking faults upon cold working and the subsequent segregation of solute upon isochronal annealing.

Impact tests on parent plate and synthetic heat-affected zone samples of A-212B pressure-vessel steel were conducted following irradiation at about 120°F in the ORR to doses of the order of 10^{19} neutrons/cm^2 (> 1 Mev). The increase in the Charpy V-notch fracture transition temperature upon irradiation was roughly the same, about 225°F, for the parent plate and two types of weld heat-affected zone samples.

10. Properties of High-Purity Iron

A digital recording system for handling all data from internal friction, resistivity measurement, creep, and other types of experiments, with a 90% reduction in man-hours, is nearing completing.

Twinning in iron at room temperature, when intergranular fractures occur, is attributed to high microscopic strain rates produced in grains whose boundaries participate in the fracture process.

11. Single-Crystal Spheres of Copper, Silver, and Gold Grown from the Melt

Single-crystal spheres of copper, silver, and gold, ranging in diameter from 75 to 600 μ, have been grown by the Bridgman technique (slightly modified) in graphite crucibles. The surface-tension properties and freedom from foreign inclusions are important in minimizing multiple nucleation.

12. $Au_{0.82}Hg_{0.18}$: A Transmutation Alloy

Single-crystal spheres of gold <0.015 in. in diameter were subjected to thermal-neutron fluxes of sufficient magnitude to produce 18 wt % of mercury in gold by transmutation at ~85°C. A solid-solution-alloy single crystal results, which under

normal thermodynamic conditions cannot form below ~400°C.

13. Electron Microscope Studies

Electron microscope studies of fission-fragment tracks in thin films indicate that tracks arise from electron excitation and ionization; however, the different behavior of metal films and UO_2 suggests basically different mechanisms by which tracks are produced in the thin films in metals as compared with UO_2. Twenty-four-Mev nitrogen ion irradiation of thin platinum films produced narrow tracks which are different from those produced by fission fragments.

14. Ar^+ Ion Bombardment of Solid Surfaces (Copper, Germanium, and Indium Antimonide)

Yields are reported for Ar^+ ions of normal incidence upon polycrystalline and monocrystalline copper and upon monocrystalline germanium. These ratios have been determined at ion energies from 1 to 5 kev.

Atom ejection patterns were obtained for the three major planes of a copper monocrystal, for copper surfaces not aligned with the principal direction, and for one plane of indium antimonide. Patterns with structure could not be obtained for any of the principal planes of germanium in the energy range studied.

The ion beam was analyzed for neutral argon atoms and (4 ± 3)% of the beam consisted of neutral particles. Therefore the experimental uncertainty, taking into consideration instrument error, neutrals, and double-charged ions, is ±8%.

PART III. NONMETALS

15. Semiconductor Studies and Studies of Insulators

Current Recombination and Annealing Studies. – Additional measurements have been made to determine the activation energy of the annealing of recombination centers in germanium. In addition, lifetime measurements are being extended to lower temperatures. Initial results demonstrated interesting behavior in this range.

Recombination Studies. – An extensive study has been made of radiation-induced recombination centers in germanium. The results emphasize the importance of doping impurities in radiation-effects studies. An analysis which correlates the various types of behavior observed, using different kinds of radiation and different doping impurities, has been performed.

Thermoelectric Power in Germanium. – In connection with the measurement of thermoelectric power of germanium, methods have been developed for scanning the sample temperature and for automatic recording of the experimental parameters. Two gamma irradiations have been made on 2-ohm-cm *n*-type germanium. The Seebeck coefficient, Hall mobility, and carrier concentration have been measured.

Gamma Irradiation of Silicon. – Introduction rates for net acceptor levels at 0.17 and 0.5 ev below the conduction band have been determined in a number of silicon samples that had been grown by a vacuum floating-zone technique. These are compared with introduction rates in pulled samples, which contain considerably more oxygen. The 0.17-ev acceptor level, which has been attributed to a center composed of an oxygen atom and a vacancy, is introduced in all samples of resistivities greater than 1 ohm-cm, which is not surprising in view of the fact that even floating-zone purification cannot remove all dissolved oxygen. The deep level is strongly dependent upon oxygen content and resistivity, appearing more rapidly in material of low oxygen content and low resistivity.

The introduction rates of the two acceptor centers are also compared in identical samples irradiated with gamma rays of different intensities. For a difference of a factor of 3 in the photon flux, no change in introduction rate per incident gamma ray was observed.

Some early measurements on the introduction of net donors in *p*-type silicon indicate that the introduction of these centers, too, may be affected by the oxygen content of the silicon.

Annealing Studies of Irradiated Germanium. – The annealing of germanium which had been irradiated by Co^{60} gamma rays at 77°K shows that the annealing involves at least two processes. One process has an activation energy of 0.787 ev.

Thermal-Neutron-Induced Recoil and Transmutation Effects in Semiconductors. – Nuclear reactions accompanying thermal-neutron capture in semiconductors have been employed to examine recoil effects, chemical impurity introduction, and impurity

compensation effects. A replacement-type collision model, which accounts for the fact that the transmuted atoms exert their expected influence on carrier concentrations irrespective of whether or not the specimen has been thermally annealed, is discussed.

Studies on Cu_2O: Recrystallization Processes. – Work on Cu_2O during the last year has been directed toward a better understanding of the conditions necessary for single-crystal preparation and the factors that influence grain growth. The temperature range of 1000 to 1130°C is being explored for parameters associated with this grain growth. One inflection in the resistivity of the sample is reported.

Solid State Division Co^{60} Gamma Source. – The original facility No. 1 has been emptied and water-cooled and will be reloaded with ~11,000 curies of Co^{60}, providing a central intensity of $\sim 10^7$ r/hr.

Electron Excess Centers in KCl. – Comparison of the optical absorption in the F band of KCl with the paramagnetic contribution to the low-temperature susceptibility has yielded values for the oscillator strength of the F band of 0.9 and 0.7, respectively, in additively and irradiation-colored material. The variation of these numbers from sample to sample was too great to ascribe any significance to the difference between the averages obtained for the additively colored and gamma-ray-colored material.

Bleaching and annealing produced M centers in the samples. Changes in the optical absorption and magnetic properties were consistent with a model recently proposed, in which two F centers coalesce to form an M center, which absorbs light both in the M and F band.

Magnetic Susceptibility of Potassium Hexachlororhenate(IV) and Potassium Hexabromorhenate(IV) from 5 to 300°K. – The Curie points of K_2ReCl_6 and K_2ReBr_6 obtained from magnetic susceptibility measurements are 12.4 ± 0.5 and 15.3 ± 0.5°K, respectively, which confirm that cooperative-type transitions observed in the heat capacities of these compounds with maxima at 11.9 ± 0.1 and 15.2 ± 0.1°K, respectively, represent transitions to the antiferromagnetic state. Evidence is presented that the ratios of the next-nearest-neighbor to nearest-neighbor superexchange interactions in the two compounds are approximately equal. An estimate of the spin-orbit coupling constants in the crystals is given and compared with other estimates.

Radiation Effects in Uranium-Doped Zirconia. – Samples were doped with depleted and enriched uranium concentrations of the proper magnitude so that the effects of fast neutrons, fission fragments, and uranium as a chemical impurity could be assessed. The results indicated that the monoclinic-to-fcc phase transition is produced by fission fragments only, not by fast neutrons, and that uranium, as a chemical impurity in concentrations less than 0.4 wt %, does not act as a catalyst or stabilization nucleus for the transformation.

Thermal Conductivity. – A cryostat for thermal conductivity measurements between 2 and 100°K is being constructed.

16. Covalent Crystals and Glasses

Introduction of the OH Radical into Silica and Its Effect on the E_1 Center. – A hydrogen-free silica was heated in H_2O vapor at 900°C for increasing periods of time. The intensity of the E_1' center for constant gamma-ray irradiation dose was observed as a function of the intensity of the stretching mode of the hydroxyl group at 2.7 μ. The relation derived from these observations is

$$\eta_{E_1} = b - a\,\eta_{(OH)},$$

where η_{E_1} = concentration of E_1 centers, $\eta_{(OH)}$ = concentration of OH bonds, and b and a are constants. On the basis of this result, it is suggested that the OH enters the silica in such a way as to destroy E_1 sites, or else to prevent the E_1 sites from trapping electrons.

Oscillator Strength of the E_1' Center in Silica. – The concentration of E_1' centers in silica has been measured by static magnetic susceptibility and electron spin resonance techniques. The concentrations measured by the two techniques are in good agreement. The concentration thus measured was used to calculate an oscillator strength, f, for the optical absorption of the E_1' center, and it was found that $f = 0.16$.

Paramagnetic Properties of the E_2' Center in Crystalline Quartz. – The g tensors of the E_2' centers in irradiated quartz single crystals were calculated. Each line, observed for c axis parallel to H orientation, has six sites per unit cell and each is approximately axially symmetric; however, for the line ($g_{c\ axis} = 2.0008$) $g_1 = 2.0015$, $g_2 = g_3 = 2.00057$, and for the line ($g_{c\ axis} = 2.0010$) $g_1 = 2.0022$, $g_2 = 2.00067$, $g_3 = 2.00050$. It may be

that the E_2' centers have their origin in the removal of an O ion and the subsequent trapping of an electron on the uncompleted Si orbital.

Aluminum Impurities and the 4600-A Band in Quartz. – The optical absorption from 1 ev to 8.5 ev in a single crystal of synthetic quartz has been observed as a function of Co^{60} gamma-ray irradiation followed by heat treatments, and subsequent reirradiation. Electron spin resonance measurements on the same specimen were used to observe the Al resonance. A threefold increase in the Al resonance after the second irradiation was not accompanied by an increase in the optical absorption in the 4600-A region. Concentration measurements of the Al resonance indicated that most of the Al present in the crystal was in substitutional positions. These results have raised serious questions with respect to the correlation of the ESR signal with the optical bands in the region of 4600 A and have raised doubts about the diffusion mechanism which was proposed to explain the enhancement of the optical absorption in this region.

Electric-Field Distribution in Gamma-Irradiated Lead Glass. – A simplified calculation of the electric-field intensity inside a gamma-irradiated lead-glass window fails to account for the planar discharges observed in such windows, though such a field seems sufficient to aid in the propagation of a discharge initiated by other means.

Vacuum-Ultraviolet Absorption Studies of Irradiated Silica and Quartz. – The optical absorption properties of Co^{60}-irradiated fused silica and crystalline quartz have been studied in the vacuum-ultraviolet region.

17. Stored Energy in Graphite

From more than 100 postannealing core samples taken from the reactor following the September 1960 anneal, it was calorimetrically determined that the extent of the anneal conforms to the maximum temperatures reached during the operation. Between 3.5 and 4.5 Mwhr of stored energy was released in a 15-ft-diam core region, and the maximum graphite temperature reached was 236°C, thus demonstrating the efficacy of the low-temperature–reverse air flow technique for annealing in the Graphite Reactor.

18. Ceramics

The annealing of some of the radiation-induced property changes of ceramic materials is being studied by thermal analysis. Apparatus was constructed which is suitable for samples weighing about 1 g.

19. Polymers

A Comparison of Reactor Neutrons to Gamma Radiation in the Cross-Linking of Polystyrene. – The relative rates of cross-linking of polystyrene by gamma radiation alone and by the mixed neutron and gamma radiation of a reactor have been determined by measurements of the fraction soluble and by swelling in toluene. The first determination is independent of the degree of branching, while the latter is independent of both the branching and the molecular-weight distribution. Both methods indicate that a given degree of cross-linking requires that the gamma-radiation dose be about 2.3 times as high as mixed reactor radiation. Analyses were performed for trace impurities which could have increased the dose in the reactor through neutron absorption reactions. The dose contributed by the impurity content was calculated to be negligible.

Infrared Studies of Plastics and Elastomers. – Sets of simultaneous equations established from known solutions of hydrocarbon standards were solved for the infrared spectral absorption of two polybutadienes. The fraction of the theoretical total unsaturated groups found was 0.89 and 0.82 for the two samples, one high in terminal unsaturated groups, the other high in *trans* groups.

Radiation Stability of Deuterated Basic Beryllium Acetate Complex. – Previous analyses of radiolysis products were supplemented by measurements of the insoluble residue in the samples and by mass spectral analysis of the evolved gases. About 0.5% insoluble material is produced by 2.4×10^{20} ev/g. The ratio of D_2 to CD_4 was 4:3, including light hydrogen compounds, in the evolved gas.

20. Radiation Dosimetry

Calorimetric measurements were made of the gamma heating of magnesium and bismuth in Hole 71 of the ORNL Graphite Reactor. Since the photoelectric absorption of bismuth is large at low

energy, an accurate knowledge of the gamma-radiation spectrum is required to estimate self-shielding. An estimate consistent with the experimental results is given by a spectrum calculated from a differential energy spectra tabulation. Chemical dosimeters are less complex than calorimeters; however, the usual dosimeters measure energy from fast-neutron and thermal-neutron interactions. A nonhydrogenous fluorocarbon organic chloride system was calibrated with gamma sources with a view to future use in reactor dosimetry.

PART IV. REACTOR MATERIALS

21. Fuel Materials

Postirradiation evaluation studies have been performed on both beryllium- and stainless-steel-canned UO_2 fuel elements. The beryllium-canned fuel rods were supplied by the French Commissariat a l'Energie Atomique, the United Kingdom Atomic Energy Authority, and Oak Ridge National Laboratory. Although no large dimensional instability was experienced by any of the fuel elements, failures occurred in the UKAEA capsules. Exposures of 2500 Mwd per metric ton were reached at clad temperatures of 1100°F. Other fuel materials examined after irradiation were UC_2 dispersed in graphite and UO_2-BeO mixtures. The UC_2 dispersed in graphite and canned in graphite showed uranium and fission product diffusion into the can wall. The UO_2-BeO samples showed a dimensional increase of 3%. Examinations were also carried out on fuel elements under development for the Maritime and Fast Breeder Reactor Programs.

The continuous release of fission gas from UO_2 was studied in both reducing and slightly oxidizing atmospheres. The gamma-ray spectrometer analysis of the fission-gas release was markedly different in the two cases. An increase of gas release was noted upon both heating and cooling.

22. Nuclear Metals

Tube burst (stress-rupture) tests have been operated in the Oak Ridge Research Reactor with specimens of Inconel, type 304 stainless steel, niobium–1% zirconium alloy, Zircaloy-2, and beryllium. The data from special heats of Inconel have not proved the theory that boron causes the lowered rupture strength under irradiation. Irradiation considerably lowers the tangential strain at rupture for the Inconel and type 304 stainless steel specimens. Preliminary results indicate that irradiation reduces the rupture strength of niobium–1% zirconium by 12 to 15% and that no drastic change is to be expected for Zircaloy-2.

PART V. SPECIAL PROJECTS

23. Effect of Reactor Irradiation on Nickel-Iron Alloys

Magnetic hysteresis loops were measured on six different nickel-iron alloys during a low-temperature irradiation in the Graphite Reactor, after the irradiation, and during a subsequent heat treatment. No significant changes were noted in the coercive force and remanence of most of the materials until during the heat treatment. Presumably, irradiation-induced defects became mobile in the range of 200 to 350°C.

24. Search for Superconductors of High Critical Temperatures and High Critical Fields

The superconducting transition temperatures of a series of Nb-Zr alloys have been determined. The results obtained are qualitatively understood as arising from a variation in electronic density of states at the Fermi surface through the entire compositional range.

25. Recoilless Gamma Emission (Mössbauer Effect)

Studies are being made of the nuclear resonant absorption of the 77-kev level of Au^{197}, using Pt^{197} as a gamma-ray source.

CONTENTS

Part I

THEORY

THIS PAGE

WAS INTENTIONALLY

LEFT BLANK

1. RANGES OF PRIMARY ATOMS

M. T. Robinson D. K. Holmes O. S. Oen

One of the important problems of radiation damage is that of determining the spatial extent of the damaged region, particularly in the case of heavy-particle damage, and specifically for investigations involving reactor bombardments, in the case of fast neutrons. Theoretical calculations have been unable to make any real progress principally because of the difficulties in obtaining realistic interatomic potentials. Experimental results have only recently been of direct pertinence, particularly in the energy range of interest for fast-neutron damage, namely a few kev to a few hundred kev. However, within the past three years some important results have been published[1-4] in which the *ranges* of energetic atoms in solid materials have been given. Knowledge of the range of one atom does not, of course, give the full details of the extent of the damaged region resulting from the cascade of secondary, tertiary, etc., displaced atoms resulting from the primary; however, the range of the primary will in most cases be a good measure of the extent of the damage, at least in one direction. Further progress is now possible since a theoretical model of the behavior of a fast atom in a lattice which correctly predicts the range (and the final spatial distribution of primary atoms, which is available in some cases[1,2]) may be, in principle, used to calculate further details of the cascade process. The work reported here is an attempt to obtain such a successful and well-founded theoretical model.

Most of the theoretical work to date[5] has been based on the "hard-sphere" approximation. The procedure followed is that of choosing an interatomic potential, using that potential to calculate a hard-sphere radius for each relative kinetic energy between the two colliding atoms, and treating the mechanical details of the collision as if it were between two rigid spheres. The great advantage of this approximation is its simplicity (for example, the final distribution of energies of the colliding atoms is independent of energy) which allows a relatively easy analytical expression of ranges and associated quantities. It has also been supposed, following Bohr,[6] that the hard-sphere model is realistic for interatomic potentials which are falling sufficiently rapidly – for example, exponentially – with interatomic separation in the region of the distance of closest approach at the particular relative kinetic energy. However, an investigation of the differential cross sections for energy transfer using the actually assumed potential itself, rather than its hard-sphere approximation, as reported in a previous progress report,[7] led to the observation that the hard-sphere approximation was very poor as regards energy transfer (or angular deflection) cross sections, but that it was not possible to say how great the error would be in such quantities as the range. The present calculations do not employ the hard-sphere approximation and so should lead to a better model of atomic collisions, and also allow directly an evaluation of the hard-sphere model, which, for its simplicity, would be very valuable if it is, or could be made, sufficiently accurate.

The present calculations use Monte Carlo techniques on an IBM 7090 computer to obtain the ranges and distributions of primary atoms. In essence the calculation consists of following the progress of an initially introduced primary atom collision by collision as it moves through the lattice of the solid until its energy has been so degraded that it is essentially at rest as an interstitial atom. Some details of the calculation, ranges of the parameters, and basic assumptions are listed below in the sequence in which the collision history of a primary atom is developed.

---

[1] J. A. Davies *et al.*, *Can. J. Chem.* 38, 1535 (1960).

[2] J. A. Davies and G. A. Sims, *Can. J. Chem.* 39, 601 (1961).

[3] R. A. Schmitt and R. A. Sharp, *Phys. Rev. Letters* 1, 445 (1958).

[4] V. A. J. van Lint, R. A. Schmitt, and C. S. Suffredini, *Phys. Rev.* 121, 1457 (1961).

[5] D. K. Holmes and G. Leibfried, *J. Appl. Phys.* 31, 1046 (1960).

[6] N. Bohr, *Kgl. Danske Videnska. Selskab, Biol. Medd.* 18(8) (1948).

[7] D. K. Holmes, G. Leibfried, and O. S. Oen, *Solid State Div. Ann. Progr. Rept. Aug. 31, 1959*, ORNL-2829, p 1.

Initial Energy. – As mentioned above, the choice of the range of energies of the primary atoms is governed by the basic interest in radiation damage by neutrons from fission. To date, the initial energies have been confined to the range 250 to 200,000 ev. These limits are also influenced by the facts that (1) the method used is not so accurate for lower energies and (2) the computing time required increases roughly linearly with the assumed initial energy (in the high energy range), and thus costs and the likelihood of machine errors increase. Running times have been as long as 1.3 hr.

Atom-Atom Scattering Process. – The interatomic collisions in this energy range may be treated adequately by purely classical scattering theory.[7] The moving atom, whose history is being followed, is assumed to interact with at most one atom of the lattice at a given time. As a criterion for determining whether or not interaction is occurring, each atom is imagined to have a sphere of influence whose radius R is half the closest interatomic spacing in the lattice; if the center of the moving atom is within this sphere, it is interacting with the given atom; if the center of the moving atom is outside the sphere, it is interacting with some other atom, or with none, since the nonoverlapping spheres of all the lattice atoms do not fill space. As a result of the collision the moving atom is deflected through some angle with respect to its original path, and kinetic energy is transferred from the moving atom to the struck atom. The deflection angle θ (and thus the energy transferred) depends on the impact parameter s between the moving and struck atoms, as illustrated in Fig. 1.1. Of course, there is really an interaction between the two atoms at interatomic separations greater than R, and the incorrect treatment of this part of the interaction turns out to be one of the limiting assumptions of the present calculation. However, the trajectory of the moving atom for most of the cases calculated here is of the form shown in Fig. 1.1 – namely, two essentially straight-line portions, with a small region, nearest the nucleus of the struck atom, in which the principal part of the deflection occurs. For such cases the restriction of the interaction to impact parameters no greater than R is quite acceptable.

Randomizing Assumption. – In the calculations performed to date, lattice distances are preserved

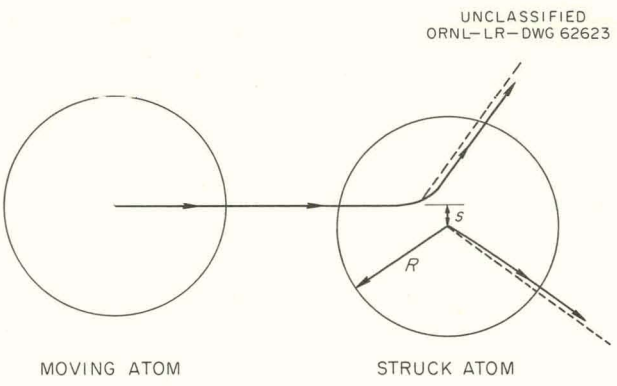

Fig. 1.1. Calculated Trajectories of a Primary and a Lattice Atom Colliding in a Screened Coulomb Potential Field. The dashed lines are the paths that would be traversed if the velocity of the primary atom did not change until reaching the turning point. The energy of the primary atom before collision was 12.4 kev, and the center-of-mass scattering angle is 107.8°.

but lattice directions are ignored. Thus, after leaving an encounter such as shown in Fig. 1.1, the moving atom is forced to enter into another collision with an atom located at the proper average distance from the atom just left in order to preserve the correct atomic density (note that this distance is not the closest interatomic spacing, since in some cases second-nearest or more distant neighbors might be struck). However, the direction of the second struck atom from the first is not correctly preserved as in the lattice, but is allowed to occur randomly. This is accomplished by choosing randomly the impact parameter for a given collision from a distribution given by:

$$P(s) = 2s/R^2 \qquad (0 \leqq s \leqq R)\ , \quad (1)$$

corresponding to picking points out of the area of a circle of radius R. At the same time, an azimuthal angle is randomly selected from a uniform distribution. This procedure has been found to be very acceptable by comparison with a calculation of the impact parameter distribution (using 100,000 samples) in a face-centered cubic lattice with an atomic site as the assumed starting position.

"Free Flight." – The lattice density is preserved by allowing a certain, extra free-flight length between every two collision points. This corresponds to the average distance traversed by the moving atom across the space not occupied

by the atomic spheres of influence. This is calculated from

$$\bar{l}_{FF} = 4V_E/S \,, \tag{2}$$

where

V_E = the unoccupied volume,

S = the surface area of the atomic spheres of influence bounding the unoccupied volume.

For example, for the fcc lattice

$$\bar{l}_{FF} = \left(\frac{4\sqrt{2}}{\pi} - \frac{4}{3}\right) R \,. \tag{3}$$

This same result may also be obtained by equating the average distance between collisions to a mean free path, as in ref 5,

$$\lambda = 1/n\pi R^2 \,, \tag{4}$$

where n is the atomic density. The correspondence between these two definitions of $\bar{l}_{FF}$ is quite general.

Distances Recorded. – The total path of the moving atom in space is represented as a series of connected straight-line segments in three dimensions. Thus the curved section of the trajectory shown in Fig. 1.1 is neglected, and the path is represented by the two asymptotes to the initial and final directions of the trajectory. In general, this approximation does not affect the position of the atom at the end of the history, but does make a small error in the total path length traversed. A further approximation is made in that the position of the asymptote intersection is not calculated precisely. The velocity change as the moving atom approaches the turning point is neglected; this method calculates the deflection angle correctly, but slightly misplaces the asymptotes of the trajectory. Again this approximation is acceptable for cases in which the curved portion of the path is limited to a small portion of the path inside the sphere of the struck atom. The position of the atom in space is followed through the calculation, so that at the end of the history the (x, y, z) coordinates of the atom are known with reference to the starting position of the moving atom and its initial direction, which is taken as the positive x axis. Figure 1.2 shows schematically how this is done. The distances shown can be calculated:

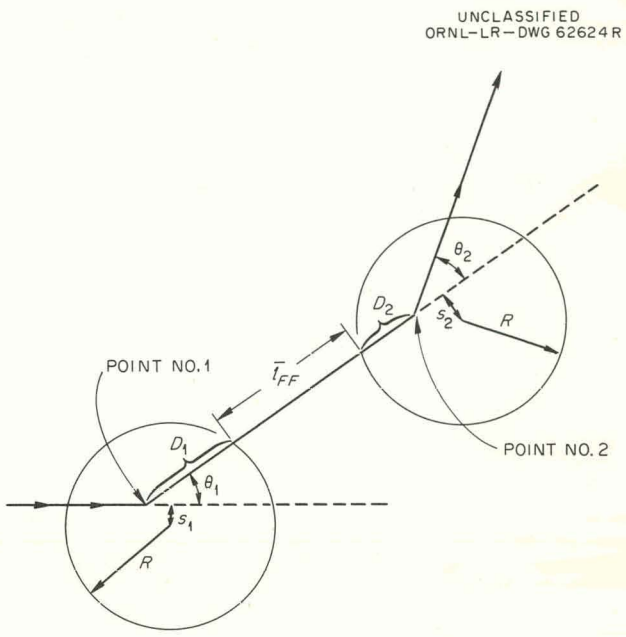

Fig. 1.2. Path Lengths Involved in the Range Calculations.

$D_1 \equiv$ the distance from the intersection of the asymptotes (in the laboratory system) to the surface of the atomic sphere and is calculable when the impact parameter s_1 has been chosen and the approximate trajectory in the laboratory system calculated.

$\bar{l}_{FF}$ is calculated from the appropriate formula [such as Eq. (3) above] and added to D_1.

$D_2 \equiv$ the distance from the surface of the second atomic sphere to the intersection point and is calculable when s_2 has been chosen.

Once θ_1 and an azimuthal angle are known, the direction cosines of the line segment $D_1 + \bar{l}_{FF} + D_2$ can be calculated from those of the preceding similar segment. Then if the total path traversed to date and the (x, y, z) coordinates are known for point number 1, the contributions to these from the segment $D_1 + \bar{l}_{FF} + D_2$ may be added in. The continuation of this process collision by collision finally gives the required quantities.

Insofar as distances are concerned, no information is reported at the end of a history as to the actual positions of the collision points, which would, in any case, not be very valuable in this randomized model.

Transferred Energy. – For a given potential, once the impact parameter is chosen, the deflection angle may be computed and, directly, the energy transferred to the struck atom. For each collision in a history this transferred energy is recorded.

Termination of a History. – The choice of an energy at which to terminate the history of a moving primary is, in general, very difficult. However, the saving feature of the range calculation is that the greater part of the distances traveled is accomplished at the early, high-energy portion of the history. To the extent that this is true, the details of the potential at lower energies and the precise energy of cutoff are not of first importance. For most cases in this work the cutoff energy has been taken as 25 ev. It should be noted that the history is terminated at any collision from which the moving atom emerges with an energy *below* 25 ev; for example, in the equal-mass case a 50,000-ev primary could suffer such a collision that its final energy is 1 ev, in which instance the history is terminated. The program also allows for the termination of a history when the primary "escapes" from the surface of the solid. This would allow for the treatment of sputtering, for example, but has not been often used to date. In fact, with realistic potentials, such as the screened Coulomb, the "forwardness" of the scattering leads to very small fractional escapes of the primary (less than 5%) from a surface imagined to be normal to the initial direction of motion of the primary and including the initial position of the primary.

Description of a Case and Final Distributions and Averages. – For most cases, to date, 1000 complete histories of primaries, all starting at the same initial energy, have been considered an adequate sample. A complete description of a single case (to which 1000 histories will be devoted) in this randomized model is given by the choice of:

1. a potential form for the interaction between the primary and the lattice atoms, with various subchoices of parameters for the potential,
2. a mass ratio, lattice atom to primary atom,
3. a radius, R,
4. an initial energy,
5. a final energy,
6. a free-flight length.

At the completion of 1000 histories, the following quantities are reported for a given case:

1. The distributions, on appropriate histograms, of:
   (a) final x-coordinate of the primary (the positive x-axis being the initial direction of motion),
   (b) final y-coordinate of the primary,
   (c) final z-coordinate of the primary,
   (d) total path traversed by the primary,
   (e) crow-flight distance from the starting point to the final position,
   (f) maximum crow-flight distance from the starting point achieved by the primary during its history,
   (g) number of collisions needed to slow the primary down over the selected energy range,
   (h) energies transferred to struck atoms along its path.
2. The following specific quantities and averages for all except the transferred energies:
   (a) average value,
   (b) average of the squares,
   (c) standard deviation,
   (d) largest value,
   (e) smallest value.

Potential. – For the most significant work done to date, the screened Coulomb or Bohr potential has been used; this may be expressed in the form:

$$V(r) = \frac{E_B}{2}\left(\frac{e^{-r/a_B}}{r/a_B}\right), \tag{5}$$

where

$$E_B = \frac{2Z_1 Z_2 e^2}{a_B}, \tag{6}$$

$$a_B = \frac{\alpha a_b}{(Z_1^{2/3} + Z_2^{2/3})^{1/2}}. \tag{7}$$

In the above equations, Z_1 and Z_2 are the atomic numbers of the primary and lattice atoms respectively; a_b is the radius of the first Bohr orbit in

hydrogen; and α is an adjustable parameter.[8] One other potential to which some attention has been devoted is the Thomas-Fermi-Firsov.[9]

Figures 1.3, 1.4, and 1.5 show some typical results for the ranges of primary copper, silver, and gold atoms in their respective lattices as a function of the initial primary energy. The various theoretical curves shown may be compared with the experimental points obtained by van Lint *et al.*,[10] which are shown in the figures with the extents of their probable errors. The quantity plotted as the range is not the same for the various theoretical curves: for the Monte Carlo calculations using the Bohr potential and the Bohr potential–hard-sphere approximation,[11] the curves shown are for the *average vector range*, that is, the average crow-flight distance from the starting point to the final position. This quantity may be shown to be the proper one to compare with the experimental data. The curves labeled "Nielsen" and "Davies and Sims" are, respectively, the total path traversed and the average distance parallel to the original direction of motion, but are the only comparable quantities obtainable from the calculations of Nielsen[12] and Davies and Sims.[13]

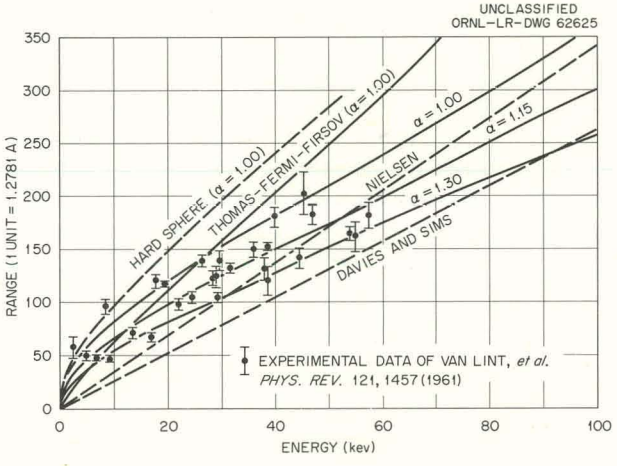

Fig. 1.3. Range of Cu^{62} in Copper.

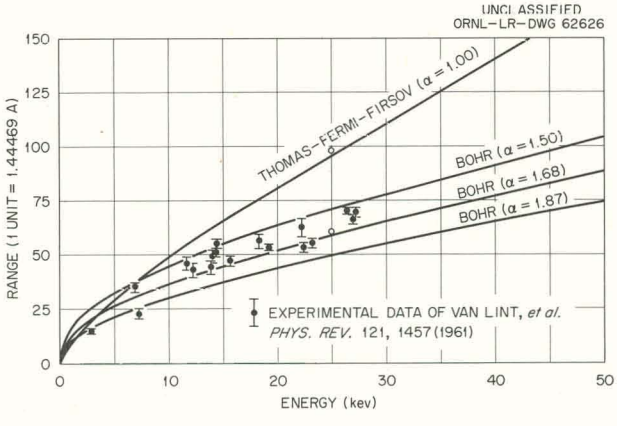

Fig. 1.4. Range of Ag^{106m} in Silver.

It is concluded from the results shown in Fig. 1.3 that a value of $\alpha = 1.15$ gives the best fit (for copper). For comparison, various values of α obtained by other authors (for copper) are:

	α_{Cu}
Present work	1.15
Bohr's original potential	1.00
Holmes and Leibfried[14] (using hard sphere and $\sqrt{\overline{r^2}}$)	2.00
Seitz and Koehler[15]	1.414
Brinkman[16]	2.96
van Lint *et al.*[10] (using method of ref 14)	1.7

The present result and that of van Lint *et al.*[10] are presumed to be the most accurate. The value of 1.7 is too high because of the use of the hard-sphere approximation and the $\sqrt{\overline{r^2}}$ as a measure

[8] For a more complete discussion of this potential see refs 5 and 7.

[9] O. B. Firsov, *J. Exptl. Theoret. Phys. (U.S.S.R.)* 33, 696 (1957); *Soviet Phys. JETP* 6, 534 (1958).

[10] V. A. J. van Lint, R. A. Schmitt, and C. S. Suffredini, *Phys. Rev.* 121, 1457 (1961).

[11] Note that $\sqrt{\overline{r^2}}$ was used in ref 5 for the hard-sphere approximation because $\overline{r}$ could not be easily calculated. The results shown were obtained by the Monte Carlo methods of the present calculation. The $\sqrt{\overline{r^2}}$ lies well above the $\overline{r}$ curve shown.

[12] K. O. Nielsen, in *Electromagnetically Enriched Isotopes and Mass Spectrometry*, Academic Press, New York, 1956.

[13] J. A. Davies and G. A. Sims, *Can. J. Chem.* 39, 601 (1961).

[14] D. K. Holmes and G. Leibfried, *J. Appl. Phys.* 31, 1046 (1960).

[15] F. Seitz and J. S. Koehler, "Displacement of Atoms During Irradiation," in *Solid State Physics*, vol 2, p 305, Academic Press, New York, 1956.

[16] J. A. Brinkman, *J. Appl. Phys.* 25, 961 (1954).

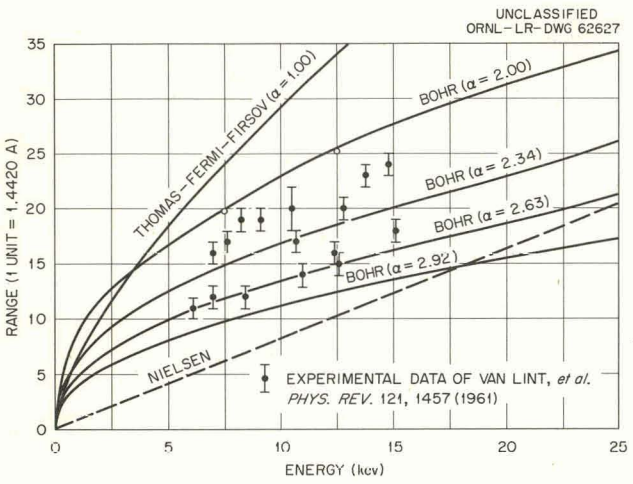

Fig. 1.5. Range of Au^{196} in Gold.

of the range, both of which tend to make the range too great, so that the screening parameter must be increased (i.e., α increased) to "spread out" the potential and reduce the range.

The range calculations of Figs. 1.4 and 1.5 for silver primaries in silver and gold primaries in gold show that the experimental data of van Lint *et al.*[10] may be fairly adequately fitted by choosing:

$$\alpha_{Ag} = 1.59 ; \quad \alpha_{Au} = 2.34 .$$

It should be noted that the experimental uncertainties alone make it impossible to specify a value of α to closer than 10–15%. The very large value of α required for gold is somewhat surprising and rather unfortunate for the method used here. This high value results from the very low experimental value for the range in gold and leads to quite large values of the interatomic potential at and beyond the radius R, so that the approximate method of calculation used here may not give the desired accuracy.

It is believed that the fault in this matter lies with the choice of the potential form, and the extension of this work will include an investigation of other potential forms. Already the Thomas-Fermi-Firsov potential[9] has been used (note curves in Figs. 1.3, 1.4, and 1.5), but again it is concluded that the value of the potential at the cutoff radius is too high to be realistic. A suggested potential is the sum of a simple exponential (Born-Mayer) and a screened Coulomb (Bohr) which gives enough adjustable parameters so that it is possible to represent the true potential well over the entire range of energies of interest.

The hard-sphere approximation remains of interest since, as may be seen in Fig. 1.3, the energy dependence is of the correct form, but the range is everywhere too great. This indicates that the criterion for choosing the hard-sphere radius[14] leads to too small a value of the radius. Simple improvements of this criterion should be explored.

In conclusion, it is now proposed to try these same calculations and extensions with an improved model in which the randomizing assumption is dropped and a more realistic model of the lattice of the solid is used. By allowing the moving atom to collide with lattice atoms placed at their correct lattice positions, it will be possible to eliminate the somewhat unsatisfactory treatment involving the addition of the free-flight length.

2. ELECTRON CROSS SECTIONS FOR ATOMIC DISPLACEMENTS

O. S. Oen

A calculational program has recently been undertaken for theoretically computing the number of atomic displacements in solids produced by irradiation with fast electrons. These calculations are planned for a large variety of substances extending over a large range of electron and displacement-threshold energies and thus will supplement the rather limited number of theoretical calculations reported in the literature.[1]

The work is being done with the aid of an IBM 7090 computer. Results to date have been found for the primary displacement cross sections in carbon, aluminum, and copper for electron energies ranging from threshold up to 10 Mev, using sharp atomic displacement thresholds from 5 to 50 ev. For light elements the primary displacement cross sections are evaluated directly from the McKinley-Feshbach version of the Mott-Rutherford equation.[2] However, for heavy elements the McKinley-Feshbach equation is no longer accurate, and it becomes necessary to evaluate numerically the Mott series to determine the cross sections.[3] In addition, to evaluate the total displacement cross section it is necessary to use a model to calculate the additional atoms which may be displaced in the cascade initiated by the primary displaced atom.

[1] W. D. Compton and G. W. Arnold, *J. Appl. Phys.* 31, 621 (1960).

[2] F. Seitz and J. S. Koehler, p 305 in *Solid State Physics*, vol 2, ed. by F. Seitz and D. Turnbull, Academic Press, New York, 1956.

[3] J. A. Dogget and L. V. Spencer, *Phys. Rev.* 103, 1597 (1956).

3. ELECTRON TRANSPORT IN A MAGNETIC FIELD

J. H. Barrett

By use of a method outlined previously,[1] the transport properties of electrons in a strong magnetic field can be calculated. It is convenient to define a six-component electrical and thermal current. Let J_1, J_2, and J_3 denote the x, y, and z components of the electrical current and J_4, J_5, and J_6 denote the x, y, and z components of the thermal current. A similar six-component electrical and thermal gradient may also be defined; call this F. The currents may be expressed as functions of the gradients by

$$J_i = \Sigma_j L_{ij} F_j \, .$$

The current and gradient components may be classified as longitudinal or transverse to the magnetic field. For free electrons the transverse components of the current will depend only on the transverse components of the gradient. Attention will be concentrated on the transverse effects. The transverse components of the current may be further classified as transverse or longitudinal with respect to an applied gradient. Let the magnetic field be in the z direction; i and j will then be restricted to the values 1, 2, 4, and 5. Let the electric field E and the thermal gradient $(-\nabla T/T)$ be in the y direction.

The components of the current will be given by

$$J_i = q \left\langle V_i \right\rangle \qquad (i = 1, 2) \, ,$$

$$J_i = \left\langle \tfrac{1}{2}[(H - \zeta)\, V_i + V_i (H - \zeta)] \right\rangle \qquad (i = 4, 5) \, ,$$

where

q = charge,

H = Hamiltonian operator,

ζ = Fermi level,

V_i = component of the velocity operator.

[1] J. H. Barrett, *Solid State Div. Ann. Progr. Rept. Aug. 31, 1960*, ORNL-3017, p 8.

The expectation value of any operator can be computed by taking the trace of the product of the operator with the density matrix. The important elements of the density matrix are certain off-diagonal elements that have correlated terms as well as uncorrelated terms.[1] These correlated terms contain a factor $\partial f/\partial y_0$. If it is assumed that the occupation probability of the states is still given by the Fermi function even in the presence of electrical and thermal gradients, then

$$\frac{\partial f}{\partial y_0} = \left[qE - (\epsilon - \zeta)\frac{1}{T}\frac{\partial T}{\partial y} \right]\frac{\partial f}{\partial \epsilon},$$

where ϵ is the energy of the state.

Relatively simple expressions can be calculated for the L_{ij} under certain limiting conditions. These are: $kT \ll \zeta$, $\hbar\omega_c \ll \zeta$, $\gamma \ll \omega_c$, where ω_c is the cyclotron angular frequency and γ is the transition probability for zero magnetic field. The purely electrical coefficients, L_{11} and L_{12}, obtained are the same as those found by Argyres[2] and agree with the results obtained in the weak-magnetic-field limit. Among the other coefficients the transverse-longitudinal ones, L_{25} and L_{55}, also agree with the weak-field results, while the transverse-transverse ones, L_{15} and L_{45}, do not. The coefficients all obey the Onsager reciprocal relations: $L_{ij}(H) = L_{ji}(-H)$. Each coefficient is made up of a monotonic term and an oscillatory term. The oscillatory term is observable only for strong magnetic fields and low temperatures. The most interesting result is the relatively large oscillatory part that occurs for the electrothermal coefficients L_{15} and L_{25}. This can be illustrated by writing out the expressions for L_{22} and L_{25}:

$$L_{22} = \frac{nq}{m}\frac{\gamma}{\omega_c^2+\gamma^2}\left[1 + \frac{5\sqrt{2}}{4}\left(\frac{\hbar\omega_c}{\zeta}\right)^{1/2}\sum_{\nu=1}^{\infty}\frac{(-1)^\nu}{\sqrt{\nu}}A_1\left(\frac{2\pi^2\nu kT}{\hbar\omega_c}\right)\cos\left(\frac{2\pi\nu\zeta}{\hbar\omega_c} - \frac{\pi}{4}\right)\right],$$

$$L_{25} = \frac{nq}{m}\frac{2\pi^2}{3}\frac{(kT)^2}{\zeta}\left[1 + \frac{15\sqrt{2}}{8\pi}\left(\frac{\hbar\omega_c}{\zeta}\right)^{1/2}\left(\frac{\zeta}{kT}\right)\sum_{\nu=1}^{\infty}\frac{(-1)^\nu}{\sqrt{\nu}}A_2\left(\frac{2\pi^2\nu kT}{\hbar\omega_c}\right)\cos\left(\frac{2\pi\nu\zeta}{\hbar\omega_c} + \frac{\pi}{4}\right)\right],$$

where

$A_1(x) = x \operatorname{csch} x$,

$A_2(x) = [(x \coth x) - 1] \operatorname{csch} x$,

n = number of electrons,

m = mass of the electrons.

The functions A_1 and A_2 have similar behavior except for extremely strong magnetic fields. Hence the terms in brackets will have similar behavior except for the presence of the factor (ζ/kT) before the summation sign in L_{25}. At a temperature of 2°K this factor will be about 50, even for a Fermi energy as small as 0.01 ev. Therefore the electrothermal effects will be almost purely oscillatory functions of magnetic field in the strong-field low-temperature limit. This agrees with experimental observations of the Seebeck and Ettingshausen-Nernst effects.[3]

[2] P. N. Argyres, *Phys. Rev.* 117, 315 (1960).

[3] C. J. Bergeron, C. G. Grenier, and J. M. Reynolds, *Phys. Rev.* 119, 925 (1960).

THIS PAGE

WAS INTENTIONALLY

LEFT BLANK

Part II

METALS AND ALLOYS

PAGES 13 to 14

WERE INTENTIONALLY

LEFT BLANK

5. LOW-TEMPERATURE IRRADIATION STUDIES

R. R. Coltman T. H. Blewitt[1]
C. E. Klabunde J. K. Redman D. L. McDonald[2]

ANNEALING STUDIES OF VARIOUS NEUTRON-IRRADIATED METALS

Investigations of the general character of radiation damage in metals have continued. These studies are carried out by measurement of changes in residual resistivity during neutron bombardment near 4°K followed by isochronal annealing, during which recovery of the damage is observed.

Tungsten and Molybdenum

Tungsten and molybdenum, which are usually thought of as "high-temperature" metals, are of particular interest. Figure 5.1 shows the isochronal annealing behavior of these metals after neutron bombardment at 4.2°K. Each specimen was prepared from high-purity Johnson-Mathey stock and given a 3-hr anneal at 1000°C in a hard vacuum. The main annealing peak seen in molybdenum occurs at about the same temperature as that found in copper. Tungsten shows an ill-defined or continuous-type annealing similar to that found in gold. This similarity between these two heavy elements is inconsistent with results obtained for platinum (ref 3), which shows a large annealing peak at 20°K.

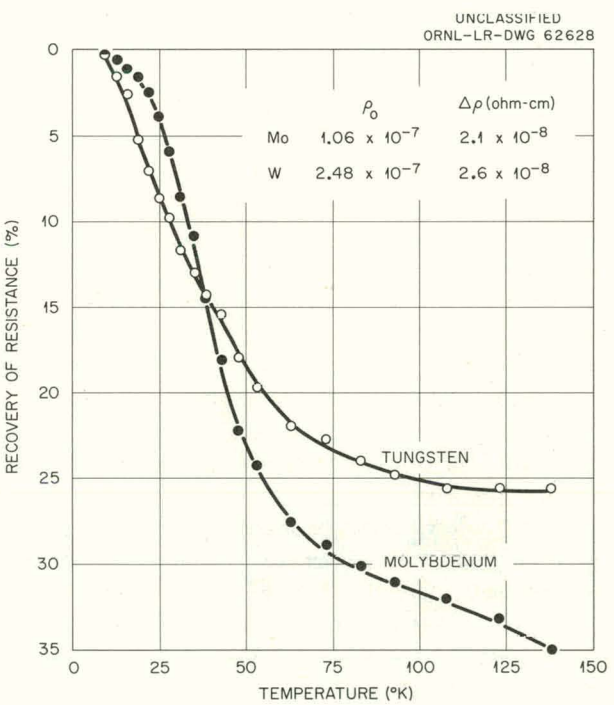

Fig. 5.1. Isochronal Annealing of Molybdenum and Tungsten. Bombardment temperature, 4.2°K; flux, 4×10^{17} *nvt*; 3-min pulses.

Niobium, Lead, and Tin

Similar studies were made on high-purity specimens of the elements Nb, Pb, and Sn. Since this bombardment was made at 4.5°K, Nb and Pb were in the superconducting state, while Sn was normal. Residual resistance measurements of Nb and Pb were made before and after bombardment and after each isochronal pulse by elevating the temperature of the specimens to just above the critical temperature of each element. Isochronal annealing results for these materials are shown in Fig. 5.2. Scatter in the data of Nb and Pb is due to the rather large temperature coefficient of resistance of these materials which persists even near the critical temperature. As a result, the detailed annealing character of these materials is not apparent, although no large peak is evident below 75°K such as is found in Cu, Ag, Al, Pt, and Ni. In the case of Sn, two successive bombardments were made on the same specimen. Additional data obtained from run 1 but not shown in Fig. 5.2 reveal 96% recovery at 300°K. The enhanced recovery of run 2 over run 1 is not understood.

Sodium

Radiation damage studies of sodium are of interest with respect to developmental work and the fundamental aspects of understanding the defect structures of a relatively simple metal. Since sodium exhibits a small magnetoresistance and can be refined to a high purity with low residual resistivity, it seems attractive for use in

---

[1] Now at Argonne National Laboratory, Argonne, Illinois.

[2] Guest scientist from Australian Atomic Energy Commission.

[3] R. R. Coltman *et al.*, *Solid State Div. Ann. Progr. Rept. Aug. 31, 1959*, ORNL-2829, p 72.

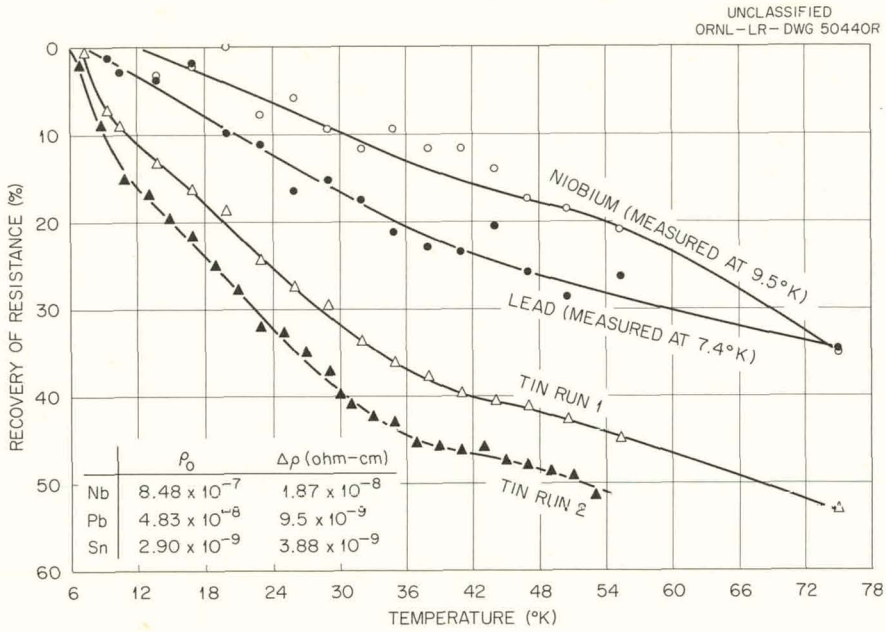

Fig. 5.2. Isochronal Annealing of Niobium, Lead, and Tin. Bombardment temperature, 4.6°K; flux, 3×10^{17} *nvt*; 3-min pulses.

high-flux electromagnets operating at low temperatures (~10°K). This approach relies on the fact that at low temperatures the thermal portion of electrical resistivity is absent and that relatively high fields can be obtained with modest power requirements. In application to thermonuclear devices, where magnet windings are subjected to irradiation, damage effects may be quite important.

A sodium sample was prepared by casting it under vacuum in a 1½-in.-long stainless steel tube with a ⅛-in. OD and a 0.004-in. wall.[4] Copper current and potential probes were silver-soldered through the wall of the tube before casting. A residual resistivity measurement of the sample at 4.2°K before bombardment gave a value of 8×10^{-8} ohm-cm, corresponding to a resistance ratio of about 60. Since ratios as high as 5000 have been obtained for sodium, it is believed that the impurity content of this specimen was high. The specimen was irradiated at 4.8°K to a flux of 4×10^{17} *nvt*. The damage rate showed a slight saturation effect, suggesting the possibility of radiation annealing. Following bombardment, isochronal annealing studies were made, and the results are shown in Fig. 5.3. Since the initial resistivity was 8×10^{-8} ohm-cm, it can be seen that complete recovery is reached at 125°K. Sodium shows considerable annealing at low temperatures, in that 4.2% of the damage was recovered after a 3-min pulse at 5.1°K. The damage rate of sodium, which is about four times that of copper, suggests that before using this material for low-temperature electromagnets, serious consideration must be given to the amount of irradiation to which they will be subjected. Undoubtedly, shielding would be necessary to maintain the desirable electrical qualities of unirradiated sodium.

As seen in Fig. 5.3, an interesting anomaly occurs in the range 125 to 225°K, where the resistivity drops well below its preirradiation value. Since virtually all of the damage has recovered below this temperature range, it is believed that the effect is independent of the bombardment. A later test on a similar but unirradiated specimen verified this. The reason for this behavior is not clear at this time. Since sodium is known to undergo a phase transformation (body-centered cubic to hexagonal close packed) near 40°K, it may be that alteration of this transformation is brought about by thermal stress or impurity content.

[4]The group is indebted to E. E. Hoffman of the Metallurgy Division for casting the sodium samples.

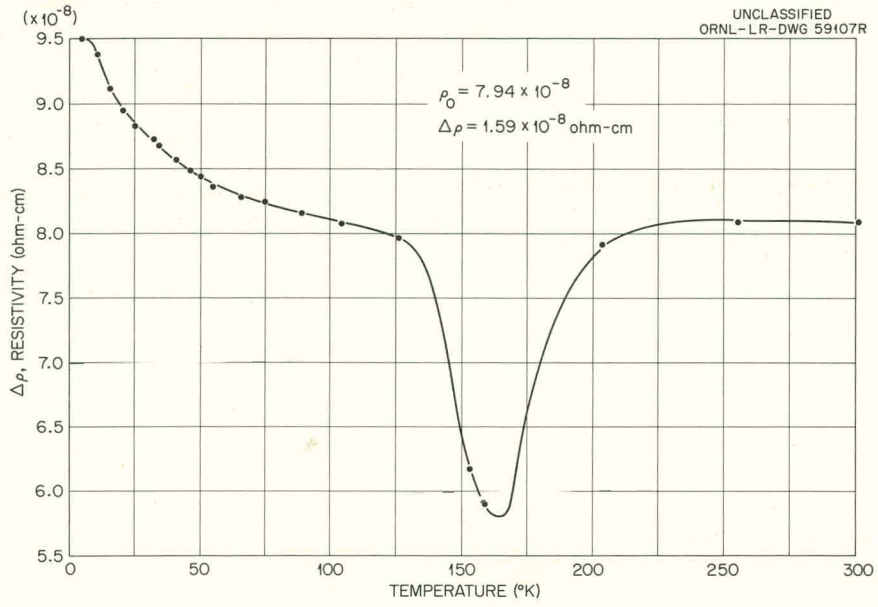

Fig. 5.3. Isochronal Annealing of Sodium. Bombardment temperature, 4.8°K; flux, 4×10^{17} *nvt*; 3-min pulses.

Pyrolytic Graphite

The resistance damage rate and the annealing of pyrolytic graphite were again studied in greater detail to pin down earlier suspicions about current carrier changes. Two conclusions were reached:

1. The rapid bend-over of the damage-rate curve, which cannot reasonably be ascribed to saturation or overlap effects at this low flux dose, can be well described in terms of carrier concentration increase with dose. Figure 5.4 shows how well the data can be fitted by a curve derived by assuming simultaneous increase in resistive scattering centers ($C\alpha\phi$) and current carrier concentration ($n_0 K\alpha\phi$). The carrier concentration increase during a 160-hr (4×10^{17} *nvt*) bombardment was found to be 90% of the original concentration.

2. The resistance rise found on subsequent anneals around 100 to 180°K cannot be ascribed to a *decrease* in carrier concentration. Otherwise, a higher damage rate should be observed upon continuation of the bombardment. Actually, as shown in Fig. 5.4, after pulse annealing to 138°K and continuing bombardment, the subsequent points may be transposed down to match very well with the original curve. If anything, a slight decrease in slope is noted, corresponding to a carrier concentration *increase* (as much as 30%). This means that the anomalous increase in resistance upon annealing must be due to some rearrangement of the irradiation-produced scattering centers, making them more effective scatterers (rather than less effective as is the usual case). This is in line with the suggestion of Hennig and Hove at the 1955 Geneva Conference that a declustering of interstitials away from the original damage regions occurs, yielding more effective carrier scattering.

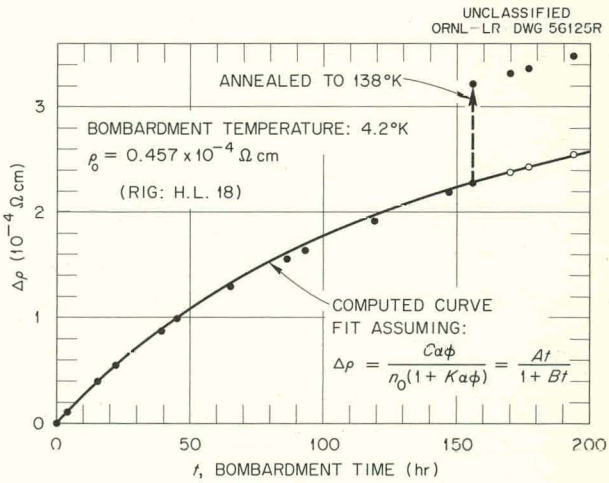

Fig. 5.4. Pyrolytic-Graphite Damage-Rate Curve.

STORED ENERGY IN IRRADIATED B^{10}-DOPED COPPER

Studies of B^{10} fission damage in copper described earlier[5] have been extended to include the measurement of stored energy after low-temperature irradiation. An 8.5-g copper specimen doped with 0.1 at. % B^{10} was prepared as shown in Fig. 5.5. With this arrangement both resistivity and stored energy could be measured on the same specimen. The assembly shown in Fig. 5.5 was then placed in a thin-walled copper can, and all leads were brought up through thin-walled stainless steel tubing and out through a vacuum-tight seal. The use of Lavite spacers and small-diameter lead wires served to allow good thermal isolation of the specimen from its housing. Before bombardment the can and its lead tube were thoroughly evacuated and then filled with hydrogen to a pressure of 5 mm and sealed. A small amount of helium exchange gas ($\sim 25\,\mu$) was introduced into the sample chamber of the liquid-helium cryostat prior to bombardment. At full reactor power this exchange gas maintained the specimen can at about 13°K. At this temperature the vapor pressure of the hydrogen in the can was capable of removing the gamma heat generated in the specimen and maintaining its temperature at about 23°K. After bombardment and with the reactor operating at $\frac{1}{3}$ full power, additional helium was introduced into the sample chamber, lowering the can temperature to 4.2°K. At this temperature the hydrogen vapor pressure in the can was reduced to less than 10^{-7} mm. With the specimen now isolated and absorbing the gamma heat input, temperature-time data from the ensuing warmup curve were recorded. After the first warmup run, during which the stored energy was released, two additional runs were made for comparison. Slopes of the warmup curves plotted as a function of temperature are shown in Fig. 5.6. Since the specific heat $C_p = \gamma \Delta t / \Delta T$, where γ is the gamma heating value during warmup (this was determined by using known specific-heat data applied to the early part of the warmup curve before any stored energy was released), a plot of C_p vs T can be made. This result is seen in Fig. 5.7. The shaded area between the curves, then, represents the stored-energy release. The resistivity recovery associated with the stored-energy release was measured on the same specimen after a second bombardment followed by an anneal to the same maximum temperature of 51°K. The stored energy released after bombardment was 4.73 cal/mole. If we assume that the recovery occurs by the annihilation of Frenkel pairs and that the formation energy of a pair is 3 ev, then the damage concentration was

$$\frac{4.73}{3 \times 2.3 \times 10^4} \times 100 = 0.0068 \text{ at. \%} .$$

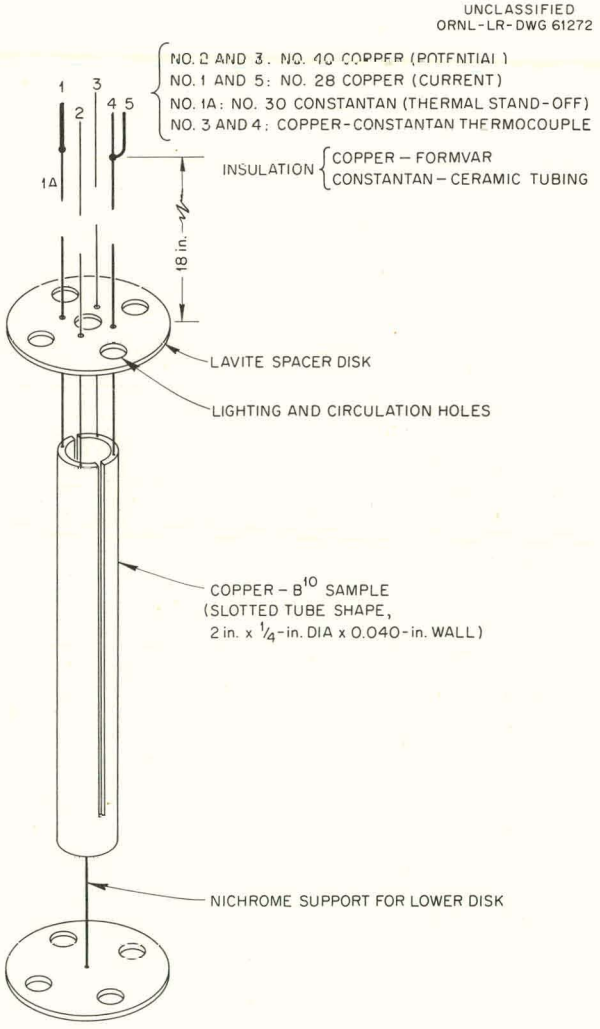

Fig. 5.5. Stored-Energy Rig for B^{10} Fission Damage in Copper.

[5] T. H. Blewitt *et al.*, *Solid State Div. Ann. Progr. Rept. Aug. 31, 1960*, ORNL-3017, p 21.

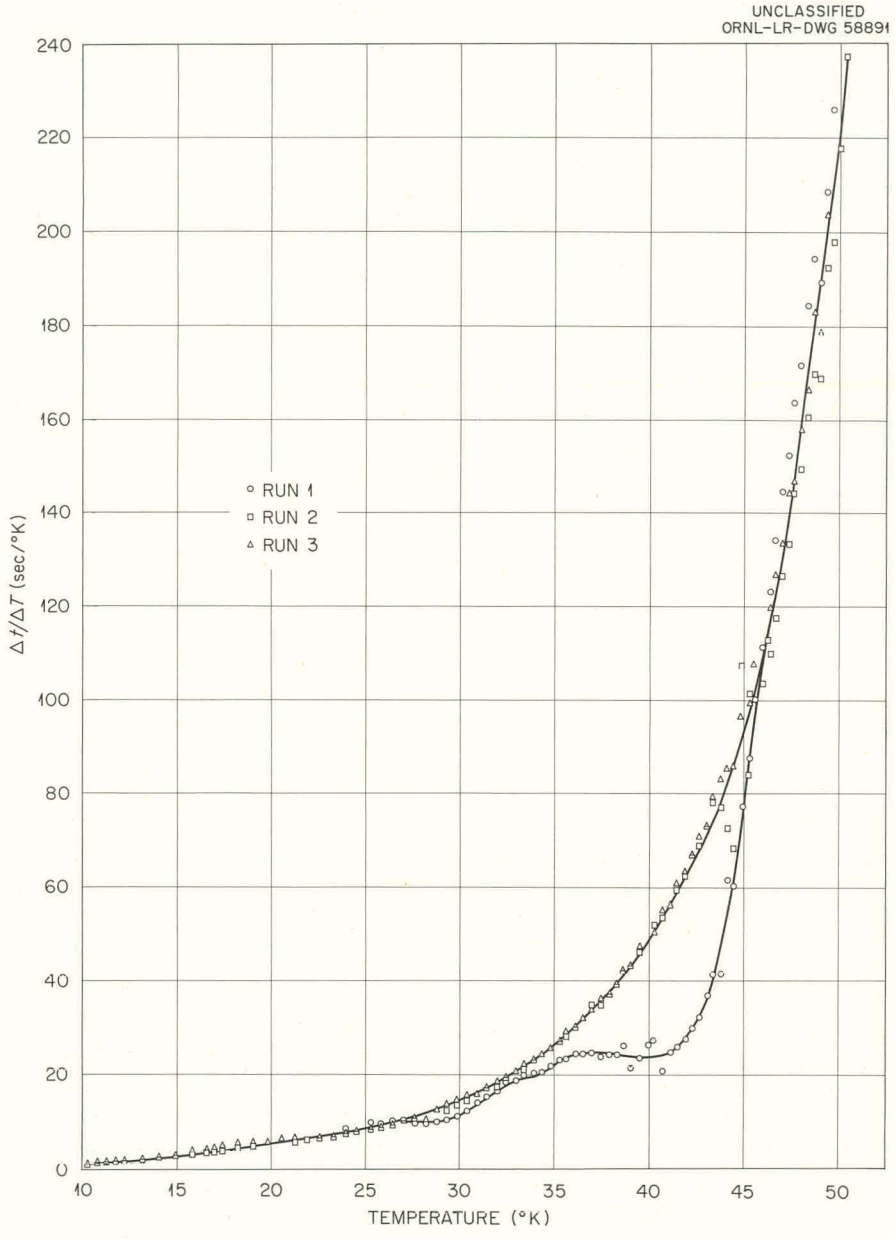

Fig. 5.6. Stored Energy Released in Irradiated Copper.

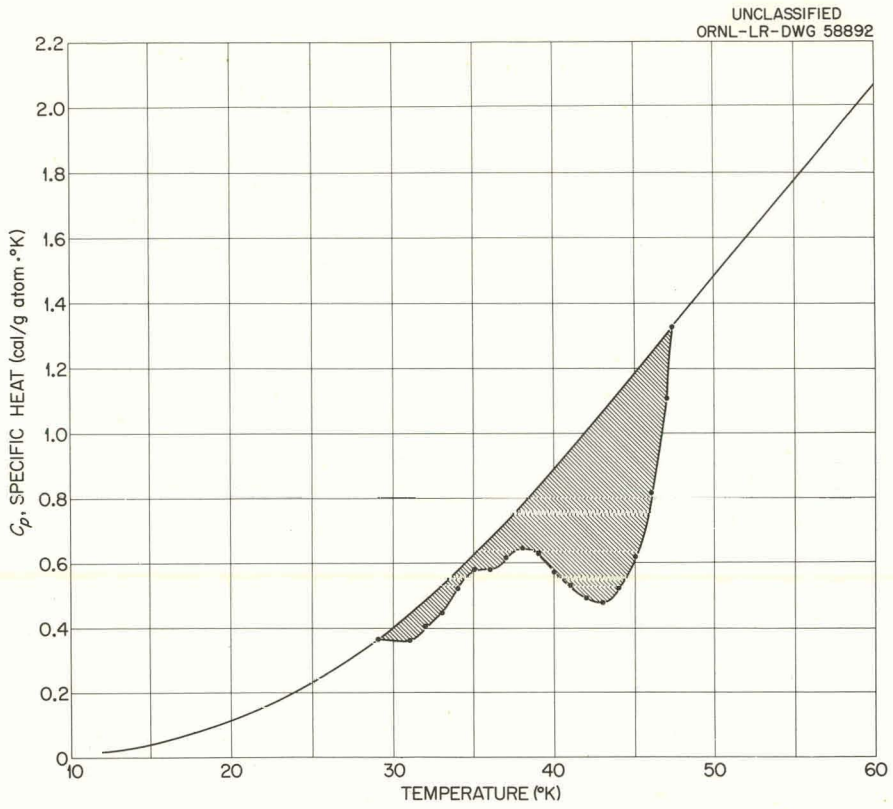

Fig. 5.7. Stored Energy Released in B^{10}-Doped Irradiated Copper.

The resistivity change associated with this recovery was 1.55×10^{-8} ohm-cm, which gives a value of 2.3×10^{-6} ohm-cm per at. % of Frenkel pairs.

LENGTH CHANGES IN IRRADIATED B^{10}-DOPED COPPER

Length-change measurements in irradiated U^{235}-doped copper and aluminum reported earlier[5] have been extended to include observations of B^{10} fission damage in copper. The principle of the bimetallic strip[5] was again employed, with one of the elements being pure copper and the other being copper with 0.1 at. % B^{10}. Based on previous resistivity changes observed in B^{10}-doped copper, the expected deflection of the strip under irradiation was only about 10% of that found for U^{235} fission damage. Therefore, a very small differential transformer and the associated detection circuits were constructed. The sensitivity of this device was better than 1% of the total radiation-induced length change but was ultimately limited by spurious vibrations. A 0.1 at. % B^{10}-doped copper resistivity specimen was also bombarded in the same rig, so that the damage rate and subsequent recovery of these two properties could be observed simultaneously. Three bombardments (one at half the flux of the other two), each followed by detailed isochronal annealing runs, were made on the same set of specimens. The bombardment temperature during each run was about 4.7°K. The results of isochronal annealing of both property changes are plotted in Fig. 5.8. Lower temperature pulses correspond to points in the upper right corner, and higher temperature pulses (up to 300°K) correspond to points nearer the origin. It is believed that some general conclusions concerning the annealing processes over this wide temperature range can be made from the results shown in Fig. 5.8.

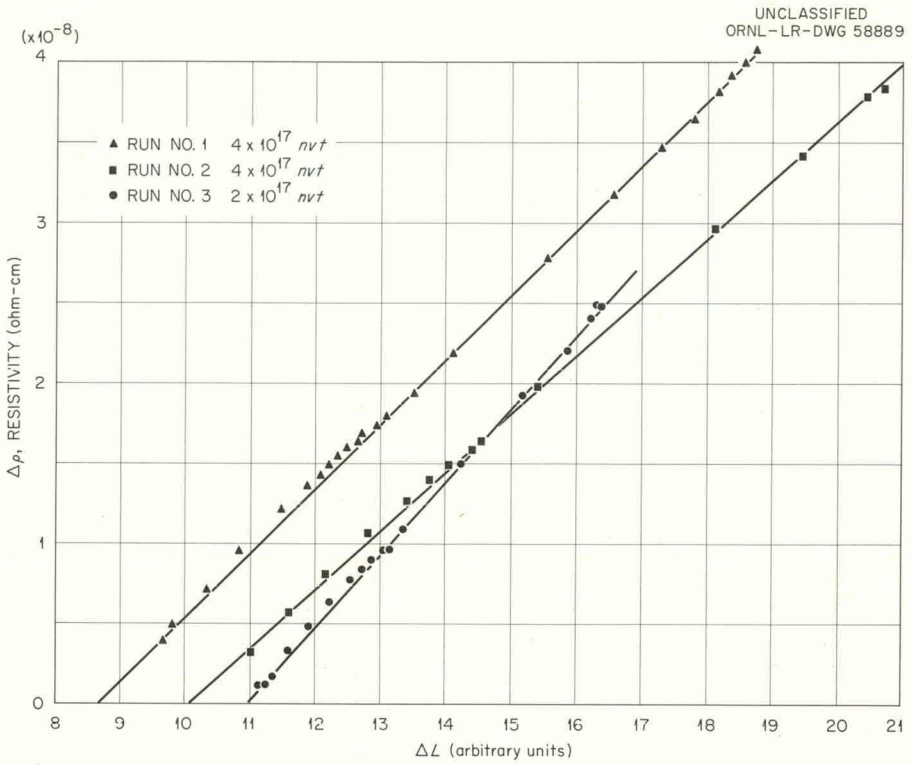

Fig. 5.8. Recovery of the Resistivity and Length Change in B^{10}-Doped Irradiated Copper.

Using specific quantities we can write the contribution to resistivity and volume change as follows:

$$\rho = n_i \rho_i + n_v \rho_v \ ,$$

$$\Delta V = n_i V_i + n_v V_v \ ,$$

where

ρ = resistivity,

ΔV = volume change due to the damage,

n_i, n_v = concentrations of interstitials and vacancies,

ρ_i, ρ_v = resistivities of interstitials and vacancies,

V_i, V_v = atomic volumes of interstitials and vacancies.

Consider now the ratio of $\rho/\Delta V = m$:

$$m = \frac{n_i \rho_i + n_v \rho_v}{n_i V_i + n_v V_v} \ . \qquad (1)$$

If we consider the annealing process of vacancy-interstitial pair annihilation, n_i is always equal to n_v, and there is a linear relationship between the recovery of these two properties. If we now impose the restriction (which physically is unlikely) that

$$\frac{\rho_i}{V_i} = \frac{\rho_v}{V_v} \qquad (2)$$

and substitute Eq. (2) into (1), we find

$$m = \frac{\rho_i}{V_i} = \frac{\rho_v}{V_v} \ . \qquad (3)$$

Since Eq. (3) is independent of the number of either kind of defect, one would obtain a linear relationship between the recovery of these properties throughout all temperature ranges regardless of the character of the annealing processes. A linear relationship between the recovery of these properties, then, implies either

that the entire recovery process is pair annihilation [the restriction imposed by Eq. (2) is not required here] or that the restriction of Eq. (2) must describe the character of the defects. If one cannot obtain a linear relationship between the recovery of these properties over a wide temperature range, then it must be concluded that the restriction expressed in Eq. (2) is impossible. Further, if a linear relationship is established over some lower temperature range and then deviates at higher temperatures, it must be concluded that the annealing processes in the two temperature ranges are different. In addition, it would seem reasonable in this case to suppose that the low-temperature annealing process is pair annihilation, for Eq. (1) indicates that either $n_i = n_v$ (pair annihilation) or that a constant relationship exists between them throughout the low-temperature annealing. The latter argument does not seem likely, since n_i undoubtedly is equal to n_v at the start of the annealing.

In Fig. 5.8 one can see deviations from linearity, suggesting that the above description might apply to this experiment. As the temperature was increased, the deviation from linearity was first noted at about 60°K, and return to the initial linear relationship occurs at about 300°K. If one assumes that the new annealing process starting near 60°K (indicated by the onset of the deviation from linearity) is the migration of interstitials to sinks other than vacancies, then it can be shown from the observed slope change that $\rho_i/V_i < \rho_v/V_v$. The analysis is also consistent with the idea that vacancy annealing occurs at the higher temperatures, where a change in slope occurs in the opposite direction.

HELIUM REFRIGERATOR MODIFICATIONS

During the past year the group has continued to make improvements upon the helium refrigerator system[6,7] used to perform the experiments described in this chapter. The addition of a new first-stage compressor (184 cfm displacement) has increased the mass flow and therefore the heat capacity of the main refrigerator system. Of greater significance is the reduced engine discharge pressure (now 8 psig) of the main refrigerator made possible by this addition. Since this pressure is below the critical pressure of helium, a standard liquefaction circuit may be incorporated which would provide an estimated heat capacity of 40 w at 4.7°K. The present heat capacity is about 5 w. This will permit the use of a cryostat with a considerably larger sample chamber and more massive experiments. Construction of the heat exchanger circuits for this higher-capacity liquefier is in progress. A heavy-duty vacuum pump (60 cfm displacement) has been installed in the suction side of the present helium liquefier circuit. With this change a bombardment temperature of 3.0°K has been reached at full reactor power. A helium gas cryostat has been constructed and attached to the helium test refrigerator operated by the group. This cryostat, which operates similarly to the main refrigerator of the irradiation facility, will be used to carry out general studies on metals from 15 to 300°K.

TWINNING IN SILVER

T. H. Blewitt[8] M. C. Wittels
J. K. Redman F. A. Sherrill

Experiments have been conducted on the tensile deformation of twinning in silver. Samples were deformed at 4.2, 77, and 300°K. The results are summarized below.

The stress required for twinning in silver is orientation-dependent, with a minimum resolved stress of 3.5 kg/mm^2 being observed with a tensile axis near the [111] direction, and a maximum of 9 kg/mm^2 with a tensile axis near the [113] direction. (The quoted values were measured at 4.2°K.)

The twinning stress monotonically increases as the tensile axis slides from the [111] to the [113] axis. There is no evidence that twinning can occur at an orientation between [113] and [100].

The twinning stress is greater at room temperature (about a factor of 2) than at 4.2°K. Room-temperature twinning was only observed with orientation near [111].

[6] R. R. Coltman *et al.*, *Solid State Div. Ann. Progr. Rept. Aug. 31, 1960*, ORNL-3017, p 31.

[7] J. T. Howe, R. R. Coltman, and T. H. Blewitt, "Liquid Helium Temperatures in an Atomic Reactor," *Proc. Cryogenic Eng. Conf., 3rd, 1957*, p 173 (1958).

[8] Now at Argonne National Laboratory, Argonne, Illinois.

High-speed photography (1000 frames/sec) has established that twin sections of millimeter thickness have formed in a time interval less than a millisecond.

When the tensile orientation is near [113] the sample twins and then detwins, so that tensile elongations of 400% have been observed. (Only about 150% elongation is usually observed.)

Some evidence for detwinning is also observed from x-ray studies. The twin is not homogeneous, since both parent and twin x-ray reflections are observed in equal amounts in the macroscopic twin. From geometrical considerations it is apparent that some of the parent reflections arise from detwinning and part from the original parent crystal.

The important conclusion from this work is that the orientation dependence of the flow stress and time for the formation make it difficult to explain the twinning in terms of a twinning dislocation pole mechanism. On the other hand, the temperature dependence and the detwinning events point toward a mechanism where the twins are formed by the separation of partial dislocations.

6. QUENCHING STUDIES IN COPPER

S. T. Sekula T. H. Blewitt[1]

Experiments on the quenching and annealing of lattice defects in copper have been undertaken in hopes that such information may prove useful in the interpretation of radiation damage phenomena.

The experimental technique is essentially one of electrically heating a length of copper wire approximately 4 cm long and 0.01 cm in diameter in a helium refrigerator. Prior to heating, the sample is maintained at a temperature of 15°K in helium exchange gas at a pressure of 400 mm Hg. Refrigeration is maintained during the heating of the sample, and the sample is quenched by merely cutting off the heating current. The reasons for heating the sample in the cold chamber are as follows: (1) The cold walls of the cryostat accelerate the quenching process. (2) The cryostat walls act as an efficient oxygen getter, thereby preventing internal oxidation of the sample with concomitant spurious changes in the electrical resistivity. (3) Measurements of the defect-induced changes in resistivity are most sensitive at low temperatures, where the thermal contribution to resistivity is the least.

The temperature of the sample during the heat treatment is obtained by using the sample itself as a resistance thermometer. The quenching rate is observed on an oscilloscope which records the voltage drop induced by a small constant current after the heating current has been cut off. Quenching rates thus determined are of the order of 8×10^3 °C/sec.

Preliminary results yield an energy of formation of vacancies in copper of 0.9 ev, in rough agreement with Airoldi *et al.*[2] If the experimentally determined self-diffusion energy of copper (2.05 ± 0.15 ev, ref 3) is combined with the above value, one infers an energy of migration of vacancies of approximately 1 ev.

Work is now in progress to obtain a more accurate value for the formation energy as well as to study the kinetics of the motion of quenched-in vacancies to obtain an independent determination of the migration energy of vacancies.

[1] Now at Argonne National Laboratory, Argonne, Illinois.

[2] G. Airoldi, G. L. Bacchella, and E. Germagnoli, *Phys. Rev. Letters* **2**, 145 (1959).

[3] A. Kuper *et al.*, *Phys. Rev.* **96**, 1224 (1954).

7. DISLOCATION INTERACTIONS

TEMPERATURE DEPENDENCE FROM 250 TO 370°K OF DISLOCATION PINNING IN COPPER SINGLE CRYSTALS BY RADIATION DEFECTS

D. O. Thompson V. K. Paré

It was first shown by Thompson and Holmes[1] that small doses of fast-neutron irradiation reduce markedly the internal friction and modulus effects due to dislocation motion in copper single crystals. They were able to interpret their results quantitatively in terms of the vibrating-string model[2,3] of dislocation motion, assuming that the irradiation introduces additional pinning points (presumably point defects) along the dislocation lines.

Subsequently, a survey[4,5] was made of the temperature dependence of the pinning process, using as irradiation facilities Hole 17-N of the ORNL Graphite Reactor for the range 100 to 350°K and the Hole 12 cryostat for a measurement at 20°K. It was found that the pinning rate under continuous irradiation increases very strongly with temperature, the rate at 350°K being more than 1000 times that at 20°K. These results indicate that in copper, at any temperature above 20°K, the pinning process depends on thermally activated migration of defects to the dislocation lines. Thus internal friction measurements can be used to study this migration, to the exclusion of other annealing processes such as recombination of close Frenkel pairs.

Early in the year a new shielded cryostat irradiation facility was placed in operation at Beam Hole HB-2 of the ORR, and the electronic equipment was modified so as to make data recording and sample-temperature regulation fully automatic. As in the earlier version of the apparatus,[6] the sample is maintained in continuous oscillation at its resonant frequency of about 15 kc, as part of a closed feedback loop. At the location of the sample, in the exterior beam hole shield, the neutron flux above 0.75 Mev is in the range 1×10^8 to 2×10^8 neutrons cm^{-2} sec^{-1}. The beam hole is equipped with a 24-in.-thick steel shutter by means of which the beam can be turned on or off within a few seconds.

The new facility was first used for a detailed study of dislocation pinning in the vicinity of room temperature. To eliminate the effects of the small changes in dislocation structure from run to run, the data are plotted in terms of the variables

$$y = \frac{(E_e - E)/E}{(E_e - E_0)/E_0} \qquad (1)$$

and

$$z = \frac{\Delta - \Delta_e}{\Delta_0 - \Delta_e} , \qquad (2)$$

where E is Young's modulus, Δ is the logarithmic decrement, subscript 0 refers to the preirradiation values, and subscript e to the values with dislocations completely pinned. Figure 7.1 shows the behavior of z during continuous irradiation at five temperatures. There appears to be a continuous increase of pinning rate with temperature. As far as the data of Fig. 7.1 are concerned, this increase could be explained either in terms of a continuous distribution in activation energy for release of the defects to the dislocation lines, or in terms of the distribution in times required for defects, all of which move with the same activation energy, to reach the dislocations from randomly located "birthplaces" in the crystal. In the latter case the delay-time distribution should be displayed directly in an experiment in which one looks for additional pinning as a function of time following a brief irradiation.

To obtain quantitative results in such an experiment it is necessary to have a linear measure of the density of radiation defect pinning points on

[1] D. O. Thompson and D. K. Holmes, *J. Appl. Phys.* **27**, 191 (1956); **27**, 713 (1956).

[2] J. S. Koehler, *Imperfections in Nearly Perfect Crystals*, p 197, Wiley, New York, 1952.

[3] A. Granato and K. Lücke, *J. Appl. Phys.* **27**, 583, 789 (1956).

[4] D. O. Thompson, T. H. Blewitt, and D. K. Holmes, *J. Appl. Phys.* **28**, 742 (1957).

[5] D. O. Thompson and V. K. Paré, *J. Appl. Phys.* **31**, 528 (1960).

[6] D. O. Thompson and F. M. Glass, *Rev. Sci. Instr.* **29**, 1034 (1958).

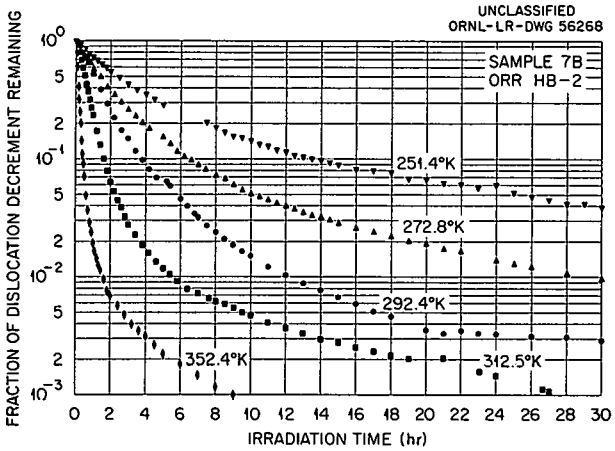

Fig. 7.1. Normalized Logarithmic Decrement Due to Dislocations, as a Function of Time Under Continuous Irradiation.

the dislocation lines. According to the vibrating-string model, one should have

$$y^{-1/2} = z^{-1/4} = \frac{l_0}{l_r} = \frac{n_0 + n_r}{n_0} = 1 + \frac{n_r}{n_0}, \quad (3)$$

where n_0 is the linear density of preirradiation pinning points, n_r is the density of radiation defect pinning points, and l_0 and l_r are the average loop lengths, respectively, before and during the pinning process. Thus $y^{-1/2} - 1$ and $z^{-1/4} - 1$ should be the required linear measures of defect density. Studies of the data show that they actually are sufficiently linear as long as their magnitude is less than 1.0; above this value they deviate from linearity, apparently because dislocations having different characteristics are being pinned.[7]

Figure 7.2 shows a comparison of the behavior of $y^{-1/2} - 1$ under continuous irradiation and after a 10-min irradiation; it can be seen that appreciable pinning occurred after the beam was turned off; in fact, the process was still going on 48 hr later. Similar experiments were done at several other temperatures in the range and interpreted in terms of a simple scheme, assuming that the irradiation produces two important types of pinning points. One type appears instantaneously at the dislocation lines and gives a pinning rate S_u; the other is delayed and would give a pinning rate S_0 if the irradiation were continued long enough to establish a steady state in the migration process. The delay of the second type is characterized by a delay function $N(t)$, defined as the fraction of delayed pinning points, created at $t = 0$, which have appeared at time t. The limiting values of this function are $N(0) = 0$ and $N(\infty) = 1$. The behavior in a continuous irradiation run is then described by

$$\frac{n_r}{n_0} = S_u t + S_0 \int_0^t N(t')\, dt'. \quad (4)$$

In the interrupted type of run the above equation is followed until the irradiation is stopped at time t_1; at that point there is a slope change whose value is S_u, and then the pinning is described by

$$\frac{n_r}{n_0} = S_u t_1 + S_0 \int_{t-t_1}^{t} N(t')\, dt'. \quad (5)$$

If t_1 is small enough compared with t, one can approximate the integral by $t_1 N(t)$ and obtain, using (3),

$$\frac{S_0}{S_u} N(t) = \frac{y^{-1/2} - 1}{S_u t_1} - 1. \quad (6)$$

Figure 7.3 shows the results obtained at several temperatures for $(S_0/S_u)N(t)$. The irradiation times used were 30 min at 281.5°K, 3 min at 373.2°K, and 10 min at the three intermediate temperatures.

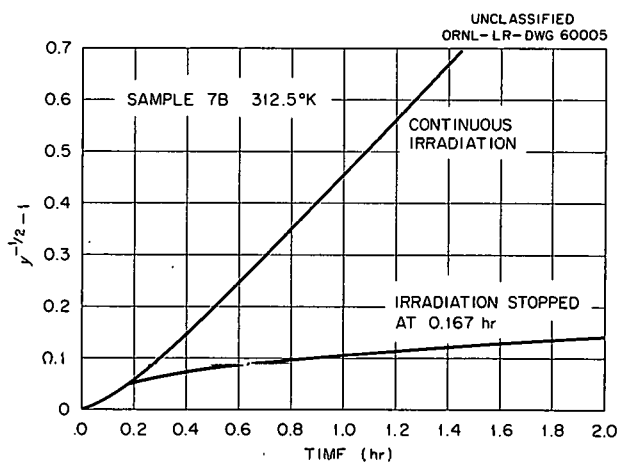

Fig. 7.2. Comparison of Continuous and Pulsed Irradiation Runs.

[7] D. O. Thompson and V. K. Paré, *Solid State Div. Ann. Progr. Rept. Aug. 31, 1960*, ORNL-3017, p 36.

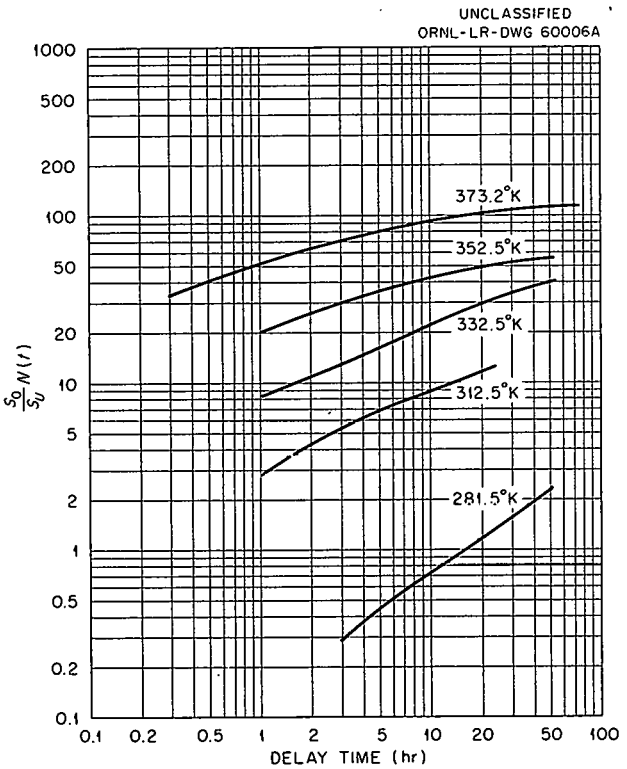

Fig. 7.3. Delay-Time Distribution Function for Dislocation Pinning at Various Temperatures.

If the delay process is governed by a single activation energy W, it should be possible to slide the curves of Fig. 7.3 horizontally into a single continuous curve, by adjusting the time scales according to the relation

$$\frac{t_0}{t} = \exp \frac{W}{k}\left(\frac{1}{T_0} - \frac{1}{T}\right), \qquad (7)$$

in which k is Boltzmann's constant, and t_0 is the time required at a reference temperature T_0 to reach a stage in the process which occurs at time t while at temperature T. The result of such an adjustment is shown in Fig. 7.4, using an activation energy of 1.063 ev. The approximation to a continuous curve is felt to be good, considering the various sources of error. The uncertainty in the activation energy is less than 0.1 ev. Thus it seems reasonable to conclude that the appearance of radiation defect pinning points on dislocations is governed in this temperature range by a single activation energy, about 1.1 ev, and that an approximate representation of the delay-time

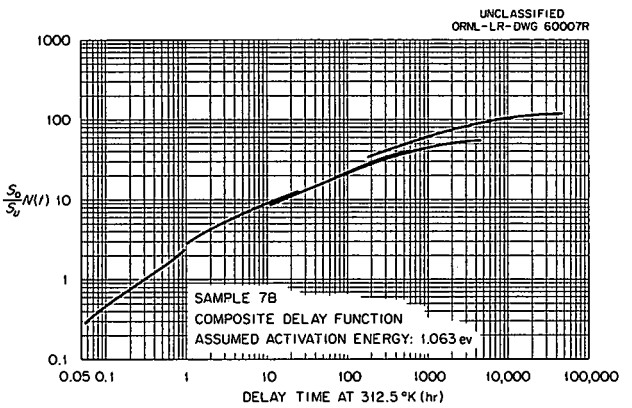

Fig. 7.4. Composite Delay-Time Distribution Function, Obtained by Converting the Delay-Time Scales of Fig. 7.3 to Equivalent Time at 312.5°K, Using an Activation Energy of 1.063 ev.

distribution function has been obtained, covering a factor of nearly 10^6 in time.

Other important aspects of the results are the following:

1. The energy obtained, 1.1 ev, appears to be a reasonable one to ascribe to vacancy migration and agrees within experimental error with the preliminary quenching data of Airoldi, Bacchella, and Germagnoli[8] and with the value of 1 ev inferred by Granato, Hikata, and Lücke.[9]

2. The value reached by $(S_0/S_u)N(t)$ at the end of the process indicates that the delayed pinning points outnumber the undelayed pinning points by a factor of more than 100. Thus the two types cannot be identified as, respectively, vacancies and interstitials, since these should be produced in equal numbers. Possibly interstitials are too mobile to form pinning points at these temperatures.

3. The average number of jumps, calculated as $(10^{13})(t) \exp(-W/kT)$, with t in seconds, is only of the order of 10^4 at the end of the process and 10^{-2} at the earliest stage observed. To exhaust the supply of defects in the whole crystal by diffusion to dislocations having a density of 10^7 cm^{-2} would require something like 10^8 jumps.

[8] G. Airoldi, G. L. Bacchella, and E. Germagnoli, *Phys. Rev. Letters* 2, 145 (1959).

[9] A. Granato, A. Hikata, and K. Lücke, *Acta Met.* 6, 470 (1958).

4. The delay function of Fig. 7.4 is much more spread out in time than would be predicted by the theory of diffusion to dislocations.[10]

The last two of these observations are not consistent with a simple picture of diffusion to the dislocations of vacancies from birthplaces scattered throughout the crystal. Further experiments are planned to test several alternative models.

A THERMALLY ACTIVATED INTERNAL FRICTION SPECTRUM IN COPPER FOLLOWING NEUTRON IRRADIATION

D. O. Thompson

The details of the mechanism whereby radiation-produced defects interact with dislocations in metals and provide dislocation pinning are unknown. Presumably, a part of this interaction occurs through a Cottrell-type potential by which the defect is bound to the dislocation. So long as the defect is thermally immobile in the lattice, or has a jump frequency smaller than that of the applied stress and the Cottrell "spring" is not broken by large stresses, it would be expected that the defect would provide a restraint to the dislocation's motion, since it is not able to follow along in phase with the driven dislocation. As the temperature is raised so that the jump frequency of the restraining defect becomes equal to or greater than that of the applied stress, then it would be expected that the impedance presented by the defect to the dislocation motion would be reduced and that the dislocation would become essentially free with respect to that particular defect. In this event the internal friction of the sample should rise rapidly with increasing temperature according to the Granato-Lücke theory[11] as the effective dislocation loop length of the sample is increased. Furthermore, it would be expected on this basis that the internal-friction spectrum would be thermally activated with the activation energy for motion of the defect in the vicinity of the dislocations. Kessler[12] showed this effect a few years ago for the case of vacancy pinning in germanium and discussed some aspects of the problem in detail. Recently, Kamel[13] has observed this kind of behavior in gold. Another instance of this phenomenon has now been found in neutron-irradiated copper and will be discussed. Further details of these experiments will be published soon.

Experimental Results and Discussion

In Fig. 7.5 are shown three internal-friction curves and a resonant-frequency curve as functions of temperature. It is particularly important to observe the differences in these internal-friction curves. These will now be presented for curves 1 and 2. Curve 3, which extends from 250 to about 330°K, will be discussed briefly later.

Curve 1 represents the final, or lowest, values of the internal friction reached during neutron irradiation at the temperature indicated. The dotted portion is an extrapolation beyond the highest bombardment temperature used to date in bombarding to saturation. It has been shown[14] in previous work that at approximately room temperature the integrated neutron flux needed to produce this final, or saturation, value is of the order of $5\text{–}10 \times 10^{12}$ neutrons/cm^2. From this curve it is apparent that the saturation value of dislocation internal friction is temperature-independent in this range of temperatures and at these measurement frequencies.

Following a bombardment at 352°K in which the decrement was reduced to the value given in curve 1 with an integrated flux of about that given above, additional amounts of bombardment were given until the total dose reached about $1\text{–}2 \times 10^{14}$ *nvt*, and then the bombardment was stopped. The temperature-dependent curve 2 was then found to have developed with a presently unspecified "incubation period." This curve was entirely reproducible during measurement with either increasing or decreasing temperatures, with the exception of the temperature interval denoted approximately by curve 3. In this interval hysteretic effects seemed to play a role. However, it is felt at present that curve 2 represents an equilibrium curve, for it was the one always

[10] F. S. Ham, *J. Appl. Phys.* **30**, 915 (1959).

[11] A. Granato and K. Lücke, *J. Appl. Phys.* **27**, 583, 789 (1956).

[12] J. O. Kessler, *Phys. Rev.* **106**, 646, 654 (1957).

[13] R. Kamel, *Acta Met.* **9**, 65 (1961).

[14] D. O. Thompson and D. K. Holmes, *J. Appl. Phys.* **27**, 191 (1956); **27**, 713 (1956).

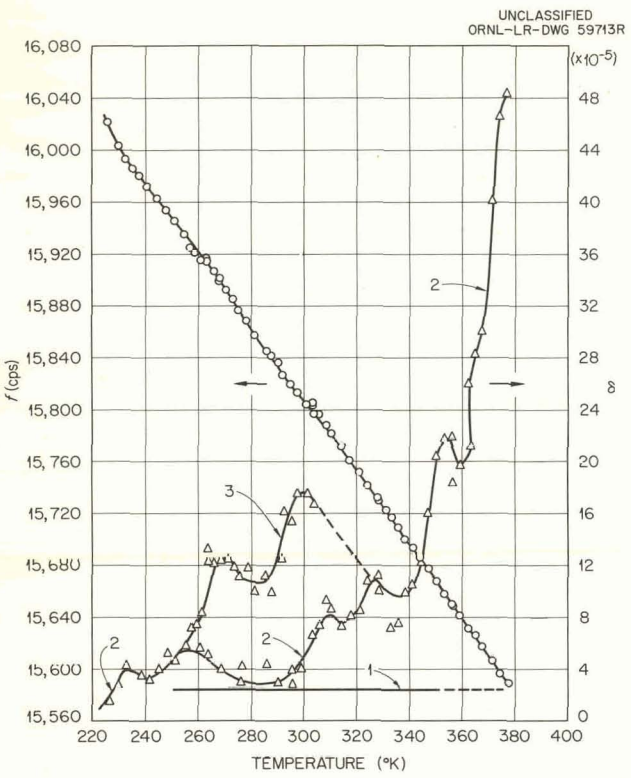

Fig. 7.5. Internal Friction and Resonant Frequency of Neutron-Irradiated Copper as a Function of Temperature at 15.7 kc. See text for meanings of curve numbers.

reached it a sufficient amount of time at temperature was allowed to elapse.

Data were also obtained on the crystal in this irradiated condition at its third harmonic (~45 kc) to determine whether or not the spectrum of Fig. 7.5 is thermally activated. Several interesting differences distinguished these results from those given in Fig. 7.5. In the first place, there was an appreciable reduction (but not complete elimination) in the amount of hysteresis. Secondly, the internal friction at the low side of the temperature interval increases with decreasing temperature rather than decreases, as is the case in Fig. 7.5. Thirdly, the whole spectrum is shifted upward in temperature. From this temperature shift thermal activation is indicated, and an activation energy can be obtained from the well-known formula

$$\ln \frac{f_2}{f_1} = \frac{W}{k}\left(\frac{1}{T_1} - \frac{1}{T_2}\right) ,$$

in which f_1 and f_2 are two measurement frequencies, W is the activation energy, k is Boltzmann's constant, and T_1 and T_2 are the absolute temperatures at which the same event occurs when measured at f_1 and f_2 respectively. The results are summarized below:

P	T_1 (°K)	T_3 (°K)	W (ev)	τ_0 (sec × 10^{13})
I	233	247	0.39	0.4
II	354	376	0.56	3.0

Here, T_1 and T_3 are used to denote the temperature of the same event at the first and third harmonic, and τ_0 is a reciprocal frequency factor also obtained from the data. The temperatures of the peaks in Fig. 7.5 and those obtained at the third harmonic are used to determine the energies rather than the large high-temperature rise in the decrement, for it is felt that they more clearly define the temperature. Furthermore, there is reason to believe that the small peaks are associated with defect motion and occur under the conditions of a Zener relaxation, that is, when $\omega\tau = 1$, in which ω is the angular measurement frequency and τ is the relaxation time of the defect. Thus W may be taken to indicate the energy of motion of the pinning defect.

It is impossible at this time to discuss the mechanism involved in the present experiment with any finality. The results indicate principally that some of the primary pinning defects introduced to the dislocations by neutron bombardment in this temperature range have undergone a conversion in the dislocation neighborhoods, so that their effectiveness as pinning points is reduced or, equivalently, that the motion energy of the converted pinning defect is smaller than that of the pinning defect initially present. This statement is based on the fact that a temperature-independent saturation-internal-friction curve becomes a temperature-dependent one, in this case after a cessation of active bombardment and an incubation time. The necessary conditions for the development of this spectrum are not presently known, but may include such quantities as the density of defects around the dislocations, "incubation" temperature and time, etc. It is to be noted that the results cannot be accounted for by supposing that an appreciable annealing out of pinning defects has taken place during the period

of measurement subsequent to bombardment. If this were true, the values of the internal friction as given by curve 2 around room temperature in Fig. 7.5 would not be maintained and be reproducible but would return toward preirradiation decrement values of around 10^{-2}. Furthermore, previous experience has indicated that annealing temperatures of the order of 650°K are necessary for any appreciable annealing to take place.

A rather consistent argument can be made which suggests that a vacancy grouping of some kind is the incubated, controlling defect in this experiment. Other work (see first part of this chapter) indicates that in this temperature range the dislocation pinning effect is most likely initiated by the diffusion of single vacancies to the dislocations. These are thought to have motion energies of the order of 1 ev in copper, and consequently might provide "hard" pinning of the dislocations in this temperature and frequency range. If the primary defect indeed be vacancies, then there is a certain probability for their recombination in the dislocation neighborhoods into higher-order clusters and particularly into divacancies. The divacancy is thought to have a binding energy of from 0.3 to 0.6 ev and a motion energy of the order of 30 to 70% of that of the single vacancy in the bulk lattice.[15–17] Consequently, it would be expected on this basis that the divacancy would be stable against decomposition in this temperature range and, further, that the dislocation internal friction would be thermally activated with an activation energy of the order of 0.5 ev if the motion energy of the divacancy in the binding field of the dislocation is not too different from that in the lattice. This postulate, clearly, is highly speculative. Others[18] have ascribed a motion energy of 0.58 ev to the divacancy in cold-worked copper. It will be seen in the tabulation that this value agrees reasonably well for the stable, high-temperature side of the present data. In this same connection it would not be too surprising that a series of small peaks would precede the general high-temperature rise, for the motion energy of a given defect may be somewhat different in different kinds of dislocations, that is, whether they be edge, screw, or mixed. Kamel gives a value of 0.55 ev in the case of gold, in which he ascribes the results to dislocation release from single vacancy pinning, with the reservation that it could be divacancy pinning. His results yield a frequency factor, however, which is many orders of magnitude too small, so that it is not clear how much reliance should be placed upon this comparison.

The origin of the hysteretic curve 3 in Fig. 7.5 is not known. Present available information indicates that curve 3 is followed if the sample has been kept at the low-temperature side of the range and measured during warmup. However, if the sample warmup is stopped and held at constant temperature for a sufficient time (10–20 hr, depending on the hold temperature), the internal friction decays back to curve 2. It should be noted that the data in Fig. 7.5 were taken with warmup rates of about 5°/hr in such a way that the sample was warmed 2 or 3°, held for about ½ hr at temperature, and then measured. All the measurements were made in a static pressure of 500 μ helium gas to aid in the establishment of apparatus thermal equilibrium. This equilibrium was attained in times certainly less than 10 min. Curve 3 apparently can be retraced from the high-temperature side only with a sufficiently slow cooling rate and a final decay back to curve 2.

Several mechanisms have been considered in connection with the hysteretic behavior in an attempt to design future experiments to help clarify the problem. Of these, perhaps one of the more reasonable ones is a diffusion-limited condensation problem in which the distribution function for the kinds of pinning defects is a function of temperature. This notion is consistent with a reduction in the hysteresis in the third harmonic, for it is necessary to raise the temperature some 15 to 20°K in this range in order to observe the same event (assuming it to be relaxational in character). This added temperature interval may be sufficient to allow the "phase change" to progress sufficiently toward completion so that the effects are reduced. To be consistent with the argument that the high-temperature end of the present spectrum is primarily divacancy-controlled, the condensate would pre-

[15] J. H. Bartlett and G. J. Dienes, *Phys. Rev.* **89**, 848 (1953).

[16] A. C. Damask and G. J. Dienes, *Phys. Rev.* **113**, 781 (1959).

[17] V. G. Weizer and L. A. Girifalco, *Phys. Rev.* **120**, 837 (1960).

[18] Schule *et al.*, *Z. Naturforsch.* **16a** (1961).

sumably be some higher-numbered vacancy cluster with a fairly small binding energy.

Measurements of the internal friction vs strain amplitude should yield interesting results in connection with the simple model outlined previously. In particular, strain amplitude measurements at relatively low temperatures should yield information on the strength of the Cottrell binding. At higher temperatures, where the defect-jump frequency becomes equal to the measurement frequency, a change in the amplitude dependence of the decrement would also be expected. Preliminary measurements in this direction indicate that such effects do exist. It is planned to make quantitative studies along these directions in the near future.

8. INVESTIGATIONS OF METAL SURFACES

F. W. Young, Jr. L. D. Hulett L. H. Jenkins J. R. Savage

ELECTROCHEMICAL DISSOLUTION OF SINGLE-CRYSTAL COPPER[1]

Galvanostatic studies of single-crystal copper anodes of (100) orientation in oxygen-free copper sulfate solutions revealed discontinuities in the curves resulting from a plot of electrode overpotentials vs current density. Using observations of changes in electrode surface topography as supporting evidence, the discontinuities were explained on the basis of different dissolution processes occurring at different current densities. The changes in dissolution processes were related to the defect structure of the electrodes, and it was concluded that the operation of any one process was determined by the kinetic requirements impressed upon the electrode rather than the thermodynamic states of different surface areas.

CHEMICAL DISSOLUTION OF COPPER

The dissolution of copper single-crystal surfaces in solutions of hydrochloric acid and cupric chloride is being investigated. The kinetics of this reaction in dilute solutions (10^{-2} *M* HCl, 10^{-4} *M* $CuCl_2$) have been studied by measuring the change in conductivity of these solutions as a function of time. An attempt to study dissolution rates in more concentrated solutions (1.0 *M* HCl, 0.1 *M* $CuCl_2$) by measuring the rate of change of refractive index of these solutions is now being made.

It appears that, in the presence of dissolved oxygen, there are two reactions taking place at the crystal surface: (1) attack of the metal by dissolved oxygen followed by dissolution of the oxide by hydrochloric acid; (2) attack by cupric ion: $Cu^0 + Cu^{2+} \rightarrow 2Cu^+$. It is possible to exclude reaction (1), simply by removing the dissolved oxygen; but in the presence of oxygen it is not possible to eliminate reaction (2), since some Cu^{2+} is always present. The rate curves for dilute solutions indicate that reaction (2) is the faster reaction. (The over-all rate of dissolution is strongly dependent on the Cu^{2+} concentration.)

The faceting behavior on (110) and (100) copper surfaces in dilute solutions has been studied. Rectangular, troughlike pits are developed on the (110) surface, and square, flat-bottomed pits are produced on the (100) surface. The same general surface topography is developed in either the presence or absence of oxygen, which can be interpreted as further evidence that reaction (2) is the dominant reaction. The facet patterns do not appear to be related to dislocations in the metal crystal.

ETCHING OF IRRADIATED COPPER[2]

By locating the dislocations as etch pits in an annealed 99.999% copper crystal with (111) faces, irradiating the crystal with 10^{18} fast neutrons/cm^2, and relocating the dislocations as etch pits, it was determined that no sensible change in dislocation density or arrangement resulted from the irradiation. However, the texture of the surface

[1] Abstract of paper submitted for publication in the *Journal of the Electrochemical Society.*

[2] Abstract of paper to be submitted to the *Journal of Applied Physics.*

between the pits at the grown-in dislocations was different after etching the irradiated crystal. For annealed crystals this texture consisted of long terraces, but on the irradiated crystals it consisted of many small pits. It is postulated that the small pits were formed at small dislocation loops resulting from the irradiation, and the density of these loops at which pits were formed was estimated to be $\sim 10^{14}/cm^3$. The density of the loops decreased after annealing, and after 30 min at 400°C the etching characteristics were the same as for well-annealed crystals. It was necessary to assume that pits were formed only at dislocation loops of diameter greater than about 150 A in order to correlate these results with the transmission electron microscopy observations of Makin *et al.*[3]

DISLOCATION MOTION AND MULTIPLICATION IN ANNEALED AND NEUTRON-IRRADIATED COPPER CRYSTALS

The motion and multiplication of dislocations have been studied in both annealed and irradiated copper crystals which were stressed by bending, using an etch-pit technique to locate the dislocations. Since the etching could be performed either before and after or while the stress was applied, the behavior of grown-in dislocations was determined and relaxation effects were studied.

For annealed crystals it was found that the hindrances to motion of the gliding dislocations were subboundaries, dislocation interactions to form sessile dislocations, and, probably, impurities in the crystal. The interaction of gliding dislocations with subboundaries and the piling up of dislocations by obstacles were studied. Very little direct information on the mechanism of dislocation multiplication was obtained.

The motion and multiplication of dislocations in the neutron-irradiated crystals were strikingly different from the motion and multiplication in the annealed crystals. There was very little motion of the grown-in dislocations, and the slip traces formed by deformation were of an entirely different character. It appeared that the best interpretation of the results was that the hardening of copper which resulted from neutron irradiation was source-hardening.

THE YIELD STRESS OF COPPER CRYSTALS[4]

Copper (99.999% pure) crystals were deformed in tension, using an Instron tensile tester, and the dislocation density and arrangement in the crystals were determined before, during, and after the deformation, using an etch-pit technique. For crystals of low initial dislocation density it was found that a large amount of dislocation multiplication occurred prior to yielding. Experimental relationships of dislocation density vs applied stress and vs shear strain were determined. It was found that the yield stress was not related to the initial dislocation density or arrangement. The yield stress was postulated to be determined by the stress necessary to break the gliding dislocations through impurity atom barriers in the crystal.

THE ELASTIC-PLASTIC TRANSITION IN COPPER CRYSTALS AS DETERMINED BY AN ETCH-PIT TECHNIQUE[5]

Copper (99.999% pure) crystals with a dislocation density of 50 per mm^2 have been prepared. These crystals were stressed by applying a pure bending moment, and they were etched with a dislocation etch either before and after or while the stress was applied. The motion of dislocations was determined by observing the size and nature of the dislocation etch pits. The resolved stress necessary to move grown-in dislocations was about 4 g/mm^2. Examples of dislocation motion under stress, then return motion when the stress was removed, and of multiple motion under stress were observed. Multiplication of dislocations occurred at a resolved stress of about 18 g/mm^2. The observed phenomena are discussed in terms of simple dislocation theory.

[3] M. J. Makin, A. D. Whapham, and F. J. Minter, *Phil. Mag.* 6, 465 (1961).

[4] Abstract of paper to be submitted to the *Journal of Applied Physics.*

[5] Abstract of paper to be published in the *Journal of Applied Physics.*

THE FORMATION OF DISLOCATIONS AROUND PRECIPITATE PARTICLES OF Cu_2O IN COPPER[6]

Precipitates of Cu_2O were formed in single crystals of 99.999% copper with (111) faces by oxidizing them in 10 μ of O_2 at 900°C and then furnace cooling. The external oxide and some of the copper were removed by dissolving in HNO_3. After electropolishing and etching with a dislocation etch, small clusters of high dislocation content were observed, by use of the optical microscope. Often a small precipitate of Cu_2O could be seen in the center of the island of dislocations. Measurements were made of the size of the oxide precipitate particles and compared with the extent of the dislocation clusters around them. Assuming that the dislocations were formed and moved by the stress arising from the precipitate, and that the distance which dislocations were observed from the precipitate was a measure of the stress, the above measurements were analyzed. The results suggest that probably the stress was associated with the conversion of a small volume of copper to Cu_2O, rather than with the difference in coefficient of thermal expansion of the copper vs Cu_2O.

[6] Abstract of a paper presented at AIME Symposium on Direct Observation of Imperfections in Crystals, St. Louis, Mo., February 1961. Proceedings of Symposium to be published by Interscience.

ACID CUTTING AND ACID POLISHING OF COPPER CRYSTALS[7]

An acid saw and an acid polisher for cutting and polishing copper crystals are described. Evidence is presented that the cutting and polishing do not introduce dislocations into the crystals. Using these techniques, copper crystals with a dislocation density of 5×10^3 per cm^2 have been prepared.

[7] Abstract of published paper: F. W. Young, Jr., and T. R. Wilson, *Rev. Sci. Instr.* 32, 559 (1961).

9. ALLOY RESEARCH

M. S. Wechsler

INTRODUCTION

In the case of alloys, there appear to be two aspects to the effect of the production of defects by radiation, plastic deformation, or quenching. The direct effect is due simply to the presence of the defects. For example, lattice vacancies, produced at a low temperature, where they are immobile, are known to increase the electrical resistivity and decrease the density. This direct effect occurs in high-purity metals as well as alloys. For alloys, however, it is important to consider a second, less direct effect that occurs when the temperature is raised to the point where significant atomic mobility exists. This arises from the fact that a relative rearrangement of the different types of atoms in the alloy may be stimulated by the defects. Often the atomic rearrangement is reflected in larger changes in properties than those caused by the presence, per se, of the defects.

This approach to an understanding of the nature of defects in alloys is being applied to several investigations. The study of the effect of radiation on Cu-Al alloys[1-3] is being continued. Here, the motion of the radiation-produced vacancies is thought to stimulate an atomic rearrangement, probably short-range ordering of the copper and aluminum atoms. Also, work is being done on the effect of cold working on the properties and annealing behavior of Cu-Si alloys. In this case the explanation of the observations is framed in terms of defects produced by the cold working and the atomic rearrangements engendered by them below the recrystallization temperature.

[1] M. S. Wechsler and R. H. Kernohan, *J. Phys. Chem. Solids* 7, 307 (1958).

[2] R. H. Kernohan and M. S. Wechsler, *J. Phys. Chem. Solids* 18, 175 (1960).

[3] M. S. Wechsler *et al.*, *Solid State Div. Ann. Progr. Rept. Aug. 31, 1960*, ORNL-3017, pp 46–49.

The radiation enhancement of diffusion-controlled processes in alloys may be an important factor in the effect of radiation on the engineering properties of structural steels. This is indicated most strikingly by the observation[4] that neutron irradiation at about 200°C is more effective in raising the brittle-fracture transition temperature of a pressure-vessel steel than neutron irradiation above or below this temperature. This result implies that the irradiation embrittlement of steels is, in part, a reflection of an atomic rearrangement stimulated as a result of the introduction of defects by the irradiation.

IRRADIATION EFFECTS ON COPPER-ALUMINUM (15 at. % Al) ALLOYS

C. Bassani[5] R. H. Kernohan
J. M. Williams M. S. Wechsler

Flux Dependence

When Cu-Al alloy samples are irradiated with neutrons, electrons, or gamma rays, a decrease in electrical resistivity takes place.[1,3] The irradiation must be carried out at temperatures where the radiation-produced vacancies are mobile, since it is in the course of their motion that the atomic configuration of lower resistivity is achieved. For the 15 at. % Al alloy irradiated at 100°C (ref 2), the magnitude of the decrease is about 0.17 microhm-cm (about 1.4% at 100°C) and is rather insensitive to the type of irradiation or the flux. On the other hand, the *rate* of decrease in resistivity at 100°C depends markedly on the type of irradiation and the flux.

The rate dependence on flux is important, since it gives information concerning the mechanism of the annihilation of vacancies. This has been discussed by Dienes and Damask.[6] Their analysis directs attention to three possibilities for the annihilation mechanism: (1) annihilation at fixed sinks (linear annealing), (2) annihilation by recombination of interstitials and vacancies (recombination annealing), and (3) annihilation by a combination of (1) and (2). In the case of linear annealing, the time, τ, to reach a given fractional change in property is shown to be proportional to K^{-1}, whereas for the other two cases, τ is expected to be proportional to $K^{-1/2}$, where K, the defect production rate, is given by $K = \phi\sigma$, where ϕ is the flux and σ is the cross section for the production of a displacement.

An investigation is in progress to determine how the rate of decrease in resistivity upon neutron irradiation at 100°C depends upon the neutron flux. Hole C of the ORNL Graphite Reactor is being used, and the flux is varied by placing the samples at various distances in the hole. At each position a preliminary run is made in which a U^{238} fission threshold flux monitor[7] is exposed for a specified time at the same power level used for the Cu-Al samples. Immediately following the monitoring run the Cu-Al sample is placed in the same location, and the resistivity is measured at 100°C as a function of time of irradiation. The results of four such runs are shown in Fig. 9.1. In this figure, f is the fractional departure from completion of the process and is given by $f = (\rho - \rho_f)/(\rho_i - \rho_f)$, where the quantities ρ_i, ρ_f, and ρ are the initial resistivity, the final resistivity, and the resistivity at time t respectively. The total decrease, $\rho_i - \rho_f$, was approximately the same at each flux level.

In a previous report[3] the dependence of the rate of decrease in resistivity on electron flux was described. In that case the time for half-completion, $\tau_{1/2}$, was found to be roughly proportional to $K^{-1/2}$ (Fig. 9.2), where K was calculated by using the observed electron flux and the cross sections for displacements calculated by Fuchs.[8] Because of the uncertainties associated with the calculation of the defect production rate for neutron irradiation, it was decided to plot the $\tau_{1/2}$ values obtained upon neutron irradiation in such a way in Fig. 9.2 that the point for the highest flux run falls on the line labeled "$\tau_{1/2} \propto K^{-1/2}$." This procedure is equivalent to selecting $K = 8.8 \times 10^{-11}$ sec^{-1} as

[4] R. G. Berggren, "Neutron Irradiation Effects in Steel: Studies at Oak Ridge National Laboratory," p 370 in *Steels for Reactor Pressure Circuits*, Special Report No. 69, The Iron and Steel Institute, London, 1961.

[5] Guest Scientist from Gruppo Fisica Stato Solido, CCR-Euratom, Ispra (Varese), Italy.

[6] G. J. Dienes and A. C. Damask, *J. Appl. Phys.* 29, 1713 (1958).

[7] We wish to thank T. V. Blosser, Neutron Physics Division, and P. W. Reinhardt, Health Physics Division, for assistance with the flux monitoring.

[8] R. Fuchs, unpublished data.

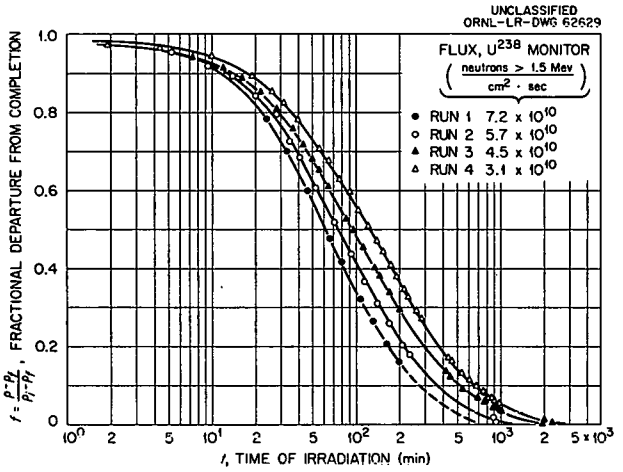

Fig. 9.1. Fractional Departure from Completion of the Decrease in Resistivity of Cu-Al (15 at. % Al) vs Time of Irradiation at 100°C. Hole C, ORNL Graphite Reactor.

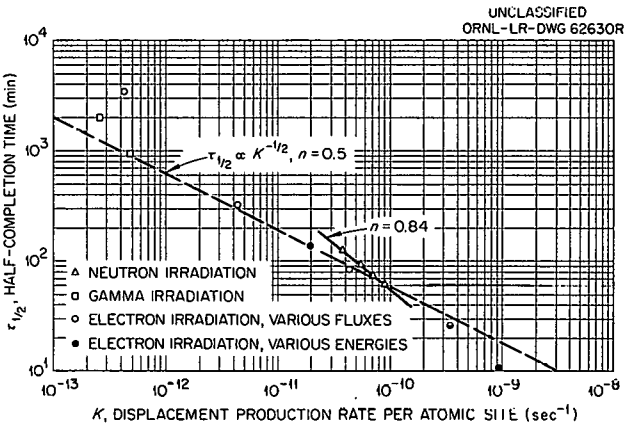

Fig. 9.2. Time Necessary To Reach Half-Completion of the Decrease in Resistivity as a Function of the Displacement Production Rate in Cu-Al (15 at. % Al). All irradiations were performed at 100°C.

the defect production rate corresponding to a flux of 7.5×10^{10} neutrons cm^{-2} sec^{-1} with energies greater than 1.5 Mev, the fission threshold for U^{238}. The values of $\tau_{1/2}$ for the lower fluxes are then plotted with proportionately reduced values of K. Let us consider the time, τ_f, to reach a given value of f to be given by

$$\tau_f K^n = \text{constant}, \qquad (1)$$

where $n = 1$ for linear annealing and $n = \frac{1}{2}$ for recombination annealing. Then Fig. 9.2 shows that $n = 0.84$ for $f = 0.5$ in the narrow neutron flux range studied thus far.

The exponent n in Eq. (1) may be determined for other values of the fractional departure from completion of the process, f. This is shown in Fig. 9.3, where it is seen that the character of the annealing appears to shift from recombination annealing ($n = 0.5$) to linear annealing ($n = 1$) during the course of the annealing process. This observation suggests that additional vacancy sinks are produced by the irradiation, which serve to increase progressively the contribution made by the linear-annealing mechanism. However, experiments will have to be carried out over a much wider range of neutron fluxes before any conclusions can be drawn concerning the mechanism of the annealing for neutron irradiation.

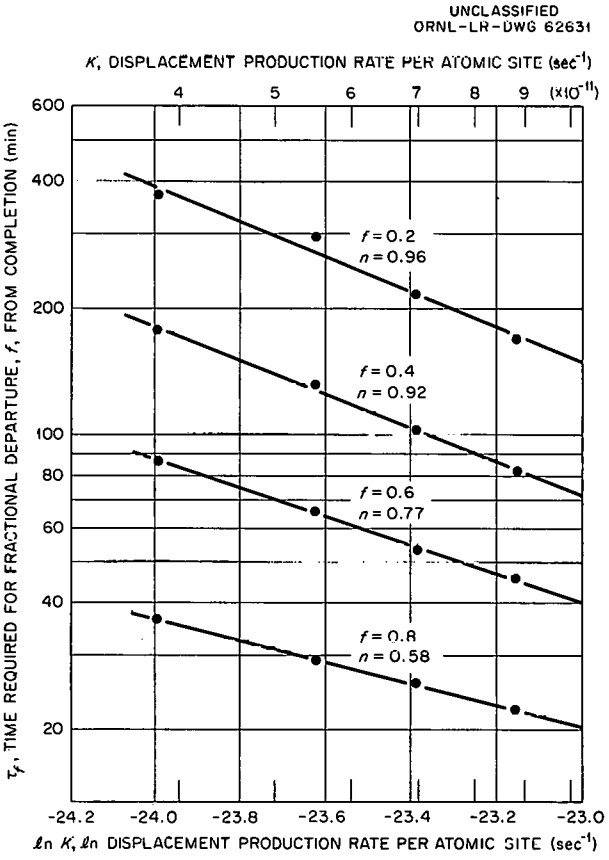

Fig. 9.3. Ln τ_f vs ln K, Where τ_f Is the Time Required for Fractional Departure, f, from Completion of the Decrease in Resistivity and K Is the Displacement Production Rate. The constant n is evaluated according to the equation $\tau_f K^n$ = constant.

It was mentioned above that experiments on structural steels suggest that atomic rearrangements are involved in the changes in mechanical properties that take place upon neutron irradiation. If this is the case, the question of the flux dependence of radiation-induced atomic rearrangements may have an important bearing on the use of structural alloys in low-flux radiation environments, as in the case of a reactor pressure vessel. The tests for the suitability of such materials are generally carried out in test reactors, where the fluxes are several orders of magnitude higher than in the service application. To correlate test results with effects in service, the assumption is usually made that the same changes in properties occur when the same total dose is received. It can be seen that this assumption corresponds to the linear-annealing case. Since K in Eq. (1) is proportional to the flux, we have from Eq. (1)

$$t_s = \left(\frac{\phi_t}{\phi_s}\right)^n t_t ,$$

where t_s and t_t are the times for a given change in properties in service and under test conditions, respectively, and the ϕ's are corresponding values of the flux. When $n = 1$, $\phi_s t_s = \phi_t t_t$ and the same radiation dose is received in service and for the test. However, if $n < 1$, the time t_s calculated on the assumption of equal property changes for equal doses will result in an overestimate of the time necessary for deterioration of properties under the low-flux service conditions.

Dependence on Temperature of Irradiation

The theory[6] of radiation-enhanced diffusion indicates that the rate of change of properties has a different temperature dependence for the different annealing mechanisms. Specifically, it is shown that for a system that exhibits pure linear annealing, there ought to be no dependence on the temperature of irradiation, whereas if some amount of recombination annealing is involved, a decided temperature dependence should prevail. The following is an abstract from a paper[2] that describes experiments on Cu-Al in which samples were irradiated at various temperatures in the range 45 to 250°C and the rate of reaction was found to increase considerably with increasing temperature:

Neutron Irradiation of Cu-Al at Elevated Temperatures. – The effect of neutron irradiation at elevated temperatures on the electrical resistivity of Cu-Al (15 at. % Al) is described. The results support the idea that at temperatures below 200°C the alloy is in a metastable state. Upon irradiation, atomic mobilities are enhanced and the metastability is eliminated, accompanied by a decrease in resistivity. An analysis is made of the temperature dependence of the rate of the atomic rearrangement stimulated by the irradiation. It is found that the activation energy for motion remains constant during the process at about 0.5 ev. A comparison is made with the results of a previous experiment in which the alloy was irradiated at lower temperatures.

Specific-Heat Measurements on Irradiated Cu-Al[9]

A study is in progress[10] at the University of Tennessee of the effect of thermal and irradiation treatments on the specific heat of Cu-Al (16.8 at. % Al). The measurements have shown that an anomalous absorption of heat takes place in the slowly cooled alloy upon raising the temperature above about 250°C. This anomaly corresponds to the excess resistivity observed[11] above 200°C. In order to compare the effects of neutron irradiation on specific heat and resistivity, samples appropriate for the measurement of these properties were irradiated simultaneously for 15 hr at 100°C in the ORNL Graphite Reactor. The irradiation produced a decrease in resistivity of 0.20 microhm-cm. The anomalous absorption of heat was observed[10] to take place in the irradiated sample at a temperature 20°C lower than for the annealed sample and was of a greater magnitude by about 30 cal/mole. It seems reasonable to suggest that the irradiated samples undergo a larger amount of disordering when the temperature is raised above 200 or 250°C, due to the higher degree of short-range order achieved at 100°C as a result of the irradiation.

[9] In collaboration with E. E. Stansbury, C. R. Brooks, and D. H. Hendrix of the University of Tennessee.

[10] C. R. Brooks, D. H. Hendrix, and E. E. Stansbury, *Application of Adiabatic Calorimetry to Metal Systems*, Report for Period Aug. 1, 1960–July 31, 1961, the University of Tennessee.

[11] M. S. Wechsler and R. H. Kernohan, *Acta Met.* 7, 599 (1959).

COLD WORKING AND ANNEALING OF A Cu-Si-Mn ALLOY[12]

J. M. Williams M. S. Wechsler

The idea that is basic to the interpretation of the irradiation effects on Cu-Al alloys discussed above is that the slowly cooled alloy is in a metastable state at room temperature. Furthermore, the metastability is eliminated by virtue of the enhancement of diffusion resulting from the motion of radiation-produced defects. In a similar way, we may expect metastable atomic arrangements in other alloys. Also, the elimination of these metastabilities may occur as a result of defects introduced by cold working. The defects may be of two types: (1) point defects, particularly vacancies, which enhance diffusion, and (2) extended defects, such as stacking faults and dislocations, which may serve as nucleation centers about which a redistribution of solute atoms takes place.

A commercial silicon-bronze alloy (Everdur 1010) of composition Cu–6.7 at. % Si–1.3 at. % Mn was chosen for this study because preliminary experiments[13] indicated large changes in the electrical resistivity upon annealing after cold working. The commercial stock was machined and drawn to 0.062-in.-diam wire with intermediate anneals and was examined under the microscope for soundness. The wires were then sealed in evacuated quartz capsules and annealed for almost 100 hr at 850°C, followed by cooling at a rate of 25°C/hr to room temperature. The grain size was about 0.024 in.

The effect of drawing at room temperature on the resistivity and hardness[14] of wire samples is shown in Fig. 9.4. Note that a 42% reduction in area produces an increase in resistivity of about 1.5 microhm-cm and a 2.6-fold increase in the diamond pyramid hardness number.

The isochronal annealing behavior of the resistivity, hardness, and yield stress was observed following cold working to 42% reduction in area.

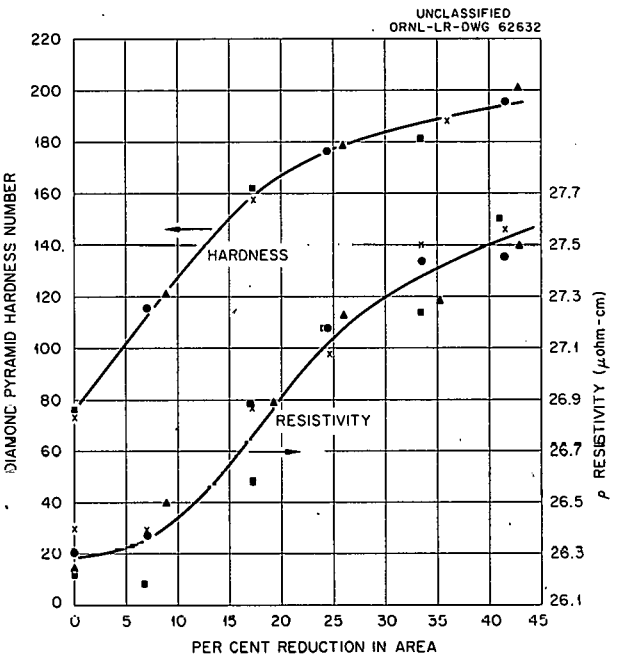

Fig. 9.4. Change in Resistivity and Hardness of Four Wire Samples of Cu–6.7 at. % Si–1.3 at. % Mn Upon Drawing at Room Temperature. Original diameter, 0.062 in. Drawing speed, 2 in./min. Resistivity measurements were made at −196°C. Previous treatment: 98.5 hr at 850°C followed by 25°C/hr cooling to room temperature.

Optical photomicrographs and x-ray diffraction patterns[15] were also obtained. The isochronal annealing was carried out in progressive steps from room temperature to 850°C, with a duration of 2 hr at each step and an interval of 50°C. For each anneal, the samples were placed in evacuated quartz capsules, held at temperature in a tube furnace, and quenched in water when the anneal was completed. The annealing of each sample was cumulative, in that each sample was subjected to all the annealing steps prior to the one at which it was removed for measurement.

The results of the isochronal annealing treatment are shown in Fig. 9.5. The curves shown in Fig. 9.5*a* indicate that the resistivity upon annealing after cold working falls far below its value prior to cold working. A minimum is reached at 400°C and, upon further increase in temperature, the

[12] In collaboration with H. M. Otte, Research Institute for Advanced Study, Baltimore, Maryland.

[13] M. S. Wechsler *et al.*, *Solid State Div. Ann. Progr. Rept. Aug. 31, 1960*, ORNL-3017, pp 46–49.

[14] We wish to thank B. C. Leslie, Metallography Group, Metallurgy Division, for making the hardness measurements and performing the metallographic work.

[15] We are indebted to F. A. Sherrill for assistance with the x-ray diffraction work.

resistivity rises again until at 600°C it achieves the value it would have had in the absence of cold working. Above 600°C there is no difference in the behavior of the cold-worked and control samples. In the range of temperatures where the resistivity is decreasing most rapidly (300–400°C), the hardness increases to a maximum (Fig. 9.5*b*). This "cold-hardening" stage following cold working has been reported previously for Cu-Zn (ref 16) and Cu-Al (ref 17). Above 400°C the hardness decreases progressively until at 700°C the value characteristic of the control sample is reached. The yield stress (Fig. 9.5*c*) begins decreasing at about 350°C and shows no maximum corresponding to the peak hardness.

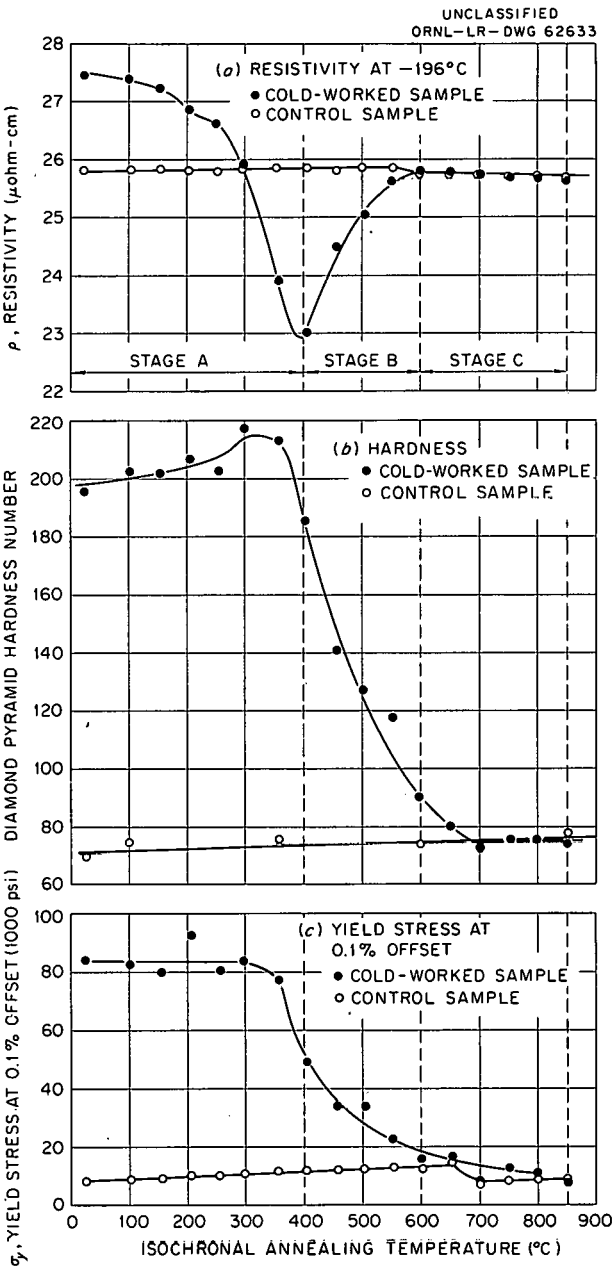

Fig. 9.5. Changes in Properties upon the Isochronal Annealing of Cu–6.7 at. % Si–1.3 at. % Mn. The samples were previously annealed 96 hr at 850°C and cooled at 25°C/hr. The cold-worked samples were cold-drawn to 42% reduction in area.

The metallographic examination resulted in the three characteristic microstructures shown in Fig. 9.6. These microstructures were observed after the anneals at 200, 450, and 600°C respectively. They are representative of the microstructures seen after anneals in the following ranges of temperatures: (*a*) 100–400°C (*b*) 450–550°C, and (*c*) 600–850°C, although in the last case more and more grain growth was observed as the annealing temperature was increased above 600°C. The photomicrograph of Fig. 9.6*a* represents flowed metal, that of Fig. 9.6*b* is indicative of a recovery stage or perhaps an early portion of the recrystallization process in which the recrystallized grains have barely begun to impinge on one another, and, finally, Fig. 9.6*c* shows the fully recrystallized structure before any large amount of grain growth has taken place. The three temperature regions indicated by the microstructure are delineated in Fig. 9.5 and labeled as stages A, B, and C.

The x-ray patterns[15] consisted of Debye-Scherrer photographs. The spottiness in the Debye-Scherrer rings characteristic of coherent recrystallized domains was faintly visible at 400°C, but was not pronounced until a temperature of 600°C was reached.

X-ray measurements of the stacking-fault probability are being made by Otte[12] at RIAS. The cold-working and annealing treatment being used is similar to that described above. A stacking-fault probability of 0.06 ± 0.03 has been measured after cold drawing to 47% reduction in area. Furthermore, the stacking-fault probability has been observed to decrease to zero upon isochronal annealing from room temperature to 350°C.

[16] R. R. Hasiguti, *J. Jap. Inst. Met.* 19, 103 (1955).

[17] R. W. Cahn and R. G. Davies, *Phil. Mag.* 5, 1119 (1960).

UNCLASSIFIED
PHOTO 55643

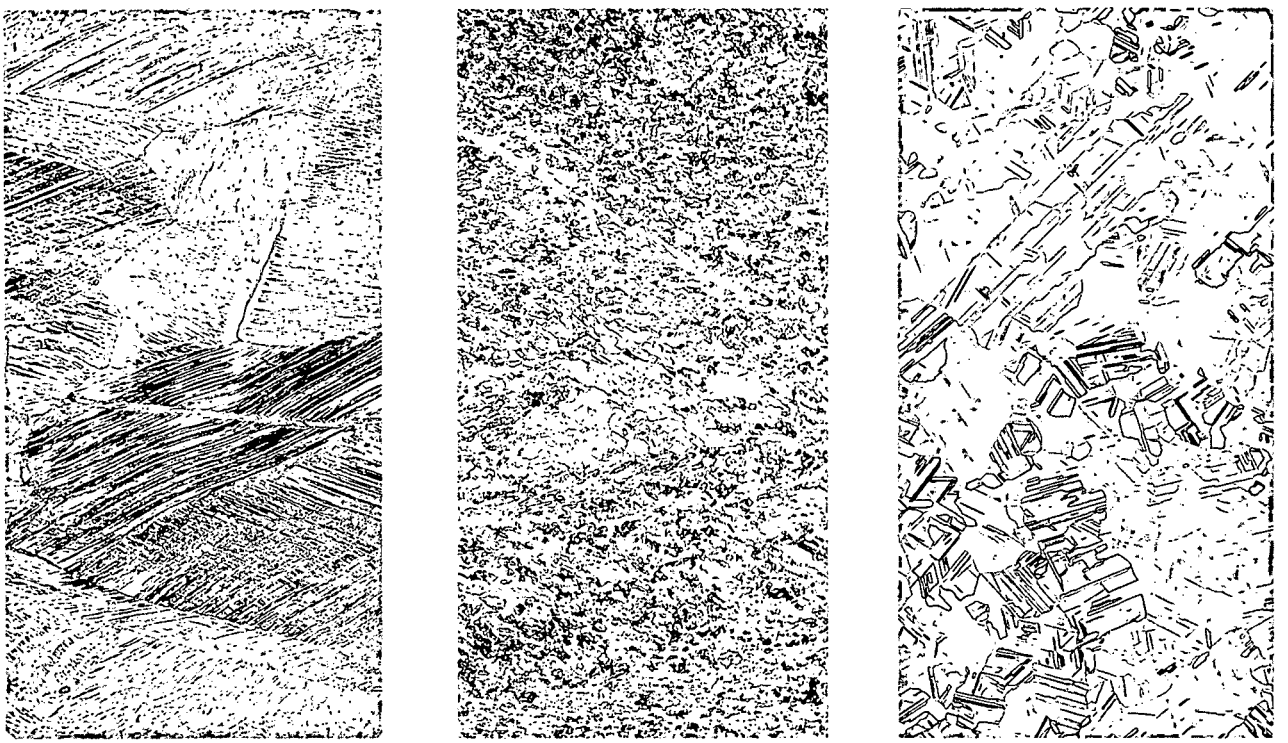

(*a*) 200°C (100 - 400°C) (*b*) 450°C (450 - 550°C) (*c*) 600°C (600 - 850°C)

Fig. 9.6. Microstructures Resulting from Isochronal (2 hr) Annealing in 50°C Steps from Room Temperature to the Temperatures Indicated for Cu–6.7 at. % Si–1.3 at. % Mn Cold-Drawn to 42% Reduction in Area. The microstructures are representative of the ranges of temperatures shown in parentheses. 100X.

An additional feature, the reversibility of the annealing behavior, is illustrated in Fig. 9.7. Two samples were cold-drawn to 42 and 45% reduction in area. The first sample was isochronally annealed up to 850°C and then isochronally annealed upon decreasing the temperature from 850°C. A similar procedure was followed for the second sample, but the maximum temperature was only 550°C. Figure 9.7 indicates that for the second sample the changes in resistivity were reversible upon increasing and then decreasing the annealing temperature. However, when the annealing was continued up to 850°C, the changes in resistivity were not reversible, since no large decrease in resistivity was observed when the temperature was again decreased.

The observed increase in resistivity of about 1.5 microhm-cm upon cold working to 42% reduction in area may be attributed to the introduction of vacancies or of deformation stacking faults. The theoretical estimates[18] of the added resistivity due to vacancies upon plastic straining vary considerably, but only the largest of these estimates appear to be capable of explaining the observed resistivity increase. The electrical resistivity of stacking faults in copper has been analyzed by Howie.[19] If his results are applied to our alloy, then the stacking-fault probability of 0.06 observed by Otte implies an increase in resistivity of about 2 microhm-cm. This calculation agrees, perhaps fortuitously, with the observed resistivity increase of 1.5 microhm-cm.

[18] A. H. Cottrell, "Point Defects and Mechanical Properties of Metals and Alloys at Low Temperatures," p 1 in *Vacancies and Other Point Defects in Metals and Alloys*, Report No. 23, The Institute of Metals, London, 1958.

[19] A. Howie, *Phil. Mag.* 5, 251 (1960).

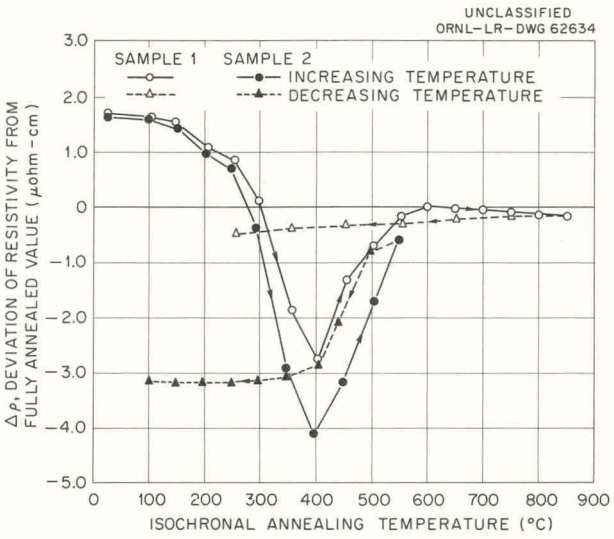

Fig. 9.7. Change in Resistivity vs Isochronal (2 hr) Annealing Temperature Upon Increasing and Then Decreasing the Temperature. Cu–6.7 at. % Si–1.3 at. % Mn, cold-drawn to 42% (sample 1) and 45% (sample 2) reduction in area. Resistivity measurements made at −196°C.

The annealing behavior is perhaps best discussed in terms of the segregation of solute, which is assumed to be supersaturated in the slowly cooled solid solution. The segregation may take place as a result of enhanced diffusion due to the added concentration of vacancies introduced by the cold working. Another possibility is the segregation at deformation stacking faults, which takes place as a result of greater solute solubility at the layer of hexagonal close-packed material at the stacking faults. In either case the cold-hardening peak at 300 to 350°C (Fig. 9.5*b*) is to be attributed to the barriers to dislocation motion imposed by the solute clusters. Furthermore, we must postulate that the clusters are no longer stable above 400°C, where the minimum in resistivity (Fig. 9.5*a*) is reached. When the temperature is raised above 400°C, the clusters become increasingly dispersed and the resistivity is increased due to higher solute concentrations in solid solution. The observations concerning the reversibility of the changes in resistivity (Fig. 9.7) indicate that the solute clusters will re-form upon the subsequent decrease in temperature, provided that recrystallization has not taken place.

It is planned to continue this investigation by studying similar effects on high-purity Cu-Si alloys.

BRITTLE FRACTURE OF IRRADIATED STRUCTURAL METALS

R. G. Berggren T. N. Jones
M. S. Wechsler

It is recognized that brittle failure is a widespread problem affecting steel structures. Many catastrophic failures in large steel structures, such as ships, bridges, pressure vessels, pipe lines, and storage tanks, have been attributed to low-temperature brittleness. It would appear that reactor pressure vessels are particularly susceptible to this type of failure. The large size of reactor pressure vessels, the thickness of the plate, the welded construction, and especially the embrittlement caused by irradiation – all contribute to the concern over the safety of reactor pressure vessels.

In large welded structures a critical point is the metallurgical condition of the weld metal and of the heat-affected zone adjacent to the weld. It is possible to study the properties of the heat-affected zone by making use of a technique developed at Rensselaer Polytechnic Institute in which samples are subjected to the same thermal treatment as would be the case during welding. This section describes the preliminary results of an investigation of the effect of radiation on the notch ductility of such simulated heat-affected zone samples.[20] The unaffected parent plate material was also studied. The material chosen corresponds to the steel used for the pressure vessels of many nuclear power reactors, including EGCR, EBWR, Maritime, and military reactors.

Charpy V-notch impact specimens were prepared from a 4-in. plate of ASTM A-212B carbon-silicon steel. The steel was from an aluminum-treated heat produced according to ASTM specification A-300 for fine-grain practice. The chemical analysis was: 0.25% C, 0.74% Mn, 0.013% P, 0.025% S, and 0.20% Si. The plate was normalized at 1625 to 1675°F, cooled with a water spray to 500°F, and stress-relieved at 1200 to 1250°F. One group of samples machined from the plate was characteristic of the parent (base) plate. Two additional groups,

[20] We wish to thank P. Patriarca of the Metallurgy Division, who initiated this investigation and arranged for the preparation of the heat-affected zone samples at Rensselaer Polytechnic Institute.

prepared at Rensselaer Polytechnic Institute,[21] were synthetic, weld heat-affected zones corresponding to energy inputs of 100,000 joules/in. (2B series) and 50,000 joules/in. (4B series). Additional information concerning the pretreatment of the samples is given in Table 9.1.

The Charpy V-notch impact curves for the unirradiated heat-affected zone samples and the parent plate samples shown in Figs. 9.8 and 9.9 are quite consistent with the results of Nippes, Savage, and Brown.[21] It is of interest that the initial transition temperature of the 2B series was higher than for the 4B series (Fig. 9.8). Metallographic examination of the parent plate showed uniformly distributed regions of ferrite and fine pearlite. The synthetic heat-affected zones appeared to be tempered bainite or tempered martensite and proeutectoid ferrite at prior austenite grain boundaries. The major microstructural difference in the synthetic heat-affected zones appeared to be in the ferrite network. This network was discontinuous in the 4B series (50,000 joules/in.) and continuous in the 2B series (100,000 joules/in.). Apparently, this continuous ferrite network contributed to the higher initial notch-impact transition temperature of the 2B series.

The two types of synthetic, weld heat-affected zone samples and the parent plate samples were irradiated in the ORR poolside facility for 1106 hr at 90 to 130°F to doses of (6 to 10) $\times$ 10^{18} neutrons/cm^2 (> 1 Mev). The effect of the irradiation on the Charpy V-notch impact strength for the three material conditions is presented in Figs. 9.8 and 9.9. A summary of the results on the basis of three transition-temperature criteria is given in Table 9.2. The radiation-induced increases in

[21] E. F. Nippes, W. F. Savage, and W. A. Brown, *Progress Report No. 2. Study of the Weld Heat Affected Zone of A-212B Steel*, Rensselaer Polytechnic Institute (February 1961).

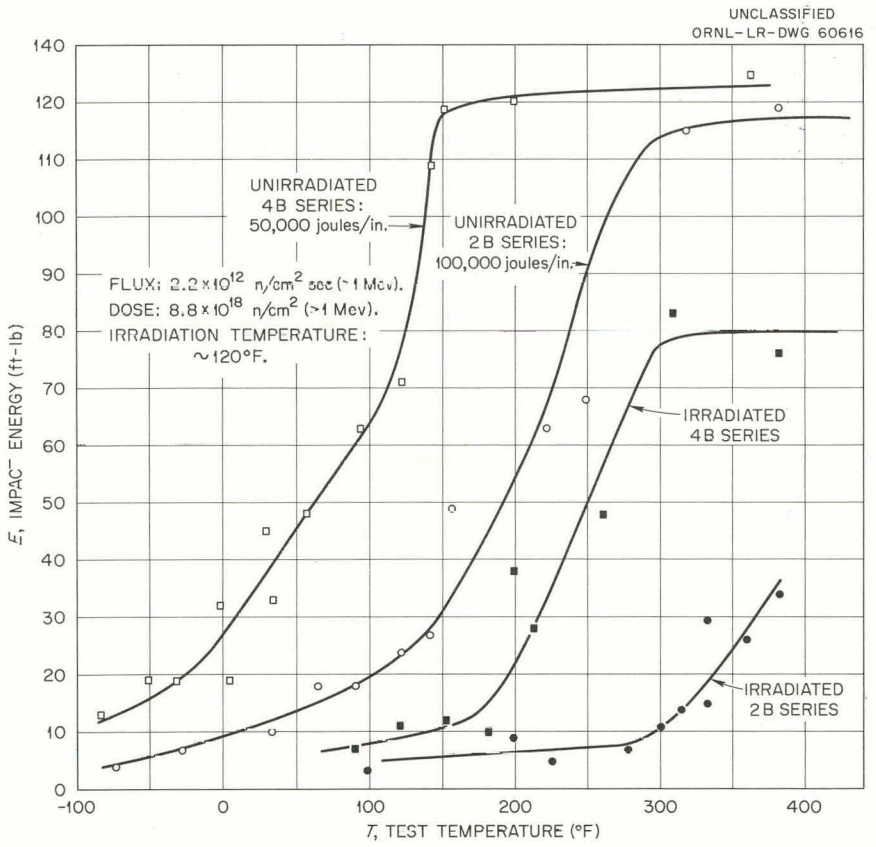

Fig. 9.8. Charpy V-Notch Impact Tests of Irradiated Synthetic Heat-Affected Zones in ASTM A-212 B Steel (Item 147).

Table 9.1. Simulated Weld Thermal Cycles and Related Properties*

Test Series	2B Series	4B Series	Parent Plate
Energy input in 1-in. plate, joules/in.	100,000	50,000	As-received
Peak temperature, °F	2400	2400	
Initial plate temperature, °F	80	80	
Post-heat treatment	1150°F, 4 hr	1150°F, 4 hr	
Cooling rate, °F/sec			
At 1000°F	13.6	43.8	
At 1300°F	31.9	83.4	
Hardness, VPN	229	280	164
Transition temperature, °F			
10 ft-lb	90	–35	–22
15-mil expansion	125	4	–7
50% shear fracture	210	25	70

*E. F. Nippes, W. F. Savage, and W. A. Brown, *Progress Report No. 2. Study of the Weld Heat Affected Zone of A-212B Steel*, Rensselaer Polytechnic Institute (February 1961).

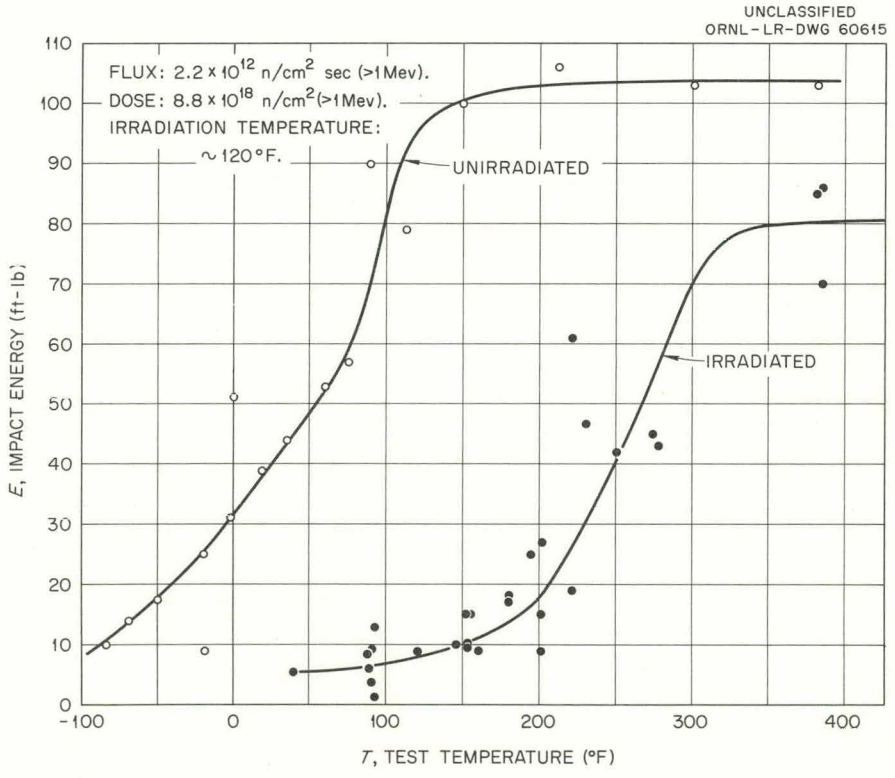

Fig. 9.9. Charpy V-Notch Impact Tests of Irradiated ASTM A-212B Steel (Parent Plate, Item 147).

Table 9.2. Effect of Neutron Irradiation at 90 to 130°F on the Fracture Transition Temperature

Neutron Dose: (6 to 10) × 10^{18} neutrons/cm^2 (> 1 Mev)

Material	Transition Temperature (°F)		
	10 ft-lb Criterion	30 ft-lb Criterion	50% of Ductile Energy Criterion
Series 2B (100,000 joules/in.)			
Unirradiated	20	150	200
Irradiated	295	365	>400
Increase	275	215	>200
Series 4B (50,000 joules/in.)			
Unirradiated	−100	10	90
Irradiated	140	215	270
Increase	240	205	180
Parent plate			
Unirradiated	−80	−5	60
Irradiated	150	230	270
Increase	230	235	210

transition temperature in these three materials are about equal and are nearly the same as for a variety of steels investigated by the Naval Research Laboratory[22] and the Oak Ridge National Laboratory.[23] A number of determinations remain to be carried out on the samples irradiated in this experiment. It is planned to measure the lateral contraction and expansion of the fractured samples and to determine their fracture appearance. Also, the microstructure of the irradiated samples will be examined metallographically. Finally, a number of samples from this irradiation experiment will be given a postirradiation recovery treatment before testing, in order to determine the manner and extent of the annealing of the radiation effects.

[22] L. F. Steele and J. R. Hawthorne, *Effect of Irradiation Temperature on Neutron-Induced Changes in Notch Ductility of Pressure Vessel Steels*, NRL Report 5629 (June 28, 1961).

[23] R. G. Berggren, "Radiation Effects in Ferritic Steels," pp 91–127 in *Status of Radiation Effects Research on Structural Materials and the Implications to Reactor Design*, TID-7588 (October 1960).

10. PROPERTIES OF HIGH-PURITY IRON

J. C. Wilson

It has been shown that high-purity iron-carbon alloys may suffer less irradiation embrittlement than ordinary steels of comparable mechanical properties.[1] The purpose of this program is to study and understand the properties of iron of the highest attainable purity in order that the mechanism of radiation effects may be more easily determined in irons and steels. Only recently has iron been purified to a high degree; at present the interactions between low-level impurities still prevent any materials from being classed as truly "high purity" as far as mechanical properties are concerned.

Removal of oxygen from iron is important because, in the absence of carbon, grain-boundary brittleness is observed in iron-oxygen alloys at room temperature and below. As a result, studies of deformation are interrupted by fracture at relatively low strains. Furthermore, deformation twins form at room temperature. A study of grain-boundary fractures has shown that twin traces appear as ridges on the surface of fractured grain boundaries. The twins are predominantly formed in grains adjacent or close to the fracture; deformation of large grains, away from the grain boundaries, does not cause twinning. It is believed that the twins are formed as a result of the high microscopic strain rates present as the grain boundary is fractured, even though the macroscopic rate of deformation is slow.

Calcium and barium, vapor deposited in vacuum on iron (0.01% oxygen) in the alpha range, were used to remove oxygen, as evidenced by the elimination of (internal) oxide particles. Other effects noted were surface terracing, a reduction in the attack of the chemical polish (oxalic acid and hydrogen peroxide) at the grain boundaries, and accelerated grain growth. Also noted, in a region of low barium concentration, was the appearance of twinned grains (brought out by metal evaporation or barium deposition) on the surface, although the material had not been heated into the gamma range. Purified calcium will be used to determine the degree of purification obtainable in large specimens. It is possible that sulfur (a major impurity, 10 ppm, in zone-refined iron) will also be eliminated by this process.

Purification of iron by lithium will also be attempted in collaboration with the Metallurgy Division. Decarburized capsules have been prepared for this purpose, and an important result will be a more positive determination of whether carbon, oxygen, or another element is responsible for the vigorous grain-boundary attack by lithium. The attack is commonly attributed to the presence of carbon, but the fact that attack can be minimized by a severe gamma quench, even after reheating to above 600°C,[2] suggests that the heat treatment results in a redistribution of oxygen rather than having any effect on the state of the carbon in the metal.

A series of preliminary internal-friction experiments (at about 1 cps) was conducted on a high-purity, vacuum-melted iron and on a zone-refined iron from 15 to 600°C at strain amplitudes of the order of 10^{-5} to 10^{-6}. The vacuum-melted iron gave curves typical of those in the literature. The zone-refined material differed in that (1) the background damping was at least a factor of 3 higher at room temperature; (2) the grain-boundary peak appeared to have some fine structure; (3) there were indications of small peaks not previously reported for iron; and (4) an increase in decrement with decreasing strain amplitude was observed below about 100°C when the material was cooled quickly from about 250°C. A thorough investigation of the internal-friction spectrum will be made up to 900°C when the data handling system described below is operating and a magnetic field is applied to reduce the magnetoelastic damping.

Approximately half the effort this year went into designing, building, and testing a data handling system in collaboration with T. A. Lewis of the Instrumentation and Controls Division. It had become obvious that data taking and reduction by hand and with conventional recorders was uneconomical where property measurements with many variables were to be made.

[1] R. G. Berggren, *Radiation Effects in Ferritic Steels*, TID-7588, pp 91–127 (October 1960).

[2] A. Herrold, P. Muller, and P. Albrecht, *Compt. rend.* 235, 658 (1952).

The data handling system consists primarily of programming, sequencing, and switching circuits; a high-speed digital voltmeter; a 1-Mc period or frequency meter; an ac-dc converter; a dc preamplifier for low-level signals; and a digital recorder. The dc voltages from 10 mv to 1000 v can be measured and recorded at the rate of five measurements per second, with an average accuracy of 0.05%. The ac voltages over the same range can be recorded with an accuracy of 0.2%. Analog clocks, feeding the digital voltmeter, allow times to be recorded in any units desired from the start of each individual experiment. The frequency meter will be used mainly for period measurements.

The main use of the apparatus will be for internal-friction measurements, where temperature, time, frequency, amplitude, and magnetic field strength can be programmed and recorded. Under these conditions the man power for obtaining and reducing data for each data point will be reduced by at least a factor of 10. Other measurements, such as electrical resistivity, creep, delay time, vacuum, power consumption, etc., can be easily programmed into the system.

The basic components of the system have been received, spot calibrated, tested for long-time stability, and operated in typical experimental apparatus to determine the effects of noise, alternating-current fields, and other sources of instability or inaccuracy. Most switching circuits are built or designed; the only missing major component is a "pulse stretcher," required for the measurement of peak amplitudes of internal-friction specimens.

11. SINGLE-CRYSTAL SPHERES OF COPPER, SILVER, AND GOLD GROWN FROM THE MELT

M. C. Wittels F. A. Sherrill J. O. Stiegler

Small spherical single crystals of copper, silver, and gold have been grown from the melt by use of the Bridgman technique with a slight modification. The modification consisted in the use of very small wires or fragments on a nearly flat graphite surface. Thus the droplets are free to grow without the external constraints of a crucible containment shell, and the growth is largely affected by the surface-tension properties of the material.

It has been shown[1] that any crystalline film or particle on the surface of the metal particle or droplet may catalyze crystal nucleation. This important factor was recognized in the studies[2,3] of metal droplets by microscopic methods. These latter studies were mainly concerned with the thermodynamics of metal crystallization in droplets ranging from 10 to 100 μ in diameter. Our studies have been concerned with the development of small, more perfect crystals, and the diameters of the spheres have ranged from $\sim$75 to 600 μ. Since it is virtually impossible to seed these small fragments with a single small impurity site to catalyze single nucleation, we have attempted to eliminate all such impurities by careful cleaning and handling, thereby avoiding multiple nucleation.

One of the advantages of crystals of this type is that they are ideal for conventional transmission x-ray diffraction studies, permitting the examination of the whole crystal mass rather than just surface layers. Another is that their size and spherical shape tend to minimize the imperfections that may be introduced through handling, and the inherent stresses are minimized as well. For radiation damage studies they also have the advantage of small mass, thereby reducing the problems of induced radioactivity.

[1] C. E. Mendenhall and L. R. Ingersoll, *Phil. Mag.* 15, 205 (1908).

[2] D. Turnbull and R. E. Cech, *J. Appl. Phys.* 21, 804 (1950).

[3] D. Turnbull, *J. Appl. Phys.* 21, 1022 (1950).

12. $Au_{0.82}Hg_{0.18}$: A TRANSMUTATION ALLOY

M. C. Wittels J. O. Stiegler F. A. Sherrill

Access to thermal-neutron fluxes in the range 10^{14} to 10^{15} neutrons cm^{-2} sec^{-1} in present-day reactors makes it possible to produce considerable numbers of nuclear transmutations in reasonable times. The gold-mercury alloy system[1] lends itself admirably to a study of the physical effects of a transmutation reaction, because a solid solution (face-centered cubic, fcc) exists at low concentrations of mercury and a new structure (hexagonal close packed, hcp) is formed with a composition Au_3Hg, containing 25 at. % Hg.

In an experimental facility of the Oak Ridge Research Reactor these compositions may be induced by thermal neutrons in gold through the transmutation reaction $Au^{197} + n \rightarrow Hg^{198}$, in only a few months of exposure time. The cross section (ref 2) for the reaction is 96 ± 10 barns, and fortunately Hg^{198} is a stable isotope; so no further secondary chemical species are produced to complicate the investigation. Mercury-199, produced through the transmutation of Au^{198} and by thermal-neutron capture by Hg^{198}, is also stable. In addition, the production of radioactive Au^{198} has the short half-life of 2.7 days, permitting safe handling of the material in about six weeks after removal from the reactor.

Small, spherical single crystals of gold, ranging from 0.003 to 0.025 in. in diameter, were grown[3] for this experiment so that the material could be examined by x-ray diffraction transmission techniques and therefore furnish information concerning the entire specimen, not just thin surface layers. The spherical shapes of the crystals also permitted a reasonable amount of handling without the dangers of inducing imperfections that are more likely to be induced in specimens having an anisotropic configuration.

The crystals were irradiated in a water-cooled test facility at 85°C, in a helium atmosphere. Cooling water made contact with the tube containing the crystals; the production of gamma heat was negligible in the small masses, as had been confirmed in numerous previous reactor experiments.

A series of x-ray diffraction patterns were taken of these single crystals before and after the reactor exposure so that a direct comparison could be made. It was first confirmed that the introduction of more than 15 at. % of Hg^{198} into the crystal lattice of gold did not destroy the long-range order, and the fcc structure was retained in a single-crystal, solid-solution matrix.

Figure 12.1 shows the superimposed single-crystal rotation diffraction patterns of a crystal before and after neutron irradiation. Identical reflections have been superimposed on the left edge of the film to emphasize the shift in lattice spacings as well as the retention of the fcc structure. From these photographs it was also evident that considerable line broadening accompanied the lattice dilatation and may partly result from possible fast-neutron damage.

Rocking curves of individual reflections confirmed the film observations that the line broadening was real, and from such curves in the back-reflection region a determination was made of the lattice expansion resulting from the growth of the solid solution. A typical set of rocking curves is shown in Fig. 12.2 for a pair of (400) reflections before and after irradiation. The peak intensities as shown in Fig. 12.2 are not directly comparable as seen, since an amplification factor of 4 had to be employed in the irradiated-crystal case to raise the peak intensity to a level comparable with the before-irradiation case. A lattice expansion of 1.29% was measured in the irradiated crystals, corresponding to a solid-solution[4] lattice containing 18 at. % Hg. This value also agrees to within ±5% with the value obtained through the measured thermal-neutron flux.

---

[1] M. Hansen, *Constitution of Binary Alloys*, p 207, McGraw-Hill, New York, 1958.

[2] D. J. Hughes and R. B. Schwartz, *Neutron Cross Sections*, BNL-325, 2d ed., GPO, Washington, 1958.

[3] M. C. Wittels and F. A. Sherrill, *Bull. Am. Phys. Soc.* 6, 352 (1961).

[4] F. Hund and H. Mosthaf, *Naturwissenschaften* 39, 209 (1952).

Since the mean free path for thermal neutrons in gold is considerably larger than the diameters of the small spheres used in this experiment, a nearly homogeneous distribution of Hg^{198} production was developed in the outer few-thousandths-inch thickness through which the x rays traveled. Severe strain in the surface layers was thus avoided, which would have resulted if larger concentrations of Hg^{198} were produced in a thin-layer skin less dense than the bulk specimen. A large resonance at 5 ev in the neutron cross-section curve for Au^{197} could also produce a similar effect, but the epithermal-neutron flux was several orders of magnitude lower than the thermal-neutron flux, and this difficulty, too, was avoided in the water-moderated Oak Ridge Research Reactor.

An $Au_{0.82}Hg_{0.18}$ solid-solution alloy, if formed from the melt,[1] freezes at about 400°C. By nuclear transmutation, an alloy of similar composition has been formed at 85°C in a single crystal.

Fig. 12.1. Single-Crystal Rotation X-Ray Diffraction Photographs of Gold Before and After Exposure to Thermal Neutrons (2.0×10^{21} neutrons/cm^2). [100] rotation axis, Cu$K\alpha$ radiation.

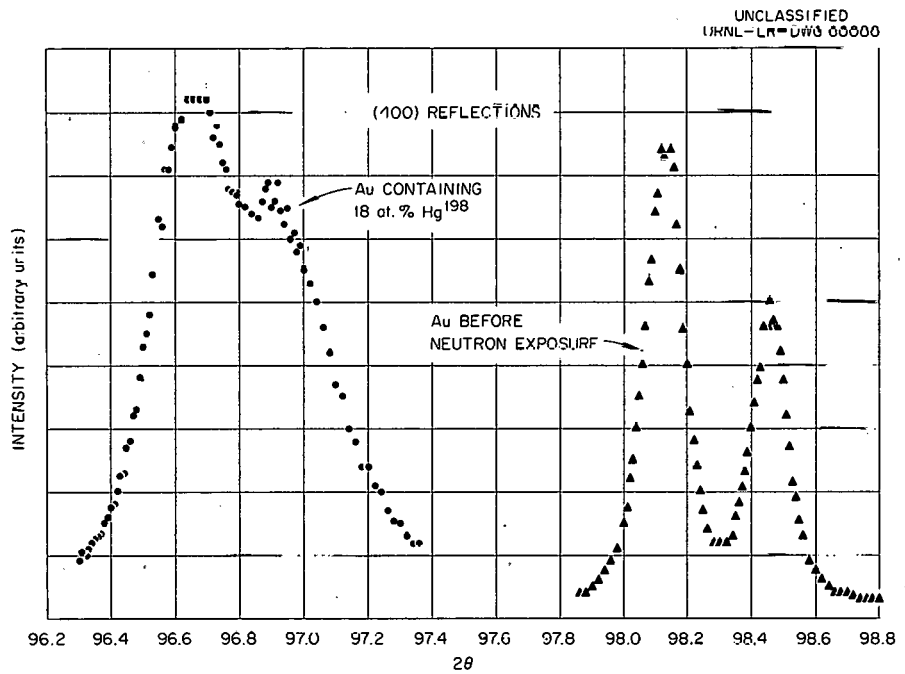

Fig. 12.2. (400) Reflections of Single-Crystal Gold Before and After Thermal-Neutron Exposure (2.0×10^{21} neutrons/cm^2).

13. ELECTRON MICROSCOPE STUDIES

T. S. Noggle J. O. Stiegler

FISSION-FRAGMENT TRACKS IN THIN FILMS OF UO_2, PLATINUM, AND PALLADIUM

Electron microscope studies of fission-fragment tracks in thin films of UO_2 previously reported[1,2] have been continued with the object of increasing the understanding of factors which determine the registration of tracks. The results have been reported,[3] describing modifications of experimental techniques which increase the information content of the tracks. From these studies it is deduced that appreciable displacement of material occurs by some process other than nuclear encounters or from thermal effects. Comparison of observations with theory indicates that track registration must occur predominantly from the energy lost by the fission fragments to the electronic system of the solid and that nuclear encounters at best can contribute only to a minor extent to track registration in the thin films. In view of this, it was suggested that appreciable displacement of atoms occurs as a consequence of multiple ionization and recoil by charge interaction of the atoms close to the fission-fragment path.

Extension of the studies to thin films of materials other than UO_2 showed that details of the track registration in metal films of platinum and palladium differ in important respects from those deduced for UO_2.[4] Figures 13.1, 13.2, and 13.3 show the microstructures of fine polycrystalline evaporated films of 25-, 100-, and 200-A-thick palladium after irradiation with an external source of fission fragments. The changes with increasing thickness from light to dark to no track contrast which are to be noted in these photomicrographs are interpreted in terms of thermal processes. The light tracks are believed to arise from vaporization, while the dark tracks represent melting and resolidification *in situ*. The absence of tracks in the thicker films (200 A and greater) is believed to be due to an insufficient energy density in the region of paths of the fission fragments to give detectable changes in the films. Progressive changes with thickness such as this have not been observed in thin films of UO_2, and the behavior of the metal films is thought to arise from energy transport by the free electrons in the metal. A theoretical treatment by Ozeroff,[5] in which the electron excitation energy

Fig. 13.1. Fission-Fragment Tracks in 25-A-thick Palladium Film. 50,000X.

[1] T. S. Noggle and J. O. Stiegler, *Solid State Div. Ann. Progr. Rept. Aug. 31, 1960*, ORNL-3017, p 50.

[2] T. S. Noggle and J. O. Stiegler, *J. Appl. Phys.* 30, 2199 (1960).

[3] T. S. Noggle and J. O. Stiegler, *Fission Fragment Tracks in UO_2*, presented at 1961 Symposium on Radiation Effects, American Society for Testing Materials, Atlantic City, N.J., June 1961.

[4] T. S. Noggle and J. O. Stiegler, "Fission Fragment Tracks in Metal Films," submitted for publication to the *Journal of Applied Physics*.

[5] J. Ozeroff, *Atomic Displacements Produced by Fission Fragments and Fission Neutrons in Matter*, KAPL-205, p 22 (June 1949).

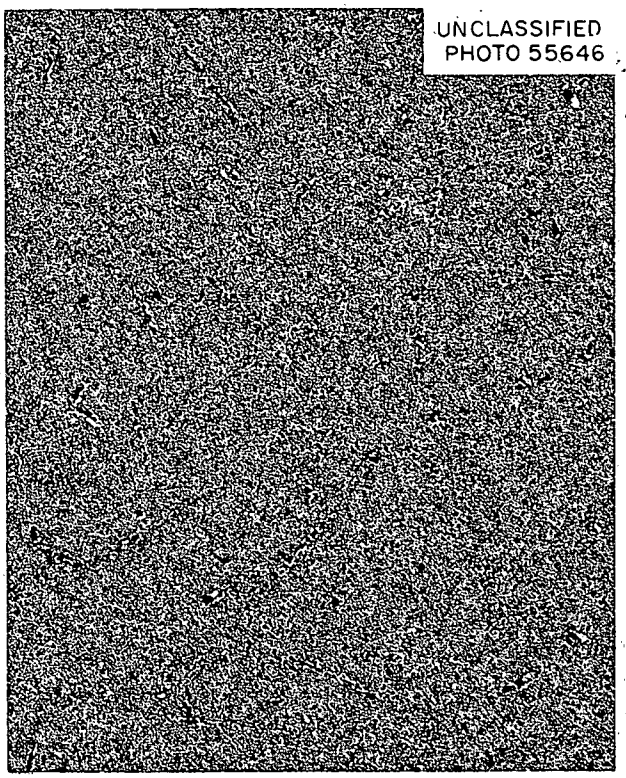

Fig. 13.2. Fission-Fragment Tracks in 100-A-thick Palladium Film. 50,000X.

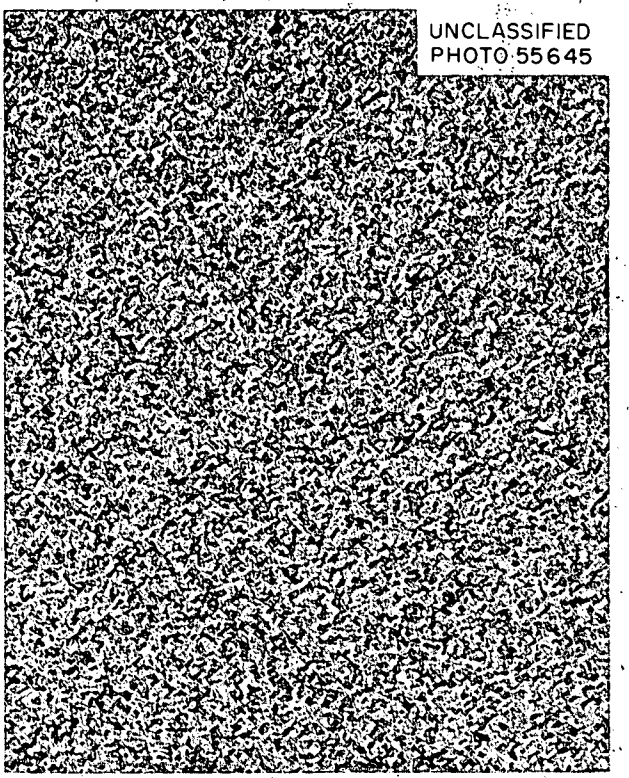

Fig. 13.3. 200-A-thick Palladium Film After Fission-Fragment Irradiation. 50,000X.

left in the wake of the fission fragment is transferred to the free electrons of the metal, gives a model which is in qualitative agreement with these observations. According to this model, the energy lost by the fission fragment to the electronic system of the solid appears as thermal energy within a cylindrical region several hundred angstroms in diameter. The energy density over this volume would be too low to melt or vaporize an appreciable fraction of the atoms in this region. However, as the film thickness becomes less than the diameter of the region in which the thermal energy may appear, the energy density will increase, since the slightly energetic free electrons carrying the energy will be constrained to the metal film and will give up their energy to the lattice in about the same distance as formerly. Thus, melting and vaporization will occur in the thinner films when the energy density is sufficient for these processes to occur to an appreciable extent.

This effect would be expected to occur only in metals and suggests that in bulk metals the electron transport of energy tends to reduce the intensity of thermal energy in the fission spike, thus minimizing irreversible thermal effects in fission damage of metals.

NITROGEN-ION BOMBARDMENT OF THIN FILMS OF PLATINUM AND UO_2

Cyclotron irradiations of platinum films (~25 A thick) and UO_2 films with 24-Mev nitrogen ions were carried out, and tracks were observed in the platinum films but not in the UO_2 films. The tracks in the platinum films are quite narrow, 25 to 50 A wide, compared with the ~400-A-wide tracks produced by fission fragments in identical films.

These observations suggest that track registration by the nitrogen ions occurs by a different mechanism than that which dominates with fission fragments in platinum. The absence of tracks in

the UO_2 (which, however, is modified in texture by the irradiation) cannot now be explained but may represent some aspects of film preparation (e.g., thickness) which limits the sensitivity in this case. Consideration of the rate of energy loss of the nitrogen ions in the platinum[6] suggests that this energy distributed over a volume extending 100 to 200 A from the ion path (as in the case of fission fragments in metal films) would not give an energy density sufficient to produce light tracks by volatilization. Therefore the tracks in the platinum are probably not basically due to thermal phenomena but to some displacement process possibly arising from charge separation, as has been suggested for the case of fission-fragment tracks in UO_2 (ref 3). These observations are as yet only preliminary, and further work is required before more definite conclusions can be made as to the detailed nature of the mechanism of track registration.

[6]Energy-loss rates of nitrogen ions have been measured in nickel by H. L. Reynold, D. W. Scott, and A. Zucker, *Phys. Rev.* 95, 671 (1954); energy-loss rates in nickel and gold have been measured by C. B. Fulmer, *Fission Fragment Studies by Magnetic Analysis*, ORNL-2320, (1959). It is assumed that the loss rate in platinum is about equal to that in gold and that the ratio of loss rates for fission fragments in gold and nickel is approximately equal to that for nitrogen ions.

14. Ar^+ ION BOMBARDMENT OF SOLID SURFACES (COPPER, GERMANIUM, AND INDIUM ANTIMONIDE)

A. L. Southern M. T. Robinson
D. R. Burrowbridge[1] W. R. Willis[2]

SPUTTERING YIELDS

One result of bombarding a solid surface with a beam of energetic ions is physical sputtering or "erosion" of the solid. The usual measure of this effect is the sputtering yield S, defined as the number of target atoms removed for each incident ion. Sputtering yield is a function of the target material and its crystalline state, the nature and energy of the ion, and the angle of incidence of the ion beam onto the target.

Yields are reported here for Ar^+ ions of normal incidence upon polycrystalline and monocrystalline copper and upon monocrystalline germanium. In all cases S has been determined as a function of beam energy in the range from 1 to 5 kev.

A description of the ion source and accelerating equipment and of the general experimental technique may be found in a previous report.[3] The earlier report contains a discussion of instrument errors and variations in beam energy and concludes that ±5% is the maximum variation of S due to these sources of error.

The copper targets were produced from American Smelting and Refining Company 99.999% copper. The polycrystalline target was cut from rolled sheet and then etched with nitric acid. The single crystals were polished on an acid polisher,[4] cleaned with a solution of equal parts of nitric, phosphoric, and glacial acetic acids, and then electropolished. The germanium target was cut from a single crystal of high purity and was then etched.

Figure 14.1 shows the sputtering yield as a function of energy for polycrystalline and monocrystalline copper. Figure 14.2 compares the sputtering yield of two crystals which were 10 and 12° away from (100) with that of a (100) crystal. Figure 14.3 (ref 5) shows the values of S obtained for polycrystalline copper by other workers. There seem to be two more-or-less distinct series of results, one from the data of

[1]Co-op student from Virginia Polytechnic Institute.

[2]Consultant, Department of Physics, West Virginia Wesleyan College, Buckhannon.

[3]A. L. Southern *et al.*, *Solid State Div. Ann. Progr. Rept. Aug. 31, 1960*, ORNL-3017, p 52.

[4]F. W. Young, Jr., and T. R. Wilson, *Rev. Sci. Instr.* 32, 559 (1961).

[5]Most of Fig. 14.3 was taken from a personal communication from D. E. Harrison, Jr.

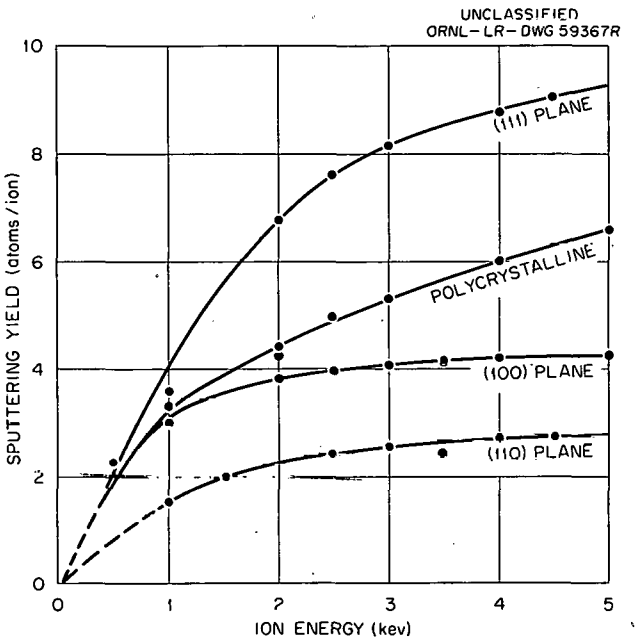

Fig. 14.1. Sputtering Yield vs Ion Energy for Poly- and Monocrystalline Copper Bombarded with Argon Ions at Normal Incidence.

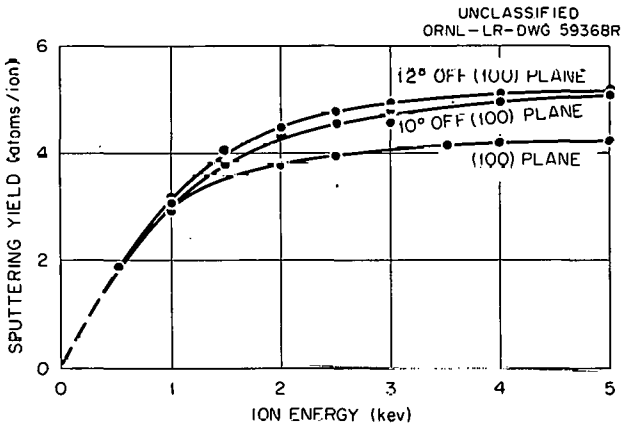

Fig. 14.2. Sputtering Yield vs Ion Energy for Copper Bombarded with Argon Ions at Normal Incidence.

European workers and the other obtained in this country, differing by more than the quoted experimental errors.

A search for sources of unresolved error in our work led to a study of the effect of species other than Ar^+ in the ion beam. It is known that the extracted beam contains both neutral argon atoms and doubly charged argon ions. Since a

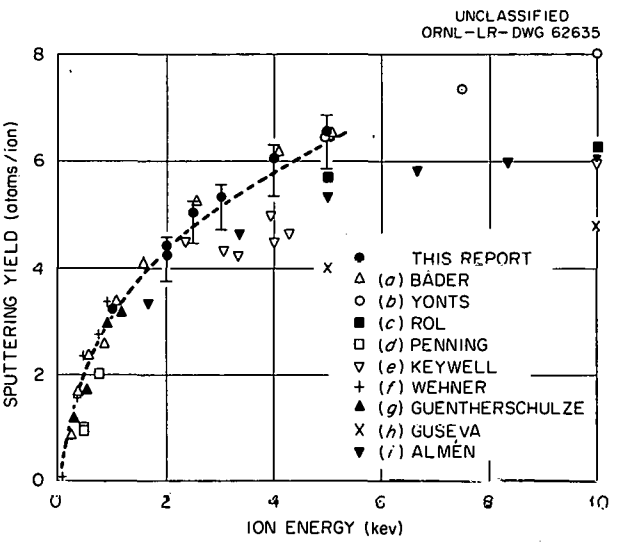

Fig. 14.3. Sputtering Yield vs Ion Energy for Polycrystalline Copper Bombarded with Argon Ions at Normal Incidence. (*a*) M. Bader, F. C. Witteborn, and T. W. Snouse, Tech. Rept. A-105, Ames Research Center, NASA, Moffett Field, California. (*b*) O. C. Yonts, C. E. Normand, and D. E. Harrison, *J. Appl. Phys.* 31, 3447 (1960). (*c*) P. K. Rol, J. M. Fluitt, and J. Kistemaker, *Physica* 26, 1000 (1960). (*d*) F. M. Penning, *Physica* 4, 71 (1937). (*e*) F. Keywell, *Phys. Rev.* 97, 1611 (1955). (*f*) N. Laegreid and G. K. Wehner, *Trans., Nat. Symposium on Vacuum Technol., 6th, 1959*, p 164. (*g*) A. Güntherschulze, *Vacuum* 3, 360 (1953). (*h*) M. I. Guseva, *Soviet Phys. Solid State* 1, 1410 (1960). (*i*) O. Almén and G. Bruce, *Nuclear Instn & Methods* 11, 257 (1961).

rough calculation indicated that there could be ~20% neutral atoms, a series of four experiments was performed to measure their effect. These atoms would cause sputtering without contributing to the beam current and would thus lead to a high value of S. The first of the four experiments was a normal sputtering measurement at 2.0 kev. The next three experiments were performed with the same technique except that the ion beam was deflected from the target by a counterfield lens and/or a permanent magnet. Analysis of these experiments shows that the neutral content of the beam contributes less than 10% and probably about (4 ± 3)% to the sputtering yield. The dashed line in Fig. 14.3 shows the results of our work corrected for the effect of neutral atoms and also shows the experimental uncertainty of ±8%.

Experience with the rf ion source indicates that there could be 5 to 6% (ref 6) Ar^{2+} in the extracted beam. The effect of the lens and wiping iris system would be to remove Ar^{2+}, so that considerably less than the above amount would strike the target. The Ar^{2+} striking the target would tend to give a lower value to S in the 1- to 5-kev energy region, although the relative change in the yield would not be as great as the relative amount of Ar^{2+} in the beam. It is believed that the presence of Ar^{2+} ions is not a significant source of error.

If the argon deposited in the target is removed only by sputtering away the surface layer, then the steady-state ratio of argon atoms to copper atoms in the irradiated volume is the reciprocal of the sputtering yield. Since the range of argon in copper is small at these energies and the rate of removal of a monolayer is high, the above assumptions are reasonable. Almén[7] found an inverse relation between S and the amount of beam material retained in the target. The material being sputtered would therefore contain from 10 to 30 at. % argon. The volume being sputtered is low enough that no appreciable effect on the loss of weight, and thus the sputtering yield, is to be expected from retained argon. However, any considerations involving the surface geometry of the crystal would be affected (see next section, "Atom Ejection Patterns"). It is interesting to note that the flux of argon ions in our experiment is $\sim 10^{14}$ to 10^{15} ions sec^{-1} cm^{-2}. At 5 kev each of these would produce about 100 displaced copper atoms,[8] giving them damage rates that are very much greater than those caused by the neutron irradiation of copper in the ORR.

Figures 14.1 and 14.2 show that there is a marked difference in sputtering yield for different crystal orientations. Rol *et al.*[9] found such a variation by changing the angle of incidence of the ion beam on a crystal face. Using a hard-sphere model for the crystal, the apparent atom density varies when the model is projected on different crystal faces. For face-centered (fcc) metals the order of decreasing density of the principal planes is (111), (100), (110), which is the order of the yield seen in Fig. 14.1. The data shown in Fig. 14.2 are also compatible with these ideas. For the germanium lattice the simple model predicts the order of decreasing yield to be (100), (111), (110). Figure 14.4 gives the sputtering yield as a function of energy for germanium monocrystals with these orientations.

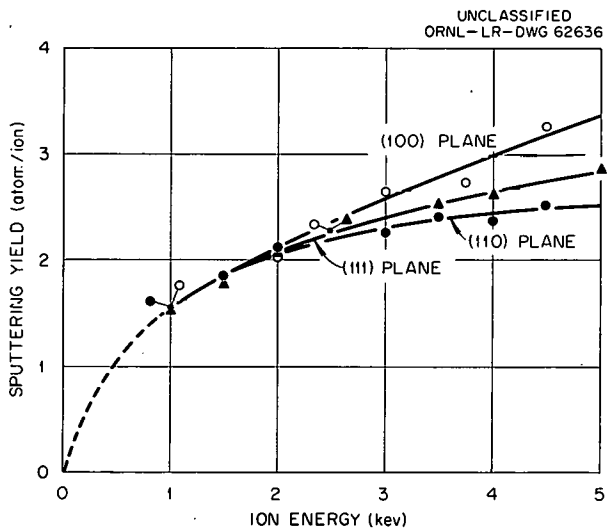

Fig. 14.4. Sputtering Yield vs Ion Energy for Germanium Bombarded with Argon Ions at Normal Incidence.

ATOM EJECTION PATTERNS

Several workers[10] have noted that material sputtered from the surface of a monocrystal is ejected in preferred directions, which seem to be the directions of closest packing in the crystal. Ejection of the material in these directions occurs up to at least 50 kev and has also been noted with material ejected from the back side of a gold target.[11] This phenomenon is believed to occur as a result of momentum

[6] Personal communication from P. H. Stelson.

[7] O. Almén and G. Bruce, *Nuclear Instr. and Methods* 11, 257 (1961).

[8] D. S. Billington and J. H. Crawford, Jr., *Radiation Damage in Solids*, Princeton University Press, 1961.

[9] P. K. Rol *et al.*, p 17 in *Proceedings of the Fourth International Conference on Ionization Phenomena in Gases*, August 1959.

[10] G. K. Wehner, *Phys. Rev.* 102, 690 (1956); K. Koedam, thesis, State Univ. Utrecht, March 1961; V. E. Yurasova, N. V. Pleshivtsev, and I. V. Orfanov, *J. Exptl. Theoret. Phys. (USSR)* 37, 996 (1959); R. S. Nelson and M. W. Thompson, *Proc. Roy. Soc. (London)* A259, 458 (1961).

[11] M. W. Thompson, *Phil. Mag.* 4, 139 (1959).

transfer within the crystal by a focusing-collision mechanism.[12] We have obtained atom ejection patterns for material sputtered from (100), (110), and (111) faces of copper monocrystals, from several copper surfaces not aligned with principal directions, and from a (111) face of an InSb monocrystal. Patterns with structure could not be obtained for germanium crystals in the energy range studied.

The equipment used to measure sputtering yields was modified so that the collector plate could be mounted in the target area and so that the angle of incidence of the beam could be adjusted. Figure 14.5 shows the target holder used. The collector plates were Pyrex glass disks, drilled in the center to allow the beam to pass. In some cases these were coated with palladium in an attempt to prevent surface migration of the depositing material. To keep the plate from charging to a high voltage, the back was covered with a mica disk, and, in some cases, a grounded tungsten screen was mounted on the mica.

Figures 14.6 and 14.7 show atom ejection patterns obtained for (100) and (111) faces of copper monocrystals. Figure 14.8 shows the pattern for a crystal cut 6° off (100) so that the normal to the face moves from [100] toward [111]. Here the central [100] spot is visible, and the four [110] spots have shifted in a manner predictable from the geometry of the crystal. It is obvious from the figure that the spot intensity depends upon the angular displacement from the crystal normal.

The placement of these spots on the horizontal plane is in all cases consistent with the known orientation of the crystal, found by x-ray analysis. If the angular distance of the spot from the crystal normal is measured, however, there is a systematic discrepancy. These measured angles are less than the ones expected from the crystal geometry. Since material is ejected from the surface at angles near the central angle of the spot, the beam of particles from the surface forms a cone with a small open angle ($\sim 12°$). This cone intersects the collector plate in an ellipse so that the center of the ellipse is not the axis of the cone. This, however, would lead one to measure an angle that is larger than the expected value. There seems to be no doubt that the atoms are ejected at angles less than the expected value. If it is assumed that the surface layers of the crystal are separated slightly along the normal because of argon retained in the structure, then the close-packed direction of the crystal would shift closer to the normal. It might be equally well assumed

[12] R. H. Silsbee, *J. Appl. Phys.* 28, 1246 (1957); G. Leibfried, *J. Appl. Phys.* 31, 117 (1960).

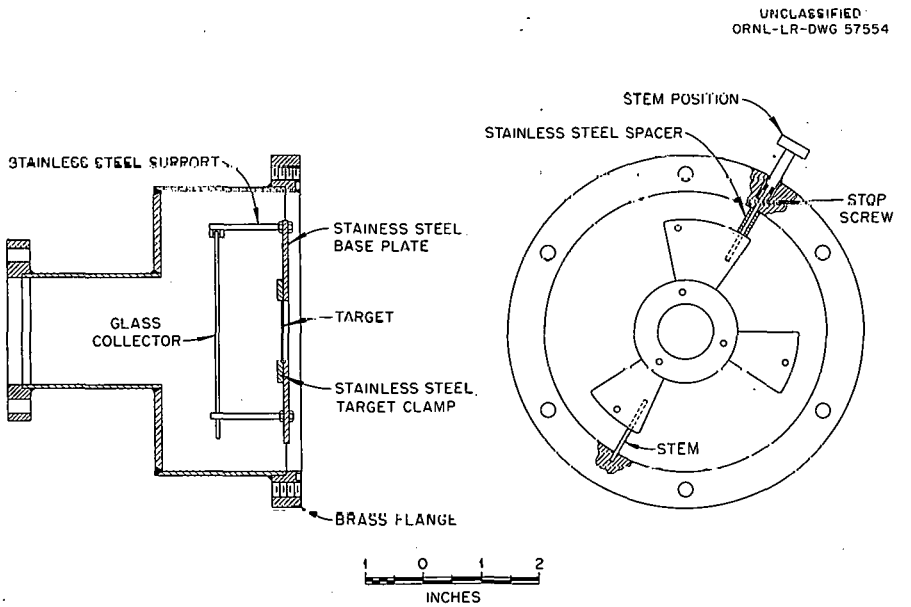

Fig. 14.5. Atom Ejection and Collector Plate Holder.

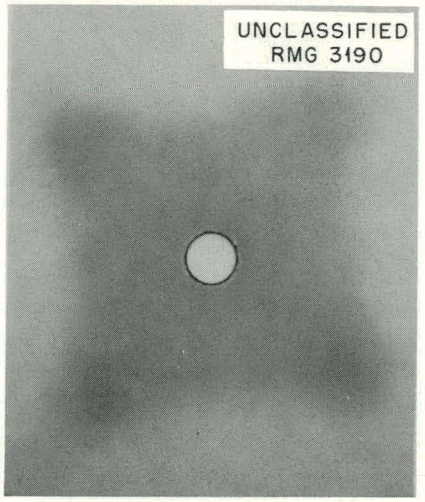

Fig. 14.6. Atom Ejection Pattern for Copper (100) Plane Bombarded with 2.5-kev Argon Ions at Normal Incidence.

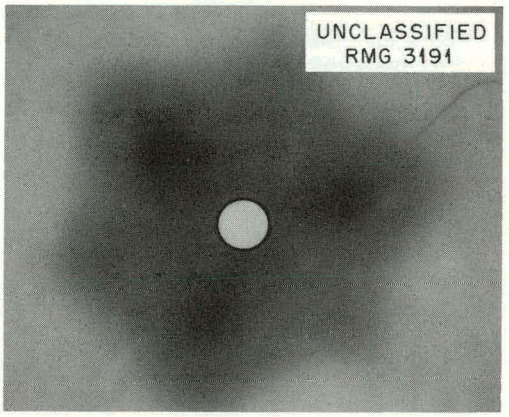

Fig. 14.7. Atom Ejection Pattern for Copper (111) Plane Bombarded with 2.5-kev Argon Ions at Normal Incidence.

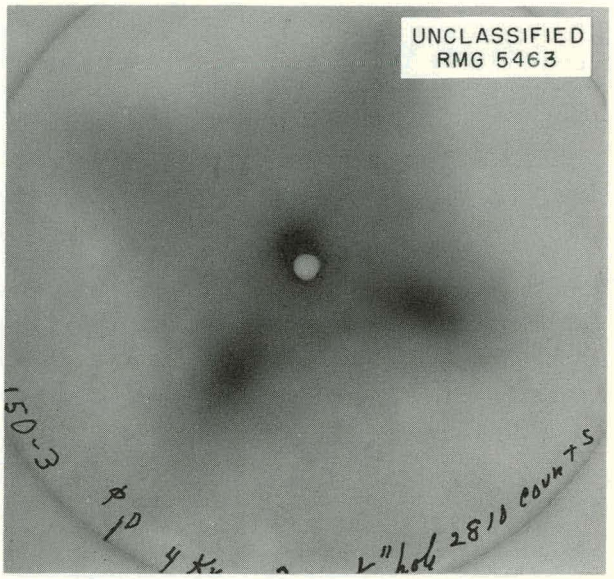

Fig. 14.8. Atom Ejection Pattern for Copper (100) Plane 6° Toward (111) Bombarded with 4.0-kev Argon Ions at Normal Incidence.

that surface forces decrease the interatomic spacing in the surface layer.

The pattern obtained for InSb did not reproduce well and is omitted. Spots were found with the expected symmetry but were "negative," that is, lighter than the general background. When a model of this crystal is studied, along the [110] directions can be seen two lines of atoms lying close together. Interference between these two lines leads to an "antifocus" of momentum along [110]; consequently, sputtering in this direction is less than the general background. This lack of efficient propagation chains toward the surface could also explain the low sputtering yields of germanium, compared with copper, in which the double lines do not occur.

THIS PAGE

WAS INTENTIONALLY

LEFT BLANK

Part III

NONMETALS

THIS PAGE

WAS INTENTIONALLY

LEFT BLANK

15. SEMICONDUCTOR STUDIES AND STUDIES OF INSULATORS

CURRENT RECOMBINATION AND ANNEALING STUDIES

O. L. Curtis, Jr. S. Othmer[1]

Although a rather extensive study[2] of carrier recombination processes in germanium was made recently, it has been felt that in several areas more detailed exploration would be desirable. For instance, a quantity which needs more careful determination is the activation energy for annealing of recombination centers. In order to make this determination, a number of isothermal anneals have been made with 1.4-ohm-cm antimony-doped germanium. Figure 15.1 displays typical annealing curves. It is observed that, following an early transient, first-order kinetics are exhibited. This behavior is typical of a diffusion-controlled reaction.[3] The rate constant obtained from the linear portion of such curves is plotted as a function of reciprocal temperature in Fig. 15.2. From these data an activation energy of 0.76 ev is obtained. This result is surprising in view of earlier results,[2] which seem to indicate that annealing of recombination centers occurs through the diffusion of vacancies. (The activation energy for motion of a vacancy has been determined to be 1.0 ev.[4]) Furthermore, the value of 0.76 ev (activation energy) obtained here is quite close to the value obtained from an analysis of annealing data at lower temperatures by Brown, Augustyniak, and Waite,[5] and by J. C. Pigg (this report). It is evident that additional data on other specimens must be obtained before final conclusions are drawn. It may be that different apparent activation energies are obtained, depending upon the individual specimen.

It was found in our recent studies[2] that very interesting recombination behavior is observed in certain specimens below 0°C. This behavior was explained[2] on the basis of the interactions between recombination and trapping levels. It would appear useful to study this behavior at still lower temperatures. Figure 15.3 shows some of our first attempts to do so. This figure, which shows lifetime plotted logarithmically as a function of

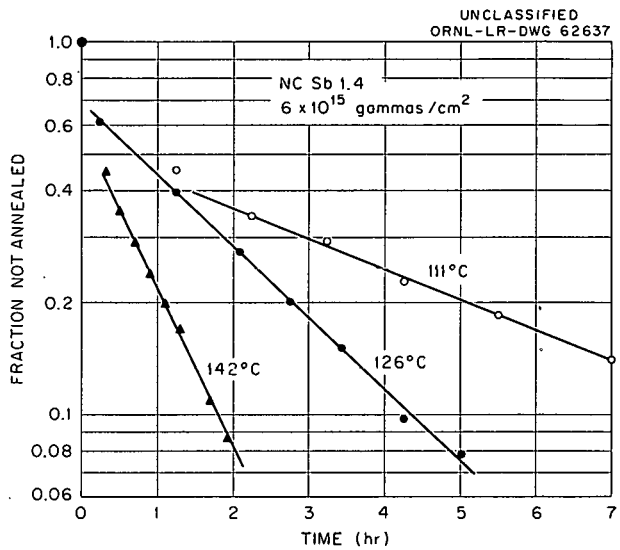

Fig. 15.1. Isothermal Annealing of 1.4 ohm-cm, Antimony-Doped Germanium Following Co^{60} Gamma Irradiations.

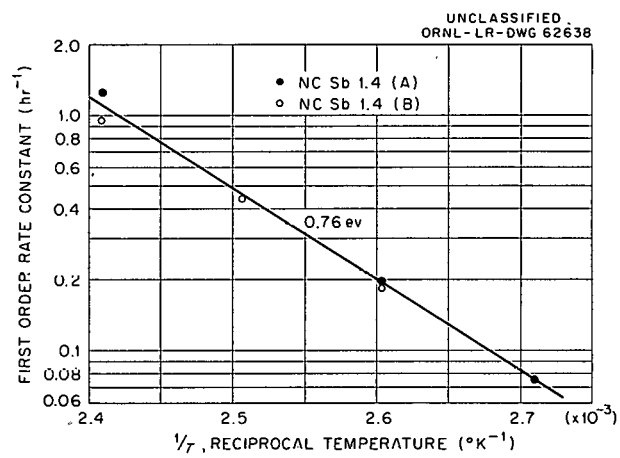

Fig. 15.2. First-Order Rate Constants as Obtained from Isothermal Anneals for 1.4 ohm-cm, Antimony-Doped Germanium as a Function of Reciprocal Temperature.

[1] Co-op student from Virginia Polytechnic Institute.

[2] O. L. Curtis, Jr., and J. H. Crawford, Jr., *The Carrier-Recombination Behavior and Annealing Properties of Radiation-Induced Recombination Centers in Germanium*, ORNL-3108 (May 15, 1961).

[3] Howard Reiss, *J. Appl. Phys.* 30, 1141 (1959).

[4] H. Letaw, Jr., W. M. Portnoy, and L. Slifkin, *Phys. Rev.* 102, 636 (1956).

[5] W. L. Brown, W. M. Augustyniak, and T. R. Waite, *J. Appl. Phys.* 30, 1258 (1959).

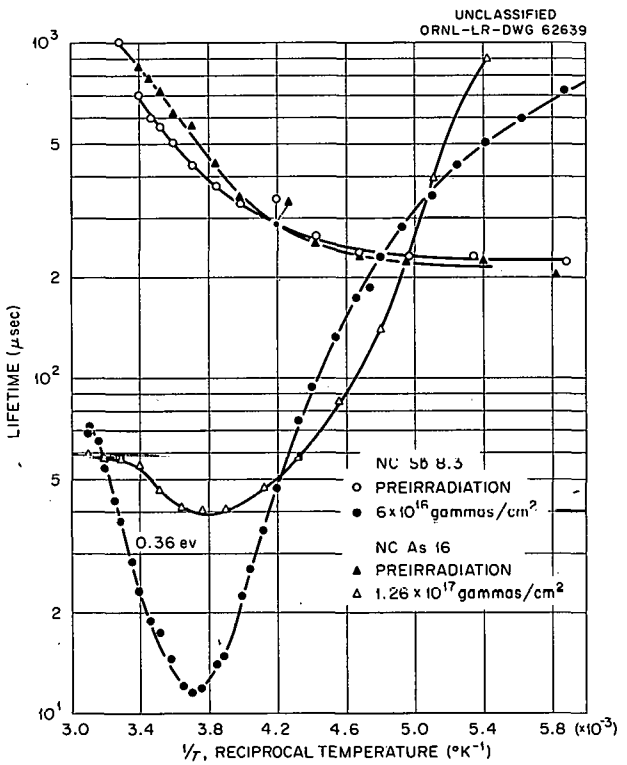

Fig. 15.3. Recombination Behavior of High-Resistivity Antimony- and Arsenic-Doped Germanium Following Irradiations by Co^{60} Gamma Rays.

reciprocal temperature, displays very interesting behavior. The large increase in lifetime at low temperatures, while the photoconductivity decay remains exponential, should provide a useful means of studying trapping centers. The behavior observed in Fig. 15.3 is typical of high-resistivity arsenic- and antimony-doped materials; however, lower-resistivity specimens display markedly different behavior.[2] No attempt will be made to interpret these data in detail until additional samples can be investigated.

RECOMBINATION STUDIES

O. L. Curtis, Jr. J. H. Crawford, Jr.

A rather complete treatment of this work has been given in the form of an ORNL report, the abstract of which follows. In addition, an abstract of a paper presented at a conference and to be published in the proceedings is included, as well as the abstract of another paper which has been submitted for publication.

The Carrier-Recombination Behavior and Annealing Properties of Radiation-Induced Recombination Centers in Germanium[6]

An investigation has been made of the carrier-recombination behavior and annealing properties of radiation-induced recombination centers in germanium. In order to analyze the recombination behavior, it has been necessary to treat the problem of recombination in the presence of trapping. A model which explains the experimental results in both *n*- and *p*-type material for various sorts of irradiation is presented. On the basis of this model, recombination occurs at an energy level 0.36 ev above the valence band in gamma-irradiated, *n*-type germanium. The position of this level is shifted slightly downward for neutron-irradiated material. Trapping levels occur in arsenic-doped germanium 0.17 ev above the valence band which are not present in antimony-doped material. An energy level apparently present in unirradiated material acts as a trapping center in *p*-type germanium. It is difficult to obtain a value for capture cross sections, but under certain assumptions a value for the electron capture cross section in *n*-type material is obtained: 7×10^{-19} cm^2. The annealing behavior of antimony-doped germanium is grossly different from that of arsenic-doped material. Although the annealing behavior is rather complicated, the results are consistent with the following model. Irradiation produces three major types of defects: interstitials, vacancies, and vacancy-interstitial pairs. The vacancy-interstitial pair evidently is responsible for a trapping level located 0.25 ev above the valence band. Both the interstitial and vacancy act as acceptors. The recombination level at 0.36 ev belongs to the vacancy. The interstitial becomes mobile above room temperature and either anneals or forms a complex with an impurity atom. It is thought that the trapping level located 0.17 ev above the valence band might be due to an arsenic-interstitial pair. The activation energy of motion for the interstitial is about 0.8 ev. At a somewhat

[6] Abstract of ORNL-3108 (May 15, 1961).

higher temperature the vacancy becomes mobile with an activation energy of motion of approximately 1.1 ev. In antimony-doped material the vacancy disappears by association with an antimony atom. This process does not occur in arsenic-doped material, and higher temperatures are required to produce annealing.

Carrier Recombination and Trapping Processes in Irradiated Germanium[7]

An investigation has been made of the carrier-recombination process in irradiated germanium. In order to analyze the recombination behavior, it has been necessary to treat the problem of recombination in the presence of trapping. A model which explains the experimental results in n-type material for various sorts of irradiation is presented. On the basis of this model, recombination occurs at an energy level 0.36 ev above the valence band in gamma-irradiated germanium. The position of this level is shifted slightly downward for neutron-irradiated material. Trapping levels which are not present in antimony-doped material occur in arsenic-doped germanium 0.17 ev above the valence band.

Radiation-Induced Recombination and Trapping Centers in Germanium. I. The Nature of the Recombination Process[8]

Extensive measurements on irradiated germanium indicate that previous analyses of the recombination process are incorrect. A model which explains the observations in both n- and p-type material is presented. According to this model, the recombination level lies 0.36 ev above the valence band in gamma-irradiated n-type germanium. Presumably due to the extensive perturbation caused by neutron irradiation, the level lies slightly lower in neutron-irradiated material. Trapping levels which are not present in antimony-doped germanium occur in arsenic-doped material $\sim$0.17 ev above the valence band. Other trapping levels are observed only in high-resistivity antimony-doped samples. It has not been possible, from the data presented, to determine the values of hole and electron capture cross sections associated with the recombination level; however, the ratio σ_p/σ_n has been determined: its value is $\sim$1000. The results for p-type material can be explained on the basis that energy levels present in unirradiated material act as traps.

THERMOELECTRIC POWER IN GERMANIUM

O. E. Schow

The measurement of the Seebeck coefficient usually is accomplished by one of two experimental methods. The first of these is the equilibrium method, which involves the manual manipulation of a potentiometer as the sample parameters are held relatively constant. This method yields a high degree of accuracy and has been reported previously.[9]

The second method is the dynamic measurement of the sample parameters by automated techniques. The dynamic method requires modest concessions in accuracy but is much faster and gives a more complete picture of the temperature range of interest. The sample is heated slowly at a uniform rate. The linearity of the heating rate is assured by the use of a special linearized -200 to $+100$°C copper-constantan slidewire in a Leeds and Northup program controller. Linearity is important due to minor differences in the thermal masses of the sample holder.

For measurements of small temperature gradients, microvolt amplifiers are required so that multipoint strip-chart recorders may be used. A Keithley model 149 millimicrovoltmeter is used to amplify the output from the differential thermal pile. Full scale sensitivity is $\pm$100 mμv. The voltage generated in the copper-germanium thermal element is amplified by a Keithley model 150-R microvoltammeter whose input impedance is higher by a factor of 10 than that of the model 149. Sample loading effects are thus minimized. These amplifiers must have stable gain and zero drift characteristics. They are powered from a regulated voltage source, $\pm$0.01% maximum deviation. The laboratory has a double-door air lock for entrance, and the temperature can be maintained to $\pm$0.03°C. The amplifiers are further thermally isolated by being mounted in a sealed relay rack with a $\frac{3}{4}$-in.

[7] Abstract of paper presented at the General Discussion of the Faraday Society, "Radiation Effects in Inorganic Solids," Saclay, France, Apr. 11–12, 1961.

[8] Abstract of paper submitted for publication in the *Physical Review*.

[9] O. E. Schow, *Solid State Div. Ann. Progr. Rept. Aug. 31, 1960*, ORNL-3017, pp 69–72.

Plexiglas front. Counterflow forced-air circulation within the sealed rack is used to prevent local heating and subsequent damage to the electronic components.

The gain accuracy and stability are verified by measuring stable microvolt input signals to the amplifiers with a Rubicon six-dial Thermofree potentiometer and simultaneously measuring the output produced by these signals.

The Rubicon potentiometer is scheduled for complete verification of its calibration by the ORNL Instrumentation and Controls Division. Consideration is being given to converting an unused range of the potentiometer so that the smallest voltage increment will be 10^{-9} v. The residual emf in the potentiometer is 2×10^{-9} v and seems to be quite stable.

Calibration of the differential thermal pile for 0°C ΔT is obtained by heating the appropriate end of the sample until the output of the copper-germanium couple is zero. The calibration technique is valid only so long as the Seebeck coefficient does not pass through zero in the temperature range in question. Figure 15.4 is a typical calibration curve for the thermal pile.

The measurement of the Seebeck coefficient is usually two or more temperature scans at ΔT values of 0.2 and 2.0°C in the normal direction of heat flow. The direction of heat flow is then reversed, and two or more scans are made at 0.1 and 0.5°C. This sequence of measurements gives some needed information as to the presence of barriers and as to the magnitude of the impurity gradient. This information is quite important in radiation damage studies, as the homogeneity of the radiation field is always a problem. There is a thermoelectric effect, Benedict's effect, which is dependent upon the temperature gradient. According to some experimental work by Trousil,[10] the contribution should be only 0.06% of our values, and this has not been detected in our experiments.

Two gamma irradiations have been made on 2-ohm-cm *n*-type germanium to date. Analysis is complete on only the first of these. Figure 15.5 shows the per cent change, due to irradiation, of the Seebeck coefficient, Hall mobility, and carrier concentration. A Hall plate from the original ingot was used to obtain the data on mobility and carrier concentration.

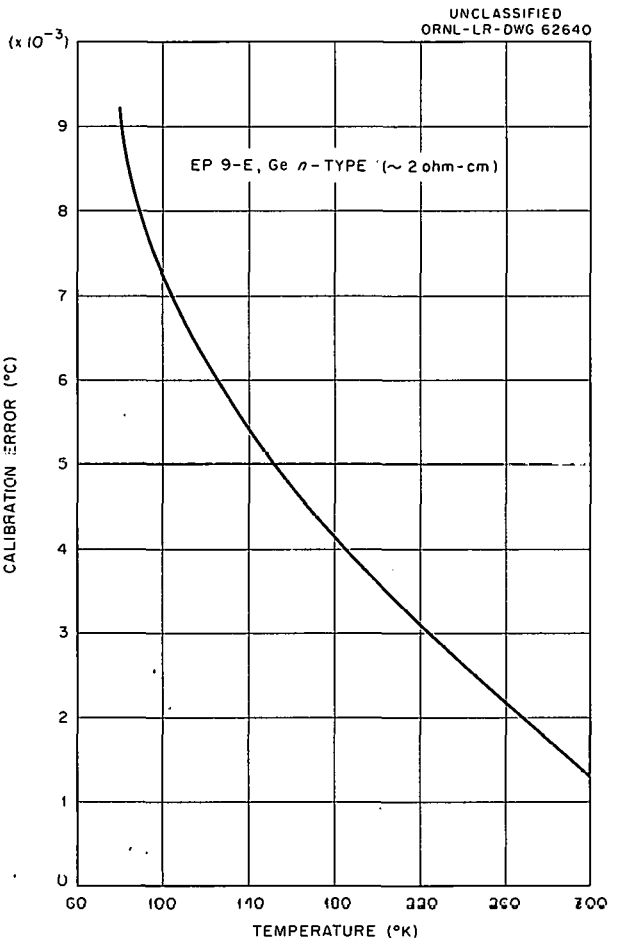

Fig. 15.4. Calibration Error of Differential Thermal Pile as a Function of Temperature.

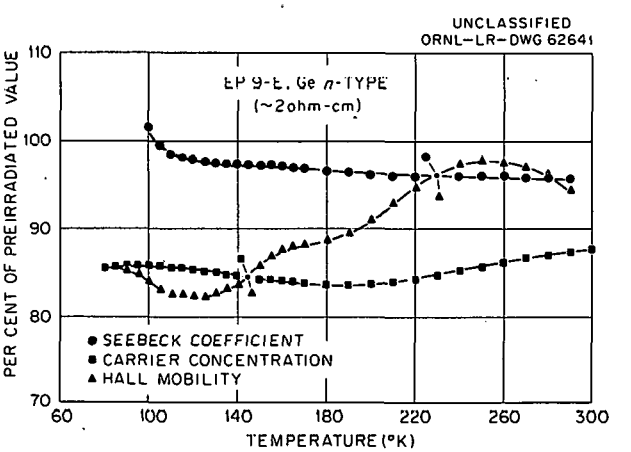

Fig. 15.5. Change of Sample Parameters Due to Co^{60} Photon Irradiation (2×10^{17} photons/cm^2) as a Function of Temperature.

[10] Z. Trousil, *Czechoslov. J. Phys.* 6, 170 (1956).

GAMMA IRRADIATION OF SILICON

L. C. Templeton E. Sonder

Effect of Oxygen Content in *n*-Type Silicon

Irradiations have been continued and the electrical properties of floating-zone-grown *n*-type silicon have been measured to obtain rates of introduction of trapping levels. Previously, a net acceptor level at 0.17 ev had been found in oxygen-containing pulled material.[11] Another had been found 0.47 ev below the conduction band,[12] in material grown by a vacuum floating-zone technique to remove oxygen. Recently, spin resonance measurements on electron-bombarded silicon have shown[13] that a center composed of a vacancy and an oxygen atom loses its paramagnetism when the Fermi level drops through the 0.17-ev level. Furthermore, three different centers were noticed which lost their paramagnetism when the Fermi level *rose* through ~0.4 ev. One of these was postulated to be a combination of a vacancy and a phosphorus donor.

The data summarized in Table 15.1 are of interest in relation to the models of the centers suggested. Comparison of the damage introduction properties of the pulled and floating-zone samples shows immediately that the deep level is generally introduced more quickly in the oxygen-free material. Moreover, the deep-level introduction rate increases when the doping (phosphorus) concentration is greater. The fact that, except for the case of one sample, the introduction of the 0.17-ev level seems to be independent of the oxygen content appears at first to contradict the theory that the oxygen-vacancy center creates the 0.17-ev acceptor level. However, once it is realized that even floating-zone purification cannot remove all the oxygen from the silicon, the contradiction disappears, especially in view of the fact that in the case of a highly doped oxygen-free sample (Du Pont 336-2) the introduction of the 0.17-ev level is not noticeable. This is shown in Fig. 15.6, where the Hall coefficient of that sample and of one of the purer ones (where the introduction of the shallow level is visible) is presented as a

[11] E. Sonder and L. C. Templeton, *J. Appl. Phys.* **31**, 1279 (1960).

[12] E. Sonder and L. C. Templeton, *Bull. Am. Phys. Soc.* **5**, 196 (1960).

[13] G. D. Watkins and J. W. Corbett, General Electric Co. Rept. 61 RL, 2629E.

Table 15.1. Introduction of Net Acceptors in *n*-Type Silicon

Specimen	Source[a]	Growth[b] Technique	Room-Temperature Resistivity (ohm-cm)	Original Donor Concentration (cm^{-3})	Introduction Rate $\left(\frac{\text{levels/cm}^3}{\text{gammas/cm}^2}\right)$	
					Deep Level	0.17-ev Level
					$\times 10^{-4}$	$\times 10^{-4}$
585-25B	M	FZ	13.8	2.9×10^{14}	12	6
553-28A	M	FZ	3.2	1.2×10^{15}	14	5
RO16	DP	FZ	9.4	4.5×10^{14}	0.7	9
12045	DP	FZ	2.3	1.6×10^{15}	10	8
336-2	DP	FZ	0.087	9×10^{16}	30	<1
1123-30	SC	P	56	7×10^{13}	0.1	7
1123-4	SC	P	30	1.2×10^{14}	0.2	7
1123-2	SC	P	12	5.0×10^{14}		10
1019-2	SC	P	2.1	2.0×10^{15}	1.3	13

[a] M = Merck; DP = Du Pont; SC = Silicon Crystals, Inc.

[b] FZ = floating zone; P = pulled out of silica crucible.

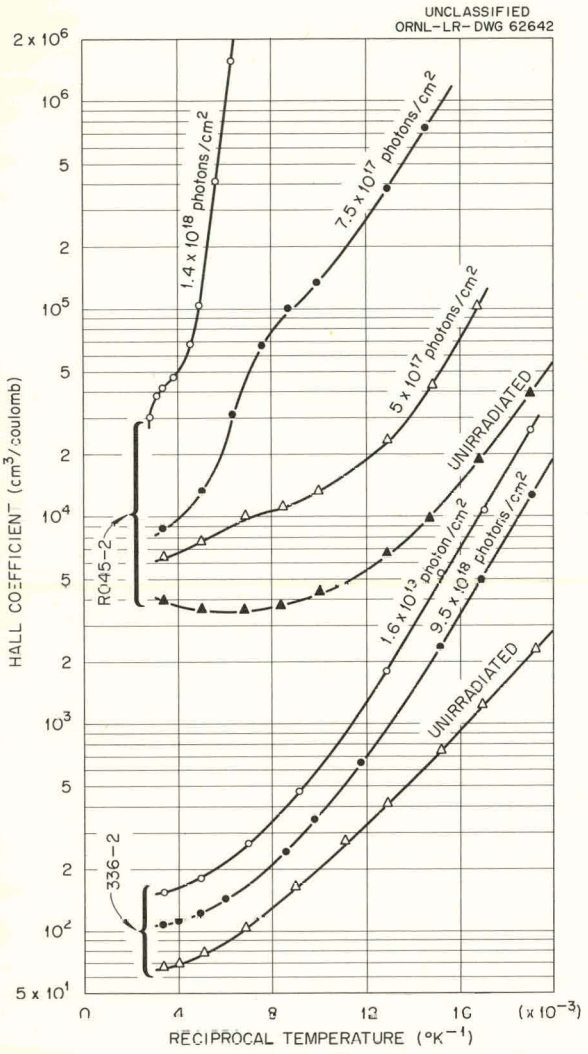

Fig. 15.6. Temperature Dependence of Hall Coefficient in Two Silicon Samples Before and After Gamma Irradiation. Comparison of the two sets of curves shows that the 0.17-ev level, which causes the inflection at $1000/T = 6$ in the curves of irradiated specimen R 045, is not apparent in the curves for sample 336-2.

function of temperature for the silicon samples before and after a number of irradiations.

Comparison of the Merck and Du Pont samples, all of which were prepared by a floating-zone technique, indicates that for samples containing 5×10^{14} donors/cm^3 the introduction rate of the deep level is much more rapid in the Merck sample. This could be because the amount of residual oxygen is less in the Merck samples.

Another trend in the results summarized in Table 15.1 that might be of interest is that for material from a given manufacturer (having presumably uniform oxygen content), the introduction rate of both the deep and shallow trapping levels seems to be greater in low-resistivity than in high-resistivity material. Since the room-temperature (irradiation temperature) Fermi level is higher in low-resistivity material, this might suggest that the vacancy is more mobile when it is negatively charged, a situation which would be more likely to exist with the higher Fermi level.

Dependence of Introduction Rate on Rate of Gamma Irradiation

The availability of two gamma sources of similar geometries, but with fluxes differing by a factor of 3, made it possible to determine whether there is a large effect of irradiation rate on the damage properties of n-type silicon. A number of irradiations on two specimens from the same 3-ohm-cm oxygen-free n-type silicon ingot were performed, and the Hall coefficient was measured between 50 and 300°K. From the Hall coefficients, the density of shallow (0.17-ev)[11] and deep electron traps was calculated and is plotted in Fig. 15.7

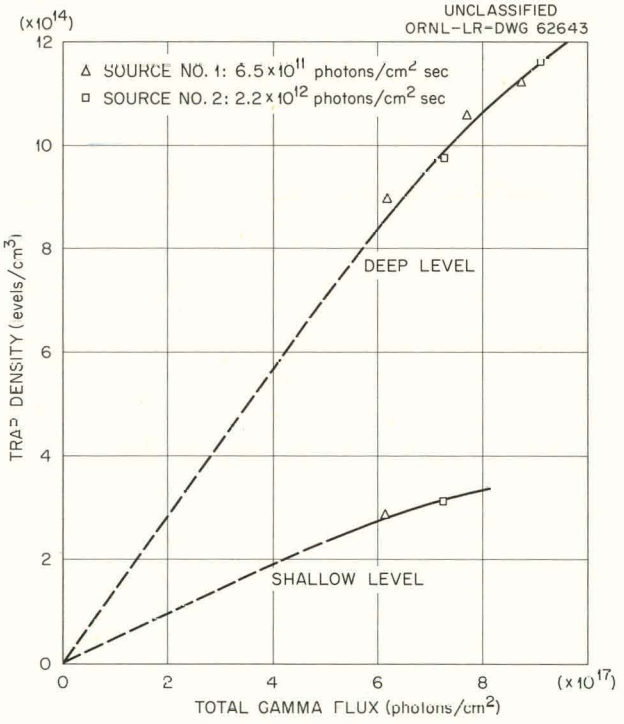

Fig. 15.7. Introduction of Net Acceptor Levels in n-Type Silicon.

vs total number of photons per square centimeter impinging on the samples. There is no difference between the results obtained in the two sources, both for the case of the shallow (0.17-ev) level and the case of the deep (~0.5-ev) level. Therefore, for the range of radiation intensity, there is no evidence of a dose-rate effect.

p-Type Silicon. – Investigation of the effect of Co^{60} gamma irradiation on the electrical properties of p-type silicon has begun. Figure 15.8 shows how the temperature dependence of the Hall coefficient is changed by irradiation. Data are shown for two samples of comparable resistivities and identical doping agents (boron). One (1189-1), obtained from Silicon Crystals, Inc., had been grown by standard pulling techniques and therefore probably contains $\sim 10^{18}$ oxygen atoms per cubic centimeter. The other, obtained from Merck and grown by a floating-zone method, should be purer, as far as oxygen is concerned, by at least a factor of 100. The curves look similar; in both cases a net donor level (hole trap) is created by the irradiation. Detrapping takes place above room temperature, indicating that the location of the level or levels is $\gtrsim 0.2$ ev above the valence band. This location is consistent with that of a level found by Wertheim[14] in electron-irradiated p-type silicon.

The introduction rates for the two samples are compared in Table 15.2. The introduction of damage seems to be greater by more than a factor of 2 in the sample containing the greater amount of oxygen. More work is necessary before any definite statement can be made concerning the reason for this difference. Presumably, as is the case in the n-type material, the presence of oxygen causes the radiation-produced primary defects to stabilize differently than they would in the absence of oxygen, producing different electronic levels.

Paramagnetism of Irradiation-Induced Centers in n-Type Silicon. – By measuring the magnetic susceptibility of a sample as a function of temperature in the liquid-helium range, it is possible to determine the density of one-electron centers.[15] In neutron-irradiated silicon, it had been found that irradiation at first removes a large fraction of the paramagnetic centers, but that after more irradiation, as the Fermi level drops below 0.2 ev (below the conduction band), magnetic centers reappear.[16] Unfortunately, in the neutron case the damage introduced is of a complicated nature, making analysis difficult.[17] In electron- or gamma-irradiated silicon, some of this difficulty is not present.

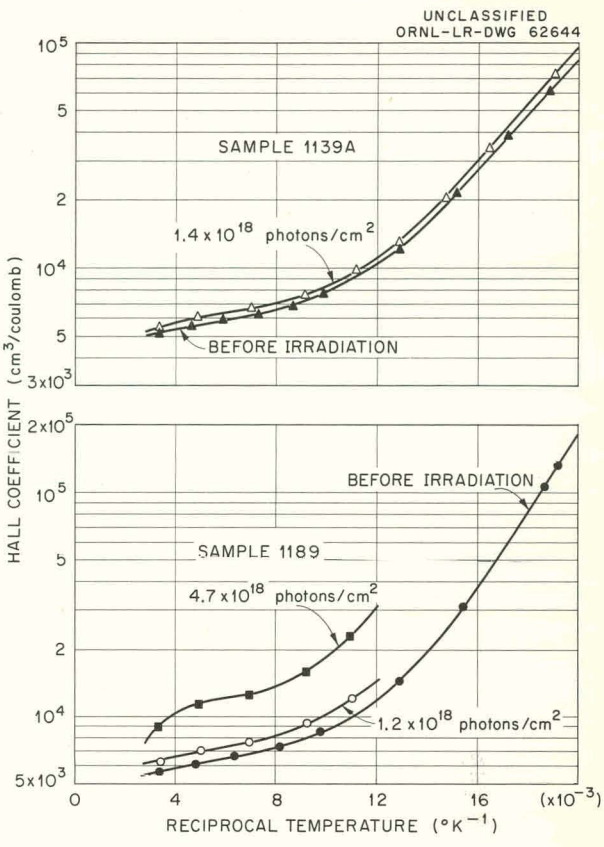

Fig. 15.8. Temperature Dependence of Hall Coefficient in Irradiated p-Type Silicon. Sample 1139A was prepared by a floating-zone technique; sample 1189 was pulled from a silica crucible.

One of the samples irradiated with gamma rays had a high enough original donor concentration to make magnetic susceptibility measurements feasible. In Table 15.3 are shown the results of these measurements. The donor density as obtained from the room-temperature Hall coefficient (see Fig. 15.6) decreased from 9.6 to 4.2×10^{16} cm^{-3};

[14] G. K. Wertheim, *Phys. Rev.* **110**, 1272 (1958).

[15] E. Sonder and D. K. Stevens, *Phys. Rev.* **110**, 1027 (1958).

[16] E. Sonder, *J. Appl. Phys.* **30**, 1186 (1959).

[17] B. Gossick, *J. Appl. Phys.* **30**, 1214 (1959).

Table 15.2. Introduction of Net Donor Levels in *p*-Type Silicon

Specimen	Source	Growth Technique	Room-Temperature Resistivity (ohm-cm)	Net Acceptor Density (cm^{-3})	Total Irradiation Flux (gammas/cm^2)	Introduction Rate $\left(\frac{\text{levels/cm}^3}{\text{gammas/cm}^2}\right)$
				$\times 10^{15}$	$\times 10^{18}$	$\times 10^{-4}$
1189	Silicon Crystals, Inc.	Pulled	16.5	1.01	0	
				0.90	1.23	0.9
				0.54	4.67	1.0
				0.09	9.14	1.0
1139A	Merck	Floating-zone	15.7	1.21	0	
				1.15	1.43	40

Table 15.3. Comparison of Donor Density with Concentration of Magnetic Centers for Specimen 336-2

Treatment	Net Donor Density (cm^{-3})	Magnetic Centers (cm^{-3})
	$\times 10^{16}$	$\times 10^{16}$
Before irradiation	9.6	9.7
After 1.6×10^{19} photons/cm^2	4.2	4.2

that is, 5.4×10^{16} electrons are trapped in centers, whose highest electronic level is below ~0.25 ev (below the conduction band). Since the density of magnetic centers decreases by the same amount, it is plain that as long as the Fermi level is ~0.2 ev (its value at the low temperatures at which the susceptibility measurements were made), electrons are trapped in pairs, so that the electron spins can align antiparallel to form singlet states. These results are in agreement with conclusions drawn from spin resonance measurements.[13]

ANNEALING STUDIES OF IRRADIATED GERMANIUM

J. C. Pigg

The annealing studies previously reported have been continued.[18] The irradiations have all been conducted at 77°K with Co^{60} gamma rays. The samples were cut from ingot EP8.[18]

Since little change in carrier concentration is produced by raising the sample to 273°K (see Fig. 10.3, ref 18), it was possible to conduct isochronal anneals and make measurements at both 77 and 273°K. The results of such an experiment are shown in Fig. 15.9. The curves show that at least two processes are taking place, one which predominates below 400°K and one which predominates above 400°K. The minima at 365 and

[18] J. C. Pigg, *Solid State Div. Ann. Progr. Rept. Aug. 31, 1960*, ORNL-3017, p 66.

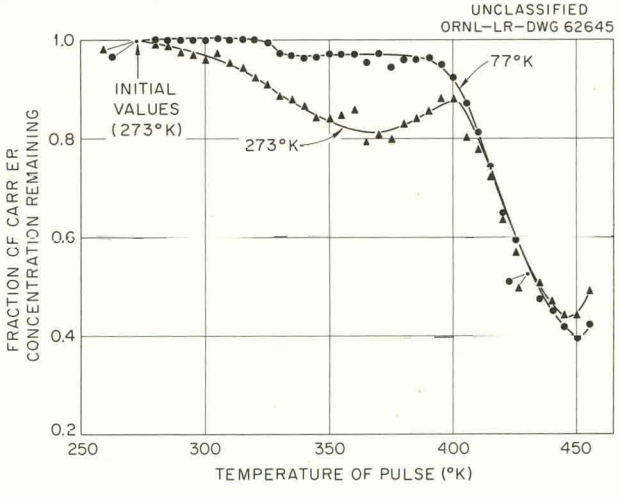

Fig. 15.9. Isochronal Anneal of Co^{60}-Gamma-Induced Carrier Change in *n*-Type Germanium.

445°K are real and are observed also in isothermal anneals.

A survey of the results of isothermal anneals for measurements at 77°K is shown in Fig. 15.10. The two processes indicated in Fig. 15.9 are clearly evident here also. The values of Fig. 15.9 are essentially a cross section of Fig. 15.10. The plateau reached by the 444.5°K anneal is clearly lower than that reached by the 455°K anneal.

The time of half anneal of the major process of Fig. 15.10 is plotted against reciprocal temperature in Fig. 15.11. Samples I, L, G, and F show an activation energy ϵ_1 of approximately 0.8 ev. This is the value found by Brown *et al.*[19] for the annealing of the change in carrier concentration produced by 1-Mev electron bombardment at 77°K.

When analyzed by the method of Holmes and Schweinler,[20] the data of Brown *et al.* yield a frequency factor of 3×10^9. Since this is probably indicative of a diffusion process, the same analysis should yield a frequency factor for samples I, L,

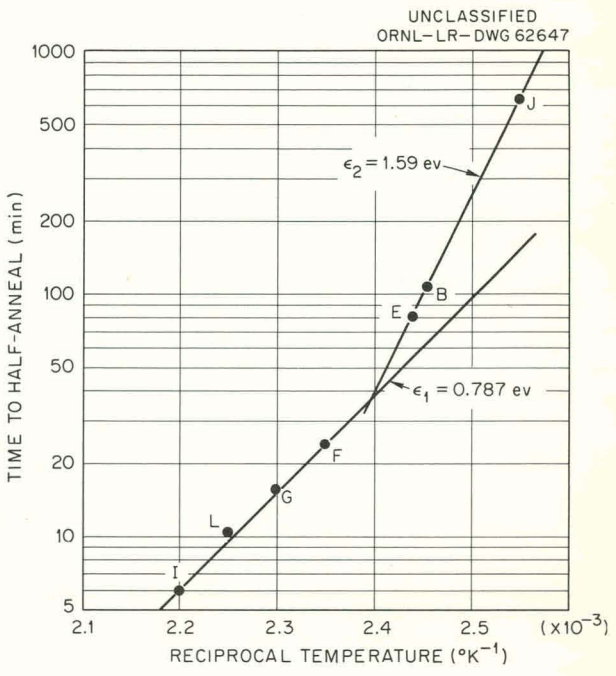

Fig. 15.11. Time to Half-Anneal vs Reciprocal Temperature.

[19] W. L. Brown, W. M. Augustyniak, and T. R. Waite, *J. Appl. Phys.* **30**, 1258–68 (1959).

[20] D. K. Holmes and H. C. Schweinler, *Approximate Treatment of Annealing with a Spectrum of Activation Energies and First-Order Kinetics*, ORNL-2829, p 58.

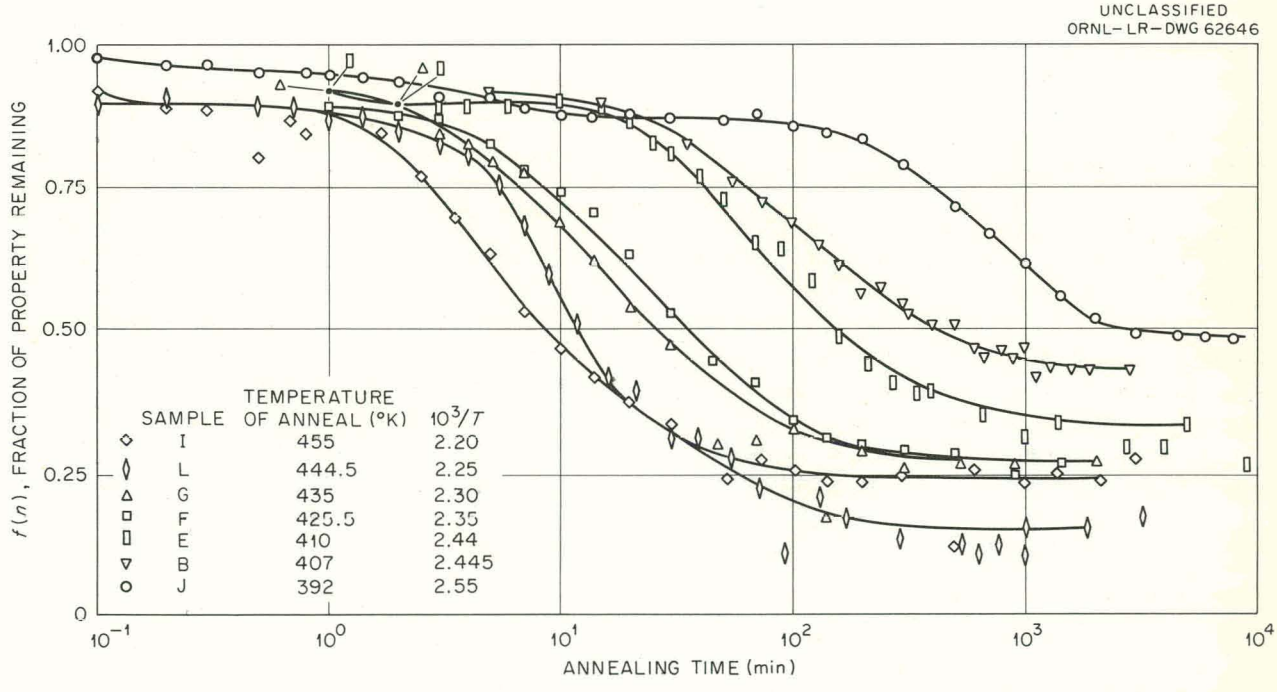

Fig. 15.10. 77°K Values of Co^{60}-Gamma-Induced Carrier Change as a Function of Isothermal Anneal.

G, and F which would differ from that of Brown's data only by the contribution produced by the different concentrations of defects. The defect concentration in Brown's samples was of the order of 10^{15}. The defect concentration in the samples reported here is of the order of 10^{14}. The frequency factor found here is 2.3×10^{7}.

THERMAL-NEUTRON-INDUCED RECOIL AND TRANSMUTATION EFFECTS IN SEMICONDUCTORS

J. W. Cleland R. F. Bass
J. H. Crawford, Jr.

"Transmutation Doping and Recoil Effects in Semiconductors Exposed to Thermal Neutrons"[21] and "Transmutation Doping and Recoil Effects in Isotopic Enriched Ge^{74} Exposed to Thermal Neutrons"[22] are previous descriptions of experiments that have now been extended to include a greater range of initial carrier concentrations and total dosages, other semiconducting materials, and irradiations conducted at 77°K, 195°K, and reactor ambient temperature (~40°C).

Table 15.4 summarizes the per cent abundance, thermal-neutron absorption cross section, per cent relative absorption, and end product for the (n, γ) reaction of those isotopes of interest. Also listed is the kinetic energy of recoil on emission of capture gamma rays. The kinetic energy (in ev) of recoil, T_γ, is related to the energy (in Mev) of the gamma ray, E_γ, by the relation

$$T_\gamma = 537 E_\gamma / A \ , \qquad (1)$$

where A is the atomic weight of the isotope in question. The recoil energy distribution for the capture gamma-ray spectrum has been analyzed from extensive tabulations of nuclear-energy-level diagrams and principal transition measurements when available,[23] or it has been estimated from the binding energies of the nucleus.

Table 15.5 summarizes the per cent relative absorption, radioactive decay scheme, and maximum recoil energy associated with the decay process. It should perhaps be emphasized that these transmutation-induced reactions occur long after the initial (n, γ) induced recoil, and the average kinetic energy of recoil on decay is probably less than the maximum value listed.

The usual criterion for the number of secondary displacements ν produced by a primary recoil of kinetic energy T would be

$$\nu = T/2E_d \ , \qquad (2)$$

where E_d is the threshold displacement energy. Application of Eq. (2), using the estimates of the kinetic energy of recoil tabulated in Table 15.4, indicates that one would expect ~26 interstitial-vacancy pairs (Frenkel-type defects) in Si, ~6 in normal isotopic Ge, ~5 in isotopically enriched Ge^{74}, ~3 in InAs and InSb, and ~5 in GaAs.

Table 15.6 is a summation of some of the principal experimental results obtained, which are discussed below:

1. The rate of removal of conduction electrons in normal isotopic germanium at 40°C was unity per actual thermal-neutron absorption within the precision of the flux determination (10%). It was also observed that the removal rate was independent of initial carrier concentration (~10^{12} to 10^{16} electrons per cm^3) and of any appreciable influence of a large amount of pre-existing lattice disorder introduced by prior fast-neutron irradiation. The removal rate of conduction electrons at 195°K was increased to −1.7 to −2.0 per actual absorption; however, no appreciable annealing was observed between 195 and 300°K. The removal rate of conduction electrons at 78°K was, apparently, further increased to −2.0 to −2.5 per actual absorption; however, appreciable annealing occurred between 78 and 300°K, and the net removal rate, −1.0 to −1.3, was less than the corresponding values for the 195°K irradiations.

2. The rate of addition of conduction electrons in 95.8% isotopically enriched germanium at 40°C was 0.1 per actual thermal-neutron absorption, where ~76% of the absorptions has transmuted to donor-type As^{75} (82-min half-life) by the time of measurement. The removal rate of conduction electrons at 78°K, however, was essentially identical, −1.7 to −2.5 per actual absorption, with the values for normal isotopic germanium. Room-temperature annealing removed all evidence of any recoil-induced acceptor states and indicated an

[21] J. H. Crawford, Jr., and J. W. Cleland, *Solid State Div. Ann. Progr. Rept. Aug. 31, 1960*, ORNL-3017, p 63.

[22] J. W. Cleland, R. F. Bass, and J. H. Crawford, Jr., *Solid State Div. Ann. Progr. Rept. Aug. 31, 1960*, ORNL-3017, pp 63–66.

[23] G. A. Bartholomew and L. A. Higgs, AECL-669 (1958).

addition rate of 0.5 to 1.0 conduction electron per actual absorption.

3. The rate of removal of conduction electrons in *n*-type silicon at 40°C was approximately two per actual absorption within the precision of the flux determination. This value was approximately doubled at an exposure temperature of 78°K, and room-temperature annealing evidently restored the net removal rate to approximately the same values as those obtained at reactor ambient temperatures.

4. The total absorption cross section of In^{115} (96% abundant) is 197×10^{-24} cm^2; hence Lambert's law indicates that ~25% of an incident thermal-neutron beam is absorbed per 0.1 cm of

Table 15.4. Nuclear Reactions

Isotope	Abundance (%)	Neutron Absorption Cross Section (cm^2)	Relative Absorption (%)	Kinetic Energy of Recoil (ev)	End Product
		$\times 10^{-24}$			
		Silicon			
Si^{28}	92.28	0.08	81.9	780	Si^{29}
Si^{29}	4.67	0.27	14.0	780	Si^{30}
Si^{30}	3.05	0.12	4.1	380	P^{31}
		Germanium			
Ge^{70}	20.45	3.4	30.4	197	Ga^{71}
Ge^{72}	27.41	0.98	11.7	161	Ge^{73}
Ge^{73}	7.77	14.0	47.2	184	Ge^{74}
Ge^{74}	36.58	0.62	9.8	149	As^{75}
Ge^{76}	7.79	0.36	1.2	118	Se^{77}
		Isotopically Enriched Germanium Specimen			
Ge^{70}	0.70	3.4	2.8	197	Ga^{71}
Ge^{72}	1.10	0.98	1.3	161	Ge^{73}
Ge^{73}	1.56	14.0	25.6	184	Ge^{74}
Ge^{74}	95.80	0.62	69.9	149	As^{75}
Ge^{76}	0.80	0.26	0.4	118	Se^{77}
		Indium Antimonide			
In^{113}	4.23	58.0	1.3		Sn^{114}
In^{115}	95.77	197.0	96.5	~40	Sn^{116}
Sb^{121}	57.25	6.0	1.7		Te^{122}
Sb^{123}	42.75	2.5	0.6		Te^{124}
		Indium Arsenide			
In^{113}	4.23	58.0	1.25		Sn^{114}
In^{115}	95.77	197.0	96.5	~40	Sn^{116}
As^{75}	100	4.3	2.2	140	Se^{76}
		Gallium Arsenide			
Ga^{69}	60.2	2.1	44.0	160	Ge^{70}
Ga^{71}	39.8	5.1	13.6	160	Ge^{72}
As^{75}	100	4.3	42.4	140	Se^{76}

traverse. All the samples employed in these experiments were ~0.1 cm thick; hence we assumed an absorption total of 2.5 nvt_{th}. The rate of addition of conduction electrons for n-type InSb at 40°C was, under this assumption, +1.0 per actual absorption, where essentially all the In^{115} atoms had transmuted to Sn^{116} at the time of measurement. The rate of removal of conduction electrons at 78°K was −0.5 per actual absorption; however, annealing at room temperature evidently removed all of the recoil-induced disorder and re-established the addition rate to approximately the same values as those originally observed at reactor ambient temperatures.

5. The rate of addition of conduction electrons for n-type InAs at 40°C was 2.0 per actual thermal-neutron absorption, under the above assumption of 2.5 nvt_{th}, where essentially all the In^{115} atoms had transmuted to Sn^{116} by the time of measurement.

6. The rate of removal of conduction electrons from n-type GaAs at 40°C was ~3 per actual thermal-neutron absorption, where essentially all the gallium and arsenic had transmuted to germanium and selenium by the time of measurement. Annealing for 20 hr at 300°C returned the carrier concentration to within 80% of the preirradiation value. Presumably, the incomplete annealing of

Table 15.5. Transmutation Reactions

Reaction	Maximum Recoil Energy (ev)
$Si^{30}(n,\gamma)Si^{31} \xrightarrow[\beta]{2.6h} P^{31}$	63
$Ga^{69}(n,\gamma)Ga^{70} \xrightarrow[\beta]{20m} Ge^{70}$	13
$Ga^{71}(n,\gamma)Ga^{72} \xrightarrow[\beta]{14.2h} Ge^{72}$	24 (10%) 11 (10%) 5 (40%)
$Ge^{70}(n,\gamma)Ge^{71} \xrightarrow[K\ x\ ray]{12d} Ga^{71}$	10^{-5}
$Ge^{74}(n,\gamma)Ge^{75} \xrightarrow[\beta]{82m} As^{75}$	18.7 (85%)
$Ge^{76}(n,\gamma)Ge^{77} \xrightarrow[\beta]{12h} As^{77} \xrightarrow[\beta]{39h} Se^{77}$	78.0 (11%) 40.0 (37%) 23.4 (31%)
$As^{75}(n,\gamma)As^{76} \xrightarrow[\beta]{27h} Se^{76}$	80 (50%)
$In^{113}(n,\gamma)In^{114} \xrightarrow[\beta]{49d} Sn^{114}$	9.8 (97%)
$In^{115}(n,\gamma)In^{116} \xrightarrow[1.3\text{-Mev}\ \gamma\ \ 3\text{-Mev}\ \beta]{54.2m\ (74\%)\ 13s\ (26\%)} Sn^{116}$	52 (26%)
$Sb^{121}(n,\gamma)Sb^{122} \xrightarrow[\beta]{2.8d} Te^{122}$	8.8
$Sb^{123}(n,\gamma)Sb^{124} \xrightarrow[\beta]{60d} Te^{124}$	12 (50%)

Table 15.6. Summation of Experimental Data for n-Type Material

Material	Number of Absorptions (N_A)	Kinetic Energy of Recoil (ev)	Calculated Number of Frenkel Defects	Irradiation Temperature	Carrier Concentration Change (dn/dN_A)	Net dn/dN_A After Room-Temperature Anneal	Number and Type of Transmutations
Ge	$0.108\ nvt_{th}$	182	6	40°C	−1.0		$0.12N_A = N_{As}$
							$0.3N_A = N_{Ga}$
				195°K	−1.7 to −2.0	−1.7 to −2.0	
				78°K	−2.0 to −2.5	−1.0 to −1.3	
Ge^{74}	$0.038\ nvt_{th}$	150	5	40°C	+0.10		$0.76N_A = N_{As}$
				78°K	−1.7 to −2.5	+0.5 to 1.0	
Si	$0.007\ nvt_{th}$	780	26	40°C	−2.0		$0.04N_A = N_P$
				78°K	−3.7	−1.8	
InSb	$2.50\ nvt_{th}$	40	3	40°C	+1.0		$N_A = N_{Sn}$
				78°K	−0.5	+0.5 to 1.0	
InAs	$2.50\ nvt_{th}$	40	3	40°C	+1.8		$N_A = N_{Sn}$
GaAs	$0.14\ nvt_{th}$	150	5	40°C	−3.0		$0.33N_A = N_{Ge70}$
							$0.66N_A = N_{Ge72}$

the recoil-induced states obscures any donor action of the germanium or selenium introduced by transmutation.

Discussion

Germanium and Silicon. – It is evident from these data that there is a great disparity between the number of interstitial-vacancy pairs, or Frenkel defects, that would be expected from theory and that which is observed by experiment. Examination of the step in the Hall coefficient and resistivity curves of thermal-neutron-irradiated normal isotopic[21] germanium and isotopically enriched[22] Ge^{74} would indicate that each recoil-induced Frenkel defect probably removes two conduction electrons; hence the actual rate of defect production is only one-half the rate of electron removal indicated in Table 15.6. One might therefore summarize the experimental observations for normal isotopic n-type germanium and n-type silicon by stating that the actual rate of defect production at reactor abmient temperature, ~40°C, is less than one-tenth of that predicted by theory. Corresponding data at 78°K would indicate that the actual rate of defect production is still only about one-fifth of that predicted by theory; however, the added complication of minority-carrier trapping phenomena might serve to make these values somewhat uncertain.

Vacuum annealing at ~450°C for 20 to 40 hr has always served to remove essentially all the Frenkel-type defects introduced in germanium, silicon, or InSb by electrons, Co^{60} photons, or fast neutrons. Annealing subsequent to thermal-neutron irradiation should, therefore, permit a separate evaluation of recoil-induced defects and transmutation-produced impurity states. The expected concentration and half-life of introduction time of Ga^{71} acceptor atoms was observed in samples of n-type germanium after thermal-neutron irradiation and after thermal-neutron irradiation and vacuum annealing. These results would indicate an essentially identical behavior for atoms that had presumably recoiled by an (n, γ) reaction

to interstitial positions and later transmuted to acceptor impurity atoms and for potential acceptor type of impurity atoms that have been returned to a substitutional position by annealing. The expected concentration and half-life of introduction of Ga^{71} acceptors has also been observed in samples of *n*-type germanium that were irradiated at 78°K and then stored at 78°K. One might therefore conclude that the donor or acceptor action of As^{75} and Ga^{71} impurities in normal isotopic germanium is identical, irrespective of whether these atoms are presumably interstitial as a result of recoil or substitutional as a result of vacuum annealing.

There is no evidence for multiple defect creation by the recoils in isotopically enriched Ge^{74} as a result of ambient-temperature thermal-neutron irradiation, where any such Frenkel pairs would be expected to serve as acceptors. There is also no evidence, however, for the expected donor action of the As^{75}, since the addition rate of conduction electrons was only about one-tenth of that expected from the number of thermal-neutron absorptions. The expected concentration of As^{75} was observed, however, after a vacuum anneal.

It has been suggested[21,22] that the recoil process is actually more like a replacement process, wherein the original, recoiling atom probably remains substitutional; much of the kinetic energy of recoil is dissipated in lattice vibrations or in creating Frenkel-type defects that are relatively unstable at room temperatures. In this model the original, activated atom as a substitutional atom can later transmute as a normal chemical impurity without the possible consequences of an identical behavior having to be assumed for interstitial and substitutional donor and acceptor impurity atoms, as was indicated above.

The experimental results on normal germanium and the specimen enriched in Ge^{74} would seem to agree with this model of a replacement-type process. The removal rate of conduction electrons in normal germanium is only one-tenth of that predicted by simple damage theory, and the subsequent behavior would indicate that those atoms which recoil, and later transmute, act like normal, substitutional atoms. The atoms that recoil in the Ge^{74} material have already transmuted to As^{75} by the time of measurement. These would be expected to serve as normal donor atoms, if the replacement-type model is valid. However, their net donor action is evidently reduced by the Frenkel defects induced by the capture gamma-ray recoil. Some of the recoils in the isotopically enriched Ge^{74} are Ge^{73} atoms which are transformed to stable Ge^{74} on neutron capture. There is some uncertainty in the published values of the percentage abundance of the Ge^{73} in the isotopically enriched Ge^{74} employed;[24] however, the present experimental data indicate (1) an essential balance, within 10%, of those As^{75} atoms that have recoiled but remained substitutional and (2) the expected concentration of Frenkel defects which act as acceptor states until they are removed by an appropriate vacuum anneal.

Intermetallic Compounds. – Extensive relaxation of low-temperature-induced lattice damage has previously been observed in electron-irradiated[25,26] InSb, Co^{60}-photon-irradiated[27] InSb, fast-neutron-irradiated[28] InSb, and electron-irradiated[29] InAs following exposures conducted at 4.2 or 77°K; hence the final defect concentration and configuration resulting from room-temperature irradiation is certainly different from that which would result if no relaxation occurred.

Cobalt-60 photon irradiation at ambient temperatures (~30°C) introduces net acceptor states (electron traps) that reduce the net electron concentration of *n*-type samples of germanium (ref 30), silicon (ref 31), and InSb (ref 32). The removal rate of conduction electrons is $\sim 1 \times 10^{-3}$ per incident photon for germanium and silicon and only $\sim 1 \times 10^{-5}$ per incident photon for InSb.

---

[24] Germanium donor spin resonance results of D. K. Wilson, Bell Telephone Laboratories (unpublished data), indicate that the 1.56 at. % value listed (ref 22) for the Ge^{73} must be too high. Preliminary re-analysis by the Isotopes Division has confirmed this result; however, a new value has not yet been established.

[25] L. W. Aukerman, *J. Appl. Phys.* 30, 1239 (1959).

[26] F. H. Eisen, *Phys. Rev.* 123, 736 (1961).

[27] C. R. Whitsett, *Bull. Am. Phys. Soc.* 3, 142 (1958).

[28] J. W. Cleland and J. H. Crawford, Jr., unpublished data.

[29] L. W. Aukerman, Ph.D. thesis, Purdue University (1958).

[30] J. W. Cleland, J. H. Crawford, Jr., and D. K. Holmes, *Phys. Rev.* 102, 722 (1956).

[31] E. Sonder and L. C. Templeton, *J. Appl. Phys.* 31, 1279 (1960).

[32] J. W. Cleland and J. H. Crawford, Jr., unpublished data.

Figure 15.12, which is a graph of the logarithm of the Hall coefficient and the logarithm of resistivity vs inverse temperature of *n*-type GaAs, indicates that Co^{60} photon irradiation also introduces net acceptor states (electron traps) in this material. The removal rate of conduction electrons in *n*-type GaAs is much larger than that for the other semiconductors investigated, that is, $\sim 1.4 \times 10^{-2}$ per incident photon. The radiation-induced defects are stable at 100°C; however, the original crystalline perfection is evidently restored upon annealing at 300°C. Measurements of the rate of defect introduction were also made for irradiation with 0.667-Mev photons from a Cs^{137} source, and the apparent removal rate of conduction electrons was $\sim 5 \times 10^{-4}$ per incident photon. Similar studies have also been made[33] with 1.0-Mev electron-irradiation experiments.

Fast-neutron irradiation at reactor ambient temperatures (~30°C) also introduces acceptor states (electron traps) that reduce the net electron concentration of *n*-type samples of germanium, silicon, and InSb,[34] and these materials can be restored to essentially original conditions by thermal annealing at 350 to 450°C. Unpublished results of Aukerman and of Cleland and Bass, however, indicated that approximately one-half of the fast-neutron-induced lattice defects in GaAs could not be removed, even at annealing temperatures in excess of 600°C. It has also been previously indicated[35] that fast-neutron irradiation of *n*-type InAs at ambient temperatures apparently introduces extremely shallow *n*-type donor states that increase the apparent electron concentration, and only ~25% of the apparent increase could be thermally annealed at 350°C. Studies recently performed here with Co^{60} photons have confirmed that the rate of conduction electron increase is 1×10^{-3} per incident photon and that the change in carrier concentration could not be thermally annealed at 350°C.

Thermal-neutron-induced recoil effects in *n*-type InSb (Table 15.6) indicate that the kinetic energy of recoil is not sufficient to create stable defects, since Co^{60}-photon- and fast-neutron-irradiation results have indicated that these would behave as net acceptors in *n*-type specimens at room temperature. The net result of thermal-neutron irradiation, consequently, is a unit increase in net donor concentration for each thermal-neutron absorption (each absorption resulting in an Sn^{116} donor by the time of measurement). The transmuted atoms evidently serve as normal, substitutional donors in InSb.

The situation in *n*-type InAs, however, is markedly different (Table 15.6) in that ~1.8 donors are apparently added for each actual absorption. It has been indicated above that Co^{60} photon and fast-neutron irradiation produce stable defects that act as shallow *n*-type donors in InSb, and one would therefore suspect thermal-neutron-induced recoil also to introduce a donor-type defect. The transmutation-produced chemical impurity would further increase the total donor concentration.

The effect of Co^{60} photon and fast-neutron irradiation on *n*-type GaAs is a decrease in the net electron concentration, and the Frenkel-type defects that are expected from electron or Co^{60} photon irradiation can be annealed at 300°C. Thermal-neutron-induced recoil effects in *n*-type GaAs (Table 15.6) are very pronounced, in that ~3 conduction electrons are removed per actual absorption, even though every initially recoiling atom has transmuted to a donor-type impurity atom by the time of measurement. It was previously mentioned that fast-neutron-induced lattice defects could not be readily annealed in *n*-type GaAs. Preliminary annealing experiments on thermal-neutron-irradiated samples of *n*-type GaAs indicate that only a portion of the recoil-induced defects can be removed and thus that the expected donor action of the germanium and selenium transmutation-produced chemical impurities cannot be separately observed.

[33] L. W. Aukerman, P. C. Peters, and R. D. Graft, *Bull. Am. Phys. Soc.* 6, 177 (1961).

[34] J. H. Crawford, Jr., and J. W. Cleland, *Progress in Semiconductors* (ed. by A. F. Gibson), vol 2, p 47, Wiley, New York, 1957.

[35] J. W. Cleland and J. H. Crawford, Jr., *Solid State Div. Ann. Progr. Rept. Aug. 31, 1958*, ORNL-2614, pp 20–23.

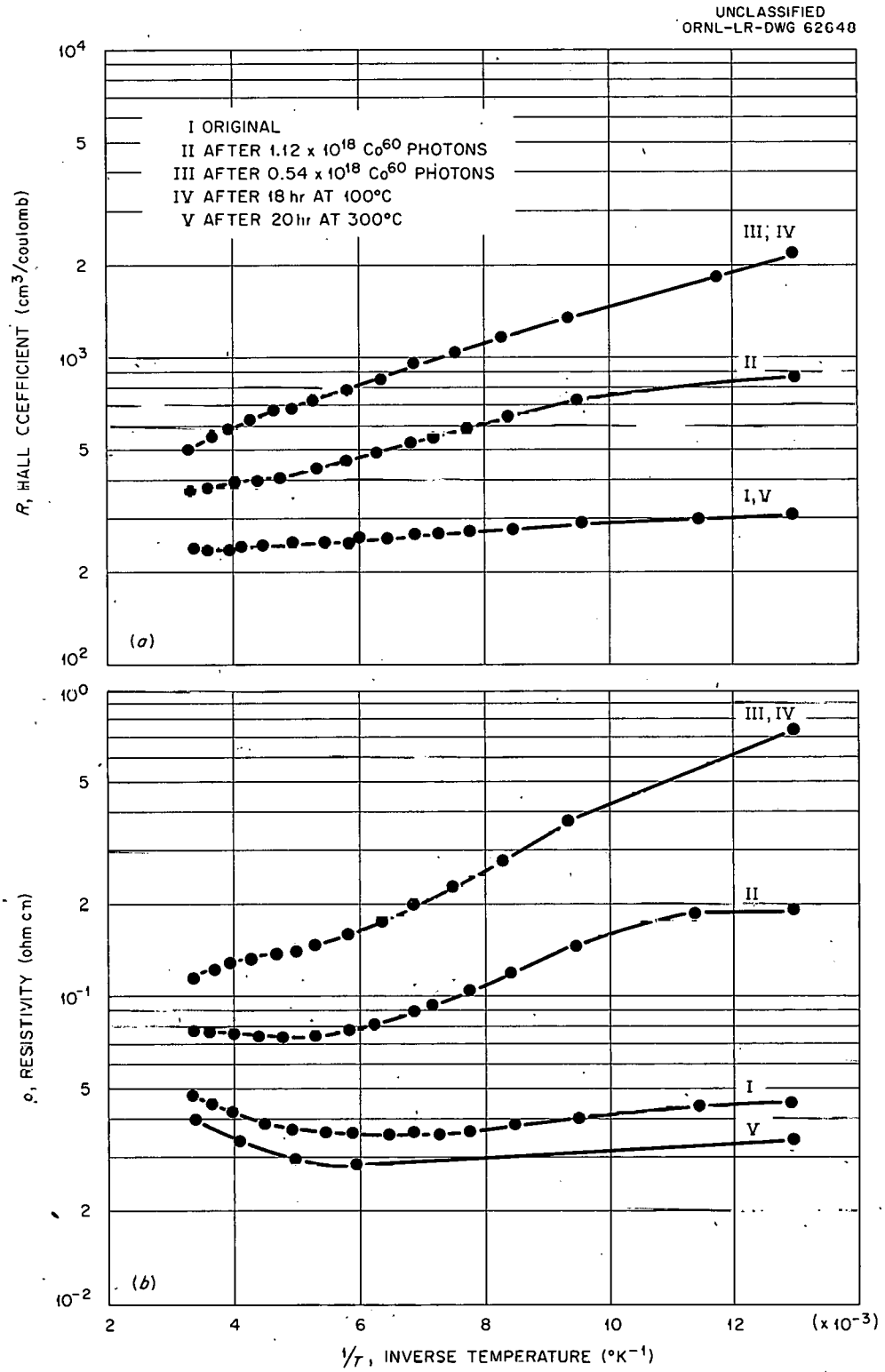

Fig. 15.12. Hall Coefficient and Resistivity vs Inverse Temperature for *n*-Type GaAs Before Irradiation, After Co^{60} Photon Irradiation, and After Annealing.

STUDIES ON Cu_2O: RECRYSTALLIZATION PROCESSES

C. C. Robinson

Recent work[36] has shown that single-crystal Cu_2O can be made by annealing polycrystalline Cu_2O in air at atmospheric pressure. A qualitative explanation of this phenomenon has been reported, although the mechanism is not yet understood. Determination of this mechanism would be of value, since perfect or near-perfect crystals are urgently needed for basic studies of the electronic properties of this material. In essence the procedure is to oxidize the copper in the region 1020 to 1050°C and anneal the resulting polycrystalline mass at higher temperatures. Both annealing time and temperature required to produce a single crystal depend on the thickness of the sample.

Work on Cu_2O during the last year has been directed toward a better understanding of the conditions necessary for single-crystal preparation and the factors that influence grain growth. Currently, 99.999% polycrystalline copper is being used in these studies, although 99.9% copper has been used in the past, and considerable grain growth has been observed. After the more important factors have been identified, it is planned that single-crystal copper will be employed as the starting material in the oxide growth process.

The present emphasis is on grain growth in completely oxidized samples. The temperature range between 1000 and 1130°C is being carefully explored for evidence of possible phase changes which might yield sufficient freedom to the ions of the lattice so that grain growth might be promoted in a given temperature interval. Both continuous resistivity measurements during cyclic temperature variations and direct visual observation of the surface of the specimens are used in these studies.

Depending on the rate of temperature change, sudden steplike changes in the resistivity of the polycrystalline specimens have been observed. One of these inflections has been studied in some detail. At 1028°C, while the temperature is increased slowly (~1°C/min), the resistance increases suddenly, decreases to a value below the extrapolated value, and then recovers to a position on the extrapolated slope of the log R vs $1/T$ curve, as shown in Fig. 15.13. The origin of this oscillatory variation is not known. Since the slope of the curve is almost the same below and above the temperature of the oscillation, it does not appear likely that it is associated with a gross crystallographic phase change in the Cu_2O lattice. It is well known that CuO is converted to Cu_2O in air near 1020°C. The change in question might be in some way connected with such a chemical transformation.

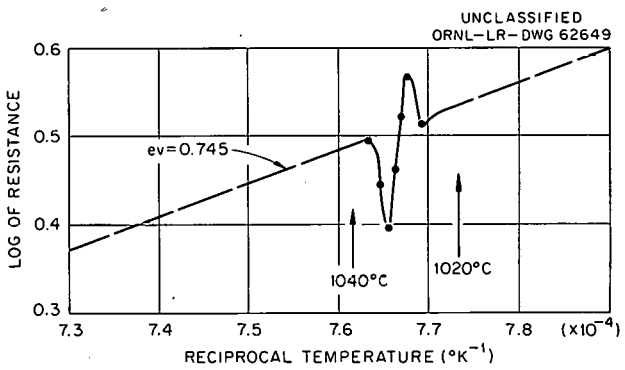

Fig. 15.13. Resistance Change in Cu_2O.

Displacements from a linear log R vs $1/T$ curve have been observed at higher temperatures. However, in each case the rate of heating was relatively rapid, and these effects have not been investigated with lower heating rates as yet. Except for these displacements, all specimens exhibited linear log R vs $1/T$ curves, with slopes corresponding to an activation energy in the range 0.7 to 0.85 ev.

A system for visually observing changes on the surface of the sample while it is in the furnace has been assembled. Examination of the sample has shown that when the temperature of a sample that has been annealed at 1100°C is lowered to between 1060 and 1070°C, the rough-appearing surface of the grains fades out completely, although grain boundaries can still be faintly seen on the sample. Refinements in the system will permit more accurate determination of the critical temperature for grain growth. It is further planned to study the sample by means of infrared photographs.

[36] R. S. Toth, R. Kilkson, and D. Trivich, *J. Appl. Phys.* 31, 1117 (1960).

SOLID STATE DIVISION Co^{60} GAMMA SOURCE

J. W. Cleland

The Solid State Division Co^{60} gamma source facility No. 1, which had an initial loading of ~1880 curies,[37] has been used for a variety of experiments during the past four years. A second facility, No. 2, which is identical with No. 1 except for the addition of water cooling, was installed in 1959 with an initial loading of ~5115 curies. This facility (No. 2) has also been used for a variety of experiments, including many irradiations at liquid-nitrogen temperature. The low-temperature irradiations were carried out using a 7-ft glass Dewar bottle (internal diameter about $1\frac{3}{8}$ in.), which was emptied after each 24-hr exposure. This evidently served to eliminate the conditions that have been known to cause explosions in this type of system.[38]

An increasing demand for large total exposures has long been felt evident; hence it was decided to reload facility No. 1. The original source tubes were removed in June 1961. No evidence of any leakage or contamination from the encapsulated Co^{60} pellets was observed. The apparatus was water-cooled, and the 24 original pellets of Co^{60} were repackaged with 96 additional pellets. It is expected that this new assembly will total ~11,000 curies and will provide a central exposure intensity of $\sim 7 \times 10^6$ r/hr.

ELECTRON EXCESS CENTERS IN KCl

E. Sonder

Oscillator Strength of the *F* Center

Magnetic-susceptibility measurements on additively colored KCl specimens in the liquid-helium temperature range have been extended to gamma-ray-colored specimens. The techniques used to obtain the oscillator strength of the *F* absorption band in additively colored KCl (ref 39) were also used for the gamma-ray-colored material. In Table 15.7 are presented the averages of the oscillator strengths measured for the two cases. It seems that the apparent oscillator strength of the gamma-ray-colored sample is a little smaller than that in the additively colored material, although the difference is hardly a significant amount in view of the large random variability observed in the results of the measurements.[40] If the dominant ultraviolet absorption center (probably the V_3 center), which is shown in Fig. 15.14, curve (a), with its absorption maximum at 5.7 ev, were paramagnetic and if its concentration were the same as that of *F* centers, then the experimentally determined oscillator strength in the gamma-ray-colored material would be half that in the additively colored samples. This would be due to the fact that in the susceptibility measurements *all* the magnetic centers would be counted, whereas in determining nf, the product of the number of centers times the oscillator strength, only *F* centers are counted. As seen from Table 15.7, no factor-of-2 difference exists. The fact that the apparent oscillator strength is less in the gamma-ray-colored KCl by an amount less than a factor of 2 might indicate that a number of centers (only one of which is paramagnetic) absorb in the broad ultraviolet band shown in Fig. 15.14, curve (a). In fact, as shown in the inset, for a different sample the shape of the absorption can be changed by a slight amount of bleaching and annealing.

Table 15.7. *F*-Center Oscillator Strength in KCl

Material	Number of Measurements	Oscillator Strength, Assuming Lorenzian Band Slope
Additively colored KCl	7	0.88 ± 0.10
Gamma-ray-colored KCl	2	0.66 ± 0.10

Magnetic Changes During *F* to *M* Conversion

When KCl containing *F* centers is bleached, the *F* band decreases and a number of secondary bands appear. The first one of these to appear is

[37] J. W. Cleland, *Solid State Div. Ann. Progr. Rept. Aug. 31, 1957*, ORNL-2413, p 75.

[38] J. C. Pigg, unpublished data.

[39] E. Sonder, *Solid State Div. Ann. Progr. Rept. Aug. 31, 1960*, ORNL-3017, p 84.

[40] The variation in f was found to be about a factor of 5 greater than would be expected due to experimental uncertainties. It stemmed mainly from random variations in impurity and *F*-center content in optical plates coming from the same ingot.

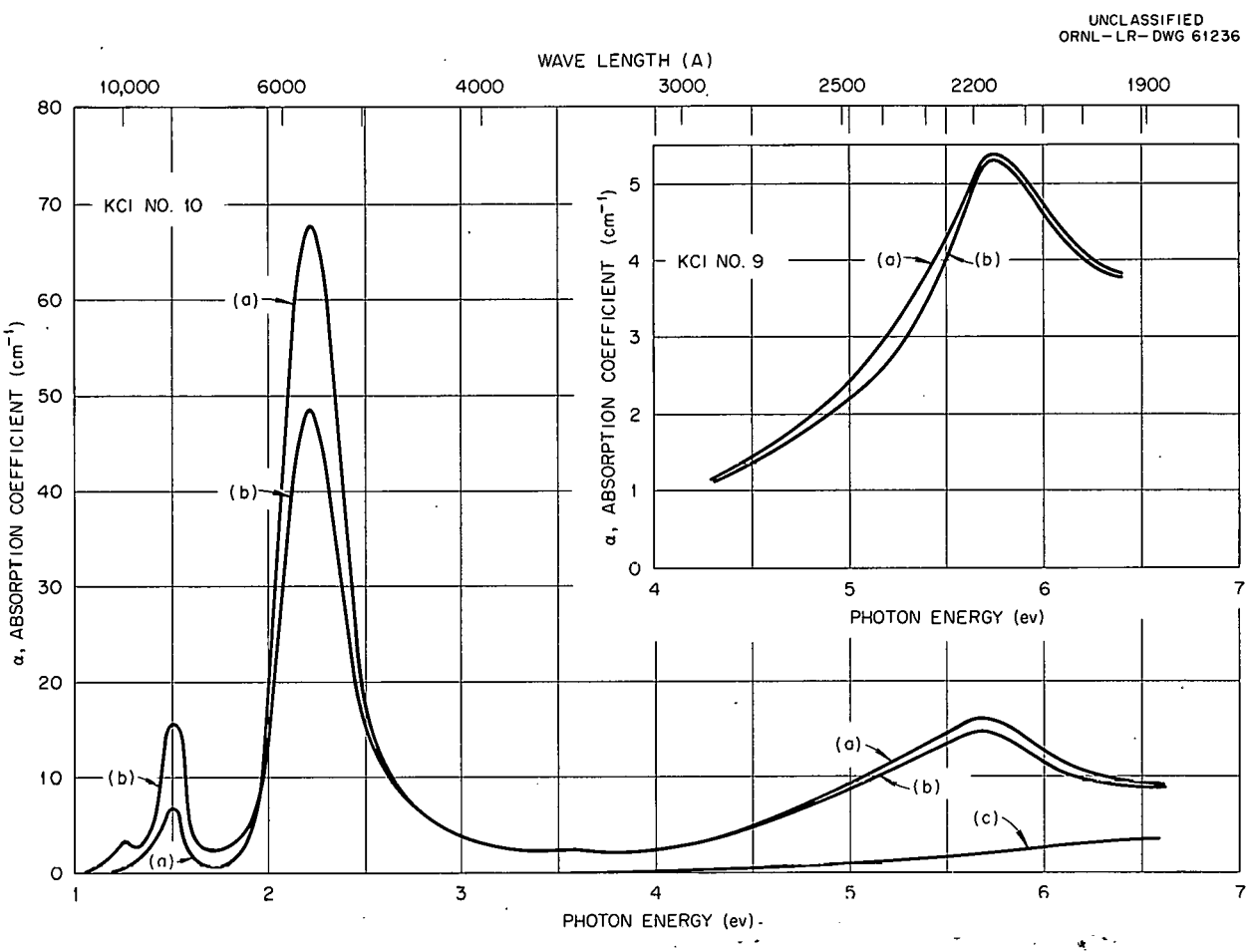

Fig. 15.14. Optical Absorption of Gamma-Ray-Colored KCl. Curve (a) was obtained after coloration before any light was permitted to fall upon the sample. Curve (b) was obtained after bleaching and annealing. Curve (c) shows the magnitude of the OH^- absorption present in the uncolored material. The curves shown in the inset are for a lightly colored sample in which the shape of the ultraviolet absorption changed upon bleaching and annealing.

the *M* band. Until recently little was known about these secondary centers. It is possible from magnetic-susceptibility and optical-absorption measurements to obtain some information about the number of electrons in such centers, since one-electron centers would contribute an electron spin paramagnetism (similarly to the *F* center), while two-electron centers would not, due to pairing of electron spins.

The results of optical and magnetic measurements before and after conversion of *F* centers to *M* centers are summarized in Table 15.8. The change in optical absorption is shown for one sample, KCl No. 10, in Fig. 15.14, curve (b). We shall discuss first the samples shown above the dashed line in Table 15.8. Even though the bleach and anneal treatments[41] were slightly varied, the results are qualitatively similar for the two additively colored and the gamma-ray-colored samples. Columns 4–7 give the density of the various centers in the samples after the stated treatments. The densities are recorded as percentage of the *original* *F*-center concentration in the sample, shown by the *upper* number for each sample in column 3. Columns 9 and 10 give the density of magnetic

[41] The bleach and anneal treatments differ slightly for the various samples. An attempt was made, using practice samples from the same ingots, to determine conditions that would, for each specimen, create *uniformly throughout the volume* the maximum *M*-center concentration consistent with reasonably small amounts of colloid and *R* centers.

Table 15.8. Change in *F*-Band Absorption and Magnetism upon Bleaching and Annealing of KCl

KCl Sample Number	Treatment	nf	*M* Centers (%)	*R* and *N* Centers (%)	Colloid Centers[a] (%)	*F* Centers Remaining After Treatment (%)	*F* Centers, Assuming *M* Absorption in *F* Band[b] (%)	n	Magnetic Centers Remaining After Treatment (%)
		$\times 10^{17}$						$\times 10^{17}$	
6[c]	Additively colored, 14 days	0.90	2					1.13	
	Bleached, 6800 A, 32 hr; annealed at 109°C, for 1 hr	0.62	7½	1	4	69	58	0.61	53
7	Additively colored, 14 days	4.11	3	~½				7.11	
	Bleached, 3900 A, 13 hr; annealed at 103°C, 1¼ hr	2.96	6	1	8	72	66	4.80	67
10	Gamma-ray-colored, 14½ hr	1.70	3					3.60	
	Bleached, 6900 A, 24 hr; annealed at 111°C, 1 hr	1.22	7	~1		72	64	2.30	63
9	Gamma-ray-colored, 1¾ hr	0.57	1					1.14	
	Bleached, 6900 A, 30 hr; annealed at 113°C, 2 hr	0.28	2½			48	45	0.76	66

[a] The colloid band is very broad and therefore difficult to resolve.

[b] See text for explanation.

[c] Ingot had been stored five months in the dark after additive coloration.

centers, as obtained from susceptibility measurements, the percentage in this case being of the number of *magnetic* centers in the originally colored specimen.

Comparison of columns 7 and 10 immediately shows that the decrease in magnetic centers is appreciably greater than the decrease of the *F*-band absorption. If the *F*-center electrons were forming even in part paramagnetic cluster centers (as for instance *M* centers of the type suggested by Seitz[42]), the opposite would happen and the magnetism would decrease more slowly than the *F*-band absorption. Even if no new paramagnetic centers were created upon destruction of *F* centers, the percentage change in columns 7 and 10 would be the same.

Recently, a nonmagnetic model has been proposed[43,44] for the *M* center. This *M* center would absorb both in its own (*M*) absorption band and under the *F* band. It is composed simply of a pair of adjacent *F* centers. Light polarized along the long axis of this center would see a charge distribution which would cause it to be absorbed with an energy difference corresponding to the *M* band. However, light traveling along the long axis of the center would be polarized in one of the two perpendicular directions and would see an *F*-center-like charge distribution, causing it to be absorbed with an energy corresponding to that of the *F* band. Qualitatively, according to this model, the true *F-center* absorption of our specimens after the bleach and anneal treatments should be the measured absorption *minus* twice the absorption on the *M* band.[45] Column 8 lists these values, again in percentages of the original *F*-center density. The agreement between columns 8 and 10 is surprisingly good.[46]

Below the dashed line in Table 15.8 are shown results of measurements on a gamma-ray-colored sample (KCl No. 9) which contained only 1×10^{17} *F* centers. This concentration is probably not much greater than the density of impurity (OH^-) ions.[47] Thus, the fact that in this case the *F*-band absorption decreased more than the susceptibility is not too surprising.[48] In all the samples an appreciable number of *F* centers (and corresponding magnetic centers) disappeared without forming *M* centers. In the case of the additively colored crystals, we found evidence of (nonmagnetic) colloid-band formation; in the case of the gamma-ray-colored KCl No. 10, there was a significant decrease of the ultraviolet absorption. In the case of the anomalous specimen, KCl No. 9, however, even though the *F* band decreased much more than in any other sample, there was little decrease *in the peak* of the ultraviolet absorption. However, the *form* of the absorption band in the ultraviolet changed appreciably, as shown in the inset in Fig. 15.14. It seems reasonable, therefore, to propose that the bleach and anneal in the case of KCl No. 9 created, in part, magnetic impurity centers and an absorption in the same wavelength range as that of the *U* and *V* absorptions bands.[49]

---

[42] See, for instance, the review article by F. Seitz, *Revs. Modern Phys.* **26**, 7 (1956).

[43] C. Z. Van Doorn and Y. Haven, *Philips Research Repts.* **11**, 479 (1956); *Ned. Tijdschr. Natuurk* **26**, 216 (1960).

[44] H. Pick, *Z. Physik* **159**, 69 (1960).

[45] This is a purely qualitative argument, in which oscillator strengths of 1 and $\frac{1}{3}$ are assumed, respectively, for the *F* and each of the three *M* absorption bands.

[46] It might be argued that for the case of the gamma-ray-colored sample, KCl No. 10, the *F*-center oscillator-strength results indicate that one of the centers contributing to the ultraviolet absorption might be paramagnetic and that a loss of such paramagnetism resulting from bleaching and annealing should be taken into consideration. Figure 15.14 shows that the *V* absorption did not change shape and decreased about 7%. If even as many as half the bleached *V* centers had been magnetic, this would still only make a difference of 3 to 4%, raising the number of magnetic *F* centers remaining (column 10 of Table 15.8) from 63 to 67%. This is still less than the remaining *F*-band absorption.

[47] The total irradiation flux used was $\sim 3 \times 10^6$ r, which was not enough to carry the sample very far into the second stage of coloration. Since first-stage coloration has been attributed to impurity-contributed vacancies [see, for instance, W. E. Bron, *Phys. Rev.* 119, 1953 (1960) and references given therein], the concentration of *F* centers and impurities should be comparable.

[48] It might also be noted that in this particular sample, due to a longer annealing time, only a $1\frac{1}{2}$% increase of *M* centers was produced, thus making it easier for impurity effects to swamp the changes created by the *M*-center production.

[49] The *U* center is not paramagnetic (ref 42). However, the oxygen atoms from the original OH^- are likely candidates for forming magnetic centers.

MAGNETIC SUSCEPTIBILITY OF POTASSIUM HEXACHLORORHENATE(IV) AND POTASSIUM HEXABROMORHENATE(IV) FROM 5 TO 300°K

R. H. Busey[50] E. Sonder

The results of susceptibility measurements on K_2ReCl_6 and K_2ReBr_6 are being published.[51] An abstract of the paper follows:

The Curie points of K_2ReCl_6 and K_2ReBr_6 obtained from magnetic-susceptibility measurements are 12.4 ±0.5 and 15.3 ±0.5°K, respectively, which confirm that cooperative-type transitions observed in the heat capacities of these compounds with maxima at 11.9 ± 0.1 and 15.2 ± 0.1°K, respectively, represent transitions to the antiferromagnetic state. Evidence is presented that the ratios of the next-nearest-neighbor to nearest-neighbor superexchange interactions in the two compounds are approximately equal. An estimate of the spin-orbit coupling constants in the crystals is given and compared with other estimates.

RADIATION EFFECTS IN URANIUM-DOPED ZIRCONIA

M. C. Wittels J. O. Stiegler
F. A. Sherrill

Conflicting interpretations describing the mechanism of the radiation-induced phase transformation[52–55] in ZrO_2 have stimulated a new study aimed at clarifying some of these controversial areas. The major differences of interpretation are of a fundamental nature insofar as radiation damage processes are concerned. Adam and Cox[54,55] have contended that either fast neutrons or fission fragments could induce the phase transition in monoclinic[56] ZrO_2 to the tetragonal or cubic forms *only* if the original material contained impurity atoms which would act as nucleation sites for the higher symmetry phases. To support these contentions they also suggested that uranium itself could act as the impurity atom and, by implication, purported to establish that this was the case even in the Wittels and Sherrill study[52] where less than 0.4 wt % natural uranium was present. Unfortunately, the phase relationships in the ZrO_2-UO_2 system[57] were misquoted in the Adam and Cox article,[54] since there are no stabilized tetragonal or cubic forms of ZrO_2 containing less than 0.4 wt % uranium below 1000°C. More recent studies in the UO_2-ZrO_2 system by Evans[58] are in full agreement with the findings of Wolten[57] in this area, and Evans states that "the high-temperature form of zirconia cannot be stabilized by the addition of UO_2."

The very difficult experiment of irradiating pure ZrO_2 with an external source of fission fragments through a thin aluminum foil to prevent uranium contamination of the sample was also conducted by Adam and Cox.[54] The results of this experiment were inconclusive – first, because of uranium leakage through the aluminum foil; and second, the conclusions were based on the questionable assumption that the damage was not produced near the beginning of the range of the fission fragment.

In their later study,[52] Wittels and Sherrill concluded that the radiation-induced transition to the face-centered cubic phase could be produced only by the action of fission fragments in small regions approximately 140 A in radius. The very large differences in energies and energy transfer mechanisms[59–63] of fast neutrons and fission fragments in solids would indicate that their damaging mechanisms would also be very different in a nonmetallic material. For these reasons an experiment was conducted which would consider

[50] Chemistry Division.

[51] R. H. Busey and E. Sonder, to be published in the *Journal of Chemical Physics*.

[52] M. C. Wittels and F. A. Sherrill, *Phys. Rev. Letters* 3, 176 (1959).

[53] M. C. Wittels and F. A. Sherrill, *J. Appl. Phys.* 27, 643 (1956).

[54] J. Adam and B. Cox, *Phys. Rev. Letters* 3, 543 (1959).

[55] J. Adam and B. Cox, *J. Nuclear Energy, Part A: Reactor Science* 11, 31 (1959).

[56] J. D. McCullough and K. N. Trueblood, *Acta Cryst.* 12, 507 (1959).

[57] G. M. Wolten, *J. Am. Chem. Soc.* 80, 4772 (1958).

[58] P. E. Evans, *J. Am. Ceram. Soc.* 43, 443 (1960).

[59] F. Seitz and J. S. Koehler, in *Solid State Physics* (ed. by F. Seitz and D. Turnbull), Academic Press, New York, 1956.

[60] J. Ozeroff, AECD-2973, 1949 (unpublished).

[61] H. Brooks, KAPL-360, August 1950 (unpublished).

[62] G. H. Kinchin and R. S. Pease, in *Reports on Progress in Physics*, vol 18, p 1, The Physical Society, London, 1955.

[63] J. A. Brinkman, *J. Appl. Phys.* 25, 961 (1954).

the effects of each of these particles, with special emphasis on the control of the number of damaging events by careful uranium doping and with due regard to chemical purity in the light of the previous studies.[52-55]

Samples of monoclinic ZrO_2 containing 35.5 ppm uranium, of which 93% was U^{235}, were prepared so that fission damage could be introduced with low concentrations of total uranium at fast-neutron doses which would be comparatively small. In addition, samples of monoclinic ZrO_2 were prepared containing 3500 ppm uranium, of which 0.022% was U^{235}. Thus the "enriched" ZrO_2 contained more than 40 times as much U^{235} as the "depleted" ZrO_2, yet the depleted samples contained total uranium in a concentration two orders of magnitude higher. With these two cases the effects of fission fragments, fast neutrons, and uranium impurity atoms were determined at exposures from 40 min to 30 days in the ORR.

The results of this investigation indicate the following:

1. Fission-fragment irradiations in the range 10^{15} to 10^{16} fissions/cm^3 produce a phase change in ZrO_2 from monoclinic to face-centered cubic.
2. The transition so produced does not require the presence of chemical impurities in concentrations sufficiently high to result in normal thermal stabilization. In particular, uranium in ZrO_2 in concentrations less than 0.5 wt % does not act as a nucleation and stabilization atom in the process.
3. Fast neutrons, solely, cannot induce the phase transition at doses up to 6.3×10^{20} *nvt*.
4. The question of stability of the phase of ZrO_2 under reactor irradiation depends entirely upon the presence of a fission-fragment flux of sufficient magnitude. Where conflicting data have been reported, it is believed that an unknown presence of fissionable impurities would explain these discrepancies.
5. Two widely different models can be used, in part, to explain the role of the fission fragment in the radiation-induced transition. One model would involve the fission fragment near the beginning of its range and an ionization-displacement[64] process. The other involves the fragment near the end of its range, where heavy concentrations of interstitials are produced through elastic collisions. In either case the pressure due to the interstitials would cause a collapse to the more dense, more symmetrical structure.
6. The contribution of temperature to the transition is problematical. It is not believed that a temperature effect would be great enough to raise the temperature of a small region more than 1000°C, but any thermal effect would probably assist the transformation.

THERMAL CONDUCTIVITY

W. T. Berg

A cryostat for the measurement of thermal conductivity in the region 2 to 100°K is being constructed. The essentials of the assembly are shown in Fig. 15.15. It is similar in design to that of Yost *et al.*,[65] except that a helium reservoir has been added in order to reach temperatures below 10°K.

The assembly is hung within the liquid-nitrogen Dewar flask. The Dewar is suspended a sufficient distance from the floor so that it may be lowered and removed without disconnecting the vacuum lines or electrical leads.

The hydrogen container is suspended in a vacuum space by thin-wall stainless steel tubes. Liquid hydrogen is introduced by means of a vacuum-jacketed siphon inserted in the inlet tube. The hydrogen outlet tube is connected to a vent system and by a valve arrangement to a high-capacity Kinney pump when the cryostat is to be cooled to the temperature of solid hydrogen.

The helium container is suspended by means of a long, thin-wall stainless steel tube which passes through the hydrogen can. By a similar valve arrangement the helium bath can be connected to the high-capacity vacuum pump.

The radiation shield and sample holder is suspended from the helium container by nylon cords. A copper wire or strap is used to improve the heat leak between the shield and the helium bath.

Cooling of the apparatus from room temperature to solid-hydrogen temperature is done by admitting a small amount of helium exchange gas into the vacuum spaces.

Not shown in the diagram are the evacuation tube for the outer vacuum space and the tube used for evacuation of the inner vacuum space and for bringing the electrical leads into the cryostat.

[64] J. H. O. Varley, *Nature* 174, 886 (1954); *J. Nuclear Energy* 1, 13 (1954).

[65] D. M. Yost *et al.*, *J. Am. Chem. Soc.* 63, 3489 (1941).

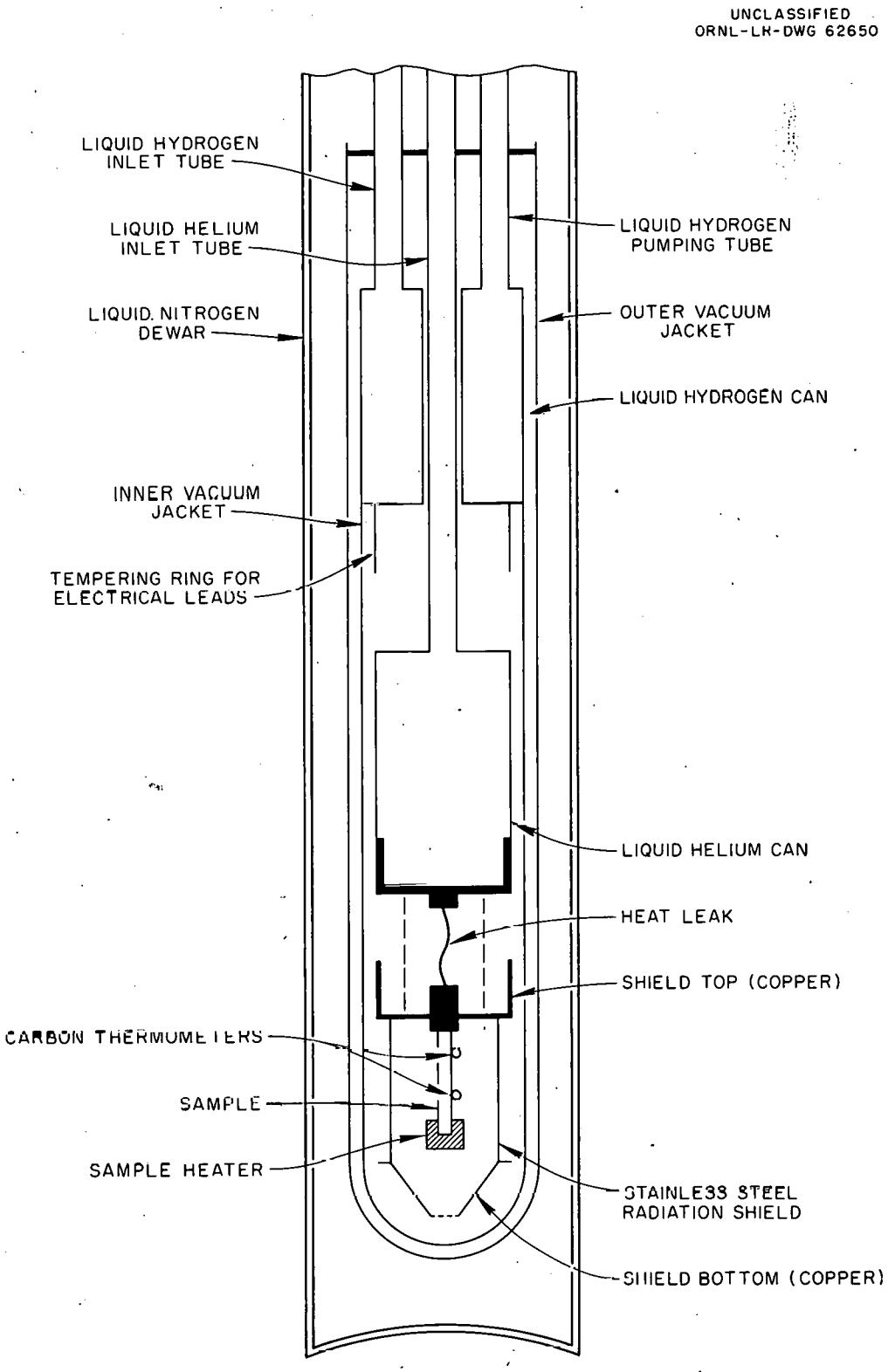

Fig. 15.15. Thermal-Conductivity Cryostat.

16. COVALENT CRYSTALS AND GLASSES

INTRODUCTION OF THE OH RADICAL INTO SILICA AND ITS EFFECT ON THE E_1 CENTER

R. A. Weeks E. Lell[1]
C. T. Butler R. C. Hudson[2]

It has been suggested[3] that the E_1 center in high-purity silica is influenced by the presence of hydrogen in the silica. The E_1 center, as has been indicated before,[4] is a fundamental defect of the quartz structure. It was noted[3] that for a constant gamma irradiation the intensity of the E_1' center (the prime indicates occupancy of the defect by an electron produced by the ionizing radiation) was apparently inversely proportional to the intensity of the 2.7-μ band arising from the O–H stretching mode.

In those specimens in which the intensity of the 2.7-μ band was high (Corning 7940), an electron spin resonance (ESR) doublet was also observed ($\Delta H \approx 70$ gauss, $g_{obs} \approx 2.00$) after irradiation.[3] This doublet was attributed to an ionization state of the hydroxyl radical. Gilliam has recently shown[5] that if the hydrogen is exchanged for deuterium the doublet disappears. This experiment gives reasonable support to the suggestion of the paramagnetism of the OH radical. However, due to the apparent low concentration of the doublet and the relatively high intensity of the 2.7-μ band, the efficiency of formation by gamma irradiation must be quite low.

In order to determine the quantitative relation between the 2.7-μ band and the E_1 center, a series of measurements have been made on a silica (Corning 7943) which initially had only a very weak 2.7-μ band. The experimental procedure was: (1) optical absorption measurements (measurements "1"), (2) Co^{60} gamma irradiation to a dose of 2×10^6 r, (3) optical measurements (measurements "1a"), (4) heat in H_2O at 900°C for 4 hr, (5) optical measurements (measurements "2"), (6) Co^{60} gamma irradiation to 2×10^6 r, and (7) optical measurements (measurements "2a"). The cycle was repeated with the heat treatment in water vapor extended to 10 hr and then to 19 hr. The specimen was prepared for the heat treatment by placing it in a quartz tube; a drop of water was inserted and then frozen. The tube was then evacuated and sealed. After each treatment the faces of the specimen had to be repolished because of etching of the surface during the treatment.

The optical measurements were made with a Perkin Elmer infrared spectrometer at 2.7 μ, a Cary model 14 at 2140 A, and a vacuum ultraviolet spectrometer in the region from 2400 to 1400 A.

The absorption coefficients at the peak of the E_1' center and OH band were found by subtracting the background absorption. These values are shown in Fig. 16.1. As noted in the experimental procedure, four values were measured. In Fig. 16.1 a straight line has been drawn through three of the points, and the fit is within experimental error. The extrapolation to zero intensity of the 2.7-μ band shows that the intensity of the E_1' center which is observed is ~10% higher than the intercept.

The optical measurements after gamma irradiation in the visible and ultraviolet region are shown in Fig. 16.2. Observation at energies in the range 5 ev down to 1 ev did not show any changes in the absorption coefficient greater than 0.6 cm^{-1} which resulted from the treatments. The optical bands introduced by the gamma irradiation are shown as $ia - i$, where i is the optical absorption measurement made after each heat treatment and ia is the measurement made after each irradiation. The heat treatments (in 900°C water) were: 1 ≡ initial condition (no treatment), 2 ≡ 4-hr treatment, 3 ≡ 10-hr treatment, and 4 ≡ 19-hr treatment. At photon energies higher than ~7.5 ev, the scattered light was equal to or greater than the light transmitted by the specimen, and therefore the data points in this region do not reflect the true absorption coefficient values. The curves, drawn through the points, have been cut off at 7.5 ev for this reason.

In addition to the E_1' band (~5.8 ev) there are two or more bands between 6.5 and 7.5 ev which decrease with the introduction of OH.

---

[1] Visiting scientist from Bausch and Lomb, Inc., Rochester, New York.

[2] Research participant from Woman's College of the University of North Carolina, Greensboro, North Carolina.

[3] *Solid State Div. Ann. Progr. Rept. Aug. 31, 1960*, ORNL-3017, p 90.

[4] R. A. Weeks and C. M. Nelson, *J. Am. Ceram. Soc.* 43, 399 (1960).

[5] O. R. Gilliam, *Bull. Am. Phys. Soc.* 6, 246 (1961).

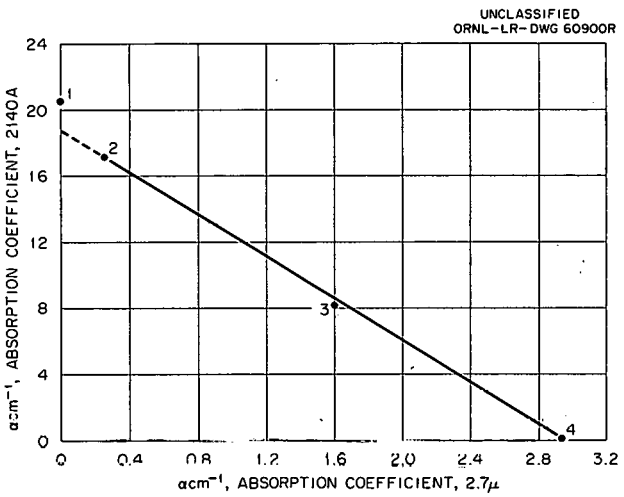

Fig. 16.1. Absorption Coefficient of the E_1' Center Produced by 3×10^6 r Co^{60} Gamma Rays at ~25°C vs Absorption Coefficient of the 2.7-μ Band After Heating in H_2O at 900°C for Various Periods of Time. The point numbers refer to heat treatments as defined in the text.

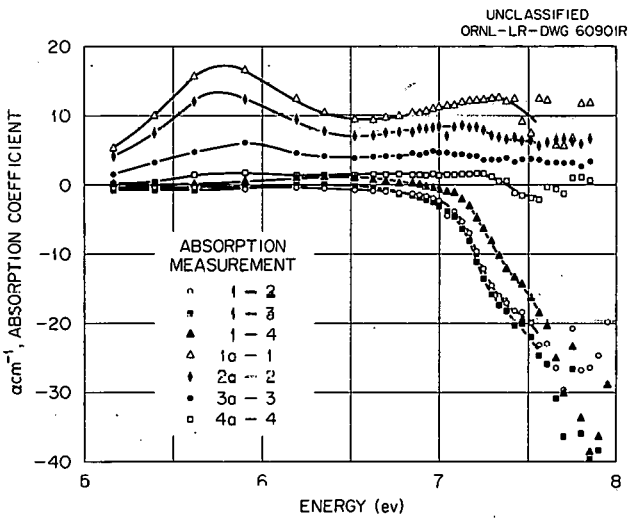

Fig. 16.2. Optical Absorption of the Silica Specimen in the Far Ultraviolet Is Shown After Each Period of Heating in H_2O. Four of the curves (1a – 1, 2a – 2, etc.) show the differences in the optical absorption before and after irradiation by 3×10^6 r Co^{60} gamma rays. The other three curves (1 – 2, –3, –4) show the differences in the optical absorption between the initial state of the specimen and after each period of heating.

The remaining curves in Fig. 16.2 were obtained by taking the difference $1 - i$, where $i = 2, 3, 4$. These curves show the effect of the heat treatment and the introduction of OH on absorption in the tail of the fundamental absorption edge. After the 4-hr treatment there is a large increase in the absorption coefficient between 7.0 and 7.5 ev. There is little change with the 10-hr treatment. With the 19-hr treatment there is a decrease of ~30%.

The curve shown in Fig. 16.1 can be described by the expression

$$\eta_{E_1} = b - a\eta_{(OH)},$$

where a and b are constants, $\eta_{E_1} \equiv$ concentration of E_1 centers, and $\eta_{(OH)} \equiv$ concentration of O–H bonds. The data in Fig. 16.1 are not sufficient for evaluation of the constants in the equation, since the oscillator strength of the O–H stretching-mode absorption is not known. This equation does show that the OH in some way prevents the formation of the E_1' center. A detailed model of the E_1' center is required before the nature of the interaction between the OH and the E_1 center can be understood. Silsbee[6] has shown that a detailed model cannot yet be derived from the ESR data. The decrease in the band at ~7.3 ev (Fig. 16.2) with the treatments does suggest that another optical band is involved in the trapping of electrons by the E_1 center.

The increase in the absorption between 7.0 and 7.5 ev after the first two treatments [curves (1 – 2) and (1 – 3)] and the decrease after the third treatment [curve (1 – 4)] indicate that the introduction of OH also affects the characteristic absorption of the unirradiated material. It is interesting to note that after the final heat treatment the absorption in this range is similar to that of the OH-containing Corning 7940 specimens.

OSCILLATOR STRENGTH OF THE E_1' CENTER IN SILICA

R. A. Weeks E. Sonder

The concentration of the E_1' center in silica produced by Co^{60} gamma irradiation was measured by an electron spin resonance (ESR) and static

[6] R. H. Silsbee, *Journal of Applied Physics*, to be published.

magnetic-susceptibility technique. The results were used to calculate the oscillator strength of the optical band and were compared with two earlier estimates of the oscillator strength.

The silica used in these experiments was a high-purity hydrogen-free material.[7] In this silica, high concentrations of the E_1' center ($\sim 10^{18}$ per cm^3) are obtained at 25°C by a relatively low gamma-ray dose ($\sim 3 \times 10^7$ r). Two specimens were used; one (Co-S1) received a dose of $\sim 3 \times 10^6$ r and the other (Co-S2) $\sim 3 \times 10^7$ r.

The ESR spectrum and the susceptibility were measured before and after irradiation; in Co-S1 a weak ESR line, probably a hole resonance, was observed prior to irradiation, and the susceptibility measurement gave $\sim 1 \times 10^{17}$ paramagnetic centers per cm^3. No ESR lines were observed in Co-S2, and the susceptibility gave $\sim 5 \times 10^{16}$ centers per cm^3. In Table 16.1 the results of the measurements are recorded. Two sets of ESR measurements were made, one in which the DPPH (diphenylpicrylhydrazyl) was crystallized from a $CHCl_3$ solution and one in which it was crystallized from CS_2 solution. It has been noted[8] that the free-radical assay in DPPH is dependent upon the solvent used and that CS_2 gives the highest assay. For this solvent the free-radical assay is 92% of that expected from the mass of the material. The results in Table 16.1 are in agreement with these facts. The values given in the last column were found by assuming that the [DPPH·CS_2] assays 100%. If the assay is indeed 92%, then the values should be reduced by 8%. Results reported earlier[9] were obtained by the ESR techniques and with [DPPH·$CHCl_3$]. If they are corrected in terms of the values given above, then they are in agreement with the DPPH·CS_2 results.

The susceptibility value for the concentration should be higher than the ESR value, since all paramagnetic centers are measured, and only the E_1' centers are counted by the ESR method. The rather close agreement ot the two methods is evidence supporting the hypothesis that the E_1' center is the primary paramagnetic center in these silicas. The concentration of other paramagnetic centers was apparently ~ 0.1 of the concentration of E_1'.

Table 16.1. Concentration of E_1' Centers in Silica

Sample	χ^a	ESR [DPPH·$CHCl_3$]	ESR [DPPH·CS_2]
Co-S1	3.8×10^{17}	6.3×10^{17}	3.9×10^{17}
Co-S2	1.09×10^{18}	1.40×10^{18}	1.10×10^{18}

[a]The assumption is made that the magnetic centers (probably hole centers) originally in the material are removed by the irradiation.

Table 16.2. Oscillator Strength of the E_1' Center

Sample	α (cm^{-1})	ΔU (ev)	f^a
Co-S1	13.1	0.8	0.17
Co-S2	35	0.8	0.16

$$^a f \approx \frac{0.07 \times 10^{17}}{n} \cdot \frac{\eta}{(\eta^2 + 2)^2} \propto \Delta U ,$$

where n = spins cm^{-3} and η = index of refraction.

The oscillator strength[10,11] of the E_1' center and the optical data are given in Table 16.2. The values for f are in excellent agreement for both specimens.

The oscillator strength of the E_2' center was also calculated by using the concentration measured by a comparison to [DPPH·$CHCl_3$]. The value was found to be $f = 0.2$. By taking the ratio of the spin concentrations for the [DPPH·$CHCl_3$] and [DPPH·CS_2] and multiplying the above f by this ratio, a corrected value, $f_{cor} \approx 0.35$ is found

[7]Corning 7943 kindly supplied by S. D. Stookey of Corning Glass, Inc.

[8]W. Duffy, Jr., Tech. Rept. No. 1, Dept. of Physics, Univ. of Santa Clara, Santa Clara, Calif., O.N.R. Contract NONR 2985(01).

[9]R. A. Weeks, *Solid State Div. Ann. Progr. Rept. Aug. 31, 1958*, ORNL-2614, p 32.

[10]The optical absorption band is assumed to have a Gaussian shape. The equation given in the table is the appropriate one for this shape function.

[11]D. L. Dexter, *Solid State Physics*, vol 6, p 371, Academic Press, New York, 1958.

PARAMAGNETIC PROPERTIES OF THE E_2' CENTER IN CRYSTALLINE QUARTZ

R. A. Weeks

The E_2' center in quartz single crystals is produced by irradiation with gamma rays or neutrons. Some of the optical and magnetic properties have been described.[4] The interaction of the spin state of E_2' centers with the lattice has been investigated as a function of temperature and is described in the section on the relaxation processes of the E' centers.[12]

With the magnetic field parallel to the c axis [00·1], two lines are observed. The orientation data indicate two sets of lines each composed of six sites per unit cell. The principal values of the two g tensors and their directions with respect to the crystalline axis have been found. Hyperfine interactions were observed and are thought to arise from an interaction with the nearby Si^{29} nuclei. A model for the defect is suggested based on the axial symmetry of the center, the direction of the axis, and the hyperfine interactions. The impurities present in the crystal are essential for the formation of the center by gamma rays and may determine the characteristics of the g tensors.

The symmetry of alpha quartz implies that, except for certain lines or planes of symmetry, an arbitrary point in the unit cell is equivalent to five other points and that the points are related by the symmetry operations of the crystal. A defect at one of these points has an equal probability of being at any one of five other symmetry-related points. For an arbitrary orientation of the crystal, a paramagnetic defect at one of the points should exhibit six electron spin resonance (ESR) lines. For the E_2' center two lines, $g_{c\,axis} = 2.0008$ and $g_{c\,axis} = 2.0010$ ($g \equiv$ observed spectroscopic splitting factor $= h\nu/\beta H$), are observed (Fig. 16.3*a*) when the applied magnetic field is parallel to the threefold axis [00·1]. Upon rotation of the magnetic field about a twofold axis [10·0], six lines are resolved. For an arbitrary orientation 12 lines have been resolved.

The Hamiltonian that can describe the lines is a spin-only one,

$$\mathcal{H} = \beta \vec{H} \cdot \overleftrightarrow{g} \cdot \overleftrightarrow{S} \qquad (1)$$

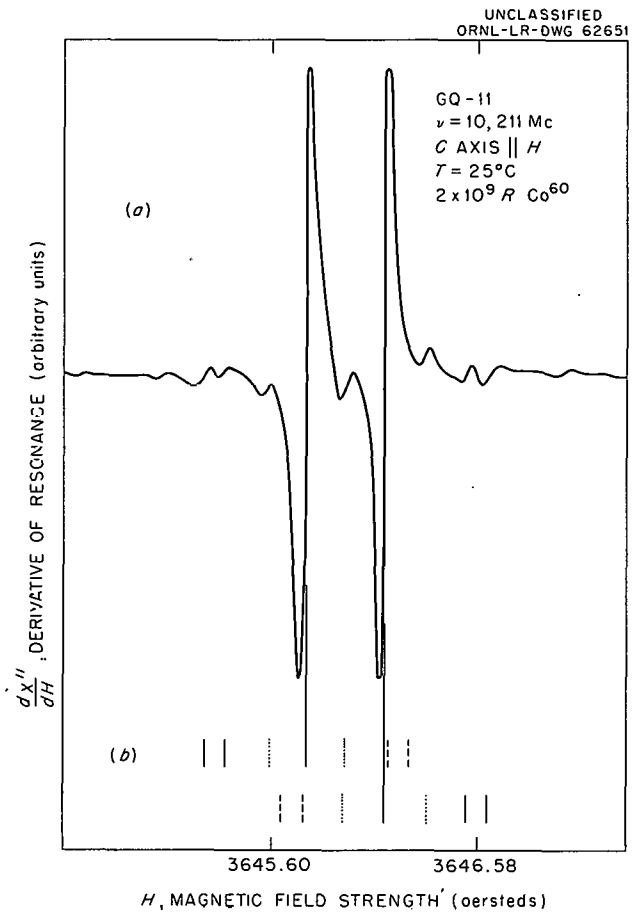

Fig. 16.3. (*a*) **Hyperfine Lines with a Very Weak Interaction.** *The two intense lines are the* E_2' lines. (*b*) Schematic Drawing of the Lines in (*a*). The solid lines are the well-resolved lines. The dotted lines are those which appear as an inflection on the shoulder of the E_2' lines. The dashed lines are the two components of the line between the two E_2' lines.

in which for the c axis parallel to H, each line is composed of six lines. Thus for arbitrary orientation 12 lines should be observed, and this is the case. This description does not take into account hyperfine interactions; an additional term is necessary for these interactions. On this basis the g tensors for the two centers were calculated and are given in Table 16.3. The eigenvalues of the g tensor are relative to the g values for the c-axis orientation. The absolute accuracy of the values for the c-axis orientation is given. The appropriate directions for the other five lines, for

[12] D. Feldman, J. Castle, and R. A. Weeks, to be published.

Table 16.3. g-Tensor Eigenvalues and Their Orientations with Respect to the Crystalline Axis

Axis	θ	ϕ
$g_{c\ axis} = 2.0008 \pm 0.0003$		
$g_1 = 2.00150 \pm 0.0001$	$61^\circ 27' \pm 3^\circ$	$-32^\circ 13' \pm 3^\circ$
$g_2 = 2.00057 \pm 0.0001$		
$g_3 = 2.00057 \pm 0.0001$		
$g_{c\ axis} = 2.0010 \pm 0.0003$		
$g_1 = 2.00223 \pm 0.0001$	$121^\circ 53' \pm 3^\circ$	$-58^\circ 10' \pm 3^\circ$
$g_2 = 2.00050 \pm 0.0001$	$35^\circ 25'$	$-31^\circ 19'$
$g_3 = 2.00067 \pm 0.0001$	$102^\circ 4'$	147°

each c-axis line, are obtained by setting $\theta' = \theta$, and $\phi' = \phi \pm 120^\circ$ and also $\theta' = (180^\circ - \theta)$ and $\phi' = -\phi \pm 120^\circ$ or $-\phi$. The errors are based on the scatter in the results for the six lines observed for rotation about a [10·0] axis. No estimate of the magnitude of systematic errors has been made.

Since two lines are observed for the [00·1] direction and each of these breaks up into three lines upon rotation about a [10·0] direction, another possible explanation is that the lines arise from one center that has $S = 1$. The orientation dependence of the lines (Fig. 16.4) does not follow the pattern expected for an $S = 1$ state.

Hyperfine interactions have been observed with nuclei of $I = \frac{1}{2}$. The lines from a very weak interaction are shown in Fig. 16.3. The intensities of these lines are ~3% of the unperturbed line. Three lines on the low-field and high-field side of the two unperturbed lines are clearly resolved, and a seventh line is resolved between the two unperturbed lines. In addition to these lines, two pairs of lines are found, each pair with a splitting of 412 gauss. When the second-order shift in the center of gravity is taken into account, these lines fall approximately on the unperturbed lines. These lines may arise from a strong interaction of the E_2' centers with a nuclei of $I = \frac{1}{2}$. Again the intensity ratio is ~0.03.

In view of the two pairs of lines with splittings of 7 or 8 gauss, which have been observed for the E_1' center,[4] a careful search was made for similar lines in the case of the E_2' centers. No lines were found with these splittings.

The evidence[4] from the neutron-irradiated crystals, the occurrence of these two lines (c-axis orientation) in all single crystals which have been gamma irradiated (two kinds of synthetic crystals and a natural crystal), and the intensity ratio of the hyperfine lines to the unperturbed lines support the hypothesis that these centers are defects of the quartz structure. The intensity ratio of the hyperfine lines to the unperturbed central lines is ~0.03 in the several crystals which have been irradiated. The kinds of impurity ions and their concentrations are of the same order in all the crystals. However, none of these have a nuclear spin of $I = \frac{1}{2}$. The only ion present in the crystal with this nuclear spin is Si^{29}, and its abundance is 4.7%. The intensities of the hyperfine lines are in agreement with intensities predicted from the natural abundance of Si^{29}.

In Fig. 16.3b a schematic diagram of the hyperfine lines is shown. The lines of the strong interaction are not shown. There are no lines for a weak interaction which occurs for the E_1' center. The very weak interactions found for the E_1' center are also found for the E_2' centers. However, there is a difference; the very weak interaction for the E_1' center shows interactions with only two Si^{29} nuclei, whereas in Fig. 16.3 three lines are resolved on the low- and high-field sides of the pair of unperturbed central lines. The schematic diagram in Fig. 16.3b shows a possible reconstruction of the hyperfine lines. The relatively strong line which is midway between these two lines is the coincidence of one hyperfine line from the 2.0008 line and one from the 2.0010 line. In this construction of the hyperfine interactions, each of the centers has a strong interaction with one Si^{29} and a very weak interaction with three Si^{29}.

On the basis of the above evidence, the E_2' centers have $S = \frac{1}{2}$ and appear to be due to an electron that occupies an Si-O bond that is uncompleted. Three of the Si-O bonds are complete, but the O ion for the fourth bond is missing. The strong hyperfine interaction is probably with the nucleus of the Si ion on which the electron is trapped, and the very weak interaction may be a superexchange interaction, through the three O ions, with the nearest neighbor Si ions. The difference between the two centers is presumed to be due to a difference in crystalline fields. The source of the difference is not known.

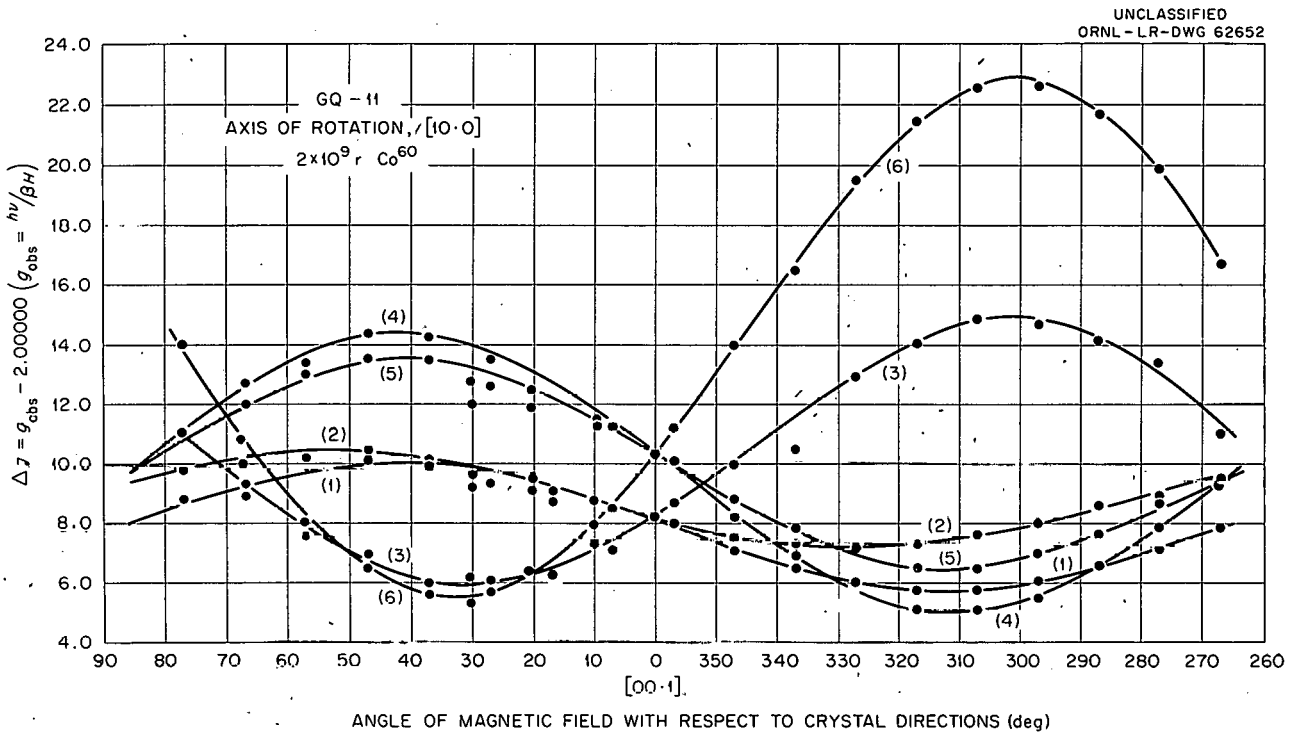

Fig. 16.4. Variation of the E_2' Lines as a Function of Angle with Respect to the Magnetic Field. Rotation axis is a twofold axis, [10·0]. The observations were made at ~25°C in the *TE* cavity, 10,200 Mc.

Electron spin relaxation[13] of the E_1' and E_2' centers has been observed over a temperature range of 2 to 300°K. The observed relaxation times are consistent with the spin state of both centers being $S = \frac{1}{2}$. At temperatures between ~10 and 250°K, an unusual temperature dependence of the relaxation was observed.

ALUMINUM IMPURITIES AND THE 4600-A BAND IN QUARTZ

R. A. Weeks C. T. Butler

The electron spin resonance (ESR) of a defect in quartz single crystals has been ascribed to a hole trapped on an aluminum ion which was substituted for a silicon ion.[14,15] The hole is produced by gamma or x-ray irradiation. It has been suggested that this trapped hole also produces optical absorption bands at ~4600 A and 6250 A.[15] On the basis of this assumption, an enhancement of the optical band at 4600 A by a cycle of neutron irradiation followed by a heat treatment was attributed to a diffusion of interstitial aluminum into substitutional sites.[16]

Recently a cycle of treatments was carried out on a synthetic quartz crystal.[17] The cycle consisted of Co^{60} gamma irradiation to ~10^9 r; heat treatments at 200°C for 30 min, 300°C for 30 min, and 440°C for 30 min; and gamma irradiation to ~10^9 r. In Fig. 16.5 the absorption coefficient observed after each of these treatments is shown. With the heat treatments there was a decrease in

[13] The relaxation-time measurements were carried out at Westinghouse Research Laboratory by D. Feldman, J. Castle, and R. A. Weeks.

[14] J. H. E. Griffiths, J. Owen, and I. M. Ward, p 81 in *Report of the Conference on Defects in Crystalline Solids*, The Physical Society, London, 1955.

[15] M. C. M. O'Brien and M. H. L. Pryce, pp 88–91 in *Report of the Conference on Defects in Crystalline Solids*, The Physical Society, London, 1955.

[16] E. W. J. Mitchell and E. G. S. Paige, *Phil. Mag.* 1, 1085–115 (1956); A. J. Cohen, *J. Chem. Phys.* 25, 908 (1956).

[17] The synthetic quartz used in these experiments was kindly sent by C. S. Brown of General Electric Limited, England.

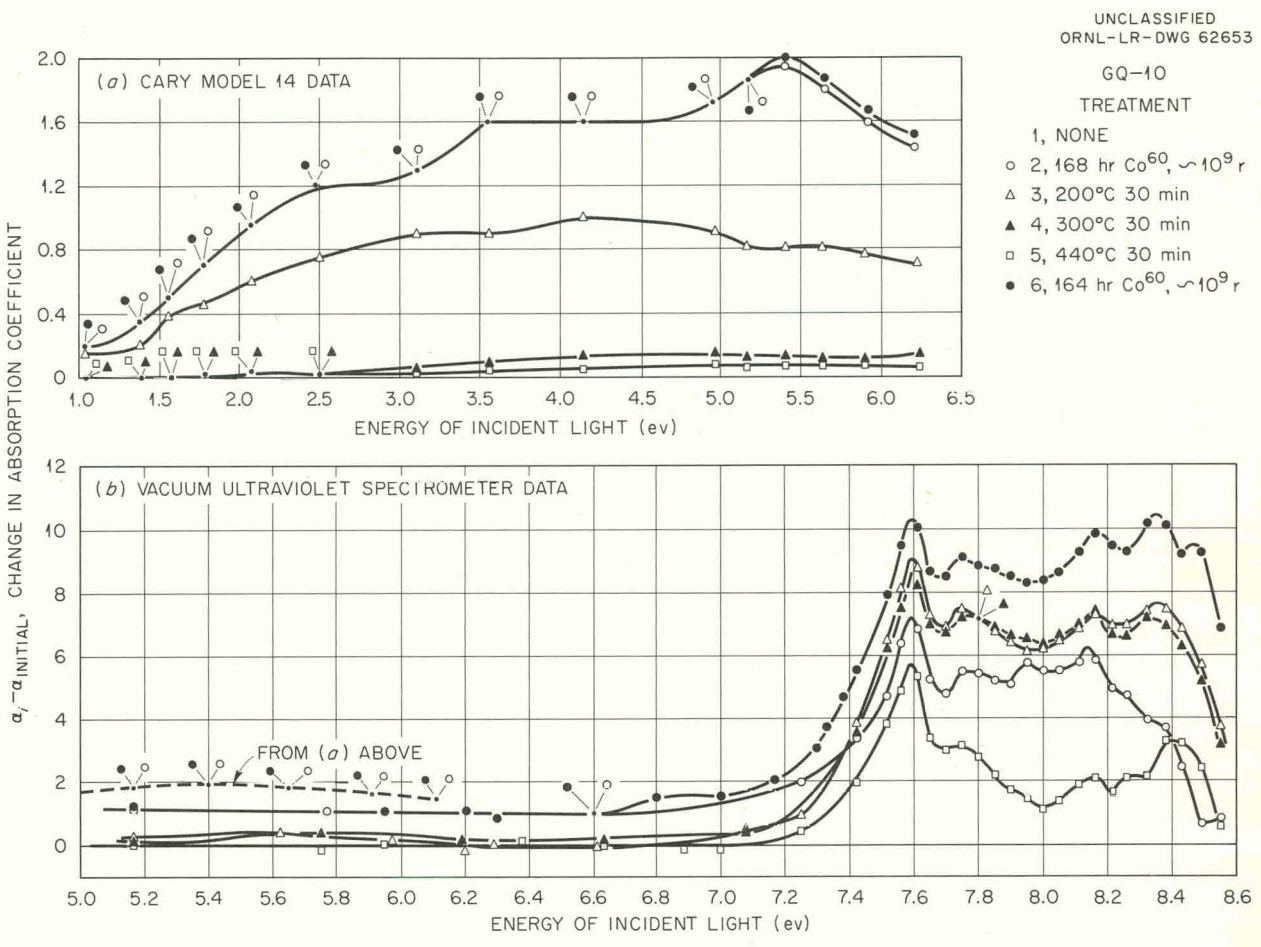

Fig. 16.5. Optical Absorption of a Synthetic Crystal After a Series of Treatments. The crystal was oriented so that the incident light was parallel to [00·1]. The absorption of the unirradiated crystal was subtracted from the absorption after the treatments indicated in the figure.

the absorption below ~7 ev and an enhancement at energies greater than ~7 ev. After the 440°C treatment there was an over-all decrease in the absorption. The exception is the small increase in absorption in the region of 6 ev after heating at 300°C for 30 min. This effect has been described elsewhere.[4] The absorption at energies greater than 7 ev is much greater than for energies less than 7 ev. The absorption in the region of 2.7 ev (4600 A) is an order of magnitude less than in the 7.5- to 8.5-ev region. The bands below 7 ev are very weak after the heat treatment at 300°C for 30 min, whereas most of the bands at higher energies are enhanced. Two bands in this region decrease after this treatment; they are at ~7.3 and 7.9 ev. It is also evident that this cycle of treatments has not enhanced the absorption in the the region of 2.7 ev (4600 A). The absorption in this band after the second irradiation is the same as after the first irradiation.

Electron spin resonance (ESR) measurements were also made at the same time as the optical measurements. Many lines were observed, and among these were the lines which have been attributed to a hole trapped on a substitutional aluminum ion.[14] The resonance is shown after the first irradiation in Fig. 16.6*a* and after the second irradiation in Fig. 16.6*b*. The observations were made at 78°K with the applied magnetic field, H, directed along the c axis, [00·1]. In this orientation the three sites per unit cell have the same g

UNCLASSIFIED
PHOTO 55647

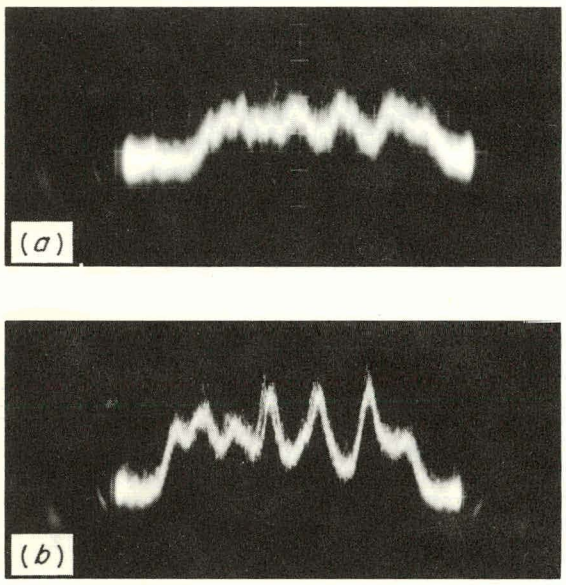

Fig. 16.6. Aluminum Resonance in the Crystal Used for the Optical Measurements. Other resonances do not appear in these photographs. They are found on the high-field side of the aluminum resonance. The crystal was at 78°K. (*a*) Resonance after the first irradiation. (*b*) Resonance after the sequence of heat treatments and second gamma-ray irradiations, shown in Fig. 16.5. The applied field was parallel to [00·1].

value. Since the magnetic field is not parallel to an axis of symmetry for any of the three sites, forbidden transitions arising from the quadrupole interaction occur. The observed spectrum is not simply the six lines expected from the hyperfine interaction of the paramagnetic hole with the aluminum nucleus ($I = \frac{5}{2}$).[15]

A comparison of Fig. 16.6*a* with Fig. 16.6*b* shows that there has been an approximately threefold increase in the intensity of this center after the second irradiation. The intensity of these lines was also compared with a known amount of diphenylpicrylhydrazyl (DPPH). The necessary conditions[18,19] were met for a comparison of the number of spins in DPPH with those in the specimen, provided that the filling factor of the specimen was taken into account. The DPPH was placed at the maximum of the magnetic component of the oscillating magnetic field. The two resonances are shown in Fig. 16.7. The concentration of spins in the aluminum resonance was 5×10^{17} spins/cm^3 ± 50%. The concentration of aluminum in the crystal was measured by a spectrographic method and was found to be 70 aluminum atoms per million silicon atoms or 1.9×10^{18} per cm^3.

UNCLASSIFIED
ORNL-LR-DWG 55359

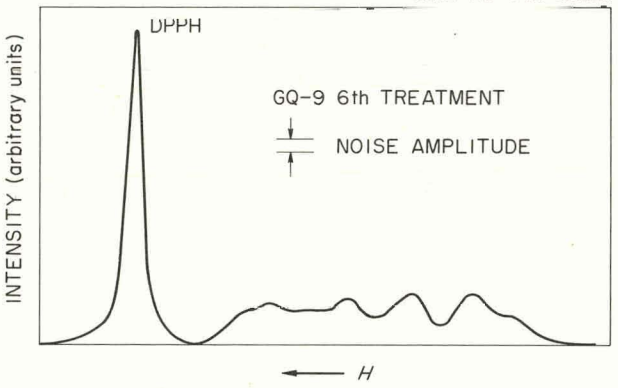

Fig. 16.7. Aluminum Resonance and Resonance of a DPPH Crystal. The DPPH crystal was crystallized from chloroform, and it was assumed that the concentration of spins was approximately six-tenths the number determined from the mass of the crystal.

Discussion

A comparison of the optical and ESR data does not support the correlation of the optical bands in the region of 2.7 ev with the ESR of substitutional aluminum.[15] The threefold enhancement of the aluminum resonance which occurs after the second irradiation is not accompanied by an enhancement of the optical absorption in the region of 2.7 ev. The absorption in this region after the second irradiation is identical with that found after the first irradiation. In view of these results, the enhancement of the optical absorption in this region which has been observed[16] cannot be attributed to the diffusion of interstitial aluminum into silicon vacancies. The enhancement of the aluminum resonance may be related to the fact that after the last heat treatment (Fig. 16.5, curve 5) the optical absorption in the 7.5- to 8.5-ev region has not returned to the initial value.

[18] R. H. Silsbee, *Phys. Rev.* 103, 1675 (1956).

[19] R. T. Schumacher and C. P. Slichter, *Phys. Rev.* 101, 58 (1956).

Another facet of these experiments is the correlation of an optical band with the ESR center. The 2.7-ev band is very weak in synthetic crystals which have been grown on a *Z* plate or *y* bar.[20,21] The spectrographically determined aluminum concentration in crystals with a strong band at 2.7 ev and crystals with only a very weak band at 2.7 ev is the same within an order of magnitude. In our specimens, grown on a *Z* plate, the band was very weak (Fig. 16.5). No enhancement of the optical absorption after the second irradiation in the region of 2.7 ev was observed, although the aluminum resonance increased. In the absorption spectrum the only region in which enhancement occurred after the second irradiation was between 6.5 ev and 8.5 ev. The aluminum resonance also disappears after heating at 300°C for 30 min. Therefore, only those bands which disappear with the heat treatment and are enhanced after the second irradiation can be correlated with the aluminum resonance. The optical absorption in the region of 7.3 ev appears to meet these requirements.

Another possibility is an optical band whose width at room temperature is much larger than the ~1-ev width found in those bands which are observed. There is at present no evidence to support this hypothesis.

These results indicate that the correlation of the optical absorption in the region of 2.7 ev with the aluminum resonance is in doubt. They also raise questions about the process by which the enhancement of the bands in this region takes place.

ELECTRIC-FIELD DISTRIBUTION IN GAMMA-IRRADIATED LEAD GLASS

R. C. Hudson[2] R. A. Weeks

In an attempt to explain the planarity of electrical discharges in hot-cell windows, such as that reported by Culler,[22] a calculation was made of the electric-field intensity inside a lead-glass window due to irradiation with 1.3-Mev gammas normal to the surface of the glass.[23]

The following simplifying assumptions were made: (1) that the window surface is an infinite plane, (2) that the gamma absorption is exponential, (3) that the Compton recoil electron moves about 2 mm into the glass beyond the point of ionization, (4) that saturation effects may be neglected, (5) that the conductivity of the glass is negligible, and (6) that only one ion pair with appreciable charge separation is produced by each gamma-ray absorption event.

It is believed that these simplifying assumptions, while not valid, enable one to derive a field intensity at least as large as that actually present, and of the same general form.

Results

The following expressions were obtained for the electric-field intensity E at a depth x from the incident surface into the glass.

From the incident surface ($x = 0$) to the beginning of electron deposition ($x = 0.2$ cm),

$$E = 1.1 \times 10^{-6} N(1 - e^{-0.14x}) \text{ v/cm},$$

where N = number of photons per cm^2 of incident surface. For $x \geq 0.2$ cm,

$$E = 3.1 \times 10^{-8} N e^{-0.14x} \text{ v/cm}.$$

Conclusions

1. The maximum field intensity occurs within a few millimeters of the "hot" face.
2. This field distribution is in itself insufficient to explain a planar discharge near the center of a window ten or more centimeters thick.
3. There may be, after extensive gamma irradiation, a field intensity deep within a window sufficient to aid in the propagation of a discharge initiated by other means. The planarity of the observed discharges seems to depend on some mechanical or impurity-layer effect.

VACUUM-ULTRAVIOLET ABSORPTION STUDIES OF IRRADIATED SILICA AND QUARTZ[24]

C. M. Nelson[25] R. A. Weeks

The optical absorption properties of Co^{60}-irradiated fused silica and crystalline quartz have been

[20] G. W. Arnold, *J. Phys. Chem. Solids* 13, 306 (1960).

[21] A. Cohen, *J. Phys. Chem. Solids* 13, 321 (1960).

[22] Vaughn Culler, *Gamma-Ray Induced Electrical Discharge in a Radiation Shielding Window*, Proceedings of the 7th Hot Laboratories and Equipment Conference, 1959.

[23] Constants for Pittsburgh Plate Glass Co. No. 4966 were used.

[24] Abstract of a paper published in *J. Appl. Phys.* 32, 883–86 (1961).

[25] Present address: Emory and Henry College, Emory, Virginia.

studied in the vacuum-ultraviolet region. The most prominent absorption band found in both materials has a maximum at 7.6 ev (1620 A). Optical and thermal bleaching experiments indicate that this band is not necessarily complementary to a band at 5.9 ev (2100 A), as has been assumed. Though the 7.6-ev band has approximately the same intensity in both materials for the same irradiation, the 5.9-ev band is >20 times more intense in fused silica. The 7.6-ev band is still present after the 5.9-ev band has been thermally bleached. Additional absorption bands occur at 8.0 and 8.2 ev. Also, optical and thermal bleaching experiments suggest other absorption bands at 7.2, 7.4, 7.8, and 7.9 ev. Since these bands (particularly the 7.6-, 8.0-, and 8.2-ev bands) occur in high-purity silica and quartz, it is suggested that they are associated with defects in the quartz structure and are not caused by impurities.

17. STORED ENERGY IN GRAPHITE

STORED ENERGY IN THE ORNL GRAPHITE REACTOR – 1960[1]

M. C. Wittels

The stored-energy status of the ORNL Graphite Reactor, which went into operation in November 1943, has been analyzed following a low-temperature anneal in which fission heat and a reverse-airflow system were employed. From more than 100 postannealing core samples, calorimetric studies revealed that the annealing operation was successful, and the extent of the anneal closely conformed to expectation for the maximum temperature profiles reached during the annealing cycle.

Between 3.5 and 4.5 Mwhr of stored energy in a 15-ft-diam region was released during the reactor operation, and the stored energy in that area was reduced to a level where a spontaneous release is now not possible. This was achieved with a maximum fuel-element temperature of 275°C and a maximum graphite temperature of 236°C, emphasizing the efficacy of the low-temperature method.

The peripheral regions of the fuel zone, including the outer three rows, did not reach sufficiently high temperatures for annealing, primarily because of sharply dropping thermal gradients at the edges of the moderator stack. The future stored-energy status of the reactor is discussed.

[1]Abstract of an article to be published in the *Journal of Nuclear Energy*, December 1961.

18. CERAMICS

C. D. Bopp O. Sisman R. L. Towns

ANNEALING STUDIES ON IRRADIATED MICA AND ASBESTOS

Annealing is being studied for some of the ceramic materials for which the radiation-induced changes were studied earlier.[1] Some initial results have been obtained for the release in stored energy by irradiated mica and for the radiation-induced change in the temperature of dehydration of asbestos, but this work is not yet complete. The furnace (Fig. 18.1) is heated at a smooth rate, and the temperature difference between the platinum crucible and the shield is recorded with a sensitivity of a few thousandths of a degree. The energy flow into the crucible is related to the differential thermocouple reading from calibration with materials of known specific heat. Since the apparatus is evacuated to less than 1 μ, the crucible is well insulated from the outer shield and the transfer of heat occurs by radiation. The component of the thermocouple signal which arises from the passage of the thermocouple lead wire through a thermal gradient (because of small inhomogeneities in composition or of stresses) is determined by comparing calibrations in which the rate of heating and the sample size are varied. The apparatus is designed so that the portion of the thermocouple lead wires which is exposed to a thermal gradient is not subject to bending when the apparatus is disassembled for sample loading.

The small mass of the crucible and sample gives a small time constant and high resolution for measuring thermal transitions. This feature, however, also makes the apparatus extremely sensitive to small fluctuations in the rate of heating. The rate of heating is controlled by changing the furnace voltage with a motor-driven Variac. This method has proved preferable over the alternative of using a motor drive on the set point of a controller, since changes in the rate of heating produced by the controller in holding the set point complicate the interpretation of the thermal analysis.

Several designs of apparatus for thermal analysis were considered. For work with small samples (about 1 g), it is desirable that the design be fairly simple, since the construction of such a small apparatus is difficult. Initially, it was planned to make the apparatus entirely adiabatic by installing a heater in the crucible. At high temperatures (600–1000°C), however, much trouble was experienced from breakdown of the insulation between the heater and the differential thermocouple. For this reason, and in order to simplify construction, the heater was omitted.

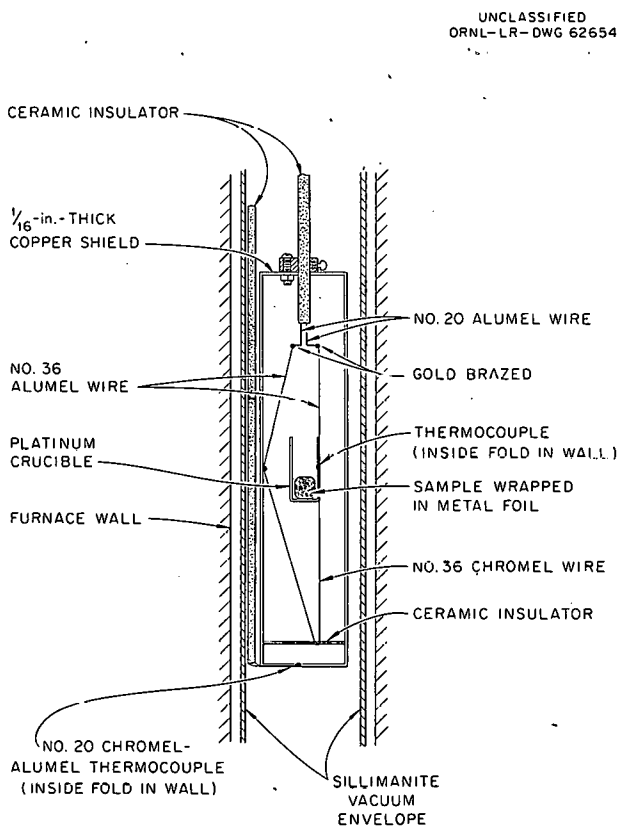

Fig. 18.1. Annealing Furnace.

[1] C. D. Bopp, O. Sisman, and R. L. Towns, *Solid State Div. Ann. Progr. Rept. Aug. 31, 1960*, ORNL-3017, p 98.

19. POLYMERS

W. W. Parkinson W. K. Kirkland O. Sisman

A COMPARISON OF REACTOR NEUTRONS TO GAMMA RADIATION IN THE CROSS-LINKING OF POLYSTYRENE

It was reported previously[1] that polystyrene required about 1300 ev per cross link produced by gamma irradiation but only 400 ev per cross link when irradiated in the mixed gamma radiation and fast neutrons of a nuclear reactor. The cross-link yields had been determined by measurement of molecular weights before and after irradiation. The molecular weights were calculated from measurements of the viscosities of dilute solutions of the polystyrene specimens. The relation between viscosity and molecular weight is somewhat dependent on the degree of branching of the polymer and the molecular-weight distribution, and these properties may change at different rates under neutron bombardment and gamma irradiation. To establish conclusively that the cross-linking yield is higher for neutron bombardment than for gamma irradiation, determinations of cross-linking by different methods have been performed.

Samples were irradiated for doses which rendered the polymer largely insoluble. The irradiated samples were then extracted repeatedly in toluene to determine the soluble fraction. The dose at which insoluble material first appears (gel point) has been shown to depend on the initial molecular-weight distribution, as well as on the average molecular weight, but the fraction insoluble has no dependence on the degree of branching. In Fig. 19.1 the fraction soluble is plotted vs dose for polystyrene irradiated in Hole 19 of the ORNL Graphite Reactor and in a Co^{60} gamma source of 2.2×10^6 r/hr. It is seen that to yield the same fraction of insoluble material, 2.2 to 2.4 times as high a dose is required from gamma radiation as from reactor radiation.

After extraction to remove soluble polymer, the insoluble portion of the specimens was weighed immediately (while in an equilibrium condition of swelling from infusion of the solvent). The specimens were then dried in a vacuum oven and the dry weight was obtained. The ratio of swollen

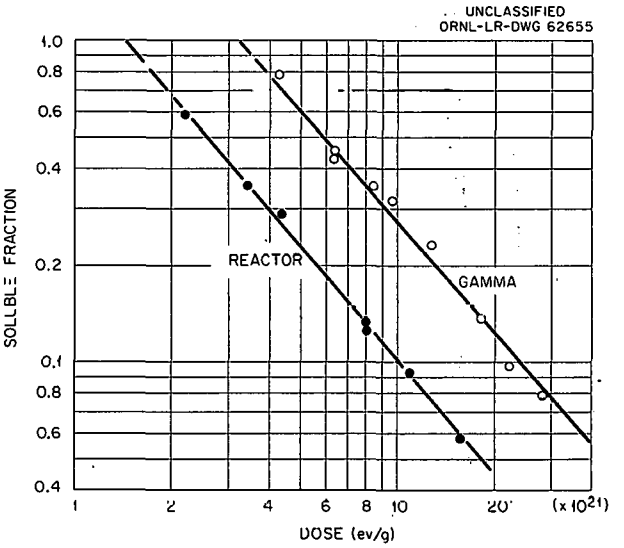

Fig. 19.1. Soluble Fraction of Irradiated Polystyrene.

to dry volume, V, was calculated, assuming that the density of the swollen polymer is that of the solvent toluene and the density of the dried sample is the same as that of the unirradiated polystyrene. It has been shown[2,3] that the swelling ratio is related to the molecular weight between cross links, M_c, by the approximate expression

$$V^{5/3} = (0.5\mu)M_c/\rho v ,$$

where μ is a constant of interaction between the polymer and solvent, ρ is polymer density, and v is the molar volume of the solvent.

The weight swelling ratios for specimens irradiated in the Co^{60} source and in the reactor are plotted vs dose in Fig. 19.2 on a logarithmic scale. Since M_c should be inversely proportional to dose, the points should fall on the line $\log V = -3/5 \log D + K$, where D is the dose and K incorporates the constants of the earlier equation. The agreement between the experimental points and the theoretical slope of $-3/5$ is only fair.

[1] W. W. Parkinson *et al.*, *Solid State Div. Ann. Progr. Rept. Aug. 31, 1960*, ORNL-3017, p 101.

[2] P. J. Flory and J. Rehner, *J. Chem. Phys.* 11, 521 (1943).

[3] A. Charlesby, *J. Polymer Sci.* 11, 521 (1953).

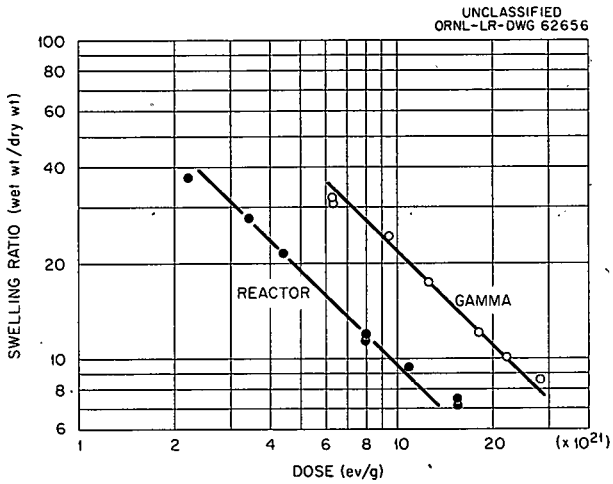

Fig. 19.2. Solvent-Swelling of Irradiated Polystyrene.

The expression is valid for moderate degrees of cross-linking – high enough so that the effect of chain ends can be ignored but low enough so that the swollen volume is much larger than the dry volume.

Since the swelling ratio accounts for the degree of branching and is independent of the molecular-weight distribution, the data demonstrate that cross-linking yields are higher for the mixed neutrons and gamma radiation of the reactor than for gamma radiation alone. From the curves, the mixed radiation of the reactor is about 2.3 times as efficient as the Co^{60} source in the production of cross links in polystyrene.

The energy absorbed by the polystyrene irradiated in the reactor was calculated from calorimetric measurements as discussed previously.[1,4] Traces of impurities having high neutron cross sections would contribute to the radiation dose in the polystyrene and could introduce a serious error in the calculated doses. The upper limit of the boron content was determined spectrographically and the nitrogen determined chemically. A neutron activation analysis was carried out for other trace impurities.[5] The concentrations for the upper limits of the trace impurities in the sheet stock, the more impure of the two sample materials, are listed in Table 19.1. Also tabulated are the estimated doses which the capture gammas and emitted particles, if any, would have contributed to the sample receiving 2.2×10^{21} ev/g from the reactor radiation field. The dose from impurities was estimated by making the simplifying approximation that the radioactive source was concentrated at the center of a 1-cm spherical sample. It is seen from the table that the total dose from impurities is negligible compared with that from the reactor field.

Table 19.1. Dose Produced by Trace Impurities in Polystyrene Sample Receiving 2.2×10^{21} ev/g from Reactor

Element	Weight Fraction	Reaction	Dose (ev/g)
	$\times 10^{-6}$		$\times 10^{17}$
B	<5	$B^{10}(n,\gamma)$	0.002
		$B^{10}(n,\alpha)$	430
Na	700	$Na^{23}(n,\gamma)$	1.2
		Na^{24} (β,γ decay)	9.2
Cl	80	$Cl^{35}, Cl^{37}(n,\gamma)$	5.9
		Cl^{38} (β,γ decay)	0.5
		$Cl^{35}(n,p)S^{35}$	0.1
Mn	4.9	$Mn^{55}(n,\gamma)$	0.1
		Mn^{56} (β decay)	0.9
Al	9.0	Al^{28} (β,γ decay)	0.1
Ag	3.5	$Ag^{108}, Ag^{110}(n,\gamma)$	0.1
		Ag^{108}, Ag^{110} (β decay)	1.9
N	2000	$N^{14}(n,p)C^{14}$	60
		$N^{14}(n,\gamma)$	3

INFRARED STUDIES OF PLASTICS AND ELASTOMERS

Infrared absorption spectra of irradiated natural and synthetic rubbers have shown significant changes in the absorption peaks characteristic of the various isomeric configurations of the olefin group ($>C=C<$). The previous report[1]

[4] C. D. Bopp, D. Binder, and R. L. Towns, *Solid State Div. Ann. Progr. Rept. Aug. 31, 1959*, ORNL-2829, p 182.

[5] Analyses were performed by M. Murray, W. R. Laing, and G. W. Leddicotte of the Analytical Chemistry Division.

described a scheme for quantitative analysis of the olefin groups by determining expressions for the optical absorption coefficient at the frequency characteristic of each group in terms of a power series in concentration. The compounds or standards for setting up the equations for *trans*, *cis*, and terminal or end >C=C< groups were *trans*-4-octene, *cis*-4-octene, and 1-octene respectively. Letting A represent the infrared absorption [log (I_0/I)] at the indicated frequency in cm^{-1}, the expressions are

$$A_{967} = t(135.4C_t - 9.05C_t^2 + 0.48C_t^3) ,$$

$$A_{910} = t(176.8C_e - 20.0C_e^2 + 1.42C_e^3) ,$$

$$A_{680} = t(29.38C_c - 0.897C_c^2 + 0.040C_c^3) ,$$

where t is thickness in centimeters and C is concentration in moles/liter of *trans*, end or terminal, and *cis* olefin groups as shown by subscript.

The olefin groups of polybutadiene occur in these three configurations, and a set of simultaneous equations can be set up for each sample by inserting the spectral absorption at the indicated frequencies and the thicknesses of the measured specimens. A small correction term must be added to the equations for absorption at 967 and 910 cm^{-1} to account for overlap of the peaks.

Sets of equations were formulated and then solved by the computer[6] for two polybutadienes, one high in terminal olefin groups, the other high in *trans* groups.[7] The resulting analyses are tabulated in Table 19.2.

The important source of uncertainty, both in determining the equation for the absorption coefficients and in measuring the samples, is the minimum thickness of specimens. For the strongly absorbing *trans* and terminal olefin groups, in octene standards as well as in polybutadiene specimens, the spectral absorption was almost complete at the thicknesses measured. Under such conditions of low light transmission, the response of the spectrophotometer is sluggish and the accuracy is poor.

Thinner liquid cells have been obtained to improve the light transmission of the hydrocarbon standards used to establish the absorption coefficient equations. Polybutadiene films of reduced thickness can be cast on salt plates, and the uniformity can be checked with a microscope. Such measurements of reduced thicknesses should improve the analytical accuracy considerably.

[6]The equations were solved on the Oracle by the group under the direction of H. P. Carter of the Mathematics Panel.

[7]The analyzed samples were obtained through W. C. Sears of the University of Georgia and J. L. Binder of the Firestone Tire and Rubber Co.

Table 19.2. Analyses of Polybutadienes for Olefin Groups

Olefin Group	Sample High in Terminal Groups			Sample High in *trans* Groups		
	Concentration		Firestone Analysis (mole %)	Concentration		Firestone Analysis (mole %)
	moles/liter	mole %		moles/liter	mole %	
trans, C_t	4.8 ±0.5	25	25	12.1 ±1	67	74
Terminal, C_e	8.8 ±0.9	45	49	3.2 ±0.4	18	18
cis, C_c	5.9 ±0.6	30	26	2.7 ±0.3	15	8
Total	19.5 ±2	100	100	18.0 ±2	100	100
Theoretical total	22			22		
% of theoretical found	89			82		

RADIATION STABILITY OF DEUTERATED BASIC BERYLLIUM ACETATE COMPLEX

An earlier report described the gas evolution and melting-point changes of deuterated basic beryllium acetate complex, $Be_4O(OCOCD_3)_6$, upon irradiation in the Graphite Reactor.[8] The reduction in melting point indicated an accumulation of decomposition products in the solid residue. An attempt to measure changes in BeO content by x-ray diffraction method had proved that the changes were below the sensitivity of the method.

Since the parent complex is soluble in many organic solvents, insoluble radiolysis products including BeO can be determined by extraction. Several samples were extracted to constant weight by refluxing in chloroform. The fraction insoluble is plotted against dose for the samples in Fig. 19.3.

The previous gas measurements had separated the evolved products only into condensible and noncondensible gases at liquid-nitrogen temperature. Two samples were irradiated and submitted for mass spectrometer analysis. The results indicate that the D_2:CD_4 ratio is 4:3, including about 25% of compounds containing light hydrogen. The analysis of compounds of masses 28 (N_2, CO, C_2 species), 32 (O_2, C_2 species), and 44 (CO_2) is tentative pending calibration of the instrument for CO_2 and C_2 species. The determination of these substances will conclude experimentation with the beryllium complex.

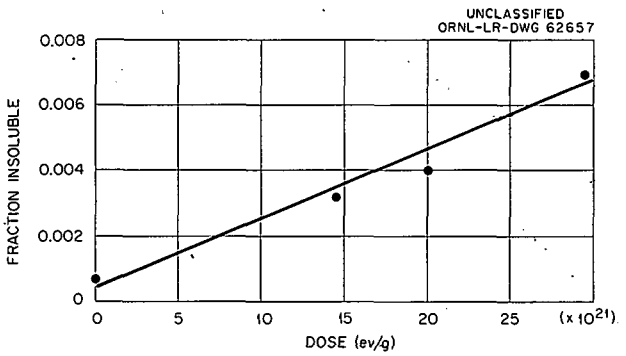

Fig. 19.3. Insoluble Fraction of Irradiated Deuterated Beryllium Acetate Complex.

[8] W. W. Parkinson, *Solid State Div. Ann. Progr. Rept. Aug. 31, 1959*, ORNL-2829, p 179.

20. RADIATION DOSIMETRY

C. D. Bopp W. W. Parkinson O. Sisman
R. L. Towns W. K. Kirkland

GAMMA HEATING IN REACTORS

A calorimeter and nonhydrogenous chemical dosimeters were developed for use in connection with the determination of energy absorption in materials exposed in reactors. The chemical dosimeters are composed chiefly of light elements in which Compton scattering is the chief energy absorption process, with photoelectric absorption making only a small contribution, as explained below. The chemical dosimeters are sensitive and convenient for use in estimating the energy absorption in other light elements. For estimation of the energy absorption in heavy elements from measurements in light elements, a knowledge of the low-energy portion of the gamma-radiation spectrum is required. The energy absorption in heavy elements may also be measured calorimetrically, but generally knowledge of the spectrum is required here, too, for estimation of the self-shielding.

The calorimeter and the chemical dosimeters are described below. The theory which is applicable to both will be stated briefly. Energy absorption from the fast-neutron component of reactor radiation is small except for very light elements (of atomic weight less than about 15), for which the energy transferred in a fast-neutron scattering event is relatively large. For this reason the fast-neutron component of energy absorption in a reactor is small for nonhydrogenous materials, which do not contain other very light elements.

Comparison of the energy absorption in a nonhydrogenous and in a hydrogenous material permits separation of the energy absorption in the hydrogenous material into the components from fast neutrons and from gamma radiation. (The correction for fast-neutron scattering by fluorine and carbon for the dosimeters described below is fairly small and may be determined by an approximate calculation such as is described for the magnesium calorimeter.) In theory, the same result could be attained with hydrogenous materials of differing hydrogen content; however, this method suffers in sensitivity when the hydrogen contents are not very different, as is the case for most organic materials. The presence of elements in the materials with large absorption cross sections for thermal neutrons complicates the analysis because of secondary radiation from thermal-neutron capture.

A further distinction arises in the consideration of energy absorption from the gamma component of reactor radiation with respect to atomic weight. For this purpose, light elements are defined as those with atomic number less than about 20. For light elements, the predominant mechanism of energy absorption from gamma radiation is by Compton scattering, but for heavier elements photoelectric absorption is also important. Compton scattering is nearly independent of the binding energy of the scattering electrons and is nearly proportional to electron density. Photoelectric absorption is greatest for the most tightly bound electrons within the inner shells and therefore increases with atomic weight. Photoelectric absorption is greatest with low-energy gamma radiation, the energy dependence being much greater than for Compton scattering. For these reasons a more accurate knowledge of the low-energy portion of the spectrum of gamma radiation is required in connection with the estimation of energy absorption for heavy elements than for light elements.

GAMMA-RADIATION CALORIMETRY IN A REACTOR

Methods of reactor calorimetry include (1) measurement of the steady-state temperature difference across a thermal resistance with calibration by an internal electric heater,[1,2] (2) measurement of the rate of temperature rise of a material which is thermally insulated from the surroundings and calibration from the specific heat,[3] and (3) measurement as in (1) but calibration from the specific heat and from the rate of approach to the steady state when the thermal equilibrium is disturbed.[4] Method (3) was chosen here for its advantage of simplicity of calorimeter construction. The calorimeter design differed from that employed previously[3] in that the temperature of the heat shield (Fig. 20.1) is measured, as well as the temperature difference between the inner cylinder and the shield. This gives greater sensitivity, since it is possible to correct for fluctuations in ambient temperature.

The calorimeter construction is greatly simplified over that of method (1), since an internal heater is not required. An external heater is used for calibration (not shown in Fig. 20.1). It consists of a length of Fiberglas-insulated Chromel wire which is placed along with the calorimeter in one of the irradiation cans normally used in the irradiation facility.

If the temperature of the outer shield were held constant, the cooling curve would be exponential. However, for experimental simplicity, the temperature of the shield was permitted to change, and the effect of this was corrected for mathematically. For reasons which will be indicated, it is advantageous if the change in temperature of the shield is kept moderate. This is accomplished by the following procedure. The heater current I_i, which gives a temperature T_{ei} (somewhat above ambient temperature), is determined. Next, the current is increased for sufficient time to raise the temperature of the inner cylinder and then shut off. When the temperature of the outer cylinder reaches T_{ei}, the current is turned on again and set at I_i. The rate of cooling of the inner cylinder is then measured. A Leeds and Northrup K3 potentiometer was used to measure the temperature difference, T, between the cylinders. The temperature of the outer cylinder, T_e, was recorded continuously.

---

[1] D. M. Richardon, A. O. Allen, and J. W. Boyle, *Proc. Intern. Conf. Peaceful Uses Atomic Energy, Geneva, 1955* **14**, 209 (1956).

[2] D. Binder, C. D. Bopp, and R. L. Towns, *Am. Soc. Testing Materials Spec. Tech. Publ.* **286**, 105 (1960).

[3] A. R. Anderson and R. J. Waite, *J. Sci. Instr.* **33**, 46 (1956).

[4] F. T. Binford, *Nucleonics* 15(3), 93 (1957).

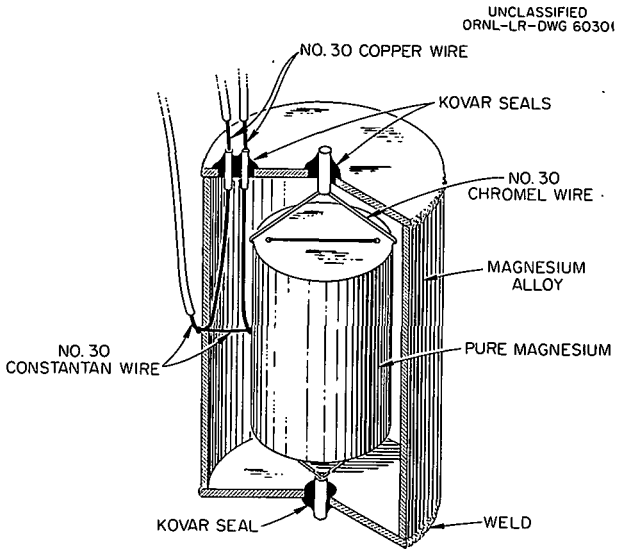

Fig. 20.1. Gamma-Radiation Calorimeter.

The rate of change of the temperature difference between the inner and outer cylinders is given by

$$dT/dt = -kT - dT_e/dt + g \,, \qquad (1)$$

where k is the time constant and is equal to the quotient of the thermal conductance of the air gap and the specific heat, and g is the gamma heating of the inner cylinder. Experimentally it was found that

$$dT_e/dt = -a - be^{-bt} \,, \qquad (2)$$

where a, b, and b are constants chosen to fit the experimental data. Combining Eqs. (1) and (2) and integrating gives

$$\ln \frac{T_0 - (g + a)/k + b/(b - k)}{T - (g + a)/k + be^{-bt}/(b - k)} = kt \,, \qquad (3)$$

where T_0 is the initial temperature difference at the time the measurements of the rate of cooling are commenced ($t = 0$).

The following procedure is used to determine g and k from the experimental data. Trial values of g and k are substituted in Eq. (3) for several values of T and t. The left side of Eq. (3) is plotted vs time. From the initial slope of the plot, an improved value of k is determined; the deviation of the plot from linearity at large t gives an indication of the adjustment required in g. Since the process converges rapidly, only a few trials fix g and k within about 2%, the reproducibility obtained for repeated experiments. The reproducibility was limited largely by fluctuations in the ambient temperature which affected the accuracy of the fit of Eq. (2) to the data.

Severe jarring changed k as much as ±10%, which is believed to have resulted from the looseness of the suspension of the inner cylinder, such that shifts in position resulted which were sufficient to affect the convective heat transfer. When the calorimeter is not jarred during a measurement, there is small disadvantage of the loose suspension, since the calorimeter is calibrated in position. For some circumstances, however, it may be advantageous to make the suspension of the inner cylinder more rigid. There is no disadvantage to the use of heavier wires as long as the heat capacity of the wires remains small in comparison to that of the inner cylinder and the thermal resistance of the wires is large in comparison to that of the air gap.

The temperature dependence of k was less than ±2% over the range from 35 to 45°C (the range used here). In this range, the emf of the copper-constantan thermocouples was 41.5 mv/°C ± 0.5% both before and after exposure to about 10^{17} epithermal neutrons/cm^2. The emf is unchanged by the radiation field.[5] Thermocouple wires were soldered in grooves machined in the surface of the inner cylinder at the locations indicated in Fig. 20.1. Since the surface-to-weight ratio for the No. 36 thermocouple wire was about 10^4 greater than that of the inner cylinder, the gamma heating of the wire produced negligible effect on the thermocouple reading.

In Table 20.1 are listed the values measured in Hole 71 with calorimeters of magnesium (with internal cylinder dimensions 3.18 cm in diameter × 3.81 cm) and bismuth (1.36 cm in diameter × 2.54 cm). The time constant k for the magnesium calorimeter was 6.1×10^{-4} sec^{-1}; for bismuth, 3.7×10^{-3} sec^{-1}.

In the case of magnesium it was necessary to correct for thermal-neutron reactions, the most important of which is the (n,γ). The fraction of the gamma radiation absorbed was estimated by the approximation that the gamma flux is composed

[5] D. S. Billington and J. H. Crawford, Jr., *Radiation Damage in Solids*, p 97, Princeton University Press, Princeton, 1961.

Table 20.1. Energy Absorption in ORNL Graphite Reactor (10^{15} ev sec^{-1} g^{-1})[a]

	Magnesium (Position B, Fig. 20.2)		Bismuth (Position A, Fig. 20.2)	
	Calorimeter Cylinder	Thin[b] Specimen	Calorimeter Cylinder	Thin[b] Specimen
(1) Total measured	7.6		9.6	
(2) Thermal-neutron component				
From radiative capture	1.0		0	
From decay of Mg^{27}	0.1		0	
(3) Fast-neutron component	0.4		0	
(4) Gamma-radiation component, (1) − [(2) + (3)]	6.1		9.6	
(5) From moderator	0.6	0.7	0.6	1.1
(6) From aluminum in liner and sample can (equivalent to a cylinder of $\frac{1}{8}$-in. wall thickness)	0.6	0.7	1.0	1.2
(7) From fuel elements, (4) − [(5) + (6)]	4.9	5.3	8.0	28

[a] In Hole 71 at a position where the thermal flux was 0.72×10^{12} neutrons cm^{-2} sec^{-1} (based on a Co^{60} cross section of 36.7 barns with no correction for the epicadmium component); the sulfur flux was 0.95×10^{10} neutrons cm^{-2} sec^{-1} [based on a cross section of 0.37 barn for the (n,p) reaction]; the reactor was operating at 3400 kw total heat power.

[b] Without self-shielding.

of particles with macroscopic absorption cross section equal to the linear energy absorption coefficient, $\mu_a \rho$. This approximation is best at fairly small values of $\mu_a \rho r$, where r is the radius of a sphere of equivalent volume. For the magnesium cylinder, $\mu_a \rho r = 0.10$ and the probability of absorption, P, is 0.07.[6] Energy absorbed by bismuth from thermal-neutron reactions is negligible, since the cross section is low and the bismuth was very pure.

For estimating the energy absorption from fast-neutron scattering, a flux spectrum calculated by the method of ref 7 was normalized to $S(n,p)$ detectors,[8] which were exposed along with the calorimeters, using the cross-section data of ref 9. This also gives the strength of the fuel elements (2.9×10^{11} fissions cm^{-1} sec^{-1}) which is used in the calculations described below. The value calculated for energy absorption from fast neutrons by magnesium agrees well with calorimetric measurements[1,2] for hydrogen and carbon when the difference in scattering cross section, the fraction of the neutron energy transferred in a collision, and the difference in source strength are taken into account.

A vertical traverse of Hole 71 (Fig. 20.2) with sulfur detectors showed local variation in flux of as much as ±15% of the mean. The sulfur detectors were spaced about 1 in. apart, and adjacent detectors showed variations less than about 5%. The spacing of the maxima and minima varied from 4 to 8 in., so that the correspondence

[6] A. M. Weinberg and E. P. Wigner, *The Physical Theory of Neutron Chain Reactors*, p 712, University of Chicago Press, Chicago, 1958.

[7] M. Goldberger, J. Stephenson, and A. M. Weinberg, *Neutron Flux in W Lattice*, CP-2439 (1945).

[8] Activation measurements by J. E. Strain, Analytical Chemistry Division.

[9] D. J. Hughes and R. B. Schwartz, *Neutron Cross Sections*, BNL-325, 2d ed., GPO, Washington, 1958.

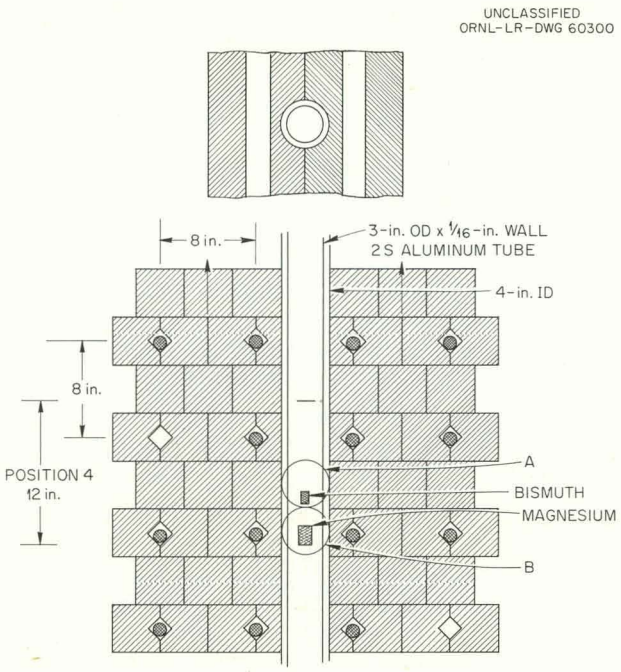

Fig. 20.2. Geometry of Hole 71, ORNL Graphite Reactor.

with fuel element spacing is not well defined. The positions of the maxima and minima were not the same for two surveys taken at an interval of about a month, though the mean value for the two surveys was nearly the same. For the survey taken nearest the time of exposure of the calorimeters, the flux was the same within a few per cent at the position of the bismuth calorimeter and at the position of the magnesium calorimeter. Approximately, this should also hold for gamma radiation, since the greater part of the gamma radiation comes from the nearest fuel elements, as is explained below. The local variation of the thermal flux in Hole 71 is roughly one-third of that of the sulfur flux, and the thermal-flux variation does not coincide with that of the sulfur flux; for this reason, the sulfur flux should prove superior to the thermal flux for monitoring exposures where the energy absorption from fast-neutron and gamma radiation is the pertinent quantity.

CALCULATED GAMMA-RADIATION SPECTRUM

The spectral shape of the gamma radiation has less effect on self-shielding by magnesium than by bismuth specimens (see also ref 10). This is shown in Table 20.1, where the calculated values of energy absorption are given for thin specimens (with no self-shielding) and for the inner cylinders of the calorimeters whose dimensions were given earlier. For the calculation the cylindrical cavity in the graphite was replaced by a spherical cavity of the same diameter. This greatly lessens the labor since, with this simplification, many of the integrals may be expressed as tabulated functions. The gamma-radiation spectrum was calculated for the positions marked A and B in Fig. 20.2. The energy absorption for thin specimens is given by integrating the spectrum weighted by the energy and the mass-energy absorption coefficient. For the calorimeter cylinders the spectrum is also weighted by the self-shielding factor.

Three sources of radiation were considered: fuel rods, radiative capture of thermal neutrons by graphite, and radiative capture by aluminum in the test hole liner and in sample containers; it is not generally necessary to attenuate this last source since there is no matter intervening between it and the sample positions. This calculation differs from that of ref 11 inasmuch as secondary radiation is considered more exactly, and more accurate values are used for the attenuation coefficients and for the energy absorption attenuation coefficients. In ref 11 the strength of the fuel-rod source is determined from the thermal flux. As already described, $S(n,p)$ detectors were used here. Both methods yield similar values, but the thermal-flux method is probably the more complex, since it is necessary to allow for flux depressions at the fuel rods and at the detector position. The depression at the detector position may be appreciable when the detectors are exposed along with samples whose exposure it is desired to monitor.

The spectrum of the fuel-rod source was taken as $Ce^{-1.1E}$ (ref 12) photons of energy E per unit energy level and per fission. This spectrum was modified in two stages: for scattering by uranium and for scattering by graphite. In each case the point-source form for the collided radiation and the differential-spectra point-source form for the uncollided radiation were integrated over the volume of the

[10] R. Fox, *Nuclear Sci. and Engr.* **6**, 33 (1959).

[11] W. Primak, *J. Appl. Phys.* **27**, 54 (1956).

source.[12,13] The flux spectrum from the first stage was converted into an equivalent line source which was used for the starting point of the second-stage integration. The spectra from the nearest and second rods were summed at positions A and B (Fig. 20.2). The calculated spectra fitted the empirical form

$$N_E = C(Me^{-1.1E} + Ne^{-2.5E})S_f , \qquad (4)$$

where N_E is the number of photons per unit energy, per second and per cm^2; S_f is the source strength in fissions cm^{-1} sec^{-1}; and M and N are parameters which depend on the distance of the fuel rods from the test position. The parameters M and N were determined at several distances and were plotted as a function of distance in order to facilitate the summing of the contributions of all the rods. The nearest and second nearest rods account for 85% of the energy absorbed from all the rods by magnesium at A, and for 80% at B. The spectrum at the surface of a fuel rod is almost entirely from the radiation originating in the rod, which is given by Eq. (4), with $M = 0.075$ and $N = 0.18$, except for flattening at about 0.5 Mev and a cutoff at about 0.2 Mev. For the spectrum from all the rods at position A, $M = 0.020$ and $N = 0.048$, except at energies in the range from 0.2 Mev to the cutoff energy (below 0.1 Mev), where the formula gives a value which is somewhat low; at position B, $M = 0.023$ and $N = 0.048$.

Since capture by the moderator contributes a relatively small part of the total energy absorption, an accurate estimate of this spectrum is not required. The calculation for the uncollided radiation from graphite is described elsewhere.[11] The secondary radiation was calculated by integrating the point-source differential spectra over an infinite space. An approximate form for the spectrum of the secondary radiation is

$$N_E = (2.3 + 11e^{-2.5E})S_v ,$$

where S_v is the source strength, the number of 5-Mev photons per unit volume and time, determined from the thermal flux and from the cross section of carbon. For the calculation of capture radiation from aluminum, the aluminum was taken as equivalent to a surrounding cylinder of $\frac{1}{8}$-in. wall thickness, and two 3.5-Mev photons per capture was assumed.

For self-shielding the energy absorption buildup tabulation was used to give the weighting factor for the point-source form as a function of the distance from the surface of the cylinder, and this form was integrated over the volume of the cylinder.

The value for the factor C in Eq. (4) ($C = 25$) was determined by setting the calculated energy absorption from fuel rods equal to the experimental data from item No. (7) in Table 20.1. That the same value within about 10% was obtained from the magnesium and bismuth data is an indication that the calculated spectrum is accurate. That the value is higher than for U^{235} ($C = 14$) (ref 12) may result in part from the inadequacy of the approximation of a uniform-volume source, in part from radiative capture by U^{238} in the natural uranium rods, and to a lesser extent from inelastic scattering of fast neutrons by uranium.

CHEMICAL DOSIMETERS

Chemical dosimeters have the advantages of simplicity and convenience of installation over calorimeters. They may be exposed along with test materials whose exposure needs to be measured. This is most advantageous in reactor irradiations, since the intensity of the radiation field may be affected by the loading of adjacent test holes or by changes in the fuel element loading. Three chemical systems have been studied: a hydrogenous system, decane, which responds to all components of a reactor radiation field; the essentially nonhydrogenous carbon disulfide–tetrabromide system; and a nonhydrogenous fluorocarbon system described in detail below.

The gas evolved from the decane was used as a measure of the dose imparted by the radiation field. The gas yields published in the literature were used after checking by irradiations in a known Co^{60} source. The doses measured in the reactor agreed with those calculated from the calorimeter measurements discussed above.

A chemical system to measure the dose imparted by gamma radiation in the presence of fast and thermal neutrons should be composed of elements of low cross section. Specifically, the hydrogen fraction should be as low as possible because

[12] H. Goldstein, *Reactor Shielding*, p 60, Addison-Wesley, Reading, Mass., 1959.

[13] R. L. French, *Nucleonics* 18(3), 114 (1960).

of its high efficiency in absorbing energy from fast neutrons. Carbon disulfide and fluorocarbon liquids are suitable with respect to neutron cross section, and a solution containing perhaps 1% of a hydrocarbon offers the possibility of using the acid production as an indication of dose while maintaining the hydrogen content at tolerable levels. The carbon disulfide requires the addition of a small amount (~1%) of carbon tetrabromide for acid production, while the fluorocarbon produces HF with hydrocarbon alone or HCl with addition of low concentrations of chlorine-containing compounds.

The replacement of chlorine by bromine reduces the thermal-neutron absorption and the secondary gamma radiation, but the longer half-life of bromine makes it inconvenient to use. Carbon disulfide has greater interaction with thermal neutrons than do the fluorocarbons, but suitable corrections can be determined from simple calibration measurements. The results of irradiations of CS_2 solutions (with 1% decane ± 1% CBr_4) are encouraging, but only a small amount of data has been obtained as yet.

FLUOROCARBON DOSIMETER

The decomposition of fluorocarbon liquids in a nuclear reactor has been shown to be moderate.[14] The yield of free radicals in mixtures of fluorocarbons and benzene irradiated in a gamma source has been found to be insensitive to concentration and in a range convenient for measurement (about 1 radical per 100 ev).[15] Wall[16] observed that the irradiation of such mixtures in glass containers resulted in considerable yields of SiF_4.

To avoid this loss of fluorine through reaction with the container, Teflon tubes were used to contain 1% solutions of decane ($C_{10}H_{22}$) in perfluorodimethyl cyclohexane (C_8F_{16}). The solutions were frozen in Teflon tubing, which was then evacuated and heat-sealed. Two samples were irradiated for about 7 and 15×10^6 rads in a Co^{60} source at 0.4×10^6 r/hr. After irradiation, the Teflon tubing was so brittle that leaks occurred during handling of the samples.

To permit the use of glass and quartz containers, fluorocarbon solutions were made up containing both decane and tetrachloroethane ($C_2H_2Cl_4$) which would produce HCl instead of HF, presumably by energy transfer or radical reactions. Solutions in C_8F_{16} were prepared in concentrations of ½ and 1% with respect to both decane and tetrachloroethane, in order to study the concentration dependence of the HCl production.

Samples for irradiation were frozen and evacuated as before and were sealed in Pyrex tubes. After irradiation the sealed tips of the containers were broken off under water to prevent the loss of gaseous HCl. The total acid content of the sample was then determined by conventional titration with a base.[17]

Samples of both ½ and 1% concentrations were irradiated at room temperature in a Co^{60} source of about 0.4×10^6 r/hr. Solutions of the higher concentration were irradiated at 50 and 80°C in a source of 5×10^6 r/hr. The acid (H^+) produced per gram of dosimeter solution is plotted vs dose in Fig. 20.3.

[17] Acid determination by B. Ginocchio, Analytical Chemistry Division.

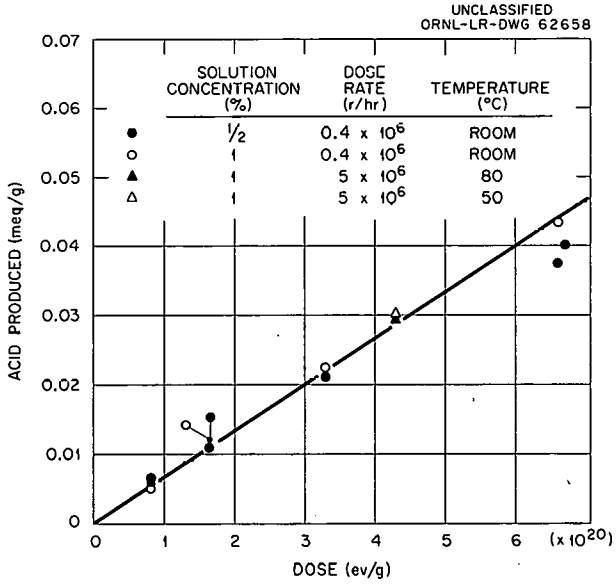

Fig. 20.3. Acid Produced in C_8F_{16}-$C_{10}H_{22}$-$C_2H_2Cl_4$ Solutions.

[14] J. H. Simons and E. H. Taylor, *J. Phys. Chem.* 63, 636 (1959).

[15] P. Y. Feng, *Proc. U.N. Intern. Conf. Peaceful Uses Atomic Energy, 2nd, Geneva, 1958* 29, 166 (1958).

[16] L. A. Wall, R. E. Florin, and D. W. Brown, *Gamma Radiation of Fluorocarbon Polymers and Prototype Substances*, WADC-TR-59-413 (1960).

The production of acid appears to be linear with dose for the 1% solution over the dose range covered. The yield for the dilute solution appears to decrease slightly at the higher doses. The results of the irradiations at the higher intensity and temperatures show promise that the yield is relatively independent of temperature and dose rate.

Based on results obtained to date, the yield of acid is 6.5×10^{-26} equivalent per electron volt, or $G = 3.9$ H^+ ions per 100 ev. This compares with G values of around 4 reported[18] for low concentrations of hydrocarbons in CCl_4 and for $CHCl_3$ and CH_2Cl_2.

[18] R. A. Back *et al.*, *Proc. U.N. Intern. Conf. Peaceful Uses Atomic Energy, 2nd, Geneva, 1958* **29**, 115 (1958).

Part IV

REACTOR MATERIALS

THIS PAGE

WAS INTENTIONALLY

LEFT BLANK

21. FUEL MATERIALS

O. Sisman

POSTIRRADIATION EXAMINATION OF EGCR PROTOTYPE CAPSULES

J. G. Morgan
M. F. Osborne
H. E. Robertson
M. T. Morgan

Examination of irradiated EGCR prototype fuel capsules, similar to those previously reported,[1] is continuing. Eighteen ORR- and ETR-irradiated capsules have been examined, and four more are under study. Parameters of greatest interest are dimensional changes in the stainless steel can, fission-gas release from the UO_2 fuel, and changes in the microstructure of the can and UO_2.

The can walls tended to collapse onto the UO_2 pellets during irradiation, especially at the higher operating temperatures.[2] Circumferential ridges, up to about 0.005 in. high, were formed at pellet interfaces in capsules irradiated at temperatures of about 1600°F (see Fig. 21.1). Profile measurements showed that capsule bowing increased with irradiation temperature to a maximum of about 0.025 in. In general, less than 1% of the fission gases generated have been released from the UO_2.[3] Metallographic examination of the can ridges formed at pellet interfaces showed considerable void formation, and significant quantities of brittle sigma-phase material were found in several samples.[4]

The UO_2 used in the earliest irradiations failed to meet specifications for purity. Consequently, the evaluation of irradiation effects was limited. No significant changes in microstructure have been

[1] *Solid State Div. Ann. Progr. Rept. Aug. 31, 1960*, ORNL-3017, p 112.

[2] *GCR Quart. Progr. Rept. Dec. 31, 1960*, ORNL-3049, p 254.

[3] *GCR Quart. Progr. Rept. Mar. 31, 1961*, ORNL-3102, p 160.

[4] *GCR Quart. Progr. Rept. June 30, 1961*, ORNL-3166, pp 131–35.

UNCLASSIFIED
PHOTO 51205

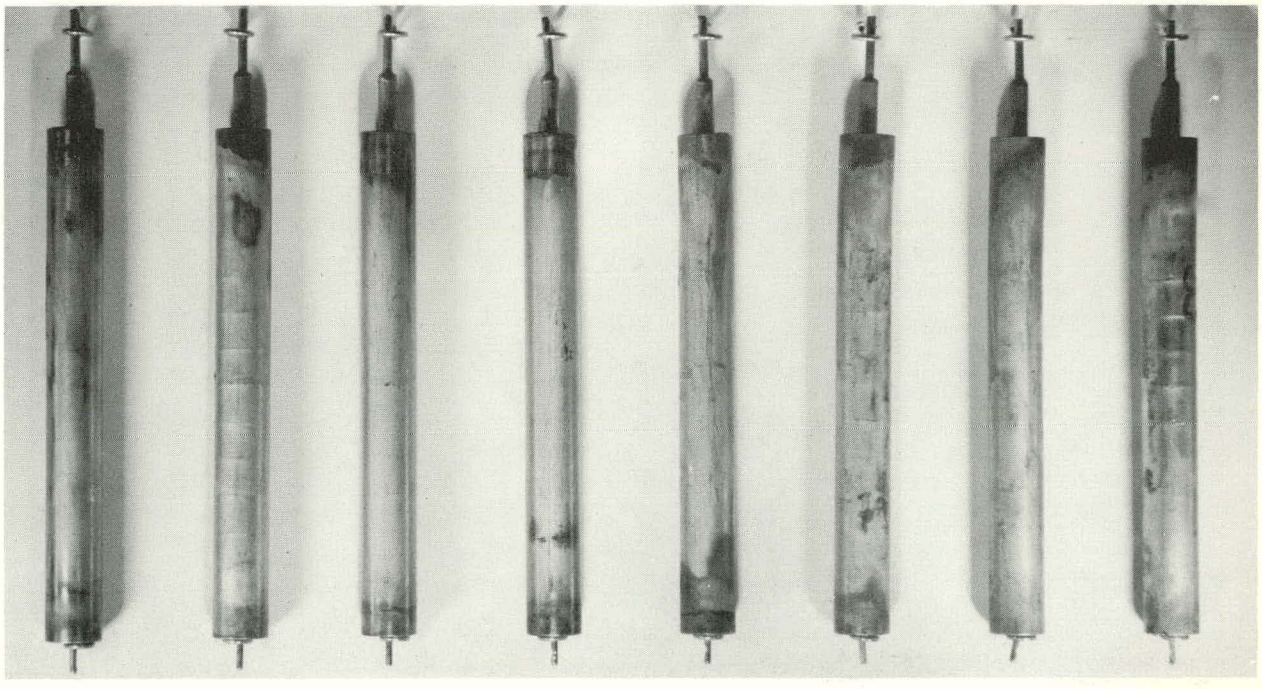

Fig. 21.1. ORR-Irradiated EGCR Prototype Fuel Capsules, Group II.

seen in relatively pure UO_2, such as that irradiated in the group II ORR capsules.[4] Uranium burnup has been determined by radiochemical analysis for long-lived fission products, such as Cs^{137} and Ce^{144}, and by mass spectrometric measurement of the U^{235}-to-U^{236} ratio. Burnup for these irradiations has ranged from 1000 to 3000 Mwd per metric ton, or about 0.1 to 0.3 at. %.[5]

Postirradiation determinations were made for the O/U ratio for some of the fuel pellets in the EGCR prototype capsules. Listed below are the results for two of the first group and two of the second group of ORR capsules. No increase in O/U ratio was found as a result of irradiation within the reproducibility of the analytical method. There is a slight indication of the UO_2 becoming more nearly stoichiometric. Preirradiation values were redetermined, with the same technique as that used on the irradiated samples in order to make the figures directly comparable.

Capsule No.	Burnup (Mwd per metric ton)	O/U Ratio		Calculated Center Temperature (°F)
		Before Irrad.	After Irrad.	
01-1	1710	2.007	2.007	2530
05-1	2610	2.015	2.002	3180
02-2	1400	2.001	2.000	2800
04-2	1680	2.001	2.002	2850

POSTIRRADIATION EXAMINATION OF BERYLLIUM-CLAD UO_2 CAPSULES

J. G. Morgan
M. T. Morgan
M. F. Osborne
J. W. Gooch
H. E. Robertson
T. W. Fulton

Six beryllium-clad UO_2 capsules were examined. The United Kingdom AEA and the French CEA joined with ORNL in fabricating two capsules each for these ORR irradiations in an effort to evaluate beryllium as a potential fuel cladding material. Capsule fabrication and operating data are summarized in Table 21.1.

Each capsule, after removal from its irradiation facility tube, was gamma-scanned, measured for dimensions, drilled for fission-gas removal, and then cut open. Individual UO_2 pellets were measured and weighed where possible, and immersion density determinations were made in some cases. Samples of UO_2 were selected for radiochemical burnup analysis. Sections of beryllium tubing, end-cap weld areas, Be-UO_2 interfaces, and UO_2 pellets were mounted for metallographic examination.

Visual examination disclosed no obvious changes in five of the capsules, while one, 05-3, had suffered a circumferential break in the weld area at

[5] *GCR Quart. Progr. Rept. Mar. 31, 1961*, ORNL-3102, p 161.

Table 21.1. Fabrication and Operating Data[a] for ORR-Irradiated Beryllium Capsules

Capsule No.	Average Outside Diameter (in.)		Enrichment (% U^{235})	External Pressure (psi)	Average Clad Temperature[b] (°F)	Burnup[c] (Mwd per metric ton)
	Be Can	UO_2 Pellets				
02-3 (ORNL)	0.594	0.513	1.82	450[d]	1048	2750
03-3 (CEA)	0.591	0.512	0.71	300[d]	1114	2350
04-3 (CEA)	0.592	0.516	0.71	450[d]	1072	2250
05-3 (AEA)	0.383	0.299	2.42	300	1140	3150
06-3 (AEA)	0.381	0.298	2.42	300	1112	2500
07-3 (ORNL)	0.380	0.299	2.42	300	1084	2300

[a] The experiment was operated by the Reactor Engineering Section of the Reactor Division.

[b] Design clad temperature was 1112° F.

[c] Burnup calculated from previous experiments.

[d] Capsules 02-3, 03-3, and 04-3 began operation at 150 psi; pressure was increased in 75-psi increments at one-month intervals to above maxima.

the bottom end cap, as shown in Fig. 21.2. Bubble testing showed that capsule 06-3 had at least two small leaks; the NaK heat transfer bath surrounding the two capsules was contaminated with fission products (confirming leakage).

Gamma scans indicated fairly uniform burnup along the capsules with the exception of 05-3, which apparently suffered a 50% flux depression at the top end, probably due to faulty positioning of a cadmium shutter used in deliberate thermal cycling (see Fig. 21.3). In some cases it was possible to distinguish each individual pellet, in addition to large gaps between pellets, by the small minima on the gamma-scan curve, as shown in Fig. 21.4.

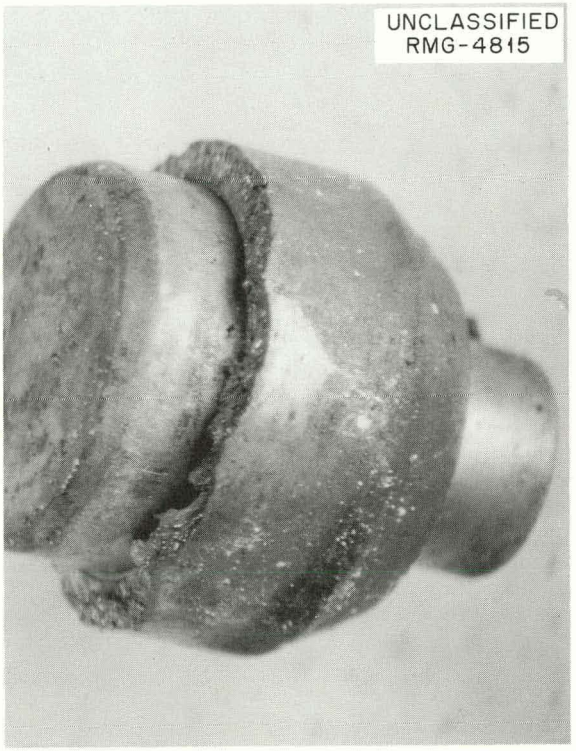

Fig. 21.2. End Cap from Capsule 05-3, Showing Break in Weld Area. 7X.

Significant changes were measured in capsule dimensions, as shown in Table 21.2. All capsules showed a general increase in diameter, reaching a maximum very near the center. Points of maximum bowing were in general not the same before and after irradiation. As expected, capsule 05-3 (the one with the broken end cap) showed the greatest dimensional changes. The only capsule on which accurate length measurements were made, 06-3, showed a decrease of 0.024 in.

Each capsule was drilled, and the contained gases were collected in an evacuated system. In addition to the two capsules known to have leaked, no fission gas was found in 04-3. It could not be determined whether this was due to an undetected leak or to a malfunction of the gas collection system. The fission-gas release from the UO_2, shown in Table 21.3, was consistent with data from similar previous experiments.

Mass spectrometer analysis of the gases showed the presence of an unusually high hydrogen concentration, about 42% in capsule 02-3. Since the capsules were filled with purified helium, it was assumed that this hydrogen had evolved from the UO_2 during high-temperature irradiation. The UO_2 had been sintered in H_2, and the subsequent degassing may have been inadequate.

Table 21.2. Beryllium Capsule Dimensional Data

Capsule No.	Average Diameter (in.)		Maximum Increase (mils)	Maximum Bow (mils)		Maximum Eccentricity (mils)	
	Before Irradiation	After Irradiation		Before Irradiation	After Irradiation	Before Irradiation	After Irradiation
02-3	0.5937	0.5944	2.9	2.0	10.4	1.0	2.0
03-3	0.5912	0.5924	3.6	10.7	18.4	1.6	2.0
04-3	0.5918	0.5923	2.1	11.0	11.1	4.4	5.0
05-3	0.3825	0.3874	9.2	9.1	33.	1.0	4.0
06-3	0.3806	0.3828	5.2	6.5	12.1	3.4	2.3
07-3	0.3804	0.3826	3.6	0.6	5.9	0.2	1.5

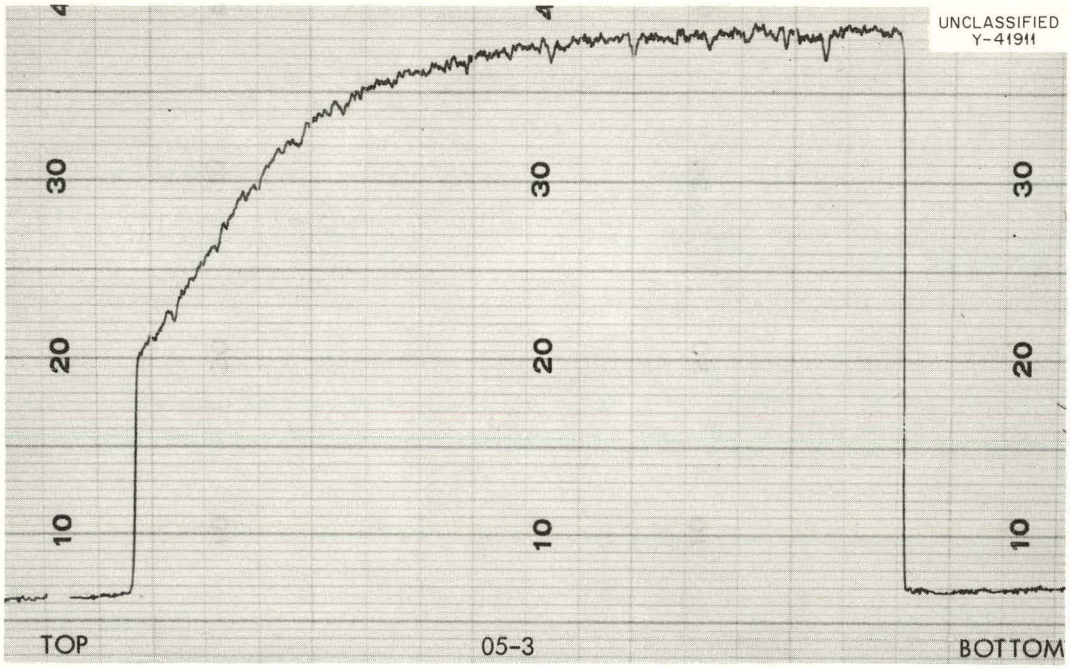

Fig. 21.3. Gamma Scan of Capsule 05-3, Showing Flux Depression near Top End.

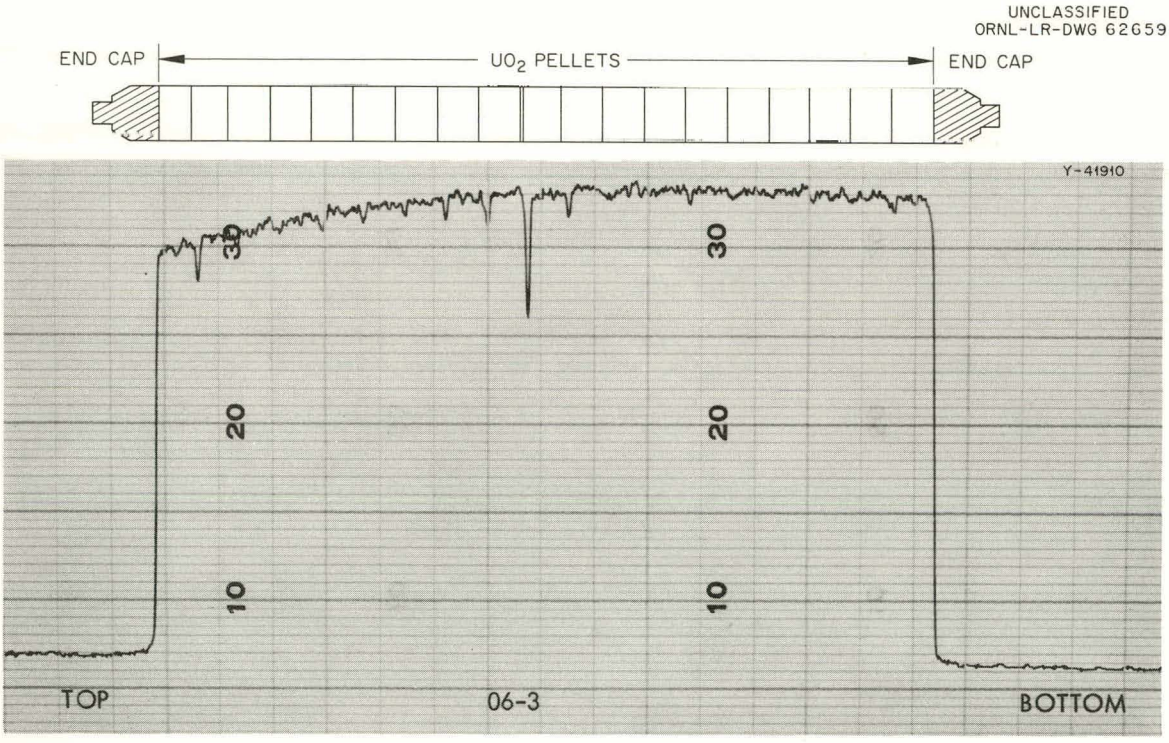

Fig. 21.4. Gamma Scan of Capsule 06-3, Showing Correlation with Fuel Pellets.

The capsules were disassembled by making circular cuts near the ends and longitudinal cuts over the central sections with a high-speed abrasive slitting wheel. Figure 21.5 shows one of the capsules after it was slit open and two of the pellets removed from that capsule. At least one pellet was removed intact from each capsule except 02-3, and the dimensions of the pellets were measured where possible. Small increases, up to about 1%, were observed in 34 measurements. One exception, a length decrease of 0.4%, was probably due to measurements being made at different positions on an asymmetrical pellet. The immersion density was determined for two pellets each from capsules 05-3, 06-3, and 07-3. Small increases, about 0.5%, were measured in all cases. This is in good agreement with data from similar previous experiments. This combined increase in dimensions and in immersion density seems to indicate that the very small cracks in the UO_2 pellets, as seen in Fig. 21.5, expose some of the originally isolated voids.

Table 21.3. Release of Kr^{85} and Xe^{133} from UO_2 in Beryllium Capsules

Capsule No.	Calculated Central UO_2 Temperature (°F)	Per Cent Release	
		Kr^{85}	Xe^{133}
02-3	3000	0.12	0.01
03-3	3000	0.34	0.05
07-3	2000	0.32	0.05

When an attempt was made to open capsule 02-3 in the described manner, one end cap broke off and the central portion of the beryllium can shattered, as shown in Fig. 21.6. This indicated that this beryllium tube was under considerably more stress than any of the other five capsules. Similar behavior has been reported as a result of heat treatment under very high external pressure (the order of 60 atm) in the absence of irradiation.[6]

Both capsules 05-3 and 06-3 were found to be completely filled with NaK, indicating that leaks had developed during operation, since both high pressure and thermal cycling would be required to

[6] M. Stohr, French CEA, personal communication.

UNCLASSIFIED
Y-42011

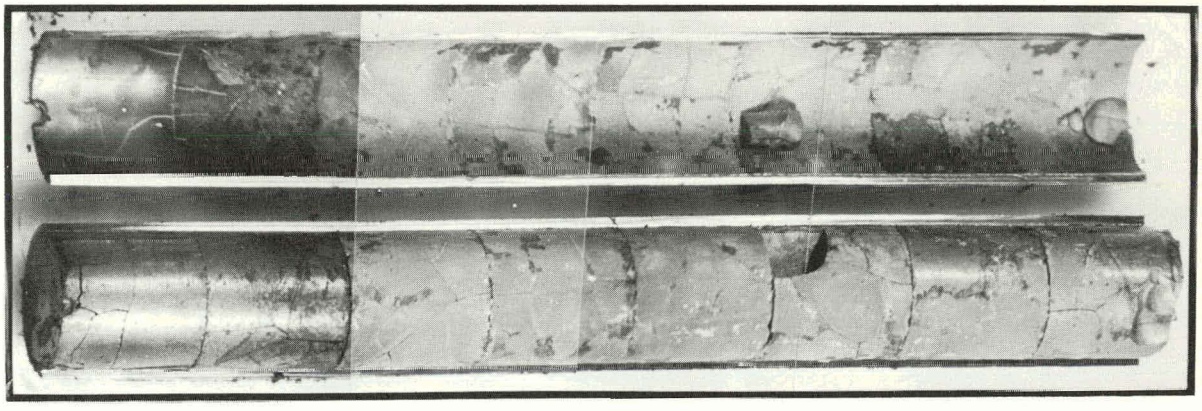

ONE INCH

Fig. 21.5. Capsule 04-3, As-Opened, with Cracked Pellets and End Caps.

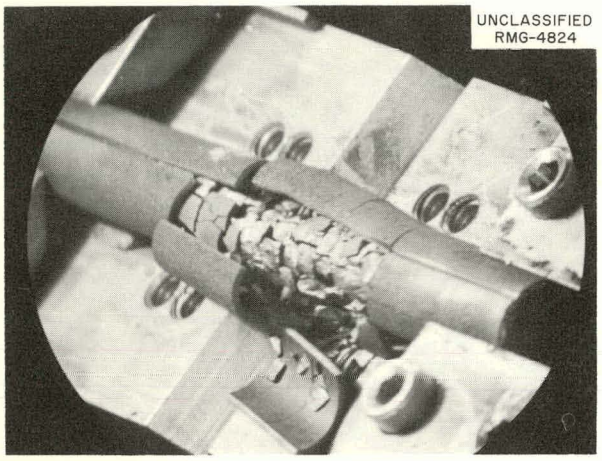

Fig. 21.6. Capsule 02-3, Showing Shattered Center Section After Partial Cut.

force NaK throughout the capsules. Preliminary metallographic examination of the beryllium clad has shown corrosion on both the inside and outside surfaces. Complete metallographic examination of all capsule components is in progress.

ADVANCED FUEL MATERIAL STUDIES

J. G. Morgan H. E. Robertson
M. F. Osborne J. W. Gooch

The advanced fuel of most current interest is UC_2 dispersed in graphite, since it will probably be used in the Pebble-Bed Reactor. Of next most interest are BeO-UO_2 and UC; UBe_{13}, USi, UN, and US are in the exploratory stage.

UC_2 Dispersions in Graphite[7]

Postirradiation examinations were made on fuel cylinders of UC_2 dispersed in graphite.[8] The fuel cylinders were canned in low-permeability graphite as shown in Fig. 21.7. Burnups of up to 20 at. % uranium were obtained with calculated central fuel temperatures of 2500°F. The third experiment in this series leaked fission products on startup through a flaw in the graphite can at the region where the end cap was sealed with Si-SiC. The dimensional changes of the fuel elements in the second irradiation were similar to those of the experiment reported previously.[9] A decrease of 4.5% in diameter and an increase of 3% in length were observed. The graphite cans surrounding the fuel elements remained dimensionally stable. While the UC_2 structure was not greatly changed in the earlier experiment, it had changed in the second irradiation. The UC_2 particles had lost their definite angular appearance. The average wall temperature of the graphite can during irradiation was 1500°F and the wall thickness was 0.4 in.

Samples from the first two experiments were obtained by core drilling radially starting at the center line of the fuel cylinder and progressing to the outer edge of the graphite can. These samples were analyzed for uranium and the fission products Sr^{89}, Zr^{95}, Cs^{137}, and Ce^{144}. Uranium analyses showed no steep gradient across the fuel pellets. However, uranium was found in the graphite-can wall surrounding the fuel. In the second experiment the amount of uranium at the outer edge of the graphite wall represented about ½% of the concentration in the fuel. In both experiments there was a decrease of about a factor of 4 in uranium concentration across the wall from inside to outside.

The fission product gradient was much steeper across the graphite wall. All the fission products mentioned above decreased by about a factor of 10^4; Zr^{95} was present in the smallest amounts.

Uranium Monocarbide

Examinations[7] were begun on the first of a series of three irradiations of specimens of arc-melted and cast UC. The pellets contained 4.8 ± 0.05 wt % carbon and had an average bulk density 96% of theoretical. The pellets were sealed in helium in a tantalum container and then irradiated to a burnup of 4000 Mwd per metric ton at an average center temperature of 2000°F. The fission-gas release based on Kr^{85} release was 1.7%. Metallographic examination showed a reaction between the tantalum and the monocarbide.

[7] *GCR Quart. Progr. Rept. June 30, 1961*, ORNL-3166, pp 141–47.

[8] The fuel elements were made by National Carbon Co., and the irradiations were performed at the MTR by the Reactor Engineering Section of the Reactor Division.

[9] *Solid State Div. Ann. Progr. Rept. Aug. 31, 1960*, ORNL-3017, pp 113–14.

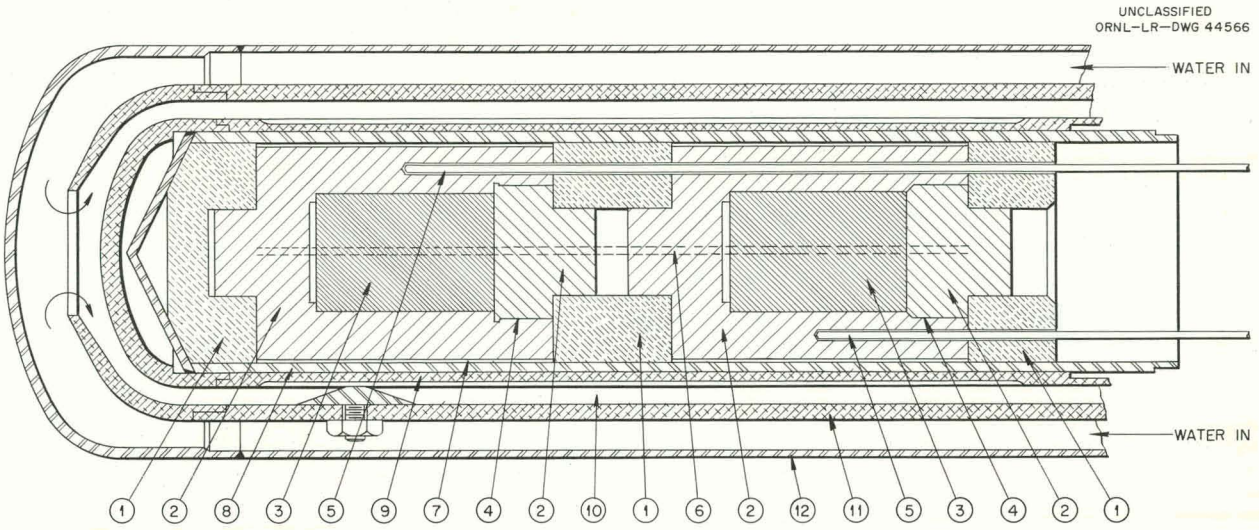

(1) POROUS CARBON-60

(2) R-0020-TYPE GRAPHITE

(3) U^{235}-FUELED GRAPHITE MATRIX

(4) GRAPHITE THREADS SEALED WITH Si–SiC

(5) TYPE 316 STAINLESS STEEL-SHEATHED MgO INSULATED CHROMEL-ALUMEL THERMOCOUPLES (THREE 120° APART PER MATRIX)

(6) FLUX MONITOR WIRES 120° APART ALONG FULL LENGTH OF BOTH MATRICES

(7) HELIUM GAS GAP, 0.010 in.

(8) INNER CONTAINMENT VESSEL, TYPE 304 STAINLESS STEEL

(9) OUTER CONTAINMENT VESSEL, 6061 ALUMINUM (WITH LONGITUDINAL GROOVES)

(10) 1/8-in. WATER FLOW ANNULUS

(11) WATER FLOW DIVIDER, 6061 ALUMINUM

(12) OUTER WATER JACKET, TYPE 304L STAINLESS STEEL

Fig. 21.7. Diagram of Assembly for ORNL-MTR-48 In-Pile Capsule Irradiation Test.

Table 21.4. LM-2 Fuel Pellet Dimensions

Pellet No.	Length			Outside Diameter		
	Before Irradiation (in.)	After Irradiation (in.)	Change (%)	Before Irradiation (in.)	After Irradiation (in.)	Change (%)
			Top			
1-2	0.2484	0.2485	0	0.1562	0.1570	0
2-4	0.2493	0.2535	+1.6	0.1560	0.1565[a] 0.1570	<1
3-7	0.2507	0.2595	+3.5	0.1565	0.1595 0.1585	+1.6
4-9	0.2490	0.2525	+1.4	0.1560	0.1575	+1
			Bottom			
8-16	0.2501	0.2565	+2.5	0.1565	0.1595	+2
6-11	0.2492	0.2575	+3.3	0.1558	0.1595	+2.4
5-10	0.2495	0.2535	+1.6	0.1561	0.1585	+1.5

[a]Two different values were obtained by rotating the sample 90°.

BeO-UO_2

Postirradiation examinations were conducted on the first of a series of capsules containing small hollow pellets of 70 vol % BeO, 30 vol % UO_2. These samples were 92% of theoretical density and were sealed in helium. The top, "a" section, operated at an average central temperature of 1900° F; the bottom, "b" section, operated at 2350° F. Both sections were irradiated to a burnup of uranium of 41,000 Mwd per metric ton, with 0.5% release of Kr^{85}. After irradiation, all eight fuel pellets were intact, with no excessive cracking. Length and outside dimensions were taken on each of the pellets except one, which was potted in place for metallographic examination. There was a general increase in dimensions, as shown in Table 21.4.

MARITIME REACTOR PROGRAM

J. G. Morgan M. F. Osborne
H. E. Robertson

Examinations were carried out on two fuel-rod bundles which had been irradiated in the pressurized water facility in the ORR.[10] Each bundle contained three fuel rods 18 in. long and 0.5 in. in outside diameter. The fuel rods were type 304L stainless steel tubes containing fused and ground Spencer Chemical Company UO_2. Both hot- and cold-swaging methods were used to fabricate the rods. The UO_2 particle size, enrichments, and swaging temperatures are listed in Table 21.5.

[10] The pressurized water facility is operated by the Reactor Engineering Section of the Reactor Division.

Table 21.5. Maritime Fuel-Rod Specifications

Fuel-Rod No.	UO_2 Particle-Size Mesh	Enrichment, U^{235} (%)	Swaging Temperature (°C)
1A1	−20 +35	2.03	25
1B1	−20 +35	2.03	25
1C1	−170 +325	2.04	25
1N1	−170 +325	0.80	25
1O1	−20	0.83	800
1P1	−20	0.83	800

The 35-mil-wall tubes were plug-welded on one end before swaging. The irradiation was carried out at 500° F clad temperature to an estimated uranium burnup of 1000 Mwd per metric ton. The rods had an approximate fission heat generation of 115,000 Btu hr^{-1} ft^{-2}.

Diameters and rod bowing measurements after irradiation showed little change from the preirradiation values. The diameter changes were less than 0.4%. Rod bowing was less than 0.008 in. except for rod 1N1, in which the bowing was 0.025 in.

Gamma scans on the irradiated rods show the burnup profile along the length as well as voids caused by fuel cracking. Figure 21.8 is the gamma scan of cold-swaged rod 1A1. The flux is lower at the top and bottom of the 18-in. rod. The rods were irradiated in vertical position and had a void space between the top of the fuel and the end plug. The rods were pierced in this region for a fission-gas sample. The results of this test are

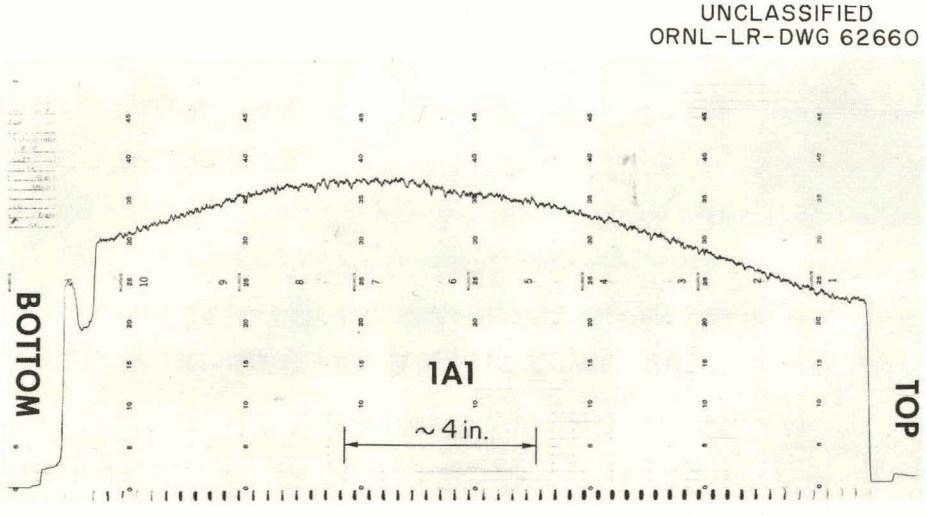

Fig. 21.8. Gamma Scan of Cold-Swaged Rod 1A1.

shown below. The release values are based on Ce^{144}/U burnup analyses:

Rod	Kr^{85} Released (%)
1A1	0.7
1B1	5.0
1C1	6.1
1N1	6.0
1O1	2.5
1P1	3.5

Each rod was sectioned at 2-in. intervals normal to the long axis, and longitudinal sections were made at the ends and in the center. Macrographs taken of these sections showed the following:

1. The free space in the top of each rod remained intact. The fuel did not redistribute itself into this region. There was no great difference in macrostructure of the fuels between the cold- and hot-swaged rods.

2. The fuel experienced extensive cracking, but no large void was found along the center line. While metallographic examination is not yet complete, it appears that some sintering took place. Figure 21.9 shows a longitudinal section in the middle of fuel rod 1A1 as compared with an unirradiated rod.

FAST BREEDER REACTOR ASSISTANCE PROGRAM

J. G. Morgan M. F. Osborne

Postirradiation evaluation studies were begun on miniature fuel plate specimens. The specimens simulate as closely as possible the roll-bonded stainless-steel-clad plates intended for the core B fuel element of the Enrico Fermi sodium-cooled reactor. Two plates, each $2 \times 0.5 \times 0.116$ in., have been irradiated in the MTR to an estimated uranium burnup of 10 at. %. Each specimen consists of a 25 vol % UO_2 core, clad on all sides with type 347 stainless steel. The uranium is 93% enriched.[11] During irradiation the plates generated 1.96×10^{15} Btu hr^{-1} ft^{-2} fission heat at a central core temperature of 1260°F. The plates were surrounded by sodium during irradiation. Pre- and postirradiation dimension and density measurements are compared in Table 21.6. The width and thickness determinations were made at three

[11] J. I. Federer, T. S. Lundy, and M. C. Ziemke, *Fast Breeder Reactor Assistance Program — Phase I — Irradiation of UO_2–Stainless Steel Fuel Specimens (ORNL-MTR-48)*, ORNL CF-60-1-14 (Jan. 7, 1960).

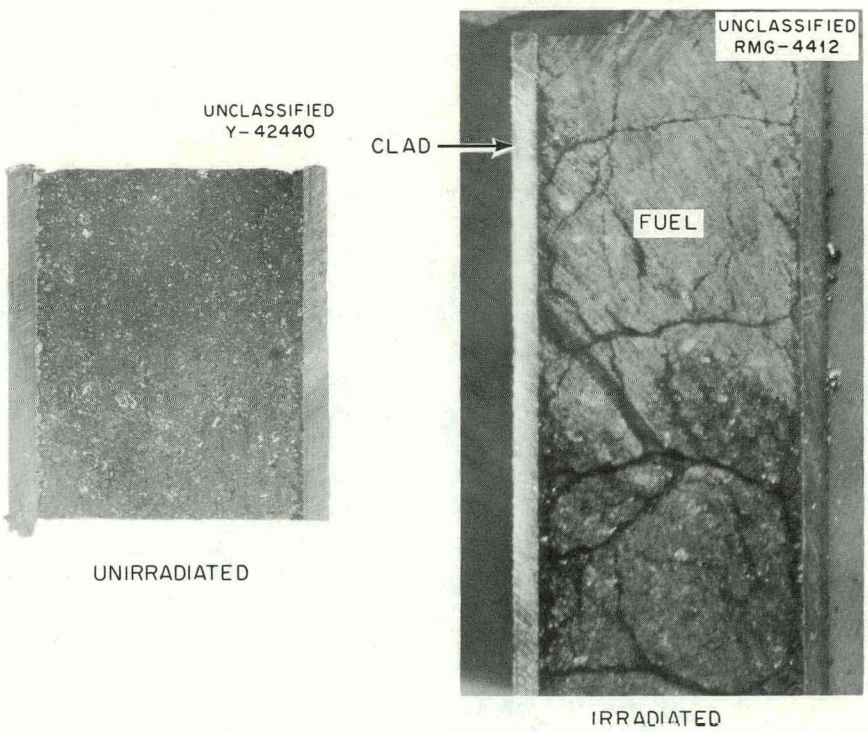

Fig. 21.9. Longitudinal Cross Section of Fuel Rod 1A1. 4X. Reduced 18%.

Table 21.6. Pre- and Postirradiation Dimension and Density Measurements

	Plate Number	
	1	10
Fermi plate dimension, in.		
Length		
Before irradiation	2.002	2.002
After irradiation	2.005	2.003
Width[a]		
Before irradiation	A 0.4972	A 0.4996
	B 0.4987	B 0.5007
	C 0.5005	C 0.5001
After irradiation	A 0.499	A 0.500
	B 0.500	B 0.502
	C 0.497	C 0.500
Thickness		
Before irradiation	D 0.1165	D 0.1212
	E 0.1160	E 0.1214
	F 0.1153	F 0.1210
After irradiation	D 0.1152	D 0.1212
	E 0.1170	E 0.1221
	F 0.1162	F 0.1215
CCl_4 immersion density, g/cc		
Before irradiation	8.16	8.14
After irradiation	8.11	8.11

[a]Letters denote locations where measurements were taken.

locations along the length of each plate. The length and width measurements are accurate to ±1 mil, and the thickness readings to within 0.4 mil. The postirradiation density results are the average values from duplicate measurements. The greatest deviation between values for a single sample was ±0.015 g/cc. There was a very slight (less than 1%) increase in thickness, which resulted in a slight decrease in density.

There were no obvious changes in the external appearance of the two plates as the result of this irradiation. Core-clad integrity checks were made on plate No. 1 with an ultrasonic test instrument, and no change was noted when compared with a standard unirradiated specimen. Fuel plate No. 1 was then step-annealed for 4-hr periods at temperatures from 1100 to 1500°F in 100°F increments. An atmosphere of argon gas at approximately atmospheric pressure was used in the furnace during the heating runs. Between anneals the plate was cooled, measured for thickness, and checked for core-clad bond integrity by the ultrasonic test instrument. A gross activity check was performed on the argon atmosphere after each anneal, and no release of radioactivity was detected. The results of these tests are listed in Table 21.7. Extraneous signals on the ultrasonic gage indicated some stratifying of the fueled region; however, this resulted in no detectable change in thickness. Metallography examinations will be made to confirm these findings.

Table 21.7. Fermi Plate Heat-Treatment Results

Temperature (°F)	Thickness (in.)			Vidigage Results
	D	E	F	
Before irradiation	0.1165	0.1160	0.1153	
After irradiation	0.1152	0.1170	0.1162	No change
1100	0.1160	0.1175	0.1162	No change
1200	0.1166	0.1172	0.1161	No change
1300	0.1166	0.1170	0.1160	No change
1500	0.1162	0.1170	0.1160	Possible rupture[a]

[a]Data not conclusive.

CONTINUOUS RELEASE OF FISSION GAS DURING IRRADIATION

R. M. Carroll J. G. Morgan
T. W. Fulton

An in-pile facility is in operation for the study of the ability of fuel materials to retain gaseous fission products during irradiation. The fuel is heated by its own fission power, which is adjusted by moving the fuel into and out of the reactor neutron flux. At constant power the temperature of the fuel is regulated by air cooling. Fission gas from the fuel is entrained in an inert sweep gas and carried outside the reactor for analysis. The neutron flux at the fuel may be determined by argon activation.

At the end of the last report period, two samples of ceramic fuel, ThO_2-UO_2, had been irradiated in the facility.[12] The total activity of the released

[12]R. M. Carroll and C. D. Baumann, *Experiment on Continuous Release of Fission Gas During Irradiation* (an interim report), ORNL-3050 (Feb. 9, 1961).

fission gas from both samples was dominated by short-lived isotopes. Measurements from 1000 to 2000°F showed that iodine, xenon, and krypton were released by a temperature-dependent process above 1300°F. Diffusion coefficients were calculated for the UO_2 sample. There was no change in thermal conductivity of 95% density UO_2 up to 2300 Mwd per metric ton burnup; in the 1000 to 2000°F range, $K = K_0 e^{-1.21T\times10^{-3}}$ ($T = °K$). An in-pile oxidation of UO_2 was indicated by a stored-energy release and a large increase of fission-gas release. A 3% hydrogen addition to the sweep gas partially reduced the fuel and decreased fission-gas release.

This facility has been used to test three additional fuel samples for their ability to retain fission products under a variety of operating conditions. The facility has been improved by the installation of a 256-channel pulse-height analyzer, replacing an obsolete single-channel analyzer. This improvement in the gamma-ray spectrometer has allowed quantitative measurements of several different isotopes in the fission gas. Transient conditions of gas release have also been determined.[13]

Although the fission-gas-release studies are the primary objectives of this experiment, measurements of electrical resistivity,[14] thermoelectric power,[14] and thermal conductivity[12] have also been obtained. A method of measuring flux by the neutron activation of a steady flow of argon was developed[15] which should have wide application.

Graphite-Clad UO_2 Fuel Sample[16]

A sample of high-density UO_2 (0.50-in. OD, 0.50-in. length with a 0.23-in. axial hole) clad in low-permeability graphite treated with a 0.001-in. coating of pyrolytic carbon was irradiated to evaluate the effectiveness of the graphite clad in retaining fission gases.

The effectiveness of the clad was determined by two methods. In the first method the ratios of the amounts of Xe^{133}, Xe^{135}, Kr^{85m}, and Kr^{88} released from the sample were compared with those for the same isotopes released from unclad UO_2. If the fission gas were retained for an appreciable time by the clad, then the isotopes with the longer half-lives would predominate. The length of time which the clad contained the fission gas can be calculated from the amounts of the various isotopes in the fission gas emerging through the clad. The clad appeared totally ineffective in retaining the fission gas.

In the second method a sudden temperature change was used to generate a burst of fission gas from the UO_2. The length of time required for the gas to pass through the clad could be measured directly by observing the time required for the increased fission-gas-release rate to appear in the flowing sweep gas. This test also showed the clad to be ineffective.

The clad sample was removed from the irradiation facility and examined in a hot cell. The graphite clad had not failed grossly and there were no obvious cracks, but the pyrolytic carbon coating had blistered and flaked away in several places. A leak test, made by placing the sample in hot oil, showed a pinhole leak.

Although the clad of this sample failed promptly and completely, the data demonstrated that the effectiveness of the clad and the time of operation before failure could be determined during irradiation.

Thin-Plate UO_2, Sample No. 2[16,17]

Two thin plates of high-density UO_2 (1 × 0.5 × 0.040 in.) were sandwiched together with thermocouples between them and pressing against the outer surfaces. The UO_2 plates were, in turn, sandwiched between two ThO_2 plates. The thermocouples were pressed tightly against the UO_2 surface by means of tungsten springs which act on the ThO_2 plates and through these on the thermocouples (Fig. 21.10).

---

[13] R. M. Carroll, *The Continuous Release of Fission Gas from UO_2 During Irradiation*, presented at 64th Annual ASTM Meeting, 1961; submitted for publication in *ASTM Journal*.

[14] M. D. Karkhanavala and R. M. Carroll, *In-Pile Measurement of the Electrical Resistivity and Thermoelectric Power of Sintered UO_2*, ORNL-3093 (Apr. 17, 1961).

[15] R. M. Carroll, "In-Reactor Thermal Neutron Flux Measurements by Continuous Argon Activation," to be published in *Nucleonics*.

[16] *GCR Quart. Progr. Rept. Mar. 31, 1961*, ORNL-3102, pp 188–96.

[17] *GCR Quart. Progr. Rept. June 30, 1961*, ORNL-3166, pp 153–60.

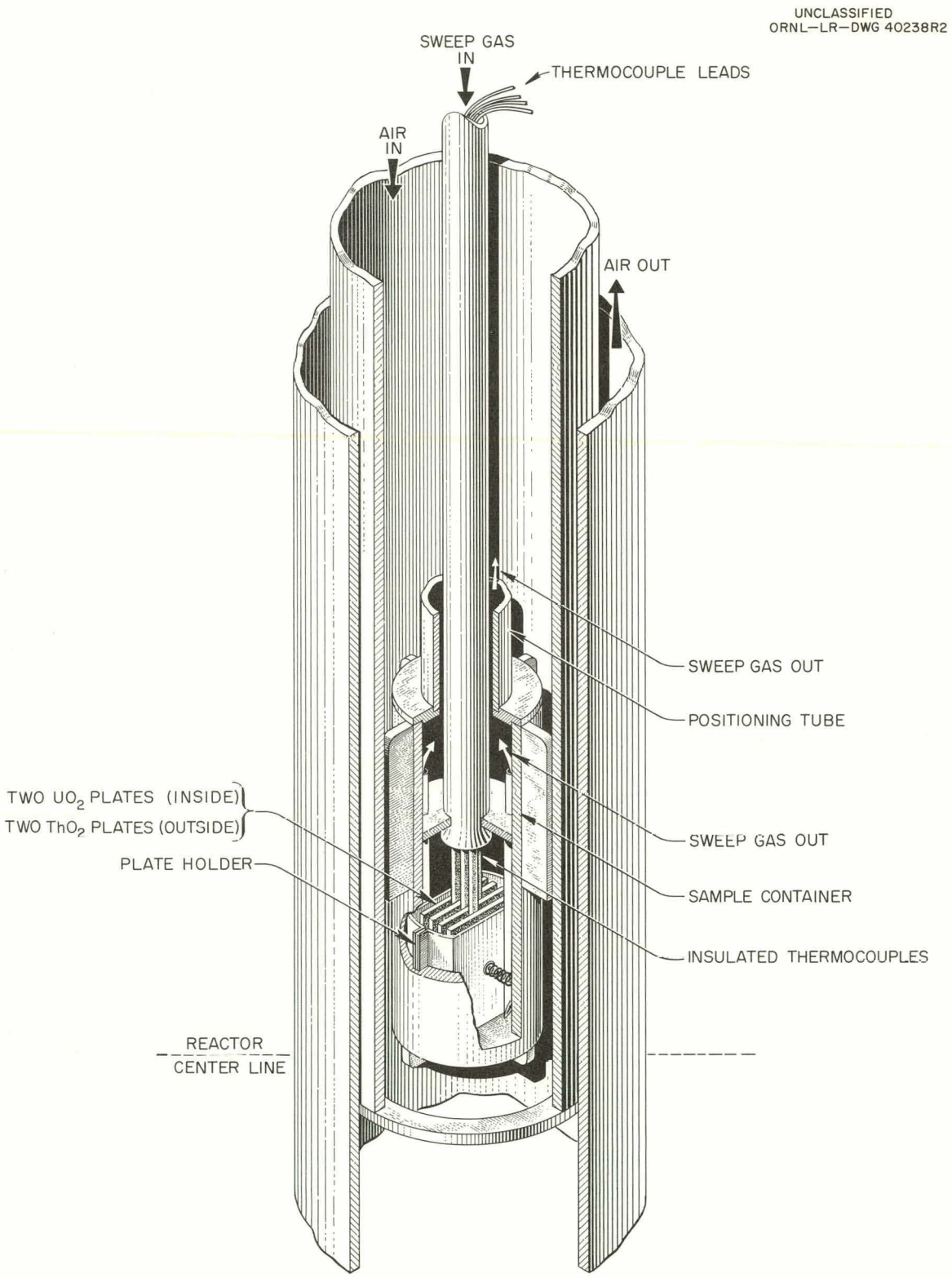

Fig. 21.10. Thin-Plate UO_2 Sample Positioned in Facility Tube.

The purpose of the ThO_2 plates was to determine whether the temperature-dependent gas release could be caused by recoil atoms embedding in the walls of the capsule. If the recoils would back-diffuse from the steel as the capsule was heated, this would produce a temperature-dependent gas release. There was no significant difference in the temperature dependence of the gas release if the UO_2 was surrounded by steel or ThO_2, so back-diffusion does not appear to be an important factor.

In order to measure the steady-state release of fission gas from the UO_2, the sample was maintained at a constant flux and temperature until the release rate of the gas was constant. The time required for equilibrium release is a function of the decay constant of the measured isotope, the temperature of the fuel, and the irradiation history of the fuel. Under steady-state conditions, equilibrium may require as long as five half-lives of the isotope. Because of this, only relatively short-lived isotopes were studied: Xe^{133} (5.3 days), Xe^{135} (9 hr), Kr^{85m} (4.4 hr), Kr^{88} (2.8 hr), and Xe^{138} (17 min).

Iodine Release and Cooling Bursts[13,17]

Only Xe^{133} and Xe^{135} of the above isotopes have long-lived precursors. Xenon-133 has a 63-min tellurium and a 20.8-hr iodine precursor. A small amount of Xe^{135} is formed directly from the fission, but the majority is born from 6.7-hr I^{135}. These iodine precursors diffuse from the UO_2 and adhere to the surfaces of the capsule and sweep system. When the iodine decays to xenon, the xenon is released from the surface and is entrained in the sweep gas. The amount of iodine emerging from the UO_2 was measured by allowing the total xenon release to obtain equilibrium and then withdrawing the sample from the reactor to measure the amount of xenon born from the iodine.

The release of $Xe^{133,135}$ during an equilibrium run is illustrated in Fig. 21.11. The sample had been irradiated for about a month at the same flux (3.7×10^{12} nv); thus the Xe^{133} was nearly at equilibrium when the run was started. When the sample was inserted into the reactor, it heated rapidly and a typical heating burst resulted. The xenon emerging from the system reached equilib-

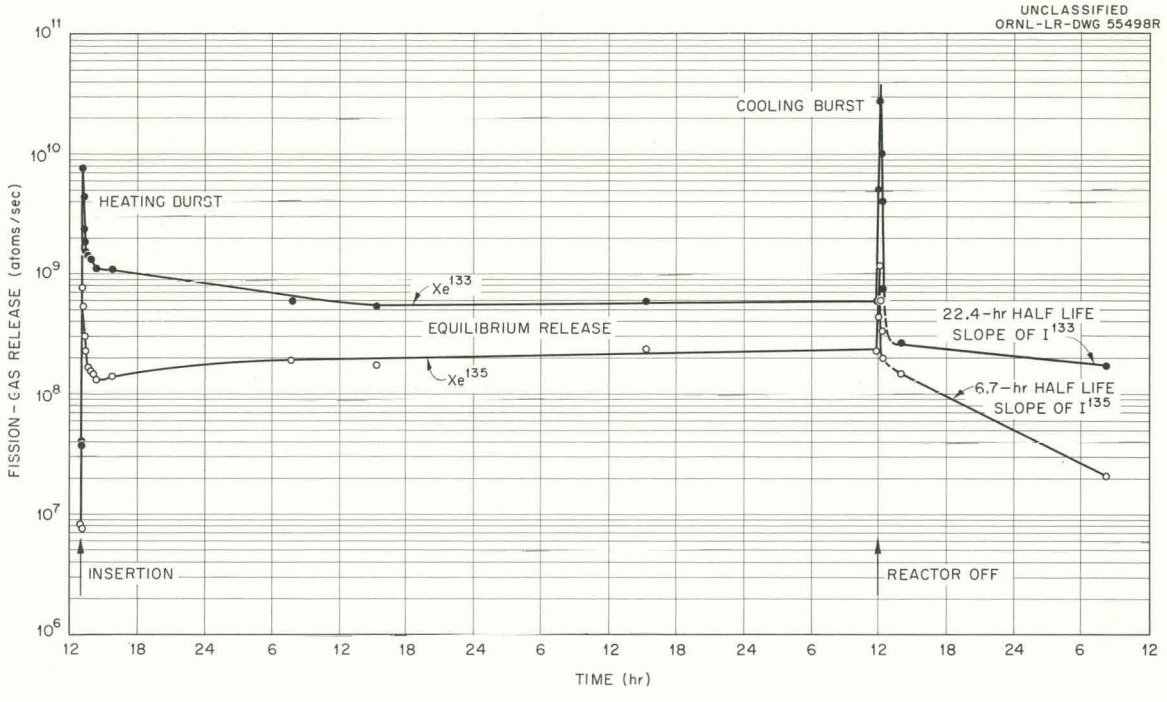

Fig. 21.11. Xe^{133} and Xe^{135} Release from UO_2 During Irradiation at 890°C, $\phi = 3.7 \times 10^{12}$.

rium after several days. The main reason that several days were required for equilibrium release of xenon is that the iodine plated on the walls of the sweep system had to reach equilibrium. When the xenon release was constant, the reactor was shut down, fission heating stopped, and the UO_2 cooled rapidly. After the cooling burst, resulting from the decrease in temperature, no more gas was released from the cold fuel. Xenon continued to be produced, however, and the amount of xenon in the sweep gas decreased with the half-life of its iodine precursor. This is because the xenon in the sweep gas was born from iodine plated on the walls of the sweep system.

If the amount of xenon due to the plated iodine is extrapolated back to the moment the irradiation stopped, the steady-state production of xenon born from the plated iodine can be found. This xenon production is equal to the steady-state release of iodine from the hot UO_2, since at equilibrium every atom of iodine that decays to xenon is replaced with an iodine atom emerging from the UO_2. This assumes that all the xenon is released when the iodine decays.

The difference between the total xenon and the xenon released from the plated iodine gives the steady-state release of xenon from the fuel itself. In this way, the steady-state release of iodine and xenon can be measured at the same time. The results of the iodine release measurements as well as measurements of the cooling bursts have been reported elsewhere[13,16,17] and are summarized below.

Iodine, Xenon, and Krypton Release[13,16,17]

The UO_2 sample was operated at a series of temperatures between 500 and 1100°C. Below 600°C, recoil release (where the atom recoils free of the fuel at the moment of fission) predominates. At temperatures above 700°C the greater part of the gas is released by a diffusion process. The temperature dependence for gas release of krypton, xenon, and iodine is the same (activation energy, 30 kcal/mole).

When the sample was operated at 1100°C a gradual increase of fission-gas release was observed. This could only be explained as a change in the structure of the UO_2. When the sample was again operated at lower temperatures, it was found that the gas release had been permanently increased, presumably by the 1100°C temperature irradiation. However, the activation energy had not been changed.

About 45% of the 133 isobar and 80% of the 135 isobar emerged from the UO_2 in the form of iodine (or a precursor) for the temperature range 700 to 1000°C.

Xenon and krypton were released in bursts when the UO_2 was heated or cooled. The amount of gas released in the cooling burst was a direct function of the steady-state release before the UO_2 was cooled. A phase change of nonstoichiometric UO_2 is most likely the cause of this cooling burst. This sample had excess oxygen, but cooling bursts have been reported[18] for oxygen-deficient samples of UO_2.

By measuring the ratio of the amounts of Xe^{133} and Xe^{135} escaping from the UO_2, the method of release (recoil, diffusion, burst) could be determined.

UO_2 Sample Irradiated in a Reducing Atmosphere

At elevated temperatures (200–1000°C), UO_2 will react with oxygen to form U_3O_8. Even small amounts of U_3O_8 in the UO_2 cause large changes in the properties of the UO_2.[12,19] In an attempt to prevent oxidation of the UO_2 sample, a sweep gas was used that contained 3% hydrogen, with the remainder either argon or helium. When this sweep gas was used on a UO_2 sample that had already been oxidized, the sample crumbled as the UO_{2+} was reduced.[12,20] A sample which had not already been oxidized should, however, retain its structure in the reducing atmosphere and also should not become oxidized.

A disadvantage of using a hydrogen trace atmosphere is that the hydrogen will affect the emf of the Pt vs Pt–10% Rh thermocouples by reacting with the high-temperature junctions. This can cause considerable error in the temperature measurements and also shorten the life of the thermocouples by embrittlement.

The fission-gas release from a thin-plate UO_2 sample irradiated in the reducing atmosphere did

[18] E. Rothwell, *The Release of Krypton^{85} from Irradiated Uranium Dioxide on Post-Irradiation Annealing*, AERE-R-3672 (March 1961).

[19] J. A. L. Robertson, *Concerning the Effects of Excess Oxygen in UO_2*, CRFD-973 (October 1960).

[20] S. Strausberg and I. E. Luebben, *Chemical Pulverization of Sintered UO_2 Bodies, Part I*, NAA-SR-3910 (Oct. 1, 1958).

not increase with time. Thus, the reducing atmosphere was apparently effective in preventing oxidation. The gamma-ray spectrum of the fission gas released was markedly different from that of fission gas released from UO_2 samples in a nonreducing atmosphere. The release of xenon was decreased relative to the release of krypton. It has been reported[12,19] that the diffusion of xenon is enhanced by excess oxygen in UO_2, and these results confirm this. The data from this sample have not yet been completely evaluated. Both heating and cooling bursts were observed, but no quantitative measurements were obtained. The experiment was prematurely terminated because of thermocouple failures.

A sample of single-crystal UO_2 is being prepared for the next irradiation. This will be operated in the reducing atmosphere, and some of the thermocouples will be of metallic sheath type to protect the junction from the atmosphere.

IN-PILE MEASUREMENT OF THE ELECTRICAL RESISTIVITY AND THERMOELECTRIC POWER OF SINTERED UO_2[14,16]

R. M. Carroll M. D. Karkhanavala[21]

Two thin plates of high-density UO_2 were sandwiched together with thermocouples between them and pressed against the outer surfaces as described above. The thermocouples were used as electrodes, and the electrical resistivity of the UO_2 was measured by the potential-drop method with corresponding arms of the thermocouples used as current lead-in wires and potential probes. The UO_2 was heated by its own fission and the electrical resistivity measured at temperatures from 50 to 972°C. Preirradiation measurements were made with an electric furnace to obtain temperatures to 750°C.

Electrical resistivity did not change with irradiation up to about 10^{18} nvt, at which point the resistivity decreased by a factor of 3. The resistivity ranged from 8.75×10^3 ohm-cm at room temperature (before irradiation) to 0.4 ohm-cm at 773°C (after $nvt > 10^{18}$). The activation energy was 0.5 ev during irradiation, as compared with 0.65 ev before irradiation.

[21] Guest scientist, from Atomic Energy Establishment, Trombay, Bombay, India.

The temperature between the plates was higher than the outside temperature during irradiation. This thermal gradient created a thermoelectric emf between the UO_2 and the platinum thermocouples. The thermoelectric emf for the Pt-UO_2-Pt system ranged from 130 $\mu v/°C$ at 162°C to 29 $\mu v/°C$ at 900°C. The UO_2 behaved similar to an n-type conductor during irradiation.

IN-REACTOR THERMAL-NEUTRON FLUX MEASUREMENTS BY CONTINUOUS ARGON ACTIVATION[15]

R. M. Carroll

A method of flux measurement has been developed that uses a steady flow of argon through the neutron flux region. The only isotope of importance in argon is Ar^{40}, which captures neutrons to become 1.83-hr Ar^{41}. The argon passes outside the reactor, where the amount of Ar^{41} per unit volume is measured by gamma-ray spectroscopy. The thermal-neutron flux at a given position is found by using an enlarged section of tubing at that position; so the probability of the argon being activated in that section is much higher than for the remainder of the tubing.

In the fuel capsule experiment[15,16] the argon was used as the fission product sweep gas and was activated by the thermal neutrons within the capsule. The flux, ϕ, was determined by the relation

$$\phi = Ar^{41}/(Ar^{40})\sigma t ,$$

where

Ar^{40} = number of atoms of Ar^{40} per second entering and leaving the fuel capsule, determined by the flow rate,

Ar^{41} = formation rate of Ar^{41}, determined by gamma-ray spectrometry,

σ = microscopic absorption cross section of Ar^{40},

t = average time (sec) the Ar^{40} atoms are exposed to the flux.

The time t of exposure is affected by the temperatures within the fuel capsule, since the argon density decreases when the gas is heated by contact with the fuel. An empirical method to correct for the effect of capsule temperature upon time of exposure was obtained by varying the temperature

of the capsule with air cooling while at constant flux.

This method of flux measurement allowed the flux to be determined within ±10% at the time the fission-gas release was being observed. The flux measurements also allowed the experimenter to correct for the drift of the neutron flux during and between reactor cycles. This drift is illustrated in Fig. 21.12.

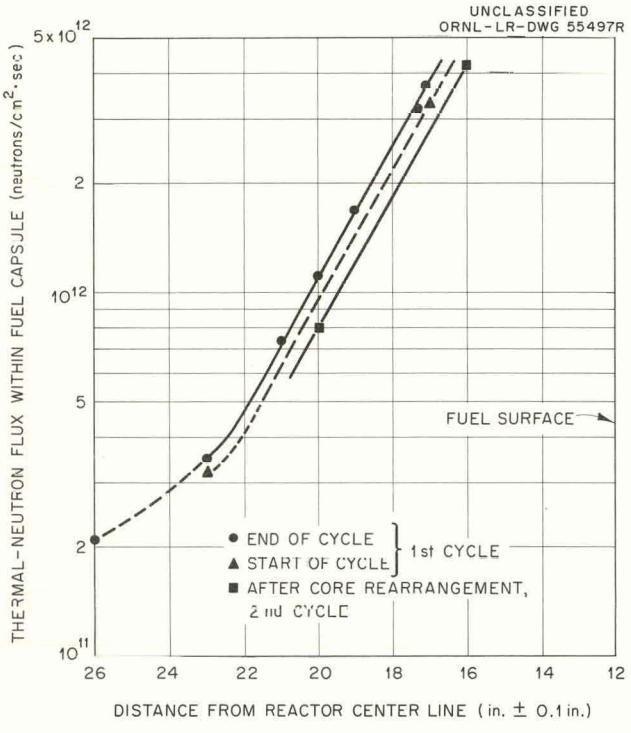

Fig. 21.12. Flux Measurements in the ORR Reactor, C-1 Position.

Although the method has been adapted to a specific experiment, it may be used in many other applications where continuous flux monitoring is desired. The only parameters to be measured are the average time an argon atom is in the flux, the amount of Ar^{41} in the gas stream, and the decay time between argon activation and measurement. This method is suitable for all neutron flux levels and is not restricted by burnup, temperature, or space limitations.

FISSION-GAS RETENTION BY GRAPHITE AND COATED GRAPHITE

P. E. Reagan C. D. Baumann
J. G. Morgan

The irradiation of advanced fuel capsules has continued in the ORR-B9 facility.[22] Eight test samples have been irradiated. Four of the samples were fueled with uranium oxide, two with a UC_2-graphite dispersion, and two with uranium oxide plus 4.5% thorium oxide. Each fuel sample was encased in a graphite can and coated with siliconized-SiC, except two samples, which were sealed in an uncoated-graphite can.

The capsule designated B9-2, containing two ThO_2-UO_2 pellets, was withdrawn from the reactor flux zone after only 7 hr at a graphite temperature of 1800°F because of coating failure.[23] The siliconized-SiC coating had crumbled and was carried by the nitrogen coolant gas to the loop filter. The graphite had completely oxidized. The two pellets had broken into seven pieces, which retained their general cylindrical contour but had their edges rounded off, possibly by being tumbled by the coolant gas.

Capsule B9-3, which contained two UO_2 cylinders clad in graphite coated with siliconized-SiC, was irradiated at 1500°F (can temperature) to a dose of 2.2×10^{20} thermal neutrons/cm^2. Both samples failed, but in different ways. Holes developed in the siliconized-SiC coating along the thermocouple trench in the top sample, as shown in Fig. 21.13. These holes were readily located by the emission of bubbles when the sample was submerged in hot silicone oil. The bottom sample failed by complete graphite separation at the bottom of the UO_2 cylinder. This was probably due to a difference in longitudinal expansion between the graphite can and the UO_2 pellet. These samples were constructed with a 0.006-in. end clearance between the UO_2 and the graphite. Calculations show that this end gap would be filled by thermal expansion at a UO_2 temperature near 2500°F if the graphite can is held at 1500°F. The two pieces

[22] P. E. Reagan, C. D. Baumann, and J. G. Morgan, *Solid State Div. Ann. Progr. Rept. Aug. 31, 1960*, ORNL-3017, p 113.

[23] *GCR Quart. Progr. Rept. Mar. 31, 1961*, ORNL-3102, p 181.

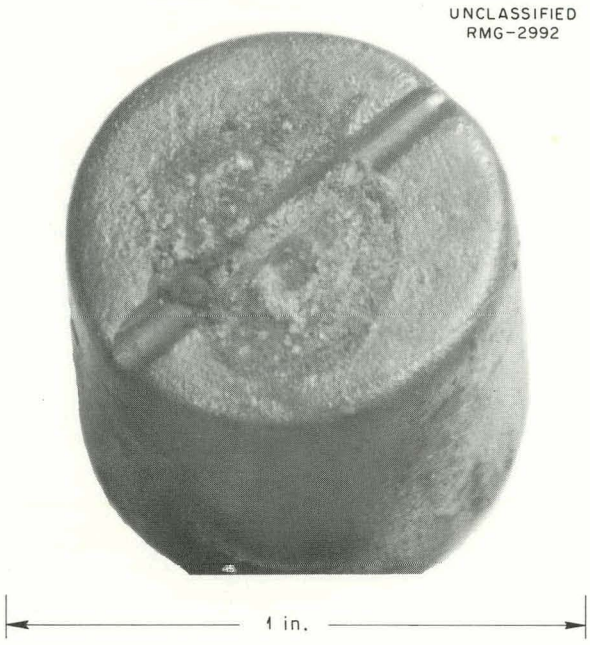

Fig. 21.13. Graphite-Clad UO_2 Pellet from Capsule B9-3, Showing Failure of Siliconized-SiC Coating Along Thermocouple Trench.

of the broken graphite can are shown in Fig. 21.14. The UO_2 cylinder was easily removed from the graphite can. A few cracks were noted along the cylinder wall. It was observed that both ends of the 0.250-in. hole through the UO_2 cylinder became filled with UO_2 during irradiation. Both samples were sectioned for metallographic examination. In both cases, UO_2 was found to have moved, probably by sublimation, from the inside walls and deposited to fill both ends of each cylinder. The UO_2 wall thickness decreased from 0.125 to about 0.090 in. A section of the bottom end of the top sample is shown in Fig. 21.15. Metallographic examination of the UO_2 deposited at the cylinder ends shows flat-sided oval-shaped voids with the flat side toward the graphite-UO_2 interface. These voids appear to have moved toward the sample center by UO_2 sublimation at the inner and hotter surface, depositing on the outer and cooler surface. They are shown in Fig. 21.16.

Capsule B9-4 contained two UO_2 cylinders encased in low-permeability uncoated graphite.[24]

[24] *GCR Quart. Progr. Rept. June 30, 1961*, ORNL-3166, pp 148–53.

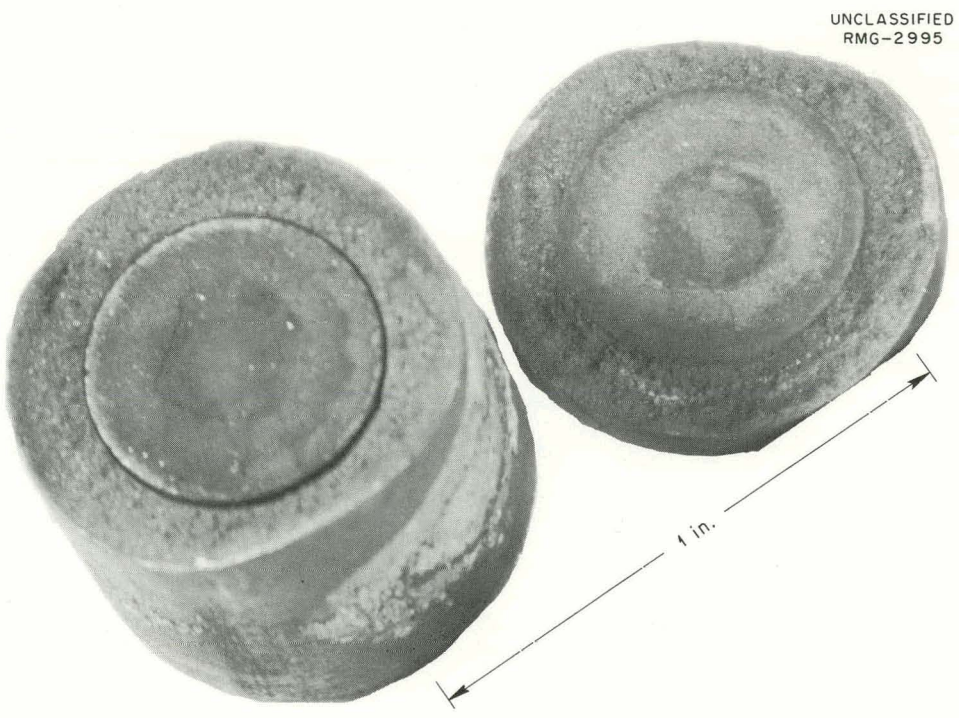

Fig. 21.14. Broken Graphite Can on UO_2 Pellet from Capsule B9-3.

These were sealed in helium in an Inconel capsule. The capsule was irradiated for 1000 hr at 1800°F. Postirradiation examination showed no graphite cracking or deformation, and no diameter changes were noted; but both samples increased in length approximately 0.010 in./in., or 1%. The samples are shown before and after irradiation in Fig. 21.17. The hot silicone oil bubble test, which indicated no leakage before irradiation, showed many holes in both graphite cans after irradiation. Both samples were sectioned for metallographic examination. No UO_2 movement was seen, as was noted in the previous test, but both cylinders showed radial cracking. The UO_2 grain size was about five times that of the unirradiated control sample.

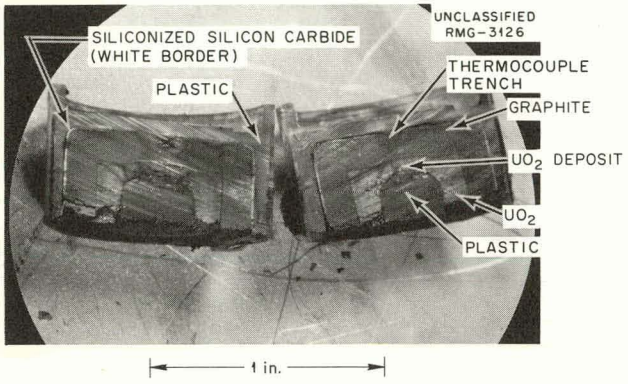

Fig. 21.15. Cross Section of Sample from Capsule B9-3, Showing UO_2 Deposit at End of UO_2 Cylinder.

Two UC_2-graphite dispersion pellets canned in graphite were irradiated in capsule B9-5.[24] These specimens differ in construction from previous samples in that the UC_2 was dispersed in a graphite matrix, a graphite shell was formed around the dispersion, and the graphite shell was coated with with siliconized-SiC. The specimens were sealed in helium in an Inconel capsule and irradiated at 1800°F in a flux of 1×10^{14} thermal neutrons

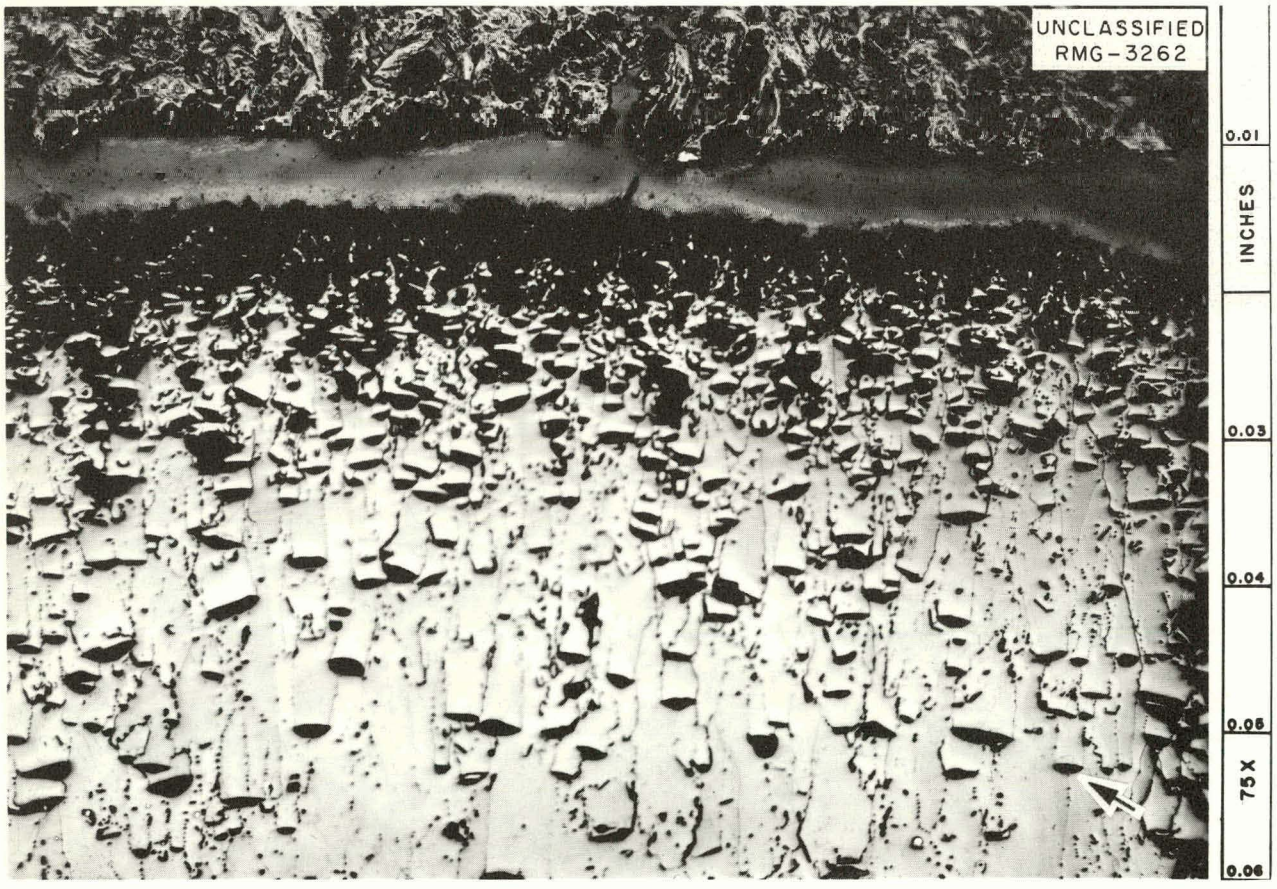

Fig. 21.16. Voids in UO_2 Deposited in Ends of Cylinder.

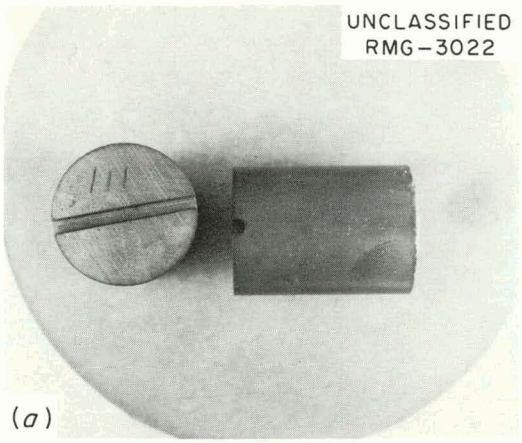

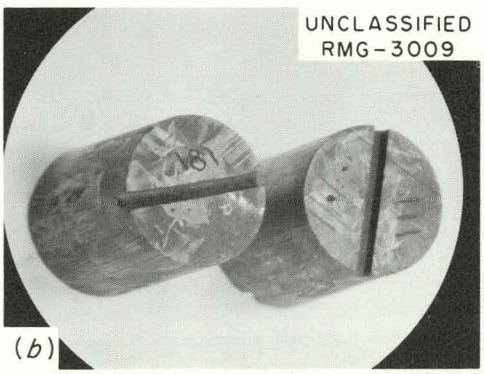

Fig. 21.17. UO_2 Cylinders Encased in Low-Permeability Graphite (*a*) Before and (*b*) After Irradiation in Capsule B9-4.

cm^{-2} sec^{-1}. The test was terminated after 170 hr because the Inconel capsule leaked; the leak was detected by the presence of fission gases in the coolant gas stream. When the samples were removed from the capsule, both were badly damaged. Metallographic examination is in progress.

The ORR-B9 facility has been changed from a nitrogen-cooled loop to a single-pass air-cooled system. The modification included the addition of helium flow lines to sweep fission gases from in-pile capsules to a gamma-ray spectrometer and a trap located in the reactor pool to collect solid daughters of short-lived fission gases.

All the specimens were fabricated by the Minnesota Mining and Manufacturing Company.

POSTIRRADIATION FISSION-GAS-RELEASE STUDIES

M. T. Morgan J. G. Morgan
T. W. Fulton

Measurements of Fission-Gas Pressure at Operating Temperatures

The first of this series of experiments was reported in the last Division progress report. Three additional EGCR prototype capsules have been heated to 1650 and 1740°F to determine the pressure contribution of any cesium and rubidium fission products which might vaporize below these temperatures. The later experiments, like the earlier ones, confirmed the linear relationship of pressure and temperature within the accuracy of the equipment, as shown in a typical graph, Fig. 21.18. Bench tests showed the pressure transducer to have a maximum deviation of ±15 mm Hg at 1700°F. The experimental apparatus for these measurements has been described in detail.[25] The pressures for capsule 06-1 were reported earlier[26] as internal capsule pressures in psia. The capsule void volume, which was estimated for calculating these pressures, has now been measured and found to differ greatly from the previously calculated value because of the porosity of the BeO central rod. This difference reduces the previously reported pressures by a factor of 2.4. Accurate values are plotted in Fig. 21.18.

Determination of the Effects of Burnup and Temperature on Fission-Gas Release

The fission-gas release from EGCR capsules has varied over several orders of magnitude[27] because of changes in several variables. Few data are available to evaluate the effect of any single variable. A postirradiation experiment is now being assembled to reheat the UO_2 from some of the ORR and LITR fuel capsules to derive more

[25] *Proceedings of the Eighth Conference on Hot Laboratories and Equipment*, Book 2, TID-7599 (December 1960).

[26] J. G. Morgan *et al.*, *Solid State Div. Ann. Progr. Rept. Aug. 31, 1960*, ORNL-3017, pp 112–13.

[27] *Ibid.*, p 110.

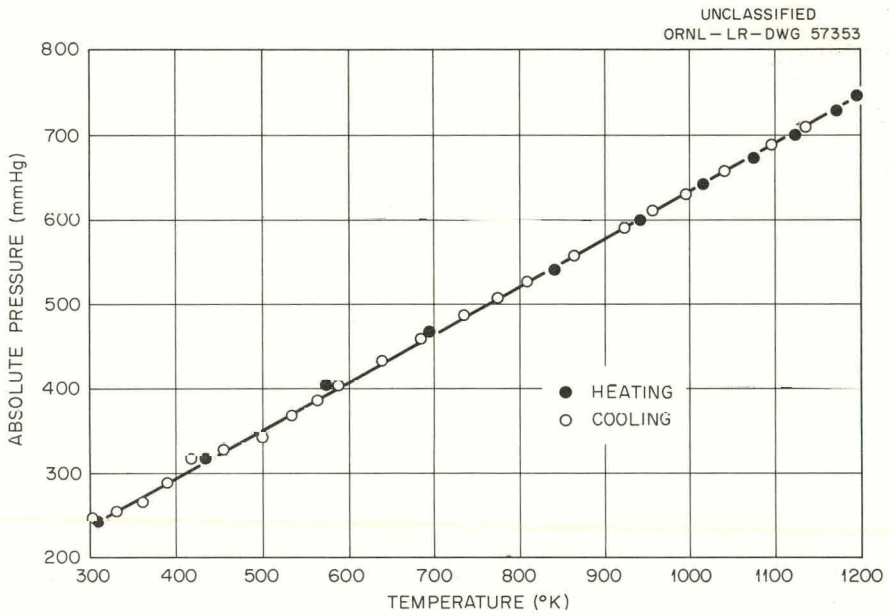

Fig. 21.18. Postirradiation Measurement of Fission Gas from ORR-Irradiated Capsule 08-1.

accurately the effect of temperature and burnup on gas release. The diffusion coefficient may be obtained from the gas-release data if the surface area as measured by the Brunauer, Emmett, Teller[28] method is known. Unfortunately, many of the pellets irradiated at high temperatures show gross changes, and since the gas surface area cannot be measured on such small samples, only those samples whose microstructure shows no changes will be used. This experiment, which is a post-irradiation annealing experiment similar to the neutron activation experiments of Toner and Scott,[29] will be put into operation in a few weeks. Samples irradiated to burnups of over 20,000 Mwd per metric ton are presently available.

[28] S. Brunauer, P. H. Emmett, and E. Teller, *J. Am. Chem. Soc.* **60**, 309 (1938).

[29] D. F. Toner and J. L. Scott, *Study of the Factors Controlling the Release of Xe^{133} from Bulk UO_2*, presented at the Annual Meeting of the American Society for Testing Materials, Atlantic City, New Jersey, June 1961.

22. NUCLEAR METALS

O. Sisman

IN-PILE STRESS-RUPTURE EXPERIMENTS

W. E. Brundage N. E. Hinkle
W. W. Davis J. T. Stanley
A. L. Johnson J. W. Woods[1]
J. C. Zukas

During the past year 15 stress-rupture experiment assemblies were irradiated in the ORR. Materials studied included Inconel, type 304 stainless steel, niobium–1% zirconium, Zircaloy-2, and beryllium. A typical assembly consists of a group of eight to ten tubular specimens stressed by internal gas pressure while the specimen is controlled at a desired temperature. The time-to-rupture at various stress levels and temperatures is measured and is compared with available data from similar tests run outside the reactor. Post-irradiation hot-cell examinations yield additional

[1] On loan from the Metallurgy Division.

information from strain measurement, rupture mode, and metallographic studies.

Techniques have been developed which permit specimens to be operated at temperatures in the range from 500 to 2000°F. The desired operating temperature must be taken into consideration in the design of an experiment. The effect of nuclear heating must be properly balanced by the heat losses to keep the temperature of the specimen below the desired operating point when the reactor is at full power. Three-section electrical heaters on each specimen supply the additional power necessary to raise the temperature to the operating point. For high-temperature operation, heat shielding is employed to lower the load on the heaters. In the lower temperature range either water-cooled or air-cooled "fingers" inside the specimen are used to aid in removing the nuclear heat.

Control equipment permits simultaneous operation of three separate experiment assemblies containing up to a total of 24 pressurized specimens and a like number of three-section heaters. Equipment now on order will permit this number to be increased to 32. Three thermocouples are attached along the specimen gage length. The emf output of each thermocouple is fed to a proportional controller which adjusts the power input to the respective furnace sections. Some sections in each experiment are directly controlled by a servo-operated variable voltage; others are roughly controlled by the same servo and then are trimmed to temperature by a proportional on-off controller.

A power and thermocouple patch panel has been installed and has proved very valuable as it permits any control instrument to be connected to any heater section in the system. This flexibility allows rapid modification of control mode when changing experiments and also permits patching to other instruments for trouble shooting or when necessitated by instrument failure. This has greatly reduced experiment down time for instrument repair.

The gas supply system purifies tank helium, supplies high-pressure helium for specimen loading, and monitors the pressure of each of the specimens every 3 min. Since some of the experimental materials are highly sensitive to contamination from their environment, the helium is purified by passing it through a liquid-nitrogen-cooled charcoal trap and over heated calcium. This purified gas is used as the atmosphere in the experiment container and to provide the pressures required for stressing the specimens (up to 5000 psig).

Inconel Tube-Burst Tests

In order to investigate the hypothesis that the presence of boron in Inconel is responsible for the observed decrease in the rupture life during neutron irradiation,[2,3] in-pile tube-burst tests in air at 1500°F have begun on six special laboratory heats of Inconel. These materials, listed in Table 22.1, contain different concentrations of natural and/or isotopic boron. The experiments (see Fig. 22.1), described previously,[4] are performed in the poolside facility of the ORR.

Results of the experiments are plotted and compared with out-of-pile data[5] in Fig. 22.2. The results, when analyzed with respect to B^{10} concentration, show no supporting trend for the proposed damage mechanism. However, when the slopes of the stress-rupture curves for the Inconel 10B and Inconel 6B10 are compared, it is seen that the out-of-pile 6B10 data and in-pile 10B data have similar slopes. Also, the data for Inconel 6B11 indicate a very large irradiation effect where none was expected, as shown by Inconel 4B11. Therefore suspicion exists that there has been a mixup of materials. The isotopic analysis is being checked, and an investigation is being made of boron concentration and distribution in these materials.

Hot-cell examination of test specimens from earlier experiments has begun. The diameters of in-pile tube-burst specimens of Inconel heat NX 8962 have been measured, and the results of these measurements are shown in Fig. 22.3. It is apparent that neutron irradiation reduces the ability of this material to deform. Figure 22.4 summarizes the stress-rupture results which have been previously reported.[2-4]

---

[2]N. E. Hinkle *et al.*, *Solid State Div. Ann. Progr. Rept. Aug. 31, 1960*, ORNL-3017, p 120.

[3]N. E. Hinkle *et al.*, *Solid State Div. Ann. Progr. Rept. Aug. 31, 1959*, ORNL-2829, p 214.

[4]J. C. Wilson *et al.*, *Solid State Div. Ann. Progr. Rept. Aug. 31, 1958*, ORNL-2614, p 106.

[5]Out-of-pile data obtained by Metallurgy Division.

Table 22.1. Boron Concentration in Inconel

Material[a]	Heat No.	Total Boron Concentration[b] (ppm)			B^{10} Concentration (ppm)
		Soluble	Insoluble	Total	
MTR Inconel	NX 8962	30	1	31	6
CX-900 Inconel	NX 5757	41	1	42	8
Special Inconels					
0B	HF 7883			< 10	< 2
2B	HF 7969			20	4
10B	HF 7970			100	20
4B11	HF 7887			40[c]	1
6B11	HF 7896			60[c]	1
6B10	HF 7885			60[d]	56

[a] Manufacturer, International Nickel Co.

[b] The soluble and insoluble analyses were supplied by Cyrus Feldman of ORNL. Where only total concentration is listed, the figure was supplied by the manufacturer and is nominal.

[c] 98% B^{11} enriched.

[d] 95% B^{10} enriched.

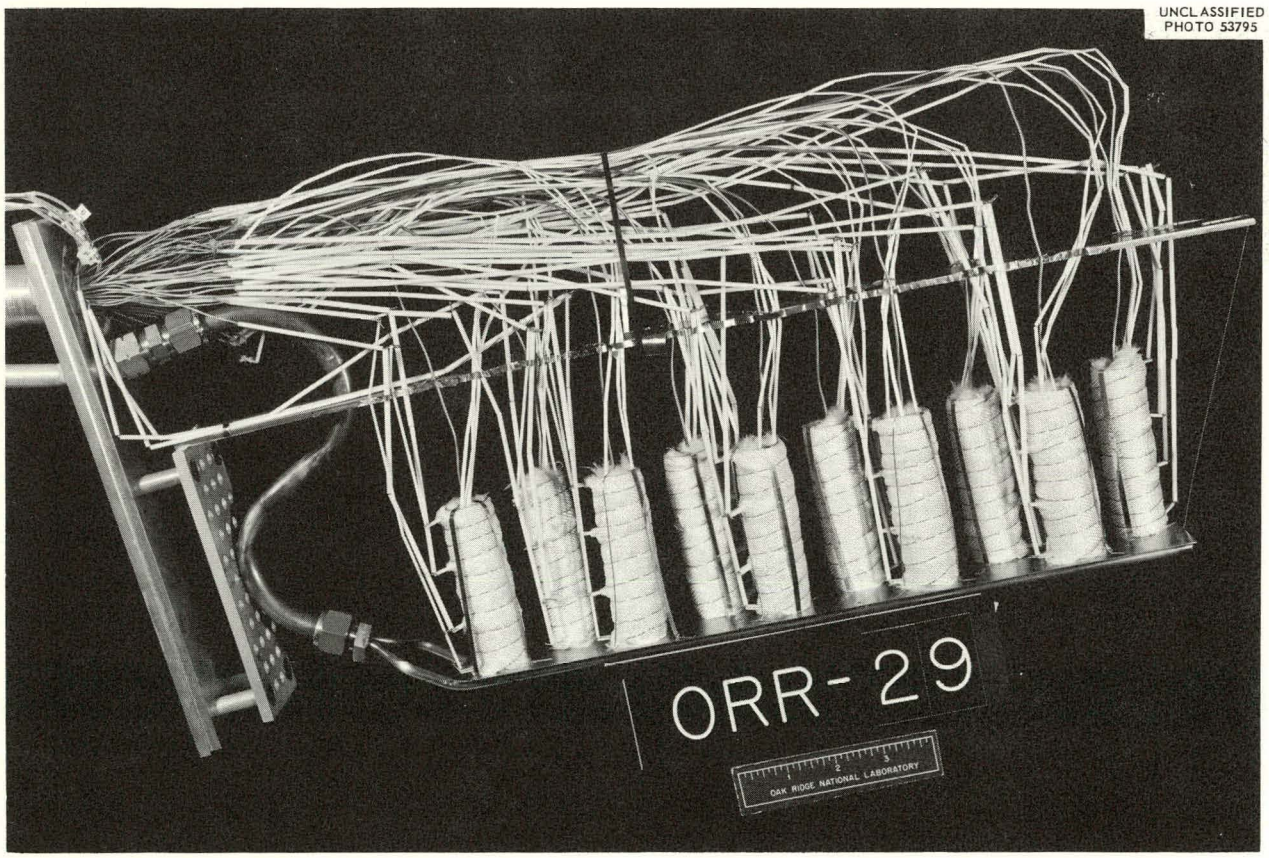

Fig. 22.1. Inconel Tube-Burst Experiment.

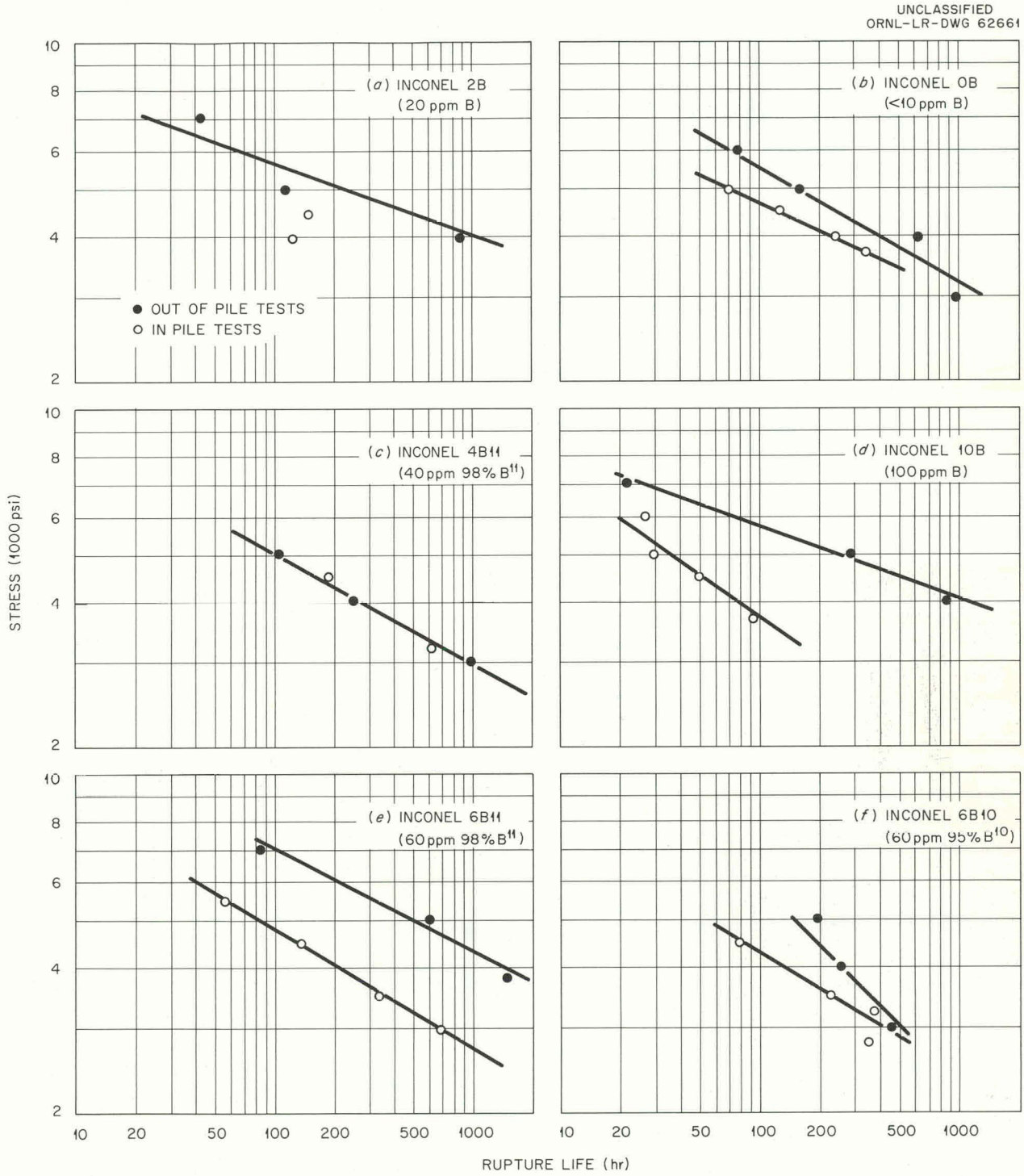

Fig. 22.2. Stress-Rupture Tests in Air at 1500°F on Special Inconel Heats. O, out-of-pile tests; ●, in-pile tests.

Stainless Steel Tube-Burst Tests

In-pile tube-burst tests on type 304 stainless steel have continued in support of the EGCR fuel-element design.[6] During the past year one experiment (ORR-17) with specimens operated at 1500 and 1600°F was completed. These results and previously reported data[6] are summarized in Fig. 22.5, in comparison with out-of-pile data[5] on the same material. The largest percentage decrease in rupture strength at a given time due to irradiation is seen at 1500°F. At 1600°F, the change appears to be smaller, possibly due to increased annealing of defects. No change in

[6]N. E. Hinkle *et al.*, *Solid State Div. Ann. Progr. Rept. Aug. 31, 1960*, ORNL-3017, p 122.

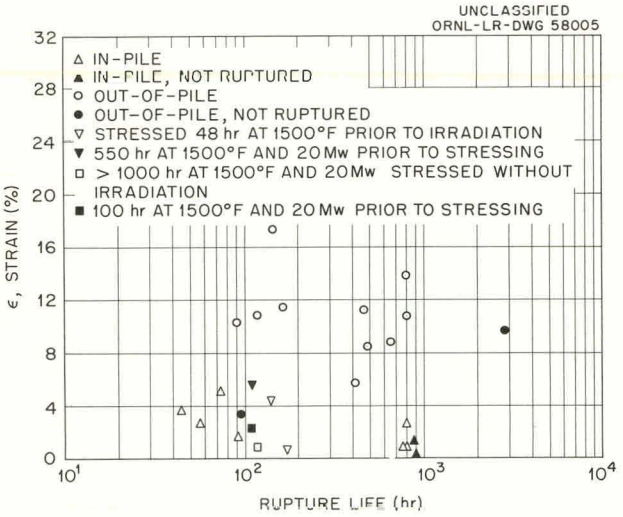

Fig. 22.3. Maximum Tangential Strain vs Rupture Life for Inconel Tube-Burst Specimens (INCO Heat No. NX 8962).

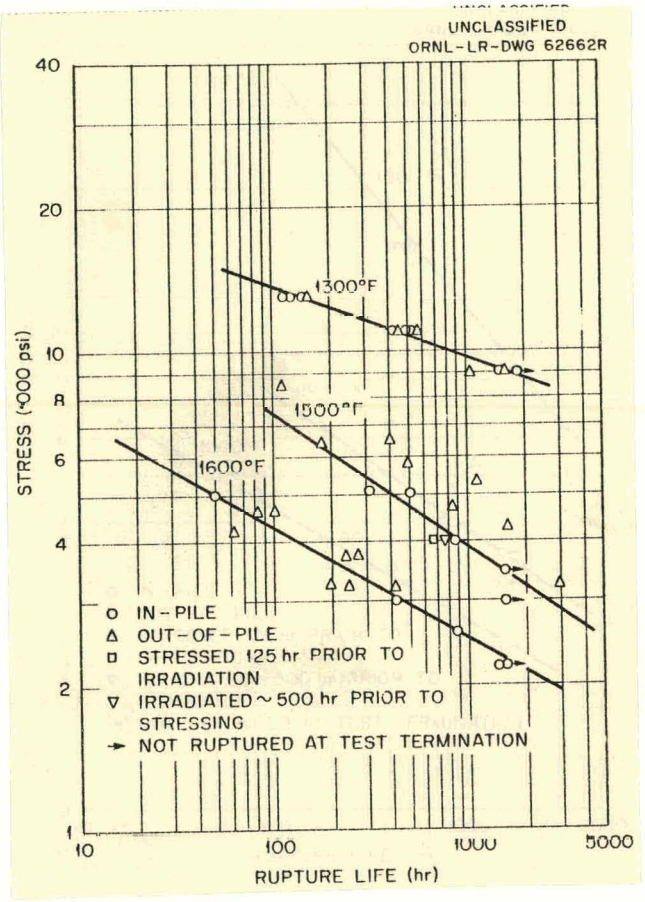

Fig. 22.5. Stress-Rupture Tests in Air on Type 304 Stainless Steel (Superior Tube Co. Heat No. 23999X).

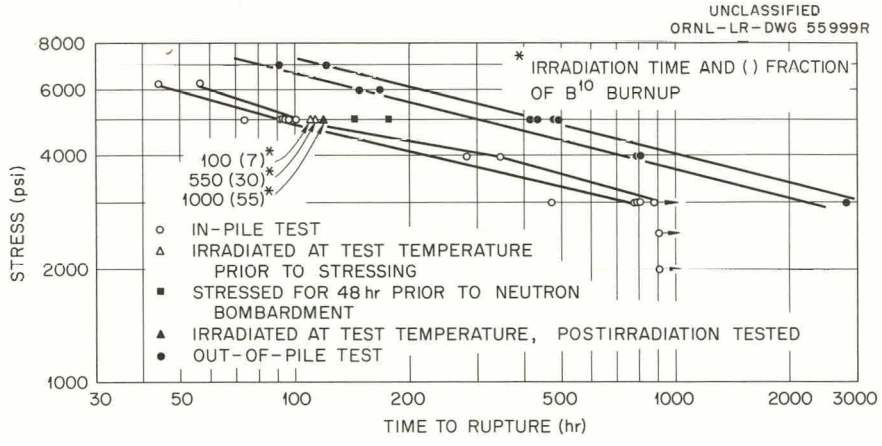

Fig. 22.4. Stress vs Time to Rupture for Inconel (INCO Heat No. NX 8962) at 1500°F in Air.

rupture strength was observed in tests at 1300°F.

Hot-cell examination of the irradiated specimens has begun with the measurement of the specimen diameters. The ductility, reported as per cent tangential strain, is shown in Fig. 22.6. The ductility at rupture is considerably less for the in-pile tests. These data also show an increasing ductility with increasing temperature but not as great as for the out-of-pile tests. The combination of reduced ductility with no change in rupture life at 1300°F suggests a lower creep rate due to neutron bombardment.

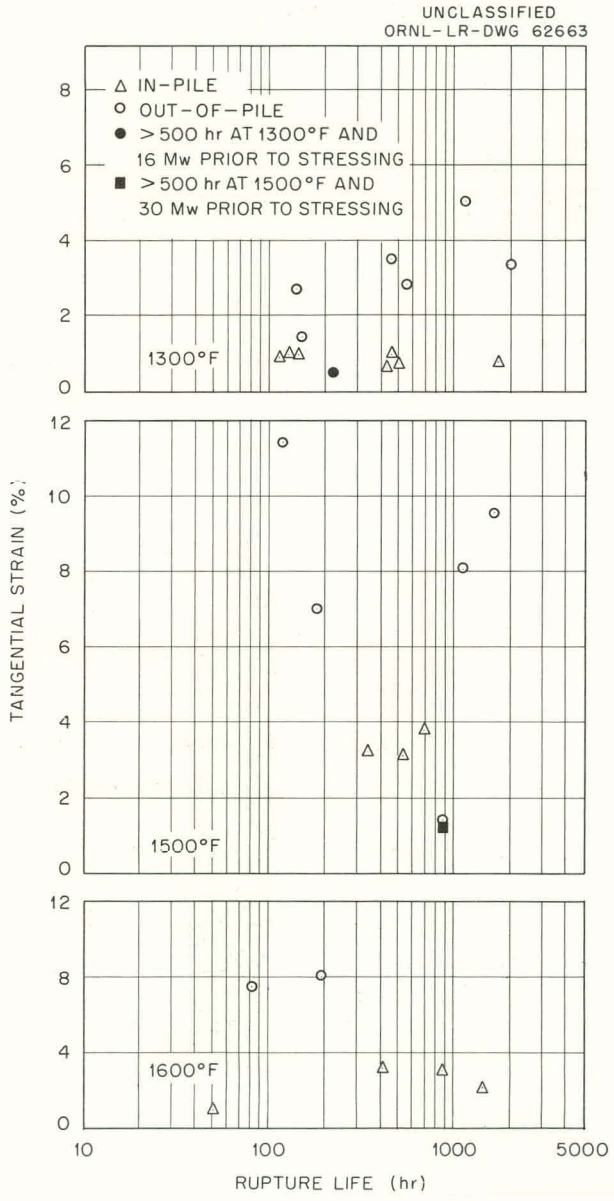

Fig. 22.6. Average Tangential Strain vs Rupture Life for Stainless Steel Tube-Burst Specimens (Superior Heat No. 23999X).

Stress-rupture tests on type 304 stainless steel will continue, with emphasis on increased range of test temperatures and increased test duration. Other heats of material will also be included.

Niobium Tube-Burst Tests

The study of the effect of neutron bombardment on the stress-rupture properties of metals has been extended to refractory metal-base alloys.[7] Three in-pile assemblies containing tube-burst specimens fabricated from an alloy of niobium–1% zirconium were operated in the poolside facility of the ORR. These experiments are identified as ORR-18, -19, and -31. Experiment ORR-18 served mostly to provide fabrication and operating experience. As a result of the information obtained in this experiment, the techniques of fabricating in-pile furnaces with mineral-insulated metallic-sheathed heater cable were refined, and experiments ORR-19 and -31 used this type of furnace. Figure 22.7 shows these furnaces at various stages of construction. Figure 22.8 shows experiment ORR-31 after completion of the assembly. The tubular parts around each furnace in Fig. 22.8 are tantalum thermal radiation shields. These experiments, operating up to 2000°F, have utilized 26-gage Chromel-Alumel thermocouple wire for temperature measurement.

The mechanical properties of the refractory alloys are drastically altered by an increase in the concentration of carbon, hydrogen, nitrogen, or oxygen in the alloy. Therefore, it is necessary to fabricate these experiments with materials which do not outgas during operation. Components of the present design are either metallic or ceramic and are degreased and baked-out prior to assembly. The components are assembled as carefully as possible to minimize contamination. Following assembly and closure of the experiment container, the apparatus is heated to about 300°F under vacuum. The apparatus is then filled with helium, cooled, and inserted in the reactor. The gas supply lines are purged with purified helium and connected to the experiment with quick-disconnect fittings, thus minimizing the entrance

[7] N. E. Hinkle *et al.*, *Solid State Div. Ann. Progr. Rept. Aug. 31, 1960*, ORNL-3017, p 123.

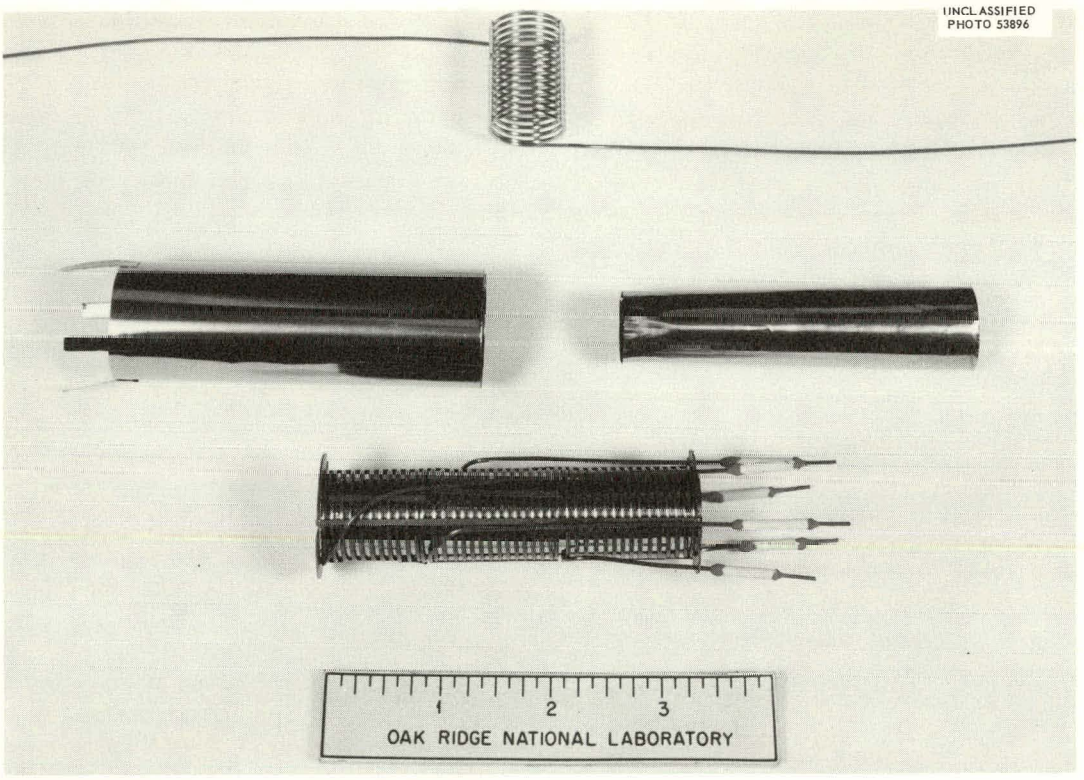

Fig. 22.7. Metallic-Sheathed Furnace.

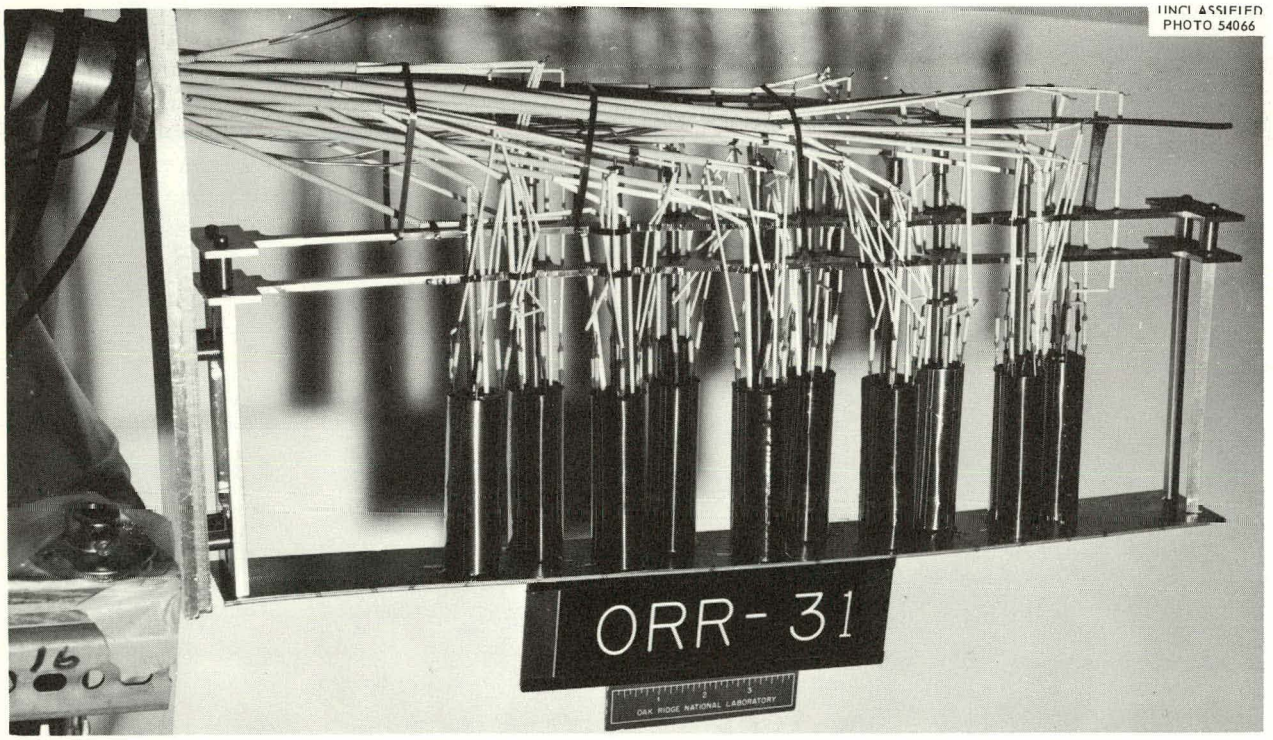

Fig. 22.8. Niobium Tube-Burst Experiment.

of impurity gases to the assembly. During operation, gettering materials, built into the experiment assembly, are maintained at an elevated temperature for the purpose of absorbing outgassed impurities.

Figure 22.9 summarizes the in-pile data obtained on the niobium–1% zirconium alloy as compared with data from the same material obtained out-of-pile in a vacuum system.[5] At 1800°F it is very difficult to obtain reproducible results due to the extreme stress dependence of the rupture life. This difficulty was increased as a result of variable tube-wall thickness. Nevertheless, the in-pile rupture strength averages about 12% lower than the out-of-pile strength. At 2000°F the in-pile data suggest a decreased rupture strength of about 15%.

Preliminary postirradiation examination of ORR-19 has been completed. Six of the specimens, all of which operated at 1800°F, showed blowout-type ruptures similar to the out-of-pile ruptures. A ruptured specimen is shown in Fig. 22.10. The specimen surfaces were still bright, indicating that the atmosphere control was good. However, confirmation of success in this area must await analysis of the material for impurity content.

In-pile tests on the niobium–1% zirconium alloy system will continue on a second heat of material. These tests will begin at 2000°F and will be extended to at least 2100°F. However, furnace material and thermocouple material will be changed to noble-metal alloys for tests above 2000°F.

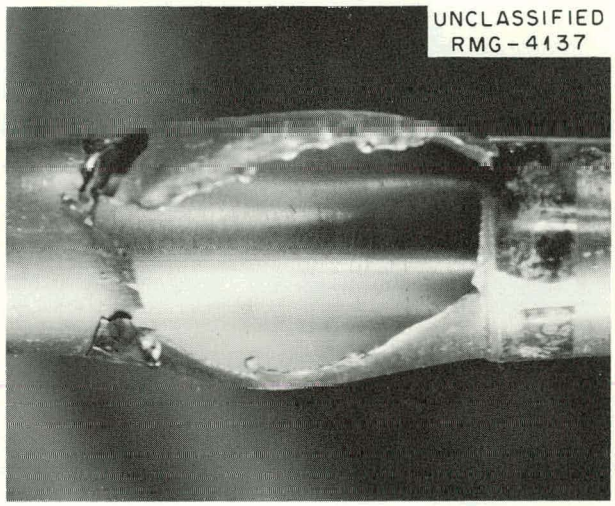

Fig. 22.10. Ruptured Niobium Specimen.

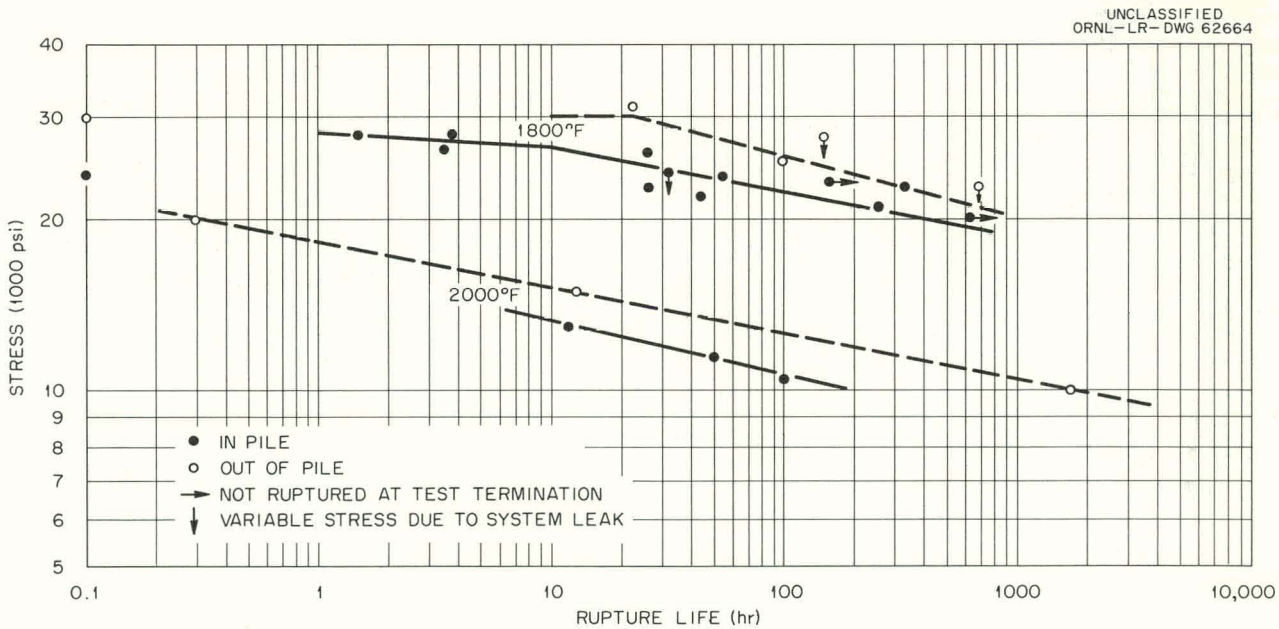

Fig. 22.9. Stress-Rupture Tests on Niobium–1% Zirconium.

Zircaloy-2 Tube-Burst Tests

The Zircaloy-2 tube-burst assembly was modified from the original design[8] to an all-Zircaloy system, since satisfactory joints could not be made from the specimen to the stainless steel cooling finger. Figure 22.11 shows the assembly ready for closure of the experiment can. Two of these assemblies were operated in the P-6 facility of the ORR. Figure 22.12 shows the time-to-rupture of the specimens of the first assembly. These were stressed after an exposure of approximately 5×10^{18} *nvt* (> 1 Mev). The same figure contains data from out-of-pile tests.[5] With the exception of one specimen at 900°F the data agree within the expected scatter band. Since the in-pile tests are performed under difficult conditions, no conclusion should be drawn from

[8] J. T. Stanley and W. E. Brundage, *Solid State Div. Ann. Progr. Rept. Aug. 31, 1960*, ORNL-3017, p 119.

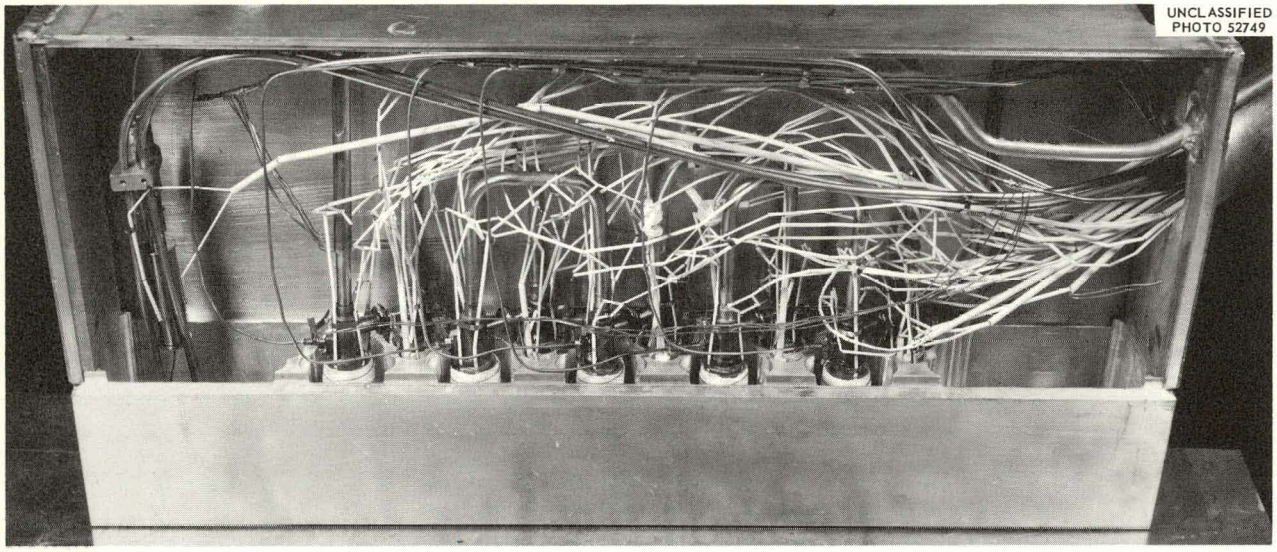

Fig. 22.11. Zircaloy-2 Tube-Burst Experiment.

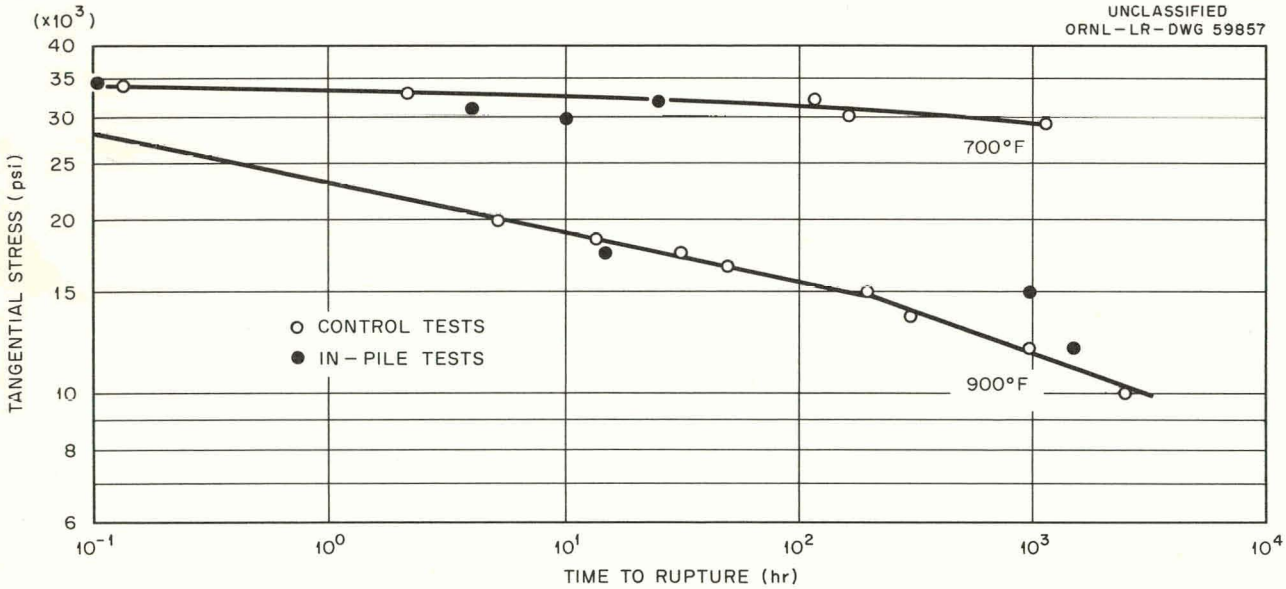

Fig. 22.12. Results of Zircaloy-2 Tube-Burst Test at 700 and 900°F in Helium.

the single exception until further information is obtained. It is possible that a loose thermocouple caused the actual specimen temperature to be lower than the indicated temperature.

Operational difficulties prevented heating of the second assembly. The specimens were irradiated at about 400°F to an exposure of about 2.5×10^{19} *nvt* (> 1 Mev). These specimens are now being removed from the assembly in the hot cell and will be subjected to postirradiation tests.

The studies on this material will be continued, with emphasis on longer irradiation times.

Beryllium

The study of the effect of neutron bombardment on the elevated temperature properties of beryllium and its alloys, in support of advanced gas-cooled reactor design, has been continued in cooperation with the Metallurgy Division. Over-all program planning and data analysis for this material are responsibilities of the Metallurgy Division, and the results of the studies have been reported in their progress report.[9]

[9] J. R. Weir, *Metallurgy Div. Ann. Progr. Rept. May 31, 1961*, ORNL-3160, p 91.

THIS PAGE

WAS INTENTIONALLY

LEFT BLANK

Part V

SPECIAL PROJECTS

THIS PAGE

WAS INTENTIONALLY

LEFT BLANK

23. EFFECT OF REACTOR IRRADIATION ON NICKEL-IRON ALLOYS

D. S. Billington

R. H. Kernohan W. L. Harman[1] P. G. Huray[2]

It is well known that the magnetic properties of magnetically soft materials are sensitive to heat treatment and to the atomic arrangement of the constituent atoms. Atomic rearrangement induced by reactor irradiation might therefore affect magnetic properties. Several Permalloy-type materials were irradiated by Schindler *et al.*[3,4] in the Brookhaven Graphite Reactor at ambient temperature. Striking changes were noted after irradiation in the size and shape of the magnetic hysteresis loops.

In an effort to extend these hysteresis loop studies, a cooperative program was undertaken with the Naval Research Laboratory in order to study changes in magnetic properties as a function of the time and temperature of irradiation. Six small commercial toroids of differing composition (see Table 23.1) were irradiated for seven weeks in Hole 50 N of the ORNL Graphite Reactor. In this facility it is possible to perform irradiation in the vicinity of liquid-nitrogen temperatures. It was estimated that the capsule containing the six specimens was irradiated at an average temperature of 90°K at a total integrated flux of 5×10^{17} *nvt* (> 1 Mev). Sixty-cycle hysteresis loops were drawn automatically on each specimen prior to irradiation, during irradiation, after irradiation, and during the subsequent isochronal heat treatment. At the end of the seven-week irradiation, the specimens were withdrawn from the reactor and allowed to remain at room temperature for three weeks while much of the radioactivity decayed. The capsule containing the specimens was then isochronally heat treated in 25°C steps; it was held for 1 hr at each temperature up to 450°C.

Table 23.1. Composition of Irradiated Toroids

Toroid	Material	Composition (%)		
		Ni	Fe	Other
P	Permalloy	79	17	4 Mo
S	Supermalloy	79	16	5 Mo
U	Mumetal	77	16	5 Cu, 2 Cr
F	Allegheny 4750	52	48	
N	Sinimax	43	54	3 Si
Q	Monimax	47	50	3 Mo

Typical hysteresis loops at different stages of the experiment are shown in Fig. 23.1 for toroid F, Allegheny 4750. In general, only small changes were observed during the low-temperature irradiation or upon warmup to room temperature. Only upon heat treatment in the range of 200 to 350°C did significant radiation-induced changes become prominent. These changes were not observed in unirradiated "control" specimens similarly heat treated. Heat treatments in the range of 350 to 450°C served to anneal the specimens and return them approximately to or toward their preirradiation values. In Tables 23.2 and 23.3 values of coercive force, H_c, and remanence, B_R, are given which were taken before and after the irradiation and after the series of heat treatments ending at 300°C. In regard to the shapes of the loops, the greatest changes were observed in Supermalloy and Allegheny 4750 (see Fig. 23.1).

The fact that no changes in the hysteresis loops were noted during the low-temperature irradiation indicates that radiation-induced defects were not mobile at 90°K and that the defects themselves did not affect the magnetic properties. These defects did begin to diffuse above room temperature, resulting in a slight amount of short-range order which increased the coercive force and decreased the remanence. If a significant critical amount of ordering had occurred, constricted hysteresis loops would have been observed.[3] The form of the heat-treatment curves indicates that diffusion occurs more readily in

[1] Co-op student from Virginia Polytechnic Institute, Blacksburg.

[2] Co-op student from the University of Tennessee; Knoxville.

[3] A. I. Schindler, E. I. Salkovitz, and G. S. Ansell, *J. Appl. Phys.* **30**, 4, 282S (1959).

[4] A. I. Schindler and E. I. Salkovitz, *J. Appl. Phys.* 31, 5, 245S (1960).

Table 23.2. Coercive Force

From room-temperature hysteresis loops

Toroid	Material	H_c (oersteds)		
		Before Irradiation	After Irradiation[a]	After 300°C
P	Permalloy	0.062	0.066	Open circuit
S	Supermalloy	0.068	0.098	0.190
U	Mumetal	0.10	0.12	0.22
F	Allegheny 4750	0.37	0.37	0.48
N	Sinimax	0.23	0.26	0.28
Q	Monimax	0.27	0.30	0.33

[a]Irradiation = 5×10^{17} $nvt > 1$ Mev at 90°K.

Table 23.3. Remanence

From room-temperature hysteresis loops

Toroid	Material	B_R (kilogauss)		
		Before Irradiation	After Irradiation[a]	After 300°C
P	Permalloy	4.8	4.8	Open circuit
S	Supermalloy	4.4	3.8	2.8
U	Mumetal	4.6	4.7	4.0
F	Allegheny 4750	11.4	11.6	5.0
N	Sinimax	9.0	9.0	7.2
Q	Monimax	11.1	11.4	8.4

[a]Irradiation = 5×10^{17} $nvt > 1$ Mev at 90°K.

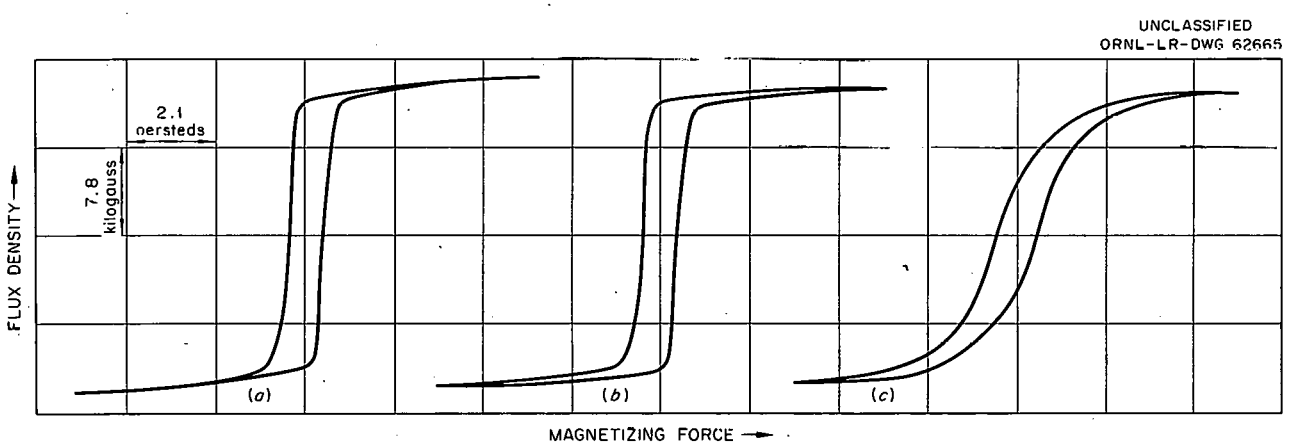

Fig. 23.1. Hysteresis Loops for Irradiated Toroid. Specimen F: Allegheny 4750 (48% Ni–52% Fe). All curves run at room temperature. (*a*) Preirradiation curve. (*b*) After 1.5×10^{17} nvt (fast) at 90°K (seven weeks in reactor). (*c*) After series of 1-hr anneals in 25°C steps ending at 300°C.

the more pure low-nickel type of alloys and that reactor irradiation at temperatures around 150°C would possibly result in greater and more rapid changes in magnetic properties.

24. SEARCH FOR SUPERCONDUCTORS OF HIGH CRITICAL TEMPERATURES AND HIGH CRITICAL FIELDS

H. C. Schweinler S. T. Sekula

The recent discovery of the superconductor Nb_3Sn with the high critical temperature, T_c, of 18°K and high critical field, H_0, of perhaps 300,000 oersteds, has aroused much interest. In search for other such superconductors, certain empirical rules of Matthias[1] have been helpful. These rules have suggested that certain "electron-to-atom ratios," e/a, are especially favorable to superconductivity. Our viewpoint has been slightly different. It is based on the BCS theory.[2] This theory leads to the equations:

$$kT_c = 1.14\hbar\omega \exp[-1/N(0)\,V] , \qquad (1)$$

$$\gamma T_c^2/H_0^2 = 0.170 \text{ (dimensionless)} , \qquad (2)$$

where $\gamma = (2/3)\pi^2 N(0)k^2$, k is the Boltzmann constant, $\hbar\omega$ is a characersitic lattice vibrational energy (say $k\Theta_D$, where Θ_D is the Debye temperature, commonly 200 to 400°K), $N(0)$ is the density of states of one spin per unit energy at the Fermi surface (unit volume of crystal understood), V is an "average" electron-phonon interaction energy, and γ is the linear term in the low-temperature heat capacity of the normal metal [$C = \gamma T + BT^3$, erg cm^{-3} $(°K)^{-1}$].

It is common to infer, correctly, from (2) that high critical field is associated with high critical temperature. From (1) and (2) we can conclude that high critical field is also associated with high density of states at the Fermi level, $N(0)$, which is equivalent to a large linear term in the heat capacity, γ.

We call attention to the fact that an experimental study of the linear term in the heat capacity of binary alloys of neighboring transition metals[3] provides a foundation for Matthias' empirical rules. These authors found strong maxima in γ for $4.5 < e/a < 5$ and $6.1 < e/a < 6.7$. All high T_c superconductors now known have e/a values within these ranges. The studies of Zr-Nb and Mo-Tc alloys were suggested by this observation.

The experimental apparatus is similar to that used for the study of resistance minima in dilute noble-metal alloys and is shown in Fig. 24.1. Samples of transition-metal alloys supplied by M. L. Picklesimer of the Metallurgy Division are placed in the helium-gas thermometer bulb which is suspended in the exchange-gas tube. A small current is passed through the samples, and the voltage drop across the sample is measured on a potentiometer which is sensitive to an emf of less than 10^{-2} μv. By pumping on the helium bath or supplying power to the Nichrome heater, the temperature interval from 1.2 to 25°K can be spanned. Calibration points for the thermometer include the normal boiling point of helium and the transition temperature of superconducting lead.

A plot of the transition temperature of Nb-Zr alloys vs concentration of niobium is shown in Fig. 24.2. The maximum transition temperature is approximately 11°K at the concentration corresponding to a valency electron/atom ratio of 4.8 and agrees with the data of Blaugher and Hulm.[4] A study of the transition temperature of Zr-Tc and Mo-Tc series is contemplated.

[1] B. T. Matthias, *Progress in Low Temperature Physics*, vol II, p 138, North Holland, Amsterdam, 1957.

[2] J. Bardeen, L. N. Cooper, and J. R. Schrieffer, *Phys. Rev.* 108, 1175 (1957).

[3] C. H. Cheng, C. T. Wei, and P. A. Beck, *Phys. Rev.* 120, 426 (1960).

[4] R. D. Blaugher and J. K. Hulm, to be published.

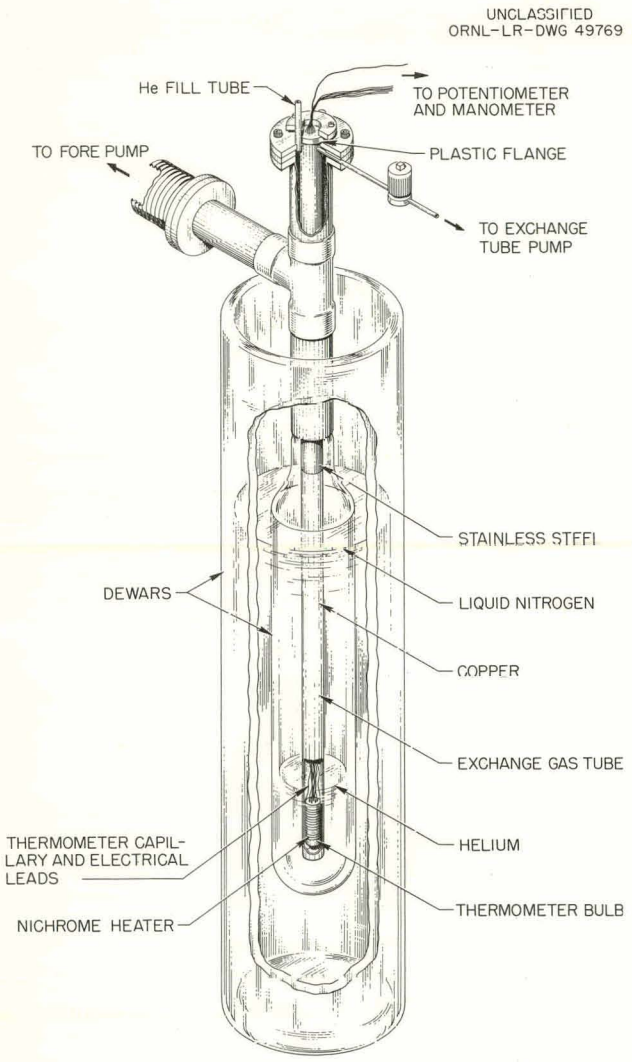

Fig. 24.1. Apparatus for Determination of Superconducting Transition Temperatures.

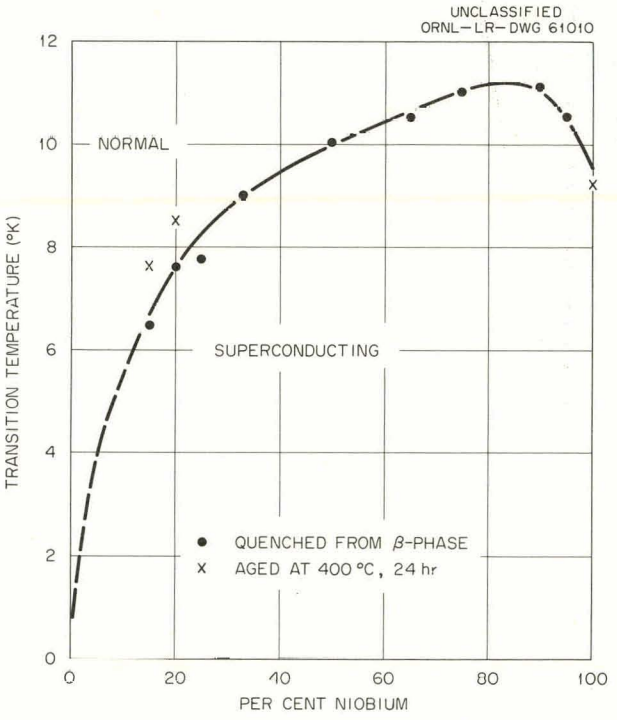

Fig. 24.2. Superconducting Transition Temperature of Nb-Zr Alloys.

25. RECOILLESS GAMMA EMISSION (MÖSSBAUER EFFECT)

H. S. Pomerance

Assistance has been given to the Physics Division in their studies of the nuclear resonant absorption of the 77-kev level of Au^{197} (ref 1). The gamma-ray source used was Pt^{197} metal prepared by neutron irradiation of Pt^{196}. A variety of absorbers have been used – gold in nickel, chromium, stainless steel, or iron; gold as the gold halides and the potassium gold halides; and the alloy Al_2Au. The magnetic splittings, the chemical shifts, and the isomeric shifts are now being compared with nuclear and molecular models. For instance, the *s*-electron binding with gold varies with the electronegativity of the partner. Pauling[2] predicts that in Al_2Au, at least 0.6 electron per gold atom must have transferred to the aluminum atoms.

Attempts to find a Mössbauer effect with Te^{125} were not successful.

[1] L. D. Roberts and J. O. Thomson, *Phys. Div. Ann. Progr. Rept. Feb. 10, 1961*, ORNL-3085, p 69.

[2] Linus Pauling, *The Nature of the Chemical Bond*, 3d ed., p 433, Cornell University Press, Ithaca, New York, 1960.

THIS PAGE

WAS INTENTIONALLY

LEFT BLANK

PUBLICATIONS AND PAPERS

THIS PAGE

WAS INTENTIONALLY

LEFT BLANK

PUBLICATIONS AND PAPERS

G. A. Alers and D. O. Thompson

"Dislocation Contributions to the Modulus and Damping in Copper at Megacycle Frequencies," *J. Appl. Phys.* **32**, 283 (1961).

R. F. Bass, J. W. Cleland, and J. H. Crawford, Jr.

"Radiation Effects on Deep-Level Impurity States in Ge," presented at Southeastern Section Meeting, American Physical Society, Louisville, Kentucky, Mar. 30–Apr. 1, 1961.

R. G. Berggren

"Brittle Fracture," presented to Oak Ridge Chapter, American Society for Metals, Oak Ridge, Tennessee, Mar. 15, 1961.

"Neutron Irradiation Effects in Steels: Studies at Oak Ridge National Laboratory," p 370 in *Steels for Reactor Pressure Circuits*, Iron and Steel Institute Special Report No. 69 (1961).

"ORNL Irradiation Tests," presented to ASME Research Committee on the Effect of Radiation on Materials and Nuclear Installations, Oak Ridge, Tennessee, Sept. 21, 1960.

"Radiation Effects in Ferritic Steels," p 91 in *Status of Radiation Effects Research on Structural Materials and the Implications to Reactor Design*, TID-7588 (1960).

R. G. Berggren, W. E. Brundage, W. W. Davis, N. E. Hinkle, and J. C. Zukas

"Tensile and Stress-Rupture Properties of Irradiated Stainless Steels and Inconel," p 205 in *Status of Radiation Effects Research on Structural Materials and the Implications to Reactor Design*, TID-7588 (1960).

D. S. Billington

"Radiation Damage (Inanimate Materials)," p 223 in *McGraw-Hill Encyclopedia of Science and Technology* (ed. by W. H. Crouse), vol 11, McGraw-Hill, New York, 1960.

"Relaxing Reliance on Empirical Data," *Nucleonics* **18**, 64 (1960).

D. S. Billington and J. H. Crawford, Jr.

Radiation Damage in Solids, vol 7 of *Investigations in Physics Series*, ed. by E. P. Wigner and Robert Hofstadter, Princeton University Press, Princeton, New Jersey, 1961.

D. Binder, C. D. Bopp, and R. L. Towns

"Measurement of Energy Absorbed from Pile Neutrons," p 105 in *ASTM Symposium on Radiation Effects and Radiation Dosimetry* (1961).

T. H. Blewitt

"Low Temperature Irradiation Studies," presented at the Fourth International Summer School on Solid State Physics, Radiation Damage in Solids, Ispra (Varese), Italy, Sept. 5–23, 1960.

"Low Temperature Studies in Neutron-Irradiated Metals," presented at Symposium on Principles of Radiation Damage on Crystals (sponsored by European Atomic Energy Society), Saclay, France, Oct. 4–7, 1960.

T. H. Blewitt, S. T. Sekula, and J. Diehl

"Energy Release in Reactor Irradiated Copper. Part II. The 600 to 700°K Release," *Phys. Rev.* **122**, 53 (1961).

T. H. Blewitt, R. R. Coltman, R. R. Jamison, and J. K. Redman

"Radiation Hardness in Copper," *Acta Cryst.* **13**, 1130 (1960).

"Radiation Hardening in Copper Single Crystals," *J. Nuclear Materials* **2**, 277 (1960).

R. H. Busey, R. B. Bevan, Jr., R. A. Gilbert, and E. Sonder

"Low Temperature Heat Capacities and Magnetic Susceptibilities of K_2ReCl_6 and K_2ReBr_6," presented at the 15th Annual Calorimetry Conference, Gatlinburg, Tennessee, Sept. 7–10, 1960.

C. T. Butler and M. T. Robinson
Photon Wavelength and Energy Conversion Tables, ORNL-3125 (July 15, 1961).

R. M. Carroll
"The Continuous Release of Fission Gas from UO_2 During Irradiation," presented at the ASTM Symposium on Radiation Effects, Atlantic City, New Jersey, June 26–30, 1961.

R. M. Carroll and C. D. Baumann
Experiment on Continuous Release of Fission Gas During Irradiation (Interim Report), ORNL-3050 (Feb. 9, 1961).

J. V. Cathcart and F. W. Young, Jr.
"Influence of Reactor Radiation on the Oxidation of Niobium," *Corrosion* **17**, 77 (1961)

J. W. Cleland
"Radiation Effects in Semiconductor Materials," presented at ASM Symposium on Recent Developments in Materials for Nuclear Applications, Albuquerque, New Mexico, Feb. 16–17, 1961.

"Transmutation Doping and Recoil Effects in Semiconductors Exposed to Thermal Neutrons," presented at the Fourth International Summer School on Solid State Physics, Radiation Damage In Solids, Ispra (Varese), Italy, Sept. 5–23, 1960.

J. W. Cleland and J. H. Crawford, Jr.
"Radiation-Induced Disorder in Semiconductors," p 299 in *Proceedings International Conference on Semiconductor Physics, Prague 1960*, Czechoslovak Academy of Sciences, Prague, 1961.

"Thermal Neutron Induced Recoil and Transmutation Effects in Isotopic Ge^{74}," *Bull. Am. Phys. Soc.* 6, 177 (1961).

R. R. Coltman, T. H. Blewitt, and S. T. Sekula
"The Effects of Annealing in Oxygen on the Resistivity of High Purity Copper," p 72 in *Colloque international sur les proprietes des metaux de tres haute purete* (International Conference on High Purity Metals, Paris, France, Oct. 10–14, 1959), Centre National de la Recherche Scientifique, Paris, 1960.

J. H. Crawford, Jr.
"Creation of Defects in Alkali Halide Crystals by Ionizing Radiation," p 21 in *Proceedings of International Conference on Color Centers and Crystal Luminescence*, ed. by G. Bonfiglioli, Turin, Italy, Sept. 8–11, 1960 (1961).

"Effect of Radiation on the Behavior of Nonmetallic Solids," presented at the Radiation Research Society Ninth Annual Meeting, Washington, D.C., May 15–17, 1961.

"Radiation Effects in Semiconductors," presented at the Colloquium on Principles of Radiation Damage on Crystals (sponsored by European Atomic Energy Society), Saclay, France, Oct. 4–7, 1960.

"Summary of Lectures on Radiation Effects in Semiconductors," presented at the Fourth International Summer School on Solid State Physics, Radiation Damage in Solids, Ispra (Varese), Italy, Sept. 5–23, 1960.

"The Influence of Radiation-Induced Defects on the Behavior of Diamond-Structure Semiconductors and Devices," p 797 in *Solid State Physics in Electronics and Telecommunications*, vol 4, "Magnetic and Optical Properties," part 2 (ed. by M. Desirant and J. L. Michiels), Academic Press, New York, 1960.

J. H. Crawford, Jr., and J. W. Cleland
"Transmutation Doping and Recoil Effects in Semiconductors Exposed to Thermal Neutrons," presented at the International Atomic Energy Agency Conference on Uses of Radioisotopes in Physical Sciences and Industry, Copenhagen, Denmark, Sept. 6–17, 1960.

J. H. Crawford, Jr., and C. M. Nelson
"Defect Interactions in Irradiated Calcium-Doped Potassium Chloride," *Phys. Rev. Letters* **5**, 314 (1960).

J. H. Crawford, Jr., and F. W. Young, Jr.
"Mechanism for the Production of F Centers in NaCl by Irradiation with Gamma Rays," *J. Appl. Phys. Letters* **31**, 1688 (1960).

O. L. Curtis, Jr.
"The Carrier-Recombination Behavior and Annealing Properties of Radiation-Induced Recombination Centers in Germanium," thesis, submitted to the Graduate Council of the University of Tennessee in partial fulfillment of the requirements for the Ph.D. degree, 1961.

O. L. Curtis, Jr., and J. H. Crawford, Jr.
"Carrier Recombination and Trapping Processes in Irradiated Germanium," presented at the Conference on Effects of Irradiation on Semiconductors (sponsored by Faraday Society), Saclay, France, Apr. 11–12, 1961.

The Carrier-Recombination Behavior and Annealing Properties of Radiation-Induced Recombination Centers in Germanium, ORNL-3108 (May 15, 1961).

W. W. Davis, N. E. Hinkle, J. R. Weir, J. W. Woods, and J. C. Zukas
Radiation Effects on Structural Materials, ORNL CF-60-10-70 (Oct. 18, 1960).

D. K. Holmes
"Approximate Methods for Treating Annealing Processes Which Involve a Spectrum of Activation Energies," presented by H. C. Schweinler at the International Atomic Energy Agency Symposium on Chemical Effects of Nuclear Transformations, Prague, Czechoslovakia, Oct. 24–27, 1960.

"Radiation Damage Studies Using Dislocation Properties," presented at the Fourth International Summer School on Solid State Physics, Radiation Damage in Solids, Ispra (Varese), Italy, Sept. 5–23, 1960.

"Terms and Concepts in Radiation Damage Theory," presented at the Fourth International Summer School on Solid State Physics, Radiation Damage in Solids, Ispra (Varese), Italy, Sept. 5–23, 1960.

D. K. Holmes and G. Leibfried
"General Outline of Topics To Be Discussed in the Lectures on Radiation Damage Theory," presented at the Fourth International Summer School on Solid State Physics, Radiation Damage in Solids, Ispra (Varese), Italy, Sept. 5–23, 1960.

M. J. Kelly, W. W. Johnston, and C. D. Baumann
"Effects of Nuclear Radiations on Thermocouples," presented at the Symposium on Temperature, Its Measurement and Control in Science and Industry (sponsored by American Institute of Physics, Instrument Society of America, and National Bureau of Standards), Columbus, Ohio, Mar. 27–31, 1961.

M. D. Karkhanavala and R. M. Carroll
In-Pile Measurement of the Electrical Resistivity and Thermoelectric Power of Sintered UO_2, ORNL-3093 (Apr. 17, 1961).

R. H. Kernohan and M. S. Wechsler
"Neutron Irradiation of Cu-Al at Elevated Temperatures," *J. Phys. Chem. Solids* **18**, 175 (1961).

C. E. Klabunde, T. H. Blewitt, and R. R. Coltman
"Radiation Effects in Pyrolitic Graphite," *Bull. Am. Phys. Soc.* **6**, 129 (1961).

J. G. Morgan
"Fission Gas Release, Post-Irradiation Results," presented at Savannah River UO_2 Information Meeting, Augusta, Georgia, Nov. 30, 1960.

"Instantaneous Fission Gas Release Experiments," presented at Savannah River UO_2 Information Meeting, Augusta, Georgia, Nov. 30, 1960.

"UO_2 Irradiation in the ORR and LITR Capsules," presented at Savannah River UO_2 Information Meeting, Augusta, Georgia, Nov. 30, 1960.

M. T. Morgan, M. F. Osborne, and H. E. Robertson
"Equipment for the Collection and Pressure Measurement of Fission Gases from EGCR Capsules," p 458 in *Proceedings of the Eighth Conference on Hot Laboratories and Equipment*, TID-7599, vol 2 (1961).

C. M. Nelson and R. A. Weeks
"Vacuum Ultraviolet Absorption Studies of Irradiated Silica and Quartz," *J. Appl. Phys.* **32**, 883 (1961).

T. S. Noggle
"Nuclear Reactors as Tools for Metallurgical Research," presented to Rocky Mountain Chapter, American Society for Metals, Denver, Colorado, Oct. 21, 1960.

T. S. Noggle and J. O. Stiegler
"Electron Microscope Observations of Fission Fragment Tracks in Thin Films of UO_2," *J. Appl. Phys.* **31**, 2199 (1960).

"Fission Fragment Tracks in UO_2," presented at the ASTM Symposium on Radiation Effects, Atlantic City, New Jersey, June 26–30, 1961.

M. F. Osborne, J. A. Canlin, and A. B. Meservey
Fission Product Disposition and Decontamination of BNL Gas-Cooled Loop, ORNL CF-61-7-49 (July 20, 1961).

W. W. Parkinson and D. Binder
"Post-Irradiation Oxidation and Molecular Weight Changes in Polystyrene and Polymethyl Methacrylate," p 224 in *Materials in Nuclear Applications*, ASTM-STP-276 (1960).

V. K. Paré and D. O. Thompson
"Temperature Dependence of Dislocation Pinning in Copper Single Crystals by Stage III Radiation Defects," presented at the 1961 Conference on Internal Friction, Ithaca, New York, July 10–11, 1961.

M. T. Robinson, O. S. Oen, and D. K. Holmes
"Fast Neutron Energy Spectra in Graphite-Moderated Reactors," *Nuclear Sci. and Eng.* **10**, 61 (1961).

H. C. Schweinler
"Distribution in Kinetic Energy of Daughter Nuclei Following Certain Primary Nuclear Transformations or Interactions," presented at the International Atomic Energy Agency Symposium on Chemical Effects of Nuclear Transformations, Prague, Czechoslovakia, Oct. 24–27, 1960.

"Energy Loss of Moving Charged Particles in a Valence or Ionic Crystal," *Bull. Am. Phys. Soc.* **6**, 176 (1961).

"Energy Loss of Moving Charged Particles in a Valence or Ionic Crystal," p 91 in *Semiconductor Nuclear Particle Detectors*, ed. by J. Dabbs and J. Walters, NAS-NRC Nuclear Science Series Report No. 32 (1961).

S. T. Sekula
"Effect of Internal Oxidation on the Residual Resistivity of Dilute Cu Alloys," *Bull. Am. Phys. Soc.* **6**, 172 (1961).

E. Sonder
"Magnetic and Color Centers in KCl," *Bull. Am. Phys. Soc.* **6**, 114 (1961).

J. O. Stiegler and T. S. Noggle
"Direct Replica Technique for Copper," *J. Appl. Phys. Letters* **31**, 1827 (1960).

"Victawet and Sodium Meta Phosphate as Parting Agents for Electron Microscope Replicas," *Rev. Sci. Instr.* **32**, 406 (1961).

D. O. Thompson
"A Thermally Activated Internal Friction Spectrum Following Neutron Irradiation," presented at the 1961 Conference on Internal Friction, Ithaca, New York, July 10–11, 1961.

D. O. Thompson and V. K. Paré
"Effect of Fast-Neutron-Induced Defects on the Internal Friction and Young's Modulus of Pure Copper Single Crystals," *Bull. Am. Phys. Soc.* **6**, 157 (1961).

M. S. Wechsler
"The Effects of Radiation on Metals and Alloys," presented at the ASM Twelfth Biennial Pennsylvania Interchapter Meeting, University Park, Pennsylvania, Sept. 10, 1960.

M. S. Wechsler, R. H. Kernohan, and J. H. Barrett
"Flux and Temperature Dependence of Irradiation-Enhanced Diffusion in Cu-Al," *Bull. Am. Phys. Soc.* **6**, 158 (1961).

M. S. Wechsler and H. M. Otte
"The Generalized Theory of the Martensitic Cubic to Orthorhombic Phase Transformation," *Acta Met.* **9**, 117 (1961); *Acta Cryst.* **13**, 1133 (1960).

R. A. Weeks
"Electron Spin Resonance in Neutron Irradiated TiO_2 Single Crystals," *Bull. Am. Phys. Soc.* **6**, 178 (1961).

R. A. Weeks and C. M. Nelson
"Irradiation Effects and Short-Range Order in Silica and Quartz," *J. Appl. Phys.* **31**, 1555 (1960).

J. C. Wilson
"A Summary of Experiment with In-Pile Thermocouples," p 140 in *High Temperature Thermometry Seminar*, TID-7586, part 1 (1960).

M. C. Wittels
"Stored Energy Review," *J. Nuclear Safety* **2**, 13 (1961).

"X-Ray Studies of Irradiated Refractory Crystals," presented at the American Ceramic Society Symposium on Ceramics in Nuclear Energy, Toronto, Canada, Apr. 23–27, 1961.

M. C. Wittels and F. A. Sherrill
"Noble Metals Grown as Small Spherical Single Crystals," *Bull. Am. Phys. Soc.* **6**, 352 (1961).

F. W. Young, Jr.
"Crystal Imperfections and the Chemical Reactivity of Metal Surfaces," presented at ASM Symposium, Chicago, Illinois, Apr. 20, 1961.

"Etch Pits at Dislocations in Copper," *J. Appl. Phys.* **32**, 192 (1961).

"On the Formation of Dislocations Around Precipitate Particles of Cu_2O in Cu," presented at the AIME Symposium on Direct Observations of Imperfections in Crystals, St. Louis, Missouri, Mar. 2, 1961.

"The Onset of Dislocation Motion in Copper," *Bull. Am. Phys. Soc.* **6**, 162 (1961).

F. W. Young, Jr., and T. R. Wilson
"Acid Cutting and Acid Polishing of Copper Crystals," *Rev. Sci. Instr.* **32**, 559 (1961).

J. C. Zukas and R. G. Berggren
"Flux Measurements and Irradiation Assemblies Used in the LITR, MTR, and ORR Reactors," p 36 in *Status of Radiation Effects Research on Structural Materials and the Implications to Reactor Design,* TID-7588 (1960).

SUMMER INSTITUTE FOR COLLEGE PHYSICS TEACHERS (ORINS-ORNL) JUNE 26–AUG. 18, 1961

Several members of the Division participated in this program. H. C. Schweinler presented eleven lectures on solid state physics. J. W. Cleland supervised laboratory demonstrations in solid state techniques, and H. S. Pomerance worked with the Reactor School to provide laboratory experiments in neutron and reactor physics.

FOURTH INTERNATIONAL SUMMER SCHOOL ON SOLID STATE PHYSICS RADIATION DAMAGE IN SOLIDS

Members of the Division were active in this Summer School, which was held at Ispra, Italy, Sept. 5–23, 1960, and sponsored by the Italian Physical Society (G. Polvani, President).

D. S. Billington was Director of the School. J. H. Crawford, Jr., presented a series of lectures on radiation damage in semiconductors, D. K. Holmes spoke on the theory of radiation damage, and T. H. Blewitt lectured on radiation damage in metals. J. W. Cleland gave a seminar on transmutation doping in semiconductors.

The entire series of lectures will appear in: *Rendiconti della Scuola International di Fisica "Enrico Fermi."*

ORNL-3213
UC-34 – Physics
TID-4500 (16th ed. Rev.)

INTERNAL DISTRIBUTION

1. J. H. Barrett
2. R. F. Bass
3. C. Bassani
4. C. D. Baumann
5. P. R. Bell
6. W. T. Berg
7. R. G. Berggren
8. U. Bertocci
9. J. O. Betterton, Jr.
10. D. S. Billington
11. E. P. Blizard
12. A. L. Boch
13. E. G. Bohlmann
14. C. D. Bopp
15. C. J. Borkowski
16. G. E. Boyd
17. M. A. Bredig
18. R. B. Briggs
19. H. Brooks (consultant)
20. F. R. Bruce
21. W. E. Brundage
22. C. T. Butler
23. N. Cabrera (consultant)
24. R. M. Carroll
25. J. W. Cleland
26. R. G. Cleland (consultant)
27. A. F. Cohen (consultant)
28. R. R. Coltman
29. J. A. Cox
30. J. H. Crawford, Jr.
31. F. L. Culler
32. J. E. Cunningham
33. O. L. Curtis
34. W. W. Davis
35. J. L. Fowler
36. J. H. Frye, Jr.
37. J. L. Gabbard
38. B. R. Gossick (consultant)
39. R. J. Gray
40. W. R. Grimes
41. D. E. Harrison (consultant)
42. N. E. Hinkle
43. A. Hollaender
44. D. K. Holmes
45. A. S. Householder
46. L. D. Hulett
47. H. B. Huntington (consultant)
48. J. T. Howe
49. L. H. Jenkins
50. L. K. Jetter
51. R. W. Johnson
52. R. J. Jones
53. R. G. Jordan (Y-12)
54. W. H. Jordan
55. C. E. Klabunde
56. G. W. Keilholtz
57. M. T. Kelley
58. R. H. Kernohan
59. E. M. King
60. J. A. Krumhansl (consultant)
61. C. Lehmann
62. G. Leibfried
63. H. Leidheiser, Jr. (consultant)
64. E. Lell
65. A. B. Lewis (consultant)
66. T. A. Lewis
67. T. A. Lincoln
68. S. C. Lind
69. R. S. Livingston
70. H. G. MacPherson
71. D. L. McDonald
72. C. J. McHargue
73. W. D. Manly
74. A. Meyer
75. A. J. Miller
76. E. C. Miller
77. J. W. Mitchell (consultant)
78. J. G. Morgan
79. K. Z. Morgan
80. M. T. Morgan
81. J. P. Murray (K-25)
82. R. B. Murray
83. C. M. Nelson (consultant)
84. M. L. Nelson
85. T. S. Noggle
86. O. S. Oen
87. M. F. Osborne
88. V. Paré

89. W. W. Parkinson
90. D. Phillips
91. J. C. Pigg
92. H. Pomerance
93. M. E. Ramsey
94. T. A. Read (consultant)
95. P. E. Reagan
96. J. K. Redman
97. A. E. Richt
98. H. E. Robertson
99. C. C. Robinson
100. M. T. Robinson
101. A. F. Rupp
102. O. E. Schow
103. H. C. Schweinler
104. H. E. Seagren
105. W. C. Sears (consultant
106. F. Seitz (consultant)
107. S. T. Sekula
108. F. A. Sherrill
109. E. D. Shipley
110. W. A. Sibley
111. R. H. Silsbee (consultant)
112. O. Sisman
113. M. J. Skinner
114. L. Slifkin (consultant)
115. G. P. Smith
116. M. J. Smith
117. A. H. Snell
118. E. Sonder
119. A. L. Southern
120. R. L. Sproull (consultant)
121. J. T. Stanley
122. E. E. Stansbury
123. C. D. Susano
124. J. A. Swartout
125. E. H. Taylor
126. W. E. Taylor (consultant)
127. L. C. Templeton
128. D. O. Thompson
129. David Turnbull (consultant)
130. M. S. Wechsler
131. R. A. Weeks
132. A. M. Weinberg
133. E. P. Wigner (consultant)
134. M. K. Wilkinson
135. J. M. Williams
136. W. R. Willis (consultant)
137. J. C. Wilson
138. C. E. Winters
139. M. C. Wittels
140. E. O. Wollan
141. F. W. Young
142. J. C. Zukas
143. Biology Library
144–146. Central Research Library
147–196. Laboratory Records Department
197. Laboratory Records, ORNL R.C.
198. ORNL – T-12 Technical Library, Document Reference Section
199. Reactor Division Library

EXTERNAL DISTRIBUTION

200. W. W. Shaver, Corning Glass Works, Corning, New York
201. S. H. Liebson, Naval Research Laboratory, Washington, D.C.
202. Boeing Airplane Company
203. Division of Research and Development, AEC, ORO
204. J. R. Johnson, Minnesota Mining and Manufacturing Co., St. Paul
205. A. E. Ruark, AEC, Washington
206. G. L. Stiehl, Convair Division of General Dynamics Corp., San Diego
207. R. O. Bolt, California Research Corp., Richmond
208. Benjamin Lax, Lincoln Laboratory, Lexington, Massachusetts
209. George H. Wagner, Linde Air Products Company, Tonawanda Laboratory, East Park Drive and Woodward Avenue, Tonawanda, New York
210. D. K. Stevens, Materials and Metallurgy Branch, Division of Research, U.S. Atomic Energy Commission, Washington, D.C.
211. R. I. Leininger, Battelle Memorial Institute, 505 King Avenue, Columbus, Ohio
212. Westinghouse Electric Corp., Research Laboratories, Pittsburgh, Pennsylvania

213. J. G. Castle, Jr., Physics Dept., Westinghouse Electric Corp., Research Laboratories, Pittsburgh, Pennsylvania
214. C. Kikuchi, University of Michigan, Willow Run Laboratory, Ann Arbor, Michigan
215. N. R. Beaudry, Office of Ordnance Research, Duke Station, Durham, North Carolina
216. J. Hitch, Office of Isotope Development, AEC, Washington
217. Ira Zartman, Division of Reactor Development, USAEC, Washington, D.C.
218. P. W. McDaniel, Division of Research, USAEC, Washington, D.C.
219. H. Y. Fan, Solid State Physics Dept., Purdue University, Lafayette, Indiana
220. T. J. Turner, Department of Physics, Wake Forest College, Winston-Salem, North Carolina
221. C. C. Webster, Testing Reactor, Westinghouse Electric Corp., P.O. Box 1075, Pittsburgh, Pennsylvania
222. J. B. Trice, Military Space Vehicle Department, General Electric Co., Philadelphia, Pennsylvania
223. T. H. Blewitt, Argonne National Laboratory, Chicago, Illinois
224. R. A. Charpie, Union Carbide Corporation, New York, New York
225. L. B. Emlet, Union Carbide Corporation, New York, New York
226. Watt Webb, Union Carbide Metals, Niagara Falls, New York
227. C. D. Yost, ARPA, Pentagon, Washington, D.C.
228. D. F. Cope, Reactor Division, Oak Ridge Operations Office
229. J. M. Simmons, Division of Reactor Development, AEC, Washington, D.C.
230. H. Shulman, Diamond Ordnance Fuse Laboratory, Washington, D.C.
231. G. D. Watkins, General Electric Research Laboratories, Schenectady, New York
232–865. Given distribution as shown in TID-4500 (16th ed. Rev.) under Physics category (75 copies – OTS)

Reports previously issued in this series are:

ORNL-1025*	Period Ending January 31, 1951
ORNL-1095	Period Ending April 30, 1951
ORNL-1128*	Period Ending July 31, 1951
ORNL-1214*	Period Ending October 31, 1951
ORNL-1261*	Period Ending January 31, 1952
ORNL-1301*	Period Ending May 10, 1952
ORNL-1359*	Period Ending August 10, 1952
ORNL-1429*	Period Ending November 10, 1952
ORNL-1506*	Period Ending February 10, 1953
ORNL-1606	Period Ending August 31, 1953
ORNL-1677	Period Ending February 28, 1954
ORNL-1762*	Period Ending August 30, 1954
ORNL-1851*	Period Ending February 28, 1955
ORNL-1852	Period Ending February 28, 1955
ORNL-1944	Period Ending August 30, 1955
ORNL-1945	Period Ending August 30, 1955
ORNL-2051	Period Ending February 29, 1956
ORNL-2052*	Period Ending February 29, 1956
ORNL-2188	Period Ending August 30, 1956
ORNL-2189*	Period Ending August 30, 1956
ORNL-2413	Period Ending August 31, 1957
ORNL-2614	Period Ending August 31, 1958
ORNL-2829	Period Ending August 31, 1959
ORNL-3017	Period Ending August 31, 1960

*Classified.